

# **Synthesis and Photophysical Studies of Analogues of the GFP Chromophore and Epicocconone**

Thesis Submitted  
in Partial Fulfilment  
of  
The Degree of Doctor of Philosophy from Macquarie University

By  
**Soumit Chatterjee, M.Sc.**  
**42278708**

**Date: 14<sup>th</sup> November, 2014**

**Principal Supervisor: Prof. Peter Karuso**  
**Associate Supervisor: A/Prof. Fei Liu**  
**Adjunct Supervisor: Prof. Anindya Datta, IIT Bombay, India**



**Chemistry and Biomolecular Sciences Department**  
**Macquarie University**  
**Sydney 2109**  
**Australia**



## Table of Contents

<b>Thesis Declaration .....</b>	<b>5</b>
<b>List of abbreviations.....</b>	<b>7</b>
<b>Summary .....</b>	<b>15</b>
<b>Chapter 1: Introduction.....</b>	<b>17</b>
<b>1.1. Fluorescence Spectroscopy: Prologue .....</b>	<b>19</b>
<b>1.2. Fluorescence: An Overview .....</b>	<b>20</b>
<b>1.3. Fluorophores .....</b>	<b>22</b>
<b>1.3.1. Protein-labelling Fluorophores .....</b>	<b>23</b>
<b>1.4. Overview of Excited State Processes .....</b>	<b>26</b>
<b>1.4.1. Photoisomerization.....</b>	<b>26</b>
<b>1.4.2. Photoinduced Electron Transfer.....</b>	<b>27</b>
<b>1.4.3. Excited State Proton Transfer .....</b>	<b>28</b>
<b>1.5. Restricted Environment Affecting Excited State Processes .....</b>	<b>32</b>
<b>1.5.1. Micelles .....</b>	<b>33</b>
<b>1.5.2. Excited State Proton Transfer in Microheterogeneous Media .....</b>	<b>34</b>
<b>1.5.3. Alteration of Non-radiative Processes in Microheterogeneous Media .....</b>	<b>35</b>
<b>1.6. Motivation of The Thesis .....</b>	<b>35</b>
<b>References .....</b>	<b>36</b>
<b>Chapter 2: Review on Epicocconone .....</b>	<b>41</b>
<b>2.1. Discovery and Elucidation of Structure of Epicocconone .....</b>	<b>43</b>
<b>2.2. Steady State Spectra.....</b>	<b>44</b>
<b>2.3. Applications in Molecular and Cellular Biology .....</b>	<b>45</b>
<b>2.4. Photophysics .....</b>	<b>45</b>
<b>2.5. Synthesis of Epicocconone Derivative .....</b>	<b>46</b>
<b>References .....</b>	<b>47</b>
<b>Introduction to Associated Publications .....</b>	<b>49</b>
<b>Conclusion.....</b>	<b>51</b>
<b>Chapter 3: Review on Green Fluorescent Protein Chromophore .....</b>	<b>53</b>
<b>3.1. Discovery and Early History of Green Fluorescent Protein (GFP).....</b>	<b>55</b>
<b>3.2. Use of GFP .....</b>	<b>55</b>
<b>3.3. The GFP Chromophore .....</b>	<b>56</b>
<b>3.4. Photophysics of <i>p</i>-HBDI in Protein.....</b>	<b>57</b>
<b>3.5. Synthesis of <i>p</i>-HBDI .....</b>	<b>58</b>
<b>3.6. The Enigma of Isolated <i>p</i>-HBDI .....</b>	<b>59</b>
<b>3.7. Recent Advances in Synthesis of Fluorescent HBDI Derivatives .....</b>	<b>62</b>
<b>References .....</b>	<b>66</b>
<b>Introduction to Associated Manuscripts .....</b>	<b>73</b>
<b>Conclusion.....</b>	<b>75</b>
<b>Chapter 4: Materials and methods .....</b>	<b>77</b>
<b>4.1. Materials and Experimental Procedure.....</b>	<b>79</b>
<b>4.1.1 Equipment.....</b>	<b>79</b>
<b>4.2. Steady State Measurements.....</b>	<b>80</b>
<b>4.2.1. Absorption Spectroscopy .....</b>	<b>81</b>

4.2.2. Fluorescence Spectroscopy .....	82
4.3. Time Resolved Fluorescence Measurements.....	83
4.3.1. Lifetime.....	84
4.3.2. Time Resolved Fluorescence Measurement in Nanosecond-Picosecond Time Regime .....	85
4.3.3. Analysis of Fluorescence Decay .....	89
4.3.4. Time Resolved Fluorescence Measurement in Picosecond-Femtosecond Time Regime .....	90
4.4. Synthesis of GFP Analogues .....	94
References .....	112
Conclusions .....	115
Acknowledgment .....	117



## Thesis Declaration

In this written submission of thesis by publication, two published papers, one submitted manuscript and a manuscript under preparation have been included. The first publication in *The Journal of Physical Chemistry A*, **2011** discusses the ultrafast dynamics of epicocconone, in which reported spectroscopic studies were performed and interpreted by the author. Dr. Tarak Nath Burai helped constructing the first draft of the paper, Prof. Anindya Datta supervised the fluorescence decay studies and final draft of the paper and Prof. Peter Karuso supplied pure epicocconone and supervised the final draft of the paper. In the second published paper in *The Journal of Physical Chemistry B*, **2013** we further investigated the excited state processes involved in epicocconone by comparing, with the help of four analogues, using steady state and dynamic fluorescence measurements. The author performed all the fluorescence studies, interpreted the result, did all the analysis of the spectra and drafted the first version of the paper. The compounds were synthesized by Agathe Boulangé and Philippe A. Peixoto, students of Dr. Xavier Franck from CNRS; University of Rouen, France. Prof. Anindya Datta supervised the fluorescence decay studies and helped to interpret the results and wrote the final draft of the paper. Prof. Peter Karuso performed the Quantum Mechanical and Molecular Modelling calculations, interpreted and wrote these up and edited the final draft of the paper. The third manuscript was submitted to *The Journal of Physical Chemistry B* on March 7<sup>th</sup>, 2015 and we are still awaiting the reviewer's comments. The author performed all the fluorescence studies, did all the spectroscopic analysis, interpreted the results and drafted the first version of the paper. The compounds were synthesized by Agathe Boulangé, a student of Dr. Xavier Franck at the University of Rouen, France. Prof. Anindya Datta supervised the fluorescence decay studies and interpreted the results and helped to write this up. Prof. Peter Karuso performed the Quantum Mechanical and Molecular Modelling calculations, interpreted and wrote these up and took

primary responsibility for the final drafts. The fourth manuscript, under preparation, will be submitted to the *Journal of the American Chemical Society* and discusses the photophysics of a novel green fluorescent protein (GFP) chromophore analogues, which were synthesized, characterized and studied by NMR spectroscopy, fluorescence and steady state spectroscopy and the results were interpreted by the author. Prof. Peter Karuso ran and interpreted the 2D NMR spectra, ran and interpreted the QM and MM calculations and helped to construct the final draft. The first draft of the paper was drafted by the author and Prof. Datta.

In addition, the author synthesized 8 more GFP chromophore analogues and characterized them. The author is currently preparing the first draft of the paper in the format for *Organic Letters*. Prof. Anindya Datta is helping to interpret the results and in the construction of the draft. Prof. Peter Karuso conceived the project, ran and interpreted the 2D NMR spectra and will take primary responsibility for the final drafts.

The author declares that this written submission represents his ideas and works, along with the help from his collaborators and his supervisors, in his own words and where others' ideas, words and works have been included, he has adequately cited and referenced the original sources. He also declares that he has adhered to all principles of academic honesty and integrity and have not misinterpreted or fabricated or falsified any idea/data/fact/source. He undertakes the responsibility that any violation of the above will cause disciplinary action by the University and can also evoke penal action from the sources which have thus not been properly cited or from whom proper permissions has not been taken when needed.

Soumit Chatterjee

Date: 14<sup>th</sup> November, 2014

42278708

## List of abbreviations

2-BFP	(4Z)-4-[(1H-imidazol-2-yl)methylene]-1-methyl-2-phenyl-1H-imidazol-5(4H)-one
A	Acceptor
ADC	Analogue to digital converter
BBO	Barium borate
CD	Cyclodextrin
CFD	Constant fraction discriminator
CI	Conical intersection
CMC	Critical Micelle Concentration
CT	Charge transfer
CTAB	Cetyltrimethylammonium bromide
D	Donor
DAO	Diaryloxazoles
DCM	Dichloromethane

DMABN	<i>N,N</i> -dimethylaminobenzonitrile
DMPI	(4 <i>Z</i> )-4-( <i>N,N</i> -dimethylaminobenzylidene)-1-methyl-2-phenyl-1,4-dihydro-5 <i>H</i> -imidazolin-5-one
DMSO	Dimethylsulfoxide
DNS-Cl	Dansyl chloride
DPSS	Diode pumped solid state
ESDPT	Excited State Double Proton Transfer
ESI	Electrospray ionization
ESIPT	Excited State Intramolecular Proton Transfer
ESPT	Excited State Proton Transfer
ESR	Electron Spin Resonance
EtOAc	Ethyl acetate
F.I.	Fluorescence Intensity
FC	Franck-Condon
FOG	Femtosecond Optically Gated

FRET	Förster Resonance Energy Transfer
FT-IR	Fourier Transform Infrared
FTICR	Fourier Transform Ion Cyclotron Resonance
FWHM	Full Width at Half Maximum
GFP	Green Fluorescent Protein
Gly	Glycine
H-bond	Hydrogen bond
H <sub>2</sub> LHBDI	(Z)-4-(5,7-dihydroxy-2,3-dihydro-1H-inden-1-ylidene)-1,2-dimethyl-1H-imidazol-5(4 <i>H</i> )-one
HMBC	Heteronuclear Multiple Bond Correlation
HOMO	Highest Occupied molecular Orbital
HPLC	High Performance Liquid Chromatography
HRMS	High Resolution Mass Spectrometry
HSA	Human serum albumin
HSQC	Heteronuclear single quantum coherence spectroscopy

HT	Hula-twist
Hz	Hertz
IC	Internal conversion
ICT	Intramolecular Charge Transfer
IRF	Instrument response function
kW	Kilowatt
LBO	Lithium triborate
LC-MS	Liquid Chromatography-Mass Spectrometry
LE	Locally excited
LIF	Laser induced fluorescence
LRMS	Low Resolution Mass Spectrometry
LUMO	Lowest unoccupied Molecular Orbital
MCA	Multichannel analyser
MeOH	Methanol

MHz	Megahertz
MM	Molecular modelling
N*	Excited normal state
NAC	Non-adiabatic crossing
NADH	Reduced nicotinamide adenine dinucleotide
NMR	Nuclear Magnetic Resonance
NOESY	Nuclear Overhauser Effect Spectroscopy
NS	Nascent state
<i>o</i> -AcBPA	( <i>Z</i> )-3-(5-oxo-2-phenyloxazol-4( <i>5H</i> )-ylidene)-2,3-dihydro-1H-inden-4-yl acetate
<i>o</i> -HBDI	(4-(2-hydroxybenzylidene)-1,2-dimethyl-1 <i>H</i> -imidazol-5( <i>4H</i> )-one)
<i>o</i> -LHBDI	( <i>Z</i> )-4-(7-hydroxy-2,3-dihydro-1 <i>H</i> -inden-1-ylidene)-1,2-dimethyl-1 <i>H</i> -imidazol-5( <i>4H</i> )-one
<i>o</i> -LHBPI	( <i>Z</i> )-4-(7-hydroxy-2,3-dihydro-1 <i>H</i> -inden-1-ylidene)-1-methyl-2-phenyl-1 <i>H</i> -imidazol-5( <i>4H</i> )-one
O.D.	Optical density
OBF	One bond flip

OLED	Organic Light Emitting Diodes
<i>p</i> -HBDI	5- (4-hydroxybenzylidene) – 3,5- dihydro-4H-imidazol-4-one
<i>p</i> -LHBDI	(Z)-4-(5-hydroxy-2,3-dihydro-1H-inden-1-ylidene)-1,2-dimethyl-1H-imidazol-5(4 <i>H</i> )-one
PE	Petroleum ether/light petroleum
PET	Photoinduced Electron Transfer
PMT	Photomultiplier tube
PO	Phenyl oxazolone
Q-TOF	Quadrupole-Time-of-Flight
ROESY	Rotating Frame Nuclear Overhauser Effect Spectroscopy
SDS	Sodium dodecyl sulphate
Ser	Serine
SFR	Sum frequency radiation
T*	Excited tautomer state
TAC	Time to amplitude converter



TCSPC	Time Correlated Single Photon Counting
TD	Torsional deformation
TICT	Twisted Intramolecular Charge Transfer
TLC	Thin Layer Chromatography
TOCSY	Total Correlated Spectroscopy
TX100	Triton X-100
Tyr	Tyrosine
UV	Ultraviolet
Vis	Visible



## Summary

Epicoconone, isolated from the fungus *Epicoccum nigrum*, is only weakly green fluorescent in aqueous solution but emits brightly in the orange-red region in presence of amines due to reversible enamine formation. This makes it an attractive fluorescent sensor for proteins as lysine is one of the commonest amino acids. However, epicoconone has a low quantum yield ( $< 0.01$ ) in water, increasing to a maximum of 0.17 in the presence of excess amine and detergent.

Studying the fluorescent decays, an ultrafast component was found responsible for the non-radiative decay of epicoconone, explaining its relatively low quantum yield. This component was found to be only a minor contributor to the relaxation of the butylamine (a mimic of lysine residues of protein) adduct of epicoconone while accompanied by a rise time that extends the fluorescence decay to well over 2 ns, explaining the higher quantum yield in epicoconone-protein adduct. These observations indicated that photoisomerization or excited-state tautomerization to be the origin of the ultrafast nonradiative process.<sup>1</sup> To have a better understanding of the excited state dynamics, four analogues were synthesized which reacted with amines in a similar fashion to epicoconone. Ultrafast dynamics of these analogues established the involvement of photoisomerization of the heptatriene side chain, rather than the tautomerism of the  $\beta$ -diketone, as the major nonradiative process in epicoconone.<sup>2</sup> Two more analogues with much higher quantum yields were synthesized. In this set of compounds the native compounds were found to be an order of magnitude more fluorescent than epicoconone in neat solutions while the quantum yields of the respective butylamine adducts were found to be about the same as epicoconone-butylamine adducts. Our results suggested that both these compounds could be useful as synthetic alternatives to epicoconone for protein staining and as dual-stains in biotechnology.<sup>3</sup>

The isolated chromophore of green fluorescence protein (*p*-HBDI) is virtually non-fluorescent at room temperature, unlike the protein, due to photoisomerization. A series of GFP analogues were synthesized via oxazolone formation, which we found a superior method to published synthetic routes.<sup>4</sup> One of the analogues exhibited dual emission at room temperature in water and was 500 times more fluorescent than *p*-HBDI.<sup>5</sup> This unprecedented result suggests that GFP analogues of this type could be useful in applications where dual fluorescence or switchable fluorescence can be used such as ultra high resolution microscopy (e.g. STORM).

# **Chapter 1: Introduction**



## 1.1. Fluorescence Spectroscopy: Prologue

When a molecule absorbs energy from a photon, it moves to an excited state. This process is so fast (*ca.*  $10^{-15}$  s) that the nuclear coordinates remain unchanged. The quantum mechanically allowed transitions are seen in the form of a spectrum, from which the energy gaps between different energy levels can be calculated. This forms the basis of absorption spectroscopy. The UV-visible region of the electromagnetic spectrum encompasses the energies required for electronic transitions of molecules. Such transitions may involve spin-paired singlet ( $\sum m_s = S = 0$ ) and spin unpaired triplet ( $\sum m_s = S = 1$ ) states. Organic molecules generally possess paired electrons, thus having a total spin multiplicity of zero ( $\sum m_s = S = 0$ ). The average time spent by a molecule in an excited state is called the lifetime of that state. Typical lifetimes for electronic states range from hundreds of femtoseconds to hundreds of nanoseconds for singlet states and microseconds to seconds, minutes or even hours for triplet states. If the ground state and the excited states possess the same spin multiplicity and a return to the ground state is accompanied by emission of a photon, then the radiative transition is called fluorescence. Transitions between an excited state and ground state, having different spin multiplicities, is called phosphorescence.<sup>6</sup>

Fluorescence spectroscopy is one of the ultra-sensitive physical techniques that allows even single molecule measurement.<sup>7,8</sup> Fluorescence is thus frequently used in analytical, biochemical and biomedical sciences, to report information on the local environment that is not accessible through any other method. The scope of the present thesis is to explore the photophysics of new fluorescent probes, the first set based on the natural product epicocconone and the other on the chromophore of green fluorescent protein (HBDI). In the next few sections, a background to fluorescence and excited state processes that affect it are developed.

## 1.2. Fluorescence: An Overview

According to the Boltzmann distribution (Equation 1.1), most of the molecules occupy the zeroeth vibrational state of the electronic ground state at room temperature.

$$\frac{n}{n_0} = e^{\frac{-\Delta E}{kT}} \quad 1.1$$

The vertical electronic excitation can access several vibrational levels of the excited electronic states ( $S_1$ ,  $S_2 \dots S_n$ ), leading to vibrational structure in the electronic absorption spectrum. Before the electronically excited molecule can return to its ground state by radiative and non-radiative processes, rapid internal conversion takes place when the initial state is  $S_2$  or above, so that any downward transition can originate from the  $S_1$  state. This is known as Kasha's rule and explains why the fluorescence spectrum is the mirror image of the absorption spectrum in the simplest case scenario, like in naphthalene or perylene (Figure 1.1).<sup>6</sup>

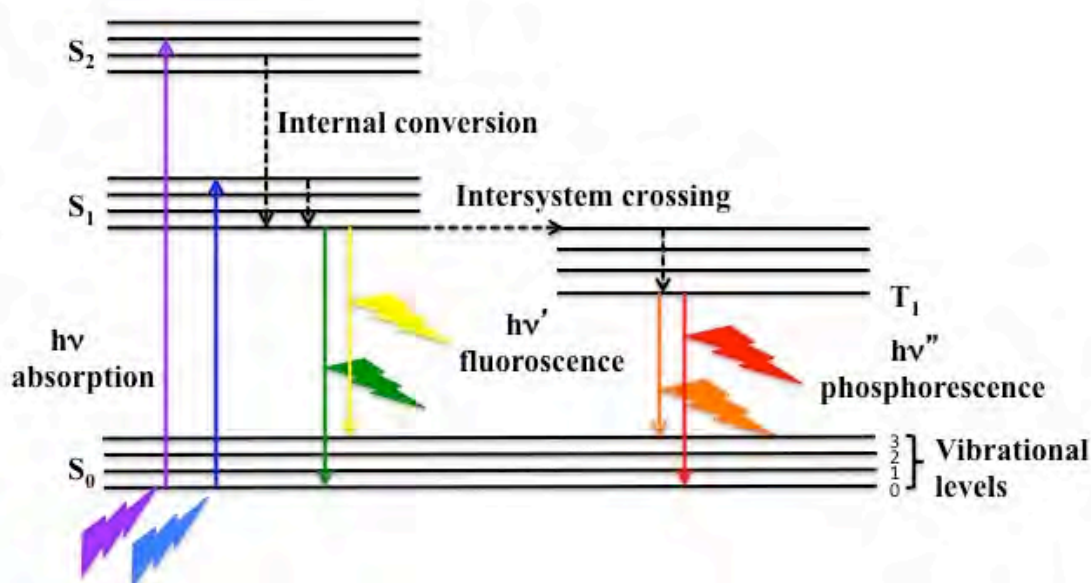


**Figure 1.1.** Schematic simplified Jablonski diagram of a molecule

The mirror image rule does not hold for many molecules, which can undergo excited state processes like photosomerization, proton transfer etc. (*vide infra*), causing a nonradiative



transition from the locally excited state to a lower energy state, which emits at a longer wavelength, if at all. The vibrational features are usually lost during an excited state process. (Figure 1.2).<sup>9,10</sup> Sometimes, the excited state process is so efficient that the LE emission is not observed at all and the fluorescence spectrum consist of a single long Stokes' shifted band.<sup>11</sup> In some other cases, the NS state is non-emissive and the signature of the excited state process is obtained as a markedly decreased quantum yield of the LE state.<sup>12</sup> In the time domain, a fast decay of the LE emission/transient absorption is observed, along with a corresponding rise in the transients of NS.<sup>13,14</sup>

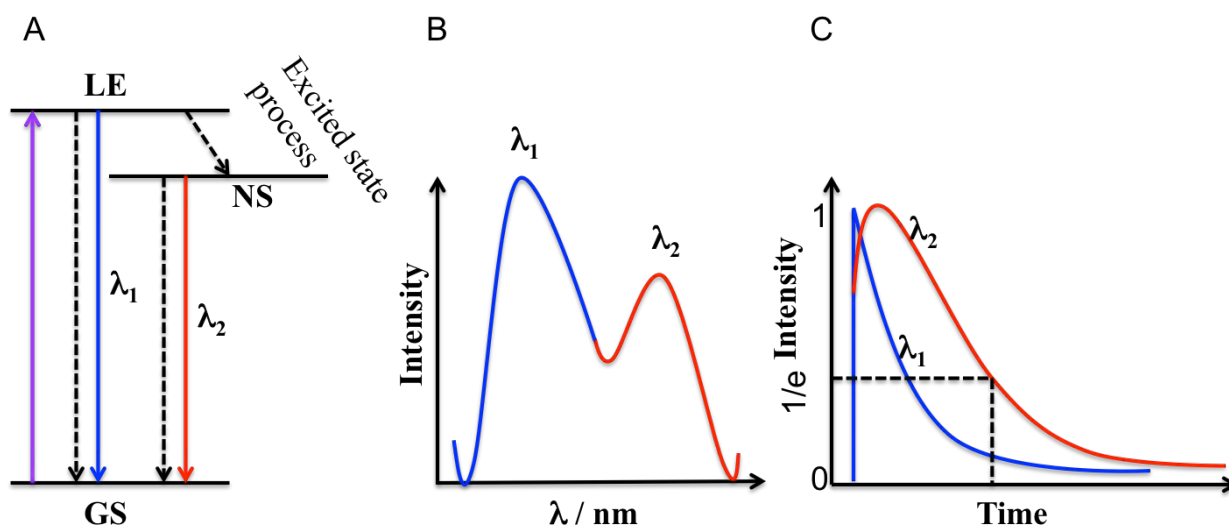


**Figure 1.2.** Schematic (a) Jablonski diagram (b) fluorescence spectrum (c) fluorescence decays resulting from an excited state process.  $\lambda_1$  and  $\lambda_2$  are higher and lower energy emission wavelengths respectively.

The fluorescence quantum yield is defined as the number of photons emitted divided by the number of photons absorbed (Equation 1.2)

$$\text{Quantum yield}(\phi_f) = \frac{\text{number of photons emitted}}{\text{number of photons absorbed}} \quad 1.2$$

If all the molecules that absorbed light are returned to the ground state with emission of a photon, then the quantum yield ( $\phi_f$ ) is 1. The quantum yield is less than 1 if molecules can

undergo non-radiative processes to return to the ground state.

As mentioned earlier, fluorescence lifetime ( $\tau_f$ ) is the average time a molecule spends in the excited state. The relationship between  $\phi_f$  and radiative and nonradiative decay is given by equation 1.3<sup>6</sup>

$$\phi_f = \frac{\Gamma}{\Gamma + k_{nr}} \quad 1.3$$

where  $\Gamma$  is the radiative rate constant,  $k_{nr}$  is the nonradiative rate constant and  $\phi_f$  is the fluorescence quantum yield and fluorescence lifetime is given by equation 1.4<sup>6</sup>

$$\tau = \frac{1}{\Gamma + k_{nr}} \quad 1.4$$

Thus the relationship between  $\phi_f$  and  $\tau$  is given by equation 1.5

$$\phi_f = \Gamma \times \tau \quad 1.5$$

### 1.3. Fluorophores

Thousands of fluorescent probes are known and can broadly be divided into two main classes; intrinsic and extrinsic fluorophores. Intrinsic fluorophores are those that occur naturally. These include the aromatic amino acids, NADH, flavins, derivatives of pyridoxyl, and porphyrins for example. Extrinsic fluorophores are added to the sample to provide new fluorescence. Extrinsic fluorophores include xanthenes, fluorescent proteins (e.g. GFP), cyanines, coumarins, pyrenes etc.<sup>6</sup> These fluorescent molecules are commonly used as markers and tracers in biology and materials science. The choice of fluorophores is governed by the questions that are to be addressed. For example, in order to measure rotational diffusion the lifetime of the fluorophore must be comparable to the timescale of the experiment of interest and fluorescence depolarization should be associated exclusively with rotational motion, without interference from an excited state process. Fluorophores that can participate in protonation

deprotonation equilibria, in ground and/or excited states, are the only suitable candidates for measurement of pH. Only probes with long excitation and emission wavelengths can be used in tissues, which display autofluorescence at short excitation wavelengths.

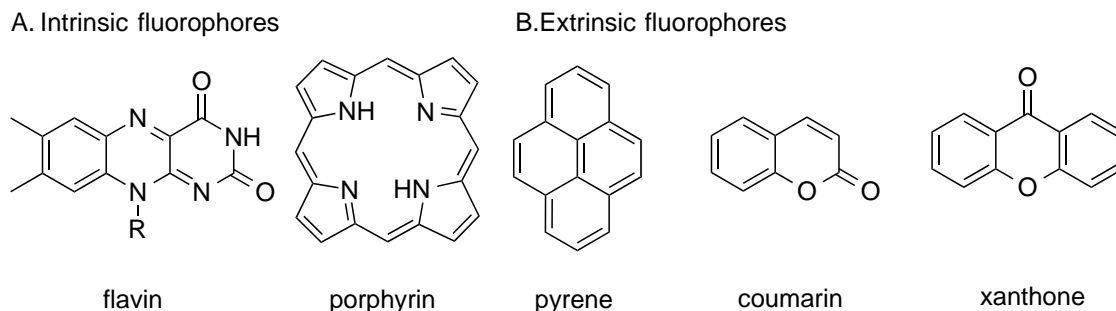


**Figure 1.3.** Examples of (A) intrinsic and (B) extrinsic fluorophores

### 1.3.1. Protein-labelling Fluorophores

A gamut of fluorophores is available for covalent and non-covalent labelling of proteins. Early reports on dansyl chloride (DNS-Cl), which is widely used to label proteins, especially where polarization measurements are anticipated, described the advantages of extrinsic probes in biochemical research.<sup>6</sup> Fluoresceins and rhodamines are also widely used as extrinsic labels. One common use of fluorescein and rhodamine is for labelling of antibodies. A wide variety of fluorescein- and rhodamine-labelled immunoglobulins are commercially available and are frequently used in fluorescence microscopy and immunoassays. High quantum yields, long wavelengths of absorption and emission, which minimize background fluorescence from biological samples and eliminate the need for quartz optics make these fluorophores popular choices.<sup>6</sup> In this thesis, we will concentrate on two such protein-labelling fluorophores that have found considerable interest in recent times.

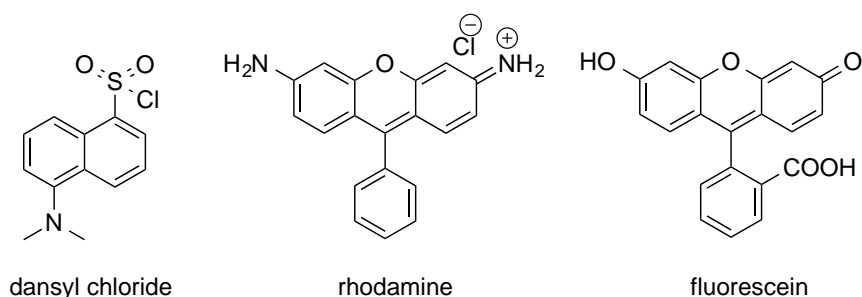


**Figure 1.4.** Examples of protein labelling fluorophores

#### 1.3.1.1. Green Fluorescent Protein

Green Fluorescent Protein (GFP) has emerged as an important tool for monitoring the location and movement of protein within living cells, because it can be genetically encoded.<sup>15-21</sup> This discovery was the subject of the 2008 Nobel Prize in Chemistry.<sup>22,23</sup> GFP was first derived from the jellyfish *Aequorea victoria*, as a companion protein to aequorin, which is a chemiluminescent protein that emits blue light ( $\lambda_{\text{em}} = 470 \text{ nm}$ ), upon binding with  $\text{Ca}^{2+}$  ions. GFP has two characteristic absorption maxima ( $\lambda_{\text{max}} = 395$  and  $470 \text{ nm}$ ) and since the chemiluminescence of aequorin is close to  $470 \text{ nm}$ , energy transfer (FRET) occurs from aequorin to GFP and a green emission at  $508 \text{ nm}$  is observed when the two proteins are within the Förster radius. Shimomura elucidated the structure of the chromophore as 4-*p*-hydroxybenzylideneimidazolinone (*p*-HBDI), formed from the cyclization of the Ser-Tyr-Gly to form an imidazolone.<sup>24-26</sup> The chromophore is centred within a beta-barrel fold of the GFP protein (Figure 1.5). GFPs with many different spectral properties have been prepared by mutating the amino acid sequence.<sup>27</sup> A discussion on GFP and its chromophore is provided in chapter 2.

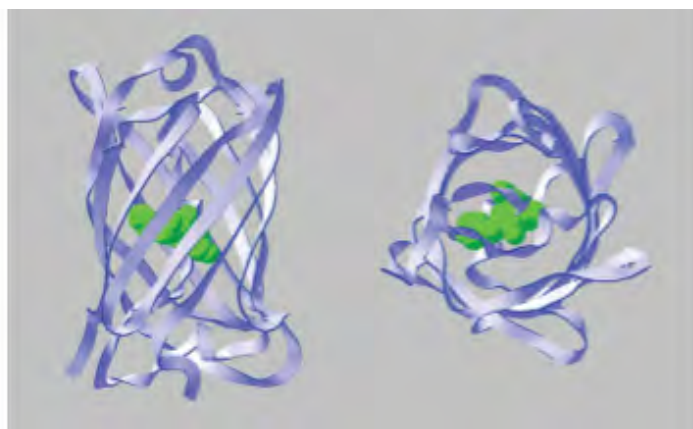


**Figure 1.5.**  $\beta$ -barrel structure of GFP, Side and top view. The chromophore is linked covalently to the protein<sup>6</sup>

#### 1.3.1.2. *Epicocconone*

Epicocconone (Figure 1.6), a novel fluorophore from fungus *Epicoccum nigrum*, is used to covalently label proteins. It is only weakly green fluorescent in aqueous solutions but becomes strongly fluorescent with an emission maximum at 610 nm upon addition of proteins.<sup>28</sup> The enhancement of fluorescence of epicocconone in proteins has been shown to be due to reversible enamine formation with lysine residues of the proteins.<sup>29</sup> This unique mechanism makes epicocconone the first reversible-covalent latent fluorophore to be discovered. A thorough discussion about epicocconone and its analogues are provided in chapter 2.

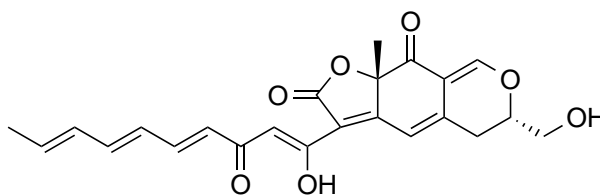


**Figure 1.6.** Molecular structure of epicocconone

Both the green fluorescent protein chromophore and epicocconone undergo various excited state processes, which govern their photophysical behaviour. These processes are affected by the properties of the immediate microenvironment of the fluorophores. An overview of some relevant excited state processes has been provided in the following sections.

## 1.4. Overview of Excited State Processes

### 1.4.1. Photoisomerization

Photoinduced cis-trans isomerization process of double bonds is known as photoisomerization.<sup>30-32</sup> An example of this process is available in the cis-trans isomerization of retinal polyenes involved in the process of vision.<sup>33-36</sup> It also drives a proton transport in bacteriorhodopsin, which has inspired attempts to devise potential applications of photoisomerization in optical switching systems and molecular electronics.<sup>37,38</sup> Different mechanisms have been proposed for photoisomerization such as one bond twist in which the Arrhenius pre-exponent is enhanced in viscous media or hula twist and bicyclic pedal mechanisms where a concerted rotation about two bonds is involved.<sup>39-41</sup> In the ground state, the potential energy surfaces of the two isomers are generally well separated by a large barrier, disfavoring isomerization. However, the excited state may have no barrier between cis and trans conformations and can return to the ground state in either conformation (Figure 1.7). This barrierless transition can occur on the femtosecond time scale.<sup>42-45</sup>

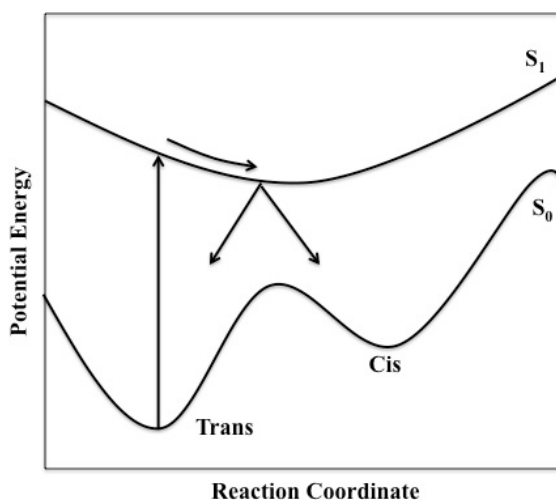


**Figure 1.7.** Schematic of potential energy surface of a molecule in the ground ( $S_0$ ) and excited state ( $S_1$ ).

### 1.4.2. Photoinduced Electron Transfer

Photoinduced electron transfer (PET) processes involve transfer of an electron from a donor to an acceptor upon photoexcitation. This process can be either intermolecular or intramolecular.<sup>46,47</sup> Intermolecular PET process is diffusion controlled and electron transfer is through space or solvent mediated while in intramolecular PET the electron transfer can take place through bonds or through space. Increasing the number of bonds between the donor and acceptor moiety leads to an exponential decrease in bond interactions while the through space interactions are observed when the donor and acceptor are close enough and allow their respective electronic wave functions to overlap. The rate of electron transfer is governed by the Marcus theory of electron transfer.<sup>48,49</sup>

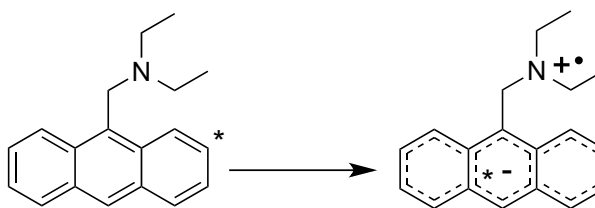


**Figure 1.8.** An example of PET in derivatized anthracene

#### 1.4.2.1. Intramolecular Charge Transfer

Intramolecular charge transfer (ICT) processes have wide application in studying micropolarity and microviscosity of a medium. A group of fluorophores may undergo a twist after ICT leading to loss in planarity of the molecule thereby restricting the back electron transfer. Such charge separated states are stabilized in polar environments and the viscosity of the environment can affect twisting. In a twisted intramolecular charge transfer (TICT) state formed by intramolecular charge transfer in an electron donor (D)/acceptor (A) molecule, the D and A subgroups have a mutually perpendicular configuration that leads to electronic decoupling of D and A. The twisted ICT (TICT) band is usually more Stokes' shifted as compared to the

ICT band. The relative intensity of the ICT and TICT band can thus give an idea about the microenvironment. A classical example of a molecule that undergoes TICT is *N,N*-dimethylaminobenzonitrile (DMABN), the photophysics of which exhibits concomitant viscosity dependence as well as polarity dependence.<sup>9,50</sup>

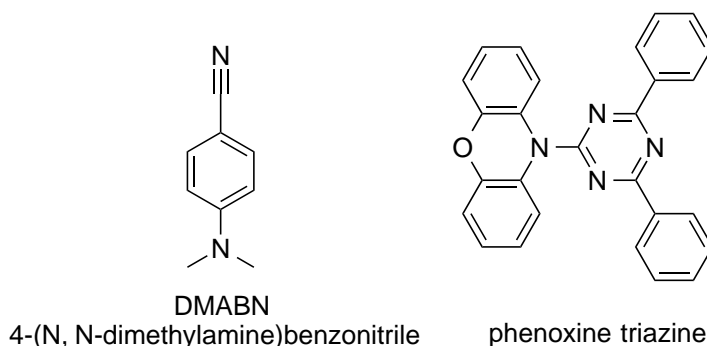


**Figure 1.9.** Examples of molecules that show ICT

### 1.4.3. Excited State Proton Transfer

The basic principle of excited state proton transfer is best understood with the help of an example. The ground state acidity of aromatic compounds, like phenols, is common knowledge and is easily explained by the stabilization of the deprotonated form by delocalization of its negative charge over the ring. From the point of view of molecular orbital theory for phenol, for example, the stabilization is associated with accommodation of the electron cloud from the oxygen atoms in the antibonding  $\pi^*$  orbitals of the phenyl ring. With this background, one may consider the situation in the presence of light that causes a  $\pi$ - $\pi^*$  transition, thereby creating a vacancy in the lower energy bonding  $\pi$  orbital for the incoming electron cloud from oxygen. Since this is a favourable situation as far as energy requirements are concerned, phenols are generally stronger acids in the excited state than in the ground state, as is manifested elegantly in an excited state  $pK_a$  ( $pK_a^*$ ) of about 2.0 for 2-naphthol, vis-à-vis the ground state  $pK_a$  of 9.2.<sup>6</sup> By similar arguments, it can be established that aromatic bases are stronger bases in their



electronically excited states. Such compounds are called photoacids and photobases respectively and find applications in proton burst experiments where a sudden change in pH is required.<sup>51,52</sup> On a different note, if photoacidic and photobasic functional groups are held in close proximity, either covalently or noncovalently, a proton transfer, that does not occur in the ground state, can take place upon electronic excitation. Such a process is termed excited state proton transfer (ESPT). The first observation of ESPT was by Weber in 1931 and was monitored using absorption and fluorescence spectroscopy.<sup>53</sup> In 1949 Förster explained the phenomenon in 1,4-naphthylamine sulphonate in the light of ESPT to develop what is known as the Förster's cycle.<sup>54</sup> This scheme has been used extensively to determine the excited state  $pK_a$  of acids.<sup>55</sup> Molecules like phenols, that have significantly less  $pK_a^*$  compared to  $pK_a$ , are called photoacids. Molecules like 7-azaindole, bipyridinediols, 7-hydroxyquinoline exhibit excited state double proton transfer (ESDPT). Electronic and structural rearrangement resulting in alteration of dipole moment of the molecule in the excited state has been observed in ESPT which was discovered by Weller *et al.* and has been manifested in various systems like in development of optoelectronic materials.<sup>56,57</sup>

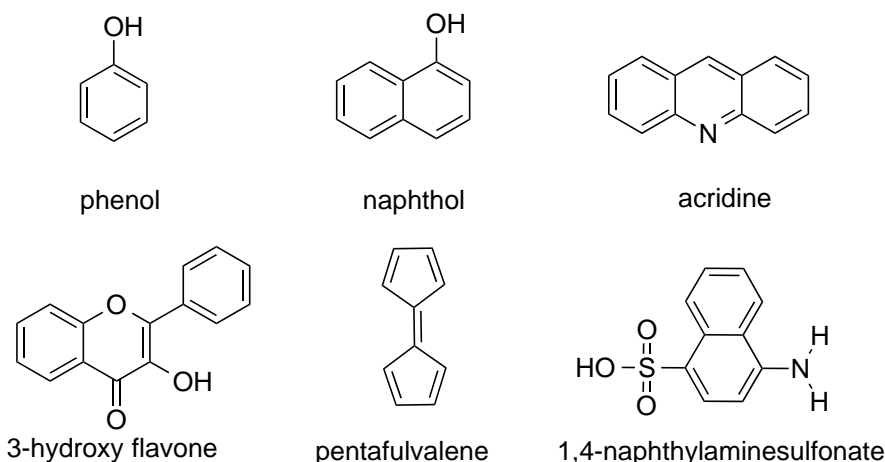


**Figure 1.10.** Examples of molecules that show excited state proton transfer

#### ***1.4.3.1. Excited State Intramolecular Proton Transfer***

When the proton donor and the acceptor moieties are in the same molecule, photoexcitation can lead to ESIPT (i.e. intramolecular ESPT). The earliest observation for ESIPT was reported in 1968 in the form of an unusually large Stokes' shifted emission in methylsalicylate.<sup>58</sup> 3-Hydroxyflavone is another probe that has been studied explicitly for ESIPT.<sup>59,60</sup> Four different kinds of possible mechanism for ESPT were proposed by Kasha.<sup>61</sup> They are: transfer of a proton within the molecule (intrinsic intramolecular transfer as found in 2-(2'-hydroxyphenyl)benzothiazole and 3-hydroxyflavone; proton transfer by a mediator (concerted biprotonic transfer) as in 7-azaindole, benzanilide dimers; static and dynamic catalysis of proton transfer (e.g. lumichrome and adenine) and proton relay transfer (e.g. 7-hydroxyquinoline, 3-hydroxyxanthone). Out of these, only the first meets the condition for ESIPT. Usually ESIPT is ultrafast and often emission from the proton transferred state only is observed.<sup>62</sup> The appearance, or absence, of the spectroscopic features of the photoisomers involved in proton transfer processes would depend on the rate at which the proton transfer process occurs. The rate, in turn depends on the potential energy surface of the ground and excited states. The potential energy surface can be either symmetric or asymmetric. An asymmetric surface can have the same asymmetry in the ground as well as the excited state or it can be reversed.<sup>63</sup> Depending on the energy barriers between the two minima, corresponding to energy of the photo-tautomers in the excited state, the rate of proton transfer can be studied. Very few examples exist where a single minimum exists for both ground and excited state.<sup>64</sup> In systems where a single minimum exists the ESIPT would be ultrafast and is observed usually in timescales of a few femtoseconds. In these cases it is likely that the newly formed tautomer is observed only in the emission spectrum as the proton back transfers in the ground state is facile. Electronic spectroscopy has proven to be a very simple and easy tool to study the dynamics of

such processes.

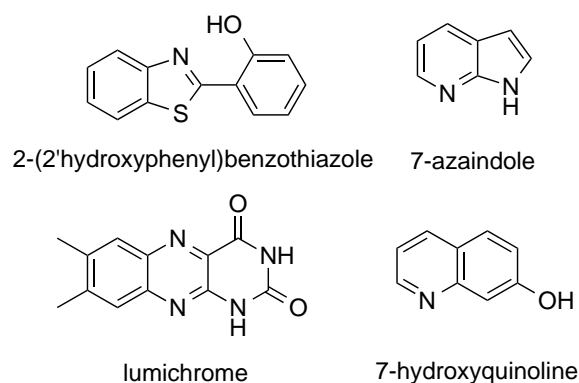


**Figure 1.11.** Examples of molecules that show excited state intramolecular proton transfer (ESIPT)

#### ***1.4.3.2. Excited State Intermolecular Proton Transfer***

The fluorophore, when it is excited, needs a mediator to lose or allow the proton abstraction in intermolecular proton transfers. Molecules where intermolecular proton transfer is frequently observed are pyridyl benzimidazole, cyanine, D-luciferin, 7-azaindole, pyranine etc. In the GFP family, photoisomerization-induced deactivation is suppressed and efficient intermolecular ESPT is observed. The investigation of photophysical properties of these types of molecules is used to develop pH sensitive sensors as well as calcium sensors (e.g. Fura-red).<sup>65,66</sup>

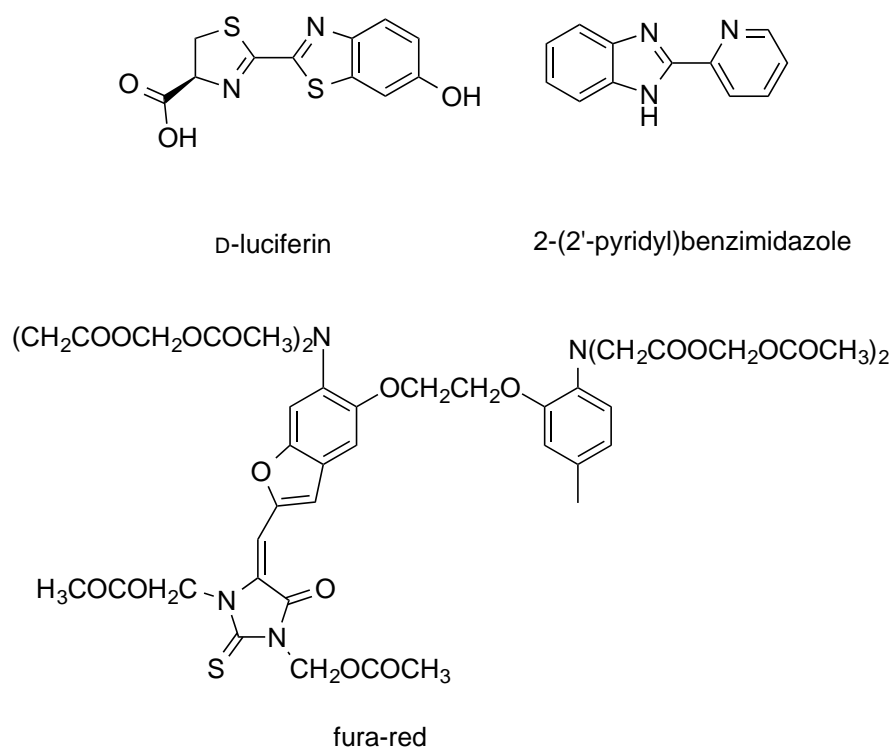


**Figure 1.12.** Examples of molecules that show excited state intermolecular proton transfer

The efficiency of ESPT can be shown by the simple example of the acid-base interaction of diaryloxazoles (DAO) in the ground and excited states in protic and aprotic solvents. The DAO are the weak bases in the ground state and the nitrogen can be protonated by strong acids such as formic acid, trifluoroacetic acid, etc. but cannot be protonated by weak acids such as acetic acid. While upon excitation the basicity of these molecules increases considerably in the excited state resulting in intermolecular proton transfer in presence of weak acids.<sup>67</sup>

## 1.5. Restricted Environment Affecting Excited State Processes

A restricted environment refers a supramolecular assembly, which form inclusion complexes with molecules by noncovalent interactions. Properties such as polarity and viscosity of the restricted environment are different from the bulk solvent. Due to different conditions inside the supramolecular host the vibrational and rotational motion of the molecule is altered and this can be observed in the excited state through fluorescence. Surfactants/membranes are

suited to mimicking biological environments because they form similar structures (vesicles). They also help us understand the fundamental properties of matter and the onset of new optical phenomena related to size that can lead the development of new materials. Examples of artificial restricted environments that mimic biological systems are micelles and cyclodextrins.

### **1.5.1. Micelles**

Aggregated surfactant molecules form micelles in aqueous solution that have a compressive core surrounded by a less compressive surface structure (Figure 1.13). The hydrophilic head group is in contact with the surrounding solvent and the hydrophobic tail is in the centre of the micelle. Each detergent has a characteristic critical micelle concentration (CMC) above which micelles form spontaneously. Temperature, nature of the surfactant, pH and ionic strength affect the CMC and size of the micelles. The shape of the micelle is usually globular but ellipsoid, cylinders and bilayers are common as determined by NMR, ESR and neutron scattering techniques. These micelles are in equilibrium with the surfactant monomer on a 1-10 ms timescale. The pH of the micellar-water interface is different from the bulk water depending on the surfactant and affects the proton transfer dynamics of the molecule. Micelles can be cationic, anionic or neutral (Figure 1.13). The local pH at the interface (Stern layer) of the anionic micelles in sodium dodecyl sulphate (SDS) is 4.8, resulting in the protonation of associated molecules with a  $pK_a > 5$ . Similarly, the pH of the interface of cetyltrimethylammonium bromide (CTAB) micelles is  $\sim 9.5$ , resulting in the deprotonation of acids with a  $pK_a < 9$ . The neutral surfactant, TX-100 also forms micelles but the thickness of the Stern layer is 25-30 Å and is called the “palisade layer”, which is difficult for small molecules to penetrate, so the properties of the incorporated molecule does not change appreciably. Van der Waals’ forces are mainly responsible for the interaction between the molecules and the micelles.

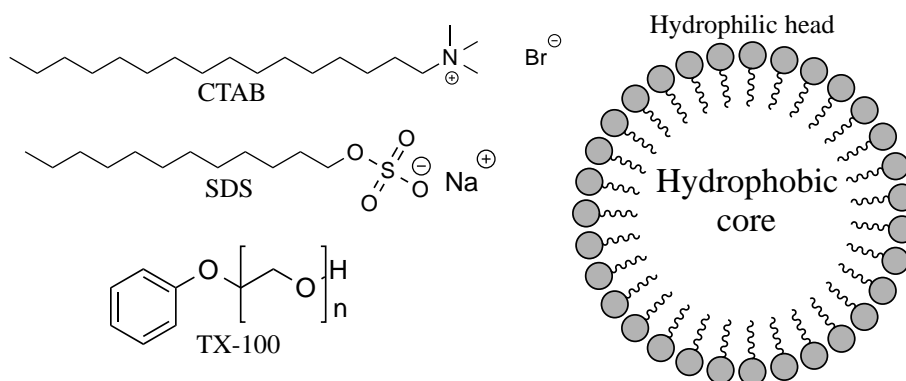


**Figure 1.13.** Molecular structures of CTAB, SDS and TX-100 and schematic representation of spherical micelles

### 1.5.2. Excited State Proton Transfer in Microheterogeneous Media

ESPT is affected significantly in microenvironments. Thus studying ESPT in different microheterogeneous media can pave the way for manipulation of the process and can have potential application in the development of lasers, optoelectronic devices etc.<sup>68-72</sup> Micelles are known to affect the ESPT; e.g. in 2- (2'-hydroxyphenyl)benzimidazole the ESPT is disrupted in micelles due to encapsulation of fluorophore preventing formation of the structures that are formed in aqueous solutions.<sup>73-75</sup> It is observed that acid-base equilibria of derivatives of flavylum salts, which are good photoacids, are affected significantly.<sup>76,77</sup> Another example is of pyranine where the ESPT is found to be drastically hindered in presence of positively charged surfactants.<sup>78</sup> ESPT has been studied in biological systems as well. The alteration of ESPT process in 4-hydroxy-5-azanaphthene has been used in measuring relative polarities of binding sites of human serum albumin (HSA) and apomyoglobin.<sup>78</sup>

### 1.5.3. Alteration of Non-radiative Processes in Microheterogeneous Media

Microheterogeneous media allow the molecular rotation to cease and thereby allowing the relaxation process of the molecule to be slower by the virtue of hydrophobic interaction. This allows the radiative rate of the molecule to predominate over the non-radiative rate and molecule tends to spend longer time in the excited state thus increasing the lifetime of the molecule which in turn results in higher fluorescence quantum yield. This finds widespread application to make a non-fluorescing or low fluorescing molecule to be highly fluorescent at room temperature and to utilize them in biotechnology, imaging and various other fields. This can also explain the fundamentals processes in the excited state of the molecule and allows synthetic modification to generate a better fluorophore. For example, epicocconone in micelles and cyclodextrins can be taken into consideration where epicocconone fluoresces strongly compared with its weak emission in aqueous medium. The reason for the non-fluorescing behaviour of epicocconone is attributed to photoisomerization, which is restricted inside the hydrophobic cores of micelles and cyclodextrins. Understanding this idea helps synthetic modification of epicocconone to stop photoisomerization and prepare highly fluorescent fluorophores that find application in protein staining, gel electrophoresis and as dual-stains.

### 1.6. Motivation of The Thesis

The aim of the present thesis is twofold. Despite the highly fluorescent ( $\phi_f = 0.8$ ) nature of green fluorescent protein, the isolated or synthesized chromophore (*p*-HBDI) is virtually non-fluorescent ( $\phi_f < 10^{-4}$ ) at room temperature. This enigmatic behaviour has been rationalized by facile photoisomerization, leading to fast internal conversion (IC), which is restricted inside the protein cavity. We have synthesized a series of GFP analogues and analysed them by spectroscopic studies to understand the origin of non-fluorescence of *p*-HBDI as well as to

provide a new direction of preparing fluorescent GFP chromophores.

Secondly, we have studied the natural product epicocconone, and several analogues, to elucidate its non-radiative decay mechanisms to help engineer better derivatives that could be more useful in biotechnology through higher quantum yields and better photostability.

## References

- (1) Chatterjee, S.; Burai, T. N.; Karuso, P.; Datta, A. *J. Phys. Chem. A* **2011**, *115*, 10154.
- (2) Chatterjee, S.; Karuso, P.; Boulange, A.; Peixoto, P. A.; Franck, X.; Datta, A. *J. Phys. Chem. B* **2013**, *117*, 14951.
- (3) Chatterjee, S.; Karuso, P.; Boulange, A.; Franck, X.; Datta, A., (Submitted to *J. Phys. Chem. B*).
- (4) Chatterjee, S.; Datta, A.; Karuso, P., (Manuscript under preparation) will be submitted to *Org. Lett.*
- (5) Chatterjee, S.; Datta, A.; Karuso, P., (Manuscript under preparation) will be submitted to *J. Am. Chem. Soc.*
- (6) Lakowicz, J. R. *Principles of Fluorescence Spectroscopy*; 3rd ed.; Springer, USA, 2006.
- (7) Dill, K.; Bromberg, S. *Molecular Driving Forces: Statistical Thermodynamics in Biology, Chemistry, Physics, and Nanoscience*, 2011.
- (8) Bolger, R.; Checovich, W. *BioTechniques* **1994**, *17*, 585.
- (9) Bhattacharyya, K.; Chowdhury, M. *Chem. Rev.* **1993**, *93*, 507.
- (10) Leinhos, U.; Kuhnle, W.; Zachariasse, K. A. *J. Phys. Chem.* **1991**, *95*, 2013.
- (11) Sengupta, P. K.; Kasha, M. *Chem. Phys. Lett.* **1979**, *68*, 382.
- (12) Albani, J. R. *J. Fluoresc.* **2009**, *19*, 399.
- (13) Lakowicz, J. R.; Balter, A. *Biophys. Chem.* **1982**, *16*, 99.



- (14) Petrich, J. W. *Int. Rev. Phys. Chem.* **2000**, *19*, 479.
- (15) Sullivan, K. F.; Kay, S. A. *Green Fluorescent Proteins*, 1999.
- (16) Zimmer, M. *Chem. Rev.* **2002**, *102*, 759.
- (17) Chudakov, D. M.; Matz, M. V.; Lukyanov, S.; Lukyanov, K. A. *Physiol. Rev.* **2010**, *90*, 1103.
- (18) Paige, J. S.; Wu, K. Y.; Jaffrey, S. R. *Science* **2011**, *333*, 642.
- (19) Addison, K.; Heisler, I. A.; Conyard, J.; Dixon, T.; Bulman Page, P. C.; Meech, S. R. *Faraday Discuss.* **2013**, *163*, 277.
- (20) Prasher, D. C. *Trends Genet.* **1995**, *11*, 320.
- (21) Haseloff, J.; Siemering, K. R.; Prasher, D. C.; Hodge, S. *Proc. Natl. Acad. Sci. U.S.A.* **1997**, *94*, 2122.
- (22) Karuso, P. *Chem. Aust.* **2009**, *76*, 24.
- (23) Karuso, P. *Chem. Aust.* **2009**, *76*, 26.
- (24) Heim, R.; Prasher, D. C.; Tsien, R. Y. *Proc. Natl. Acad. Sci. U.S.A.* **1994**, *91*, 12501.
- (25) Reid, B. G.; Flynn, G. C. *Biochemistry* **1997**, *36*, 6786.
- (26) Cubitt, A. B.; Heim, R.; Adams, S. R.; Boyd, A. E.; Gross, L. A.; Tsien, R. Y. *Trends. Biochem. Sci* **1995**, *20*, 448.
- (27) Tsien, R. Y. *Annu. Rev. Biochem.* **1998**, *67*, 509.
- (28) Bell, P. J. L.; Karuso, P. *J. Am. Chem. Soc.* **2003**, *125*, 9304.
- (29) Coghlan, D. R.; Mackintosh, J. A.; Karuso, P. *Org. Lett.* **2005**, *7*, 2401.
- (30) Tachibana, H.; Azumi, R.; Nakamura, T.; Matsumoto, M.; Kawabata, Y. *Chem. Lett.* **1992**, 173.
- (31) Zechmesteir, L. *Cis-Trans Isomers, carotenoids, Vitamin A and Arypolyenes*; Academic Press, New York, 1992.

- (32) Polalrd, M. M.; Lubomska, M.; Rudolf, P.; Feringa, B. L. *Angew. Chem. Int. Ed.* **2007**, *46*, 1278.
- (33) Birge, R. R. *Biochim. Biophys. Acta.* **1990**, *1016*, 293.
- (34) Birge, R. R.; Findsen, L. A.; Fox, G. C.; Hyde, E. W.; Tallent, J. R. *J. Am. Chem. Soc.* **1992**, *114*, 1581.
- (35) Bismuth, O.; Friedman, N.; Sheves, M.; Ruhman, S. *J. Phys. Chem. B* **2007**, *11*, 2327.
- (36) Wand, A.; Rozin, R.; Eliash, T.; Jung, K.-H.; Sheves, M.; Ruhman, S. *J. Am. Chem. Soc.* **2011**, *133*, 20922.
- (37) Lanyi, J. K.; Schobert, B. *J. Mol. Biol.* **2003**, *328*, 439.
- (38) Dér, A.; Valkai, S.; Fábián, L.; Ormos, P.; Ramsden, J. J.; Wolff, E. K. *Photochem. Photobiol.* **2007**, *83*, 393.
- (39) Saltiel, J. J. *J. Am. Chem. Soc.* **1968**, *90*, 6394.
- (40) Liu, R. S. H.; Asato, A. E. *Proc. Natl. Acad. Sci. USA* **1985**, *82*, 259.
- (41) Liu, R. S. H.; Mead, D. A.; Asato, E. *J. Am. Chem. Soc.* **1985**, *107*, 6609.
- (42) Rau, H.; Iuddecke, E. *J. Am. Chem. Soc.* **1982**, *104*, 1616.
- (43) Fujino, T.; Tahara, T. *J. Phys. Chem. A.* **2000**, *104*, 4203.
- (44) Diau, E. W. G. *J. Phys. Chem. A.* **2004**, *108*, 950.
- (45) Takeuchi, S.; Ruhman, S.; Tsuneda, T.; Chiba, M.; Taketsugu, T.; Tahara, T. *Science* **2008**, *322*, 1073.
- (46) Wieslewski, M. R. *Chem. Rev.* **1992**, *92*, 435.
- (47) Burai, T. N.; Panda, D.; Iyer, E. S. S.; Datta, A. *J. Lumin.* **2012**, *132*, 2929.
- (48) Marcus, A. R. *Rev. Mod. Phys.* **1993**, *65*, 599.
- (49) Marcus, A. R. *Adv. Chem. Phys.* **1999**, *106*, 1.
- (50) Kohler, G.; Wolschann, P.; Rotkiewicz, K. *Proc. Natl. Acad. Sci. (Chem. Sci.)* **1992**, *104*,

197.

- (51) Tolbert, L. M.; Solntsev, K. M. *Acc. Chem. Res.* **2002**, *35*, 19.
- (52) Mohammed, O. F.; Pines, D.; Dreyer, J.; Pines, E.; Nibbering, E. T. J. *Science* **2005**, *310*, 83.
- (53) Weber, K. *J. Phys. Chem.* **1931**, *15*, 18.
- (54) Förster, T. *Naturwiss* **1949**, *36*, 186.
- (55) Boyer, R.; Deckey, G.; Marzzacco, C.; Mulvaney, M.; Halpern, A. M. *J. Chem. Edu.* **1985**, *62*, 630.
- (56) Kwon, J. E.; Part, S. Y. *Adv. Mater.* **2011**, *23*, 3615.
- (57) Tang, K.-C.; Chang, M.-J.; Lin, T.-Y.; Pan, H.-A.; Fang, T.-C.; Chen, K.-Y.; Hung, W.-Y.; Hsu, Y.-H.; Chou, P.-T. *J. Am. Chem. Soc.* **2011**, *133*, 17738.
- (58) Donckt, E. V.; Porter, G. *J. Chem Soc. Faraday Trans.* **1968**, *64*, 3215.
- (59) McMarrow, D.; Kasha, M. *J. Phys. Chem.* **1984**, 88.
- (60) Schwartz, B. J.; Peteaunu, L. A.; Harris, C. B. *J. Phys. Chem.* **1992**, *96*, 3591.
- (61) Kasha, M. *J. Chem. Soc. Faraday Trans. II* **1986**, *82*, 2379.
- (62) Das, K.; Sarkar, N.; Majumdar, D.; Bhattacharyya, K. *Chem. Phys. Lett.* **1992**, *1988*, 433.
- (63) Rossetti, Z.; Rayford, R.; Haddon, R. C.; Brus, L. E. *J. Am. Chem. Soc.* **1981**, *103*, 4303.
- (64) Formosinho, S. J.; Amaut, L. G. *J. Photochem. Photobiol. A* **1993**, *75*, 21.
- (65) Grynkiewicz, G.; Martin P, P.; Y., T. R. *J. Biol. Chem.* **1985**, *260*, 3440.
- (66) Miesenbock, G.; De Angelis, D. A.; Rothman, J. E. *Nature* **1998**, *394*, 192.
- (67) Druzhinin, S. I.; Rodchenkov, G. M.; Uzhinov, B. M. *J. Chem. Phys.* **1988**, *128*, 383.
- (68) Sarkar, M.; Sengupta, P. K. *Chem. Phys. Lett.* **1991**, *179*, 68.
- (69) Pandey, S.; Dogra, S. K. *Indian. J. Chem.* **1995**, *34*, 407.
- (70) Pandey, S.; Sarpal, R. S.; Dogra, S. K. *J. Colloid Interface Sci.* **1995**, *172*, 407.

- (71) Sarkar, M.; Ray, J. G.; Sengupta, P. K. *J. Photochem. Photobiol. A* **1996**, *95*, 157.
- (72) Sarkar, N.; Datta, A.; Das, S.; Bhattacharyya, K. *J. Photochem. Photobiol. A* **1997**, *109*, 259.
- (73) Rini, M.; Kummrow, A.; Dreyer, J.; Nibbering, E. T. J.; Elsaesser, T. *Faraday Discuss.* **2002**, *122*, 7.
- (74) Nibbering, E. T. J.; Elsaesser, T. *Chem. Rev.* **2004**, *104*, 1887.
- (75) Sahoo, D.; Chakravorti, S. *Photochem. Photobiol. Sci.* **2010**, *9*, 1094.
- (76) Vautier-Giongo, C.; Yihwa, C.; Moreira, P. F. J.; Lima, J. C.; Frietas, A. A.; Alves, M.; Quina, F. H.; Macanita, A. L. *Langmuir* **2002**, *18*, 10109.
- (77) Rodrigues, R.; Vautier-Giongo, C.; Silva, P. F.; Fernandes, A. C.; Cruz, R.; Macanita, A. L.; Quina, F. H. *Langmuir* **2006**, *22*, 933.
- (78) Einen, S. A.-A. A.; Zaitsev, K.; Zaitsev, N. K.; Kuzmin, M. G. *J. Photochem. Photobiol. A* **1988**, *41*, 365.

## **Chapter 2: Review on Epicocconone**



## 2.1. Discovery and Elucidation of Structure of Epicocconone

The fungus *Epicoccum nigrum* has been the source for yellow-red pigments including several carotenoids, flavipin, and phenylalanine derived dimers such as 3,6-dibenzyl-2,5-dioxopiperazine, epicorazine A and the polyketide orevactaene.<sup>79-82</sup> Fortuitous infection of an agar plate used for the routine culturing of yeast by this fungus provided orange stained yeast cells growing near the fungus. Viewed under UV light, the yeast cells fluoresced bright red but their growth and viability were not affected by the staining. To isolate the compound responsible for the observed fluorescence, an assay was developed based on the ability of fractions to stain yeast colonies on an agar plate. The active principle was isolated by chromatography on cellulose followed by size exclusion using Sephadex LH-20 column, where the active component eluted as a deep purple band. The compound was further purified by HPLC to yield dark red crystals of epicocconone (**1**). The molecular formula of this compound was determined by high-resolution Fourier transform ion cyclotron resonance (FTICR) mass spectrometry to be C<sub>23</sub>H<sub>22</sub>O<sub>7</sub> and 2D NMR spectra, viz. TOCSY, HSQC, HMBC, ROESY and NOESY yielded the structure (Figure 2.1).<sup>28</sup>

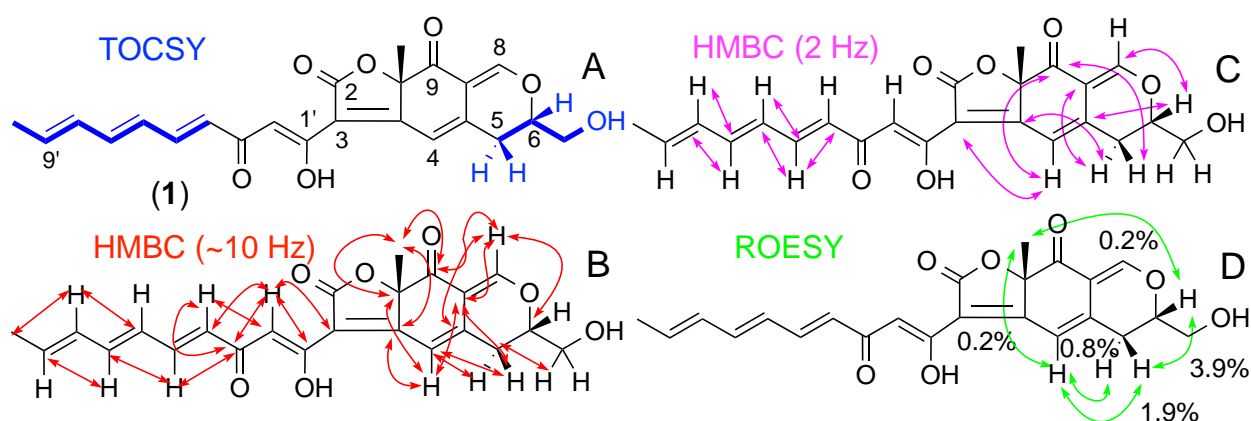
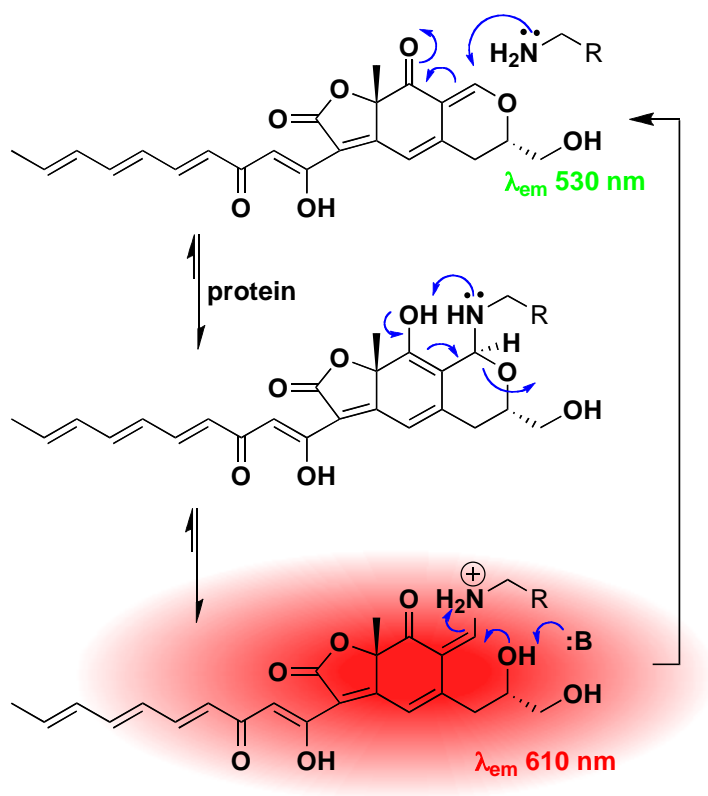


**Figure 2.1.** Molecular structure of epicocconone and key correlations from (A) TOCSY (blue), (B/C) HMBC ( $^3J_{\text{CH}}$  10 Hz red; 2 Hz magenta), and (D) ROESY experiments (green).<sup>28</sup>

## 2.2. Steady State Spectra

In aqueous solution, epicocconone fluoresces feebly ( $\phi_f < 1\%$  in water) in the green (530 nm), while a marked enhancement in its fluorescence, accompanied by a red shift in the emission maximum to 610 nm, is observed in presence of amines and proteins.<sup>28,83</sup> These properties make it a potentially good fluorescent probe for biotechnological applications like cell tracking and two-colour staining, when multiplexed with other fluorescent probes which have similar absorbances but different regions of emission.<sup>84,85</sup> Coghlan *et al.*, using *n*-butylamine, showed that the spectral change could be rationalized as formation of a stable enamine with lysine residues in proteins (Scheme 2.1).<sup>29</sup>



**Scheme 2.1.** Proposed mechanism for the reversible enamine formation of epicocconone with protein<sup>29</sup>



### 2.3. Applications in Molecular and Cellular Biology

Epicocconone forms the basis of commercial products in the ultrasensitive detection of proteins (<100 pg/band) in 2D gel electrophoresis (Deep Purple Total Protein Stain™, GE Healthcare), protein quantification in solution (FluoroProfile™; Sigma-Aldrich), live cell imaging (LavaCell™; Fluorotechnics) as well as in kinetic assays for enzymatic digestion (LavaDigest; Fluorotechnics) and makes it as good a fluorescent stain as other commercially available protein stains like SYPRO Ruby, SYPRO Orange, silver and Coomassie Brilliant Blue G-250.<sup>86-91</sup> All these applications rely on the shift in frequency and increase in quantum yield associated with enamine formation and localization in non-polar environments such as lipids or protein hydrophobic pockets. It is currently one of the most sensitive protein stains for 2D PAGE and overcomes problems like high background, speckling, and disposal of heavy metal waste associated with its major competitor, SYPRO Ruby.<sup>92</sup> In terms of mass spectral compatibility, epicocconone has the best coverage, largest number of positively identified proteins, and lowest number of false positives over other protein stains like SYPRO Ruby, Krypton and Flamingo.<sup>93,94</sup> It provides broader dynamic range than colourimetric methods and fluorescent signals in protein gels can be directly visualized.<sup>95</sup>

### 2.4. Photophysics

Epicocconone emission shows a marked dependence on solvent viscosity and polarity. The green fluorescence is enhanced in micelles.<sup>96</sup> The enhancement of the fluorescence intensity in micelles has been ascribed to a decrease in the rate of the relaxation due to a higher microviscosity. Quantum Mechanical calculations indicate that the HOMO–LUMO transition is of a  $\pi$ - $\pi^*$  type with the excited state being less polar.<sup>96</sup> These results, in addition to the viscosity dependence of the fluorescence quantum yield, lead to the conclusion that photoisomerization,

which is known to be a predominantly viscosity dependent process, is likely to be the major non-radiative process in epicocconone. The influence of microviscosity on the excited state dynamics of epicocconone is also manifested in the study of its incorporation into cyclodextrins, where the greatest fluorescence enhancement is obtained in a 1:2 complex with  $\alpha$ -cyclodextrin ( $\alpha$ -CD), which offers the most rigid microenvironment, compared with the larger  $\beta$ -cyclodextrin ( $\beta$ -CD).<sup>97</sup>

## 2.5. Synthesis of Epicocconone Derivative

Recently Franck and co-workers have synthesized a series of epicocconone analogues in which the heptatriene chain has been replaced by different cyclic groups. In addition to this, the keto-enol moiety has been forcibly changed to a di-keto group in another set of analogues, while only a single keto group has been retained in a third set. Analogues with either keto-enol or diketo group showed higher quantum yield, while analogues with single keto group exhibited even lower quantum yields than that of epicocconone in aqueous solution. All of them reacted with *n*-butylamine similar to epicocconone and showed large Stokes' shift in absorption and emission spectra.<sup>98,99</sup>

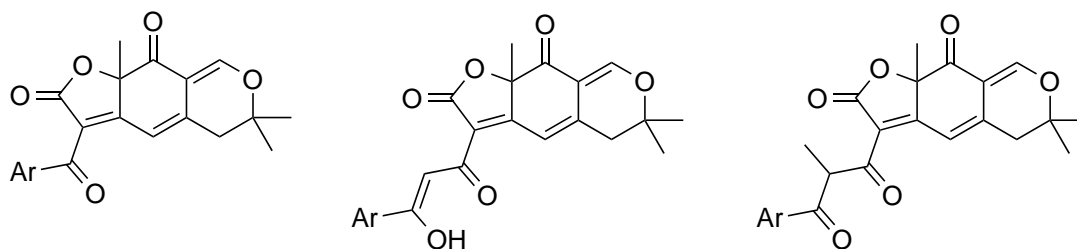


**Figure 2.2.** Molecular structures of epicocconone analogues where the heptatriene tail is replaced by an aromatic ring and the ethanol side chain by a *gem*-dimethyl.

## References

- (79) Baute, R.; Deffieux, G.; Baute, M. A.; Filleau, M. J.; Neveu, A. *Tetrahedron Lett.* **1976**, 3943.
- (80) Burge, W. R.; Buckley, L. J.; Sullivan, J. D., Jr.; McGrattan, C. J.; Ikawa, M. *J. Agric. Food Chem.* **1976**, 24, 555.
- (81) Deffieux, G.; Baute, M. A.; Baute, R.; Filleau, M. J. *J. Antibiot.* **1978**, 31, 1102.
- (82) Shu, Y. Z.; Ye, Q.; Li, H.; Kadow, K. F.; Hussain, R. A.; Huang, S.; Gustavson, D. R.; Lowe, S. E.; Chang, L. P.; Pirnik, D. M.; Kodukula, K. *Bioorg. Med. Chem. Lett.* **1997**, 7, 2295.
- (83) Choi, H. Y.; Veal, D. A.; Karuso, P. *J. Fluoresc.* **2006**, 16, 475.
- (84) Zhao, Y.; Zheng, Q.; Dakin, K.; Xu, n.; Li, W. H. *J. Am. Chem. Soc.* **2004**, 126, 4653.
- (85) Wang, L.; Cole, K. D.; Gaigalas, A. K.; Zhang, Y. Z. *Bioconjugate Chem.* **2005**, 16, 194.
- (86) Haugland, R. P. *Handbook of Fluorescent Probes and Research Products*; 9th ed.; Molecular Probes: Eugene, OR, 2002.
- (87) Mackintosh, J. A.; Choi, H. Y.; Bae, S. H.; Veal, D. A.; Bell, P. J.; Ferrari, B. C.; Van Dyk, D. D.; Verrills, N. M.; Paik, Y. K.; Karuso, P. *Proteomics* **2003**, 3, 2273.
- (88) Mackintosh, J. A.; Veal, D. A.; Karuso, P. *Proteomics* **2005**, 5, 4673.
- (89) Tannu, N. S.; Sanchez-Brambila, G.; Kirby, P.; Andacht, T. M. *Electrophoresis* **2006**, 27, 3136.
- (90) Cleemann, F.; Karuso, P. *Anal. Chem.* **2008**, 80, 4170.
- (91) Schabacker, D. S.; Stefanovska, I.; Gavin, I.; Pedrak, C.; Chandler, D. P. *Anal. Biochem.* **2006**, 359, 84.
- (92) Svensson, E.; Hedberg, J. J.; Malmport, E.; Bjellqvist, B. *Anal. Biochem.* **2006**, 355, 304.
- (93) Ball, M. S.; Karuso, P. *J. Proteome Res.* **2007**, 6, 4313.

- (94) Chevalier, F. *Materials* **2010**, *3*, 4784.
- (95) Wu, S.-Y.; Chin, L.-T.; Chen, L.-M.; Chen, H.-M. *Proteomics* **2008**, *8*, 3382.
- (96) Panda, D.; Datta, A. *Chem. Phys. Lett.* **2006**, *426*, 100.
- (97) Burai, T. N.; Panda, D.; Datta, A. *Chem. Phys. Lett.* **2008**, *455*, 42.
- (98) Boulangé, A.; Peixoto, P. A.; Franck, X. *Chem. Eur. J.* **2011**, *17*, 10241.
- (99) Peixoto, P. A.; Boulangé, A.; Ball, M.; Naudin, B.; Alle, T.; Cosette, P.; Karuso, P.; Franck, X. *J. Am. Chem. Soc.* **2014**, *136*, 15248.

## Introduction to Associated Publications

In the associated publications, we will try to unravel the nonradiative pathways responsible for the non-fluorescent nature of epicocconone. By comparing analogues with an enolizable and unenolizable  $\beta$ -diketone, we will try to establish that photoisomerization of the heptatriene side chain and not the tautomerism of the  $\beta$ -diketone, is the major nonradiative process in epicocconone. Thus analogues where the triene is replaced by the isosteric phenyl or anisyl residue possess significantly higher quantum yields. These analogues show similar reversible enamine formation with butylamine. However, unlike epicocconone, they do not show the characteristic increase in quantum yield upon reaction with amines suggesting that the heptatriene photoisomerization is not a significant relaxation pathway for the enamine of epicocconone or that subtle electronic effects of the aryl side chains stabilizes the  $\beta$ -diketone. It is also shown that intramolecular H-bonding of the enolized  $\beta$ -diketone help stabilise the excited state of the butylamine adducts. Furthermore, we focus on the excited state dynamics of two newly synthesized epicocconone analogues where the heptatriene chain is replaced with a naphthyl and an *o*-chloropyridyl group respectively. These compounds also react with amines to form enamines in a similar fashion to epicocconone but show higher quantum yield in their native form.

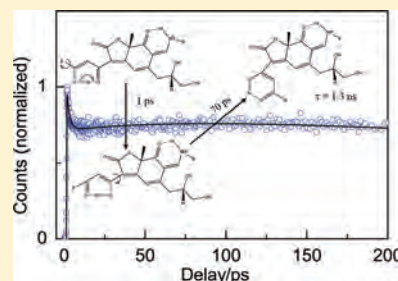


# Ultrafast Dynamics of Epicocconone, a Second Generation Fluorescent Protein Stain

Soumit Chatterjee,<sup>†</sup> Tarak Nath Burai,<sup>‡</sup> Peter Karuso,<sup>\*,†</sup> and Anindya Datta<sup>\*,‡</sup><sup>†</sup>Department of Chemistry and Biomolecular Sciences, Macquarie University, Sydney NSW 2109, Australia<sup>‡</sup>Department of Chemistry, Indian Institute of Technology Bombay, Powai, Mumbai 400076, India

S Supporting Information

**ABSTRACT:** Femtosecond upconversion experiment has been carried out for epicocconone and its butylamine adduct in acetonitrile and *tert*-butanol. An ultrafast component is found to dominate the decay of fluorescence of epicocconone in acetonitrile solution. Upon reacting with butylamine, a model for the epicocconone–protein adduct, this ultrafast component remains almost unaffected but an additional rise time occurs, indicating the formation of a highly emissive species from the locally excited state. This phenomenon is central to the extraordinary applications of epicocconone in biotechnology. The magnitude of the rise time of the butylamine adduct is similar to that of the longer component of the decay of epicocconone in acetonitrile, suggesting that the dynamics of epicocconone and its butylamine adduct are similar. The ultrafast component is slowed upon increasing the viscosity of the solvent. This results in a marked increase in quantum yield and suggests that it corresponds to rapid bond isomerization, leading to a nonradiative decay. Surprisingly, in water/sucrose mixtures, the ultrafast component remains unaffected but there is still an increase in quantum yield, suggesting that there are at least two nonradiative pathways, one involving bond isomerization and another involving proton transfer. The correct interpretation of these data will allow the design of second generation protein stains based on the epicocconone scaffold with increased quantum yields and photostability.



## INTRODUCTION

Epicocconone (Figure 1) is a cell-permeable natural product with a weak fluorescence centered at 530 nm in aqueous solutions.<sup>1,2</sup> A marked enhancement in its fluorescence, accompanied by a red shift in the emission maximum to 610 nm, is observed in the presence of amines. These spectral changes have been ascribed to the formation of a stable enamine with lysine residues in proteins (Figure S1 of Supporting Information),<sup>3</sup> which forms the basis of the commercial application of this fluorophore in the ultrasensitive detection of proteins in two-dimensional (2D) gel electrophoresis (deep purple total protein stain; GE Healthcare),<sup>4</sup> protein quantification in solution (FluoroProfile; Sigma-Aldrich),<sup>5</sup> and live cell imaging (LavaCell; Fluorotechnics) as well as in kinetic assays for enzymatic digestion.<sup>6</sup> All of these applications rely on the shift in frequency and increase in quantum yield associated with enamine formation and localization in nonpolar environments such as lipids or protein hydrophobic pockets. Fluorescence enhancement also occurs for the native fluorophore when going from polar to nonpolar solvents. A marked increase in fluorescence intensity is also observed with increasing viscosity, as is observed between acetonitrile and *tert*-butanol.<sup>2</sup> Quantum chemical calculations indicate that the HOMO–LUMO transition is of a  $\pi$ – $\pi^*$  type with the excited state being less polar.<sup>2</sup> These results, in addition to the viscosity dependence of the fluorescence quantum yield, lead to the conclusion that photoisomerization, which is known

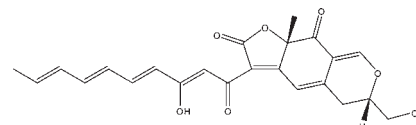


Figure 1. Molecular structure of epicocconone.

to be a predominantly viscosity-dependent process, is likely to be a major nonradiative process in epicocconone.<sup>7–9</sup> The influence of microviscosity on the excited-state dynamics of epicocconone is also manifested in the study of its incorporation into cyclodextrins, where the greatest fluorescence enhancement is obtained in a 1:2 complex with  $\alpha$ -cyclodextrin ( $\alpha$ -CD), which offers the most rigid microenvironment, compared with the larger  $\beta$ -cyclodextrin ( $\beta$ -CD).<sup>10</sup>

The time-resolved data in the picosecond–nanosecond time domain follow the same trend as the steady-state fluorescence data in restricted microenvironments. However, the steady-state and time-resolved data are different in neat solutions. For example, the fluorescence quantum yield in *tert*-butanol is markedly more than in acetonitrile, but the fluorescence decay seems to be faster in *tert*-butanol.<sup>2</sup> This anomaly suggests the

Received: June 15, 2011

Revised: August 8, 2011

Published: August 09, 2011

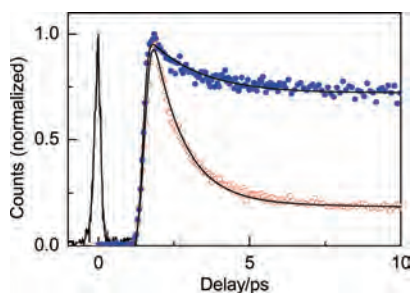


**Figure 2.** Femtosecond fluorescence transients of epicocconone in  $\text{CH}_3\text{CN}$  (red open circles) and  $\text{CH}_3\text{CN}$  + butylamine (blue solid circles).  $\lambda_{\text{ex}} = 430$  nm and  $\lambda_{\text{em}} = 530$  nm for  $\text{CH}_3\text{CN}$ , and  $\lambda_{\text{em}} = 610$  nm for  $\text{CH}_3\text{CN}$  + butylamine. The solid black lines denote the lines of best fit. The fitting parameters are provided in Table 1. The cross-correlation function of the laser pulse is shifted to the left, for the sake of clarity.

possibility of ultrafast decay pathways that dominate the quantum yields. This is the motivation for the present femtosecond fluorescence upconversion experiments on epicocconone in *tert*-butanol and acetonitrile, and in its butylamine adduct, in an attempt to unravel the ultrafast component and make the first step toward the design of second-generation protein stains with increased quantum yields and stability.

## MATERIALS AND METHODS

Epicocconone was isolated from the fungus *Epicoccum nigrum* (*E. nigrum*) as previously described.<sup>1</sup> A solution of epicocconone in dimethyl sulfoxide (DMSO; 1 mg/mL) has been used as the stock solution for each experiment. Spectroscopy grade acetonitrile from Spectrochem, Mumbai, India, has been distilled over  $\text{CaH}_2$  and the distillate has been passed over activated neutral alumina prior to the experiment. Butylamine from Qualigens, Mumbai, India, and spectroscopy grade *tert*-butanol from Spectrochem have been used as received. The absorption and fluorescence spectra have been recorded on a JASCO V 530 spectrophotometer and Varian Cary Eclipse spectrofluorimeter, respectively. The absorbance of the neat solution of epicocconone is kept below 0.1 to prevent inner filter effect for steady-state measurements and for picosecond–nanosecond time-resolved experiments. The absorbance of the neat solution of epicocconone is kept at  $\sim 1.0$  for the upconversion experiment. The absorption and emission spectra have been recorded before and after recording the femtosecond fluorescence decays, in order to verify that the samples do not get photobleached. Fluorescence quantum yields ( $\phi_f$ ) are calculated after proper correction for changes in absorbance using Lucifer yellow CH ( $\phi_f = 0.21$ ) as the reference.<sup>2</sup> Time-resolved fluorescence data were obtained using a picosecond pulsed diode laser based time-correlated single-photon counting (TCSPC) instrument from IBH (Glasgow, United Kingdom) set at the magic angle with  $\lambda_{\text{ex}} = 406$  nm. The full width at half-maximum (fwhm) of the instrumental response at this wavelength was found to be 250 ps with a resolution of 7 ps/channel. The decay traces, thus obtained, are fitted to multiexponential decays using IBH DAS 6.2 data analysis software. In some of the experiments, the emissions have been collected at the magic angle polarization using a Hamamatsu MCP photomultiplier (Model C10373). In these cases, the signal is amplified by a PAM 102-M amplifier before being routed to PicoHarp 300. The typical fwhm of this

**Table 1.** Fluorescence Decay Parameters of Epicocconone in Different Media from Upconversion Experiments

medium	$\tau_1$ (ps)	$a_1$	$\tau_2$ (ps)	$a_2$	$\tau_3$ (ps)	$a_3$
$\text{CH}_3\text{CN}$	1.10	0.80	70	0.15	770	0.05
$\text{CH}_3\text{CN}$ + butylamine	1.70	0.30	75	−0.20	1300	0.90
<i>tert</i> -butanol	3.20	0.20	55	0.40	280	0.40
water	0.05	0.90	2.1	0.07	240	0.02

system response is about 140 ps. The decay traces have been fitted to multiexponential functions using Fluofit software. The output of a femtosecond pulsed oscillator from a mode-locked Ti:sapphire laser (Tsunami, Spectra Physics) pumped by a 5 W Millennia (Spectra Physics) DPSS laser, centered at 860 nm and with a repetition rate of 80 MHz, is used as the gate pulse for the femtosecond fluorescence upconversion experiments. The second harmonic (430 nm) of this pulse has been used as the source of excitation for the sample placed in a rotating cell. The power of the second harmonic light is restricted to 5 mW at the sample, in order to minimize photobleaching. The fluorescence emitted from the sample is upconverted in a nonlinear crystal (0.5 mm BBO,  $\theta = 38^\circ$ ,  $\phi = 90^\circ$ ) by mixing with the gate pulse, which consists of a portion of the fundamental beam. The upconverted light is dispersed in a monochromator and detected using photon counting electronics. A cross-correlation function obtained using the Raman scattering from ethanol has a fwhm = 300 fs. The femtosecond fluorescence decays have been fitted using a Gaussian function of the same fwhm as the excitation pulse. The fluorescence decays have been recorded at the magic angle polarization with respect to the excitation pulse on FOG 100 fluorescence optically gated upconversion spectrometer from CDP Systems Corp., Moscow, Russia. The resolution was in appropriate multiples of the minimum step size of the instrument, i.e., 0.78 fs/step. The decays were analyzed by iterative reconvolution using a homemade program.<sup>11</sup> The lifetime found from the TCSPC has been fixed to the longest component while fitting the fluorescence decay.

## RESULTS AND DISCUSSION

In the femtosecond upconversion studies of epicocconone in acetonitrile, the decay is almost complete within 10 ps (Figure 2) and two ultrafast components have been calculated after fitting the data. In epicocconone, the short (1 ps) component dominated but in the butylamine adduct this component was less important, though still present and of approximately the same lifetime (Table 1). Instead of the longer (70 ps) decay observed with epicocconone, the butylamine adduct showed a rise time (Figures 2 and 3b, Table 1) of similar length (75 ps). This suggests that the 1 ps component, found in both molecules, arises from isomerization of the side chain while the rise time, associated only with the adduct, must be associated with the enamine portion of the molecule.<sup>3</sup> The presence of the rise time is significant. The unchanged ultrafast component as well as the similarity in magnitude and amplitude of the longer component of epicocconone decay in acetonitrile to the rise time of the butylamine adduct (Table 1) indicates that the basic dynamics involved in the excited state of epicocconone and its butylamine adduct are the same. In acetonitrile, the decay is so fast that the lifetime from picosecond–nanosecond experiment, kept fixed while fitting the upconversion data, contributes negligibly. It is likely that epicocconone, after excitation, undergoes excited-state



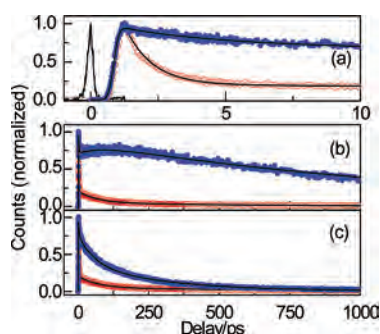
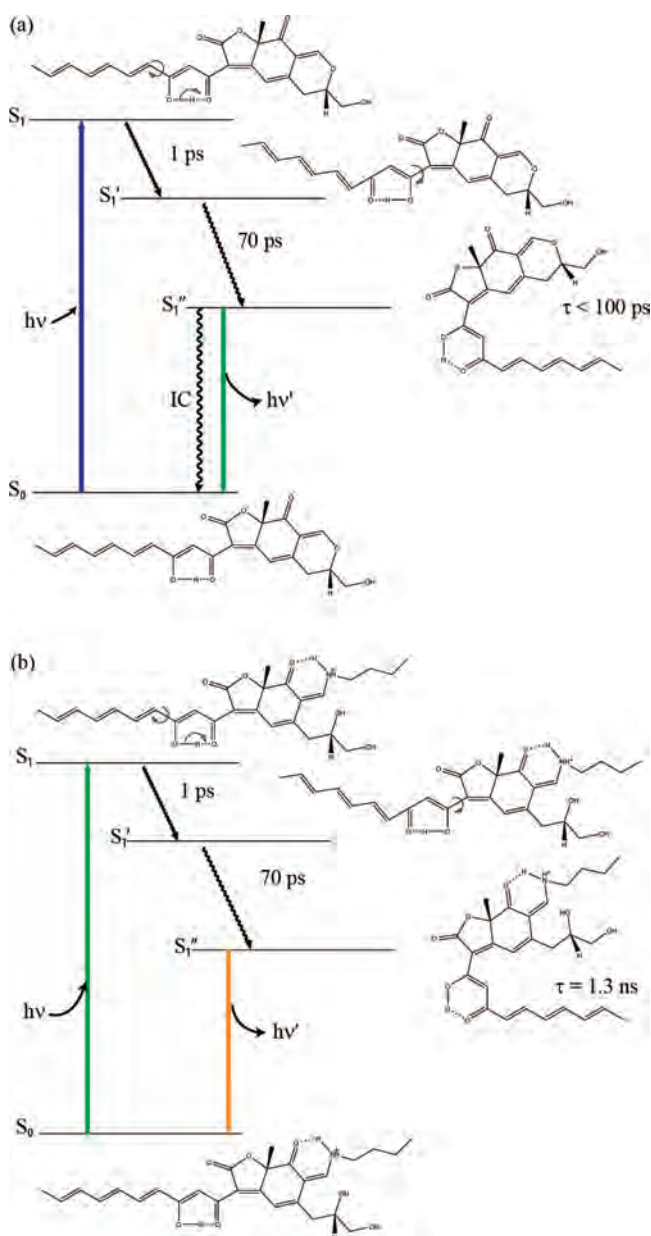


**Figure 3.** Femtosecond fluorescence transients of epicocconone in (a)  $\text{CH}_3\text{CN}$  (red open circles) and *tert*-butanol (blue solid circles), (b)  $\text{CH}_3\text{CN}$  (red open circles) and  $\text{CH}_3\text{CN}$  + butylamine (blue solid circles) in a full scale of 1 ns, and (c)  $\text{CH}_3\text{CN}$  (red open circles) and *tert*-butanol (blue solid circles) in a full scale of 1 ns.  $\lambda_{\text{ex}} = 430$  nm and  $\lambda_{\text{em}} = 530$  nm for  $\text{CH}_3\text{CN}$  and *tert*-butanol, and  $\lambda_{\text{em}} = 610$  nm for  $\text{CH}_3\text{CN}$  + butylamine. The solid black lines denote the lines of best fit. The fitting parameters are provided in Table 1. The cross-correlation function of the laser pulse is shifted, for the sake of clarity.

relaxation processes prior to coming to the ground state. With butylamine, the basic structure of epicocconone is almost unchanged apart from the higher dipole moment in the Schiffs base, which is responsible for the increased Stokes' shift. The red shift in its absorption and emission spectra has been attributed to the formation of an internal charge transfer (ICT).<sup>3</sup> The heterocyclic group, generally responsible for the fluorescence, has a longer lifetime due to enamine formation, and this is actually the emissive species. Prior to relaxation to the emissive species, the same pathway as epicocconone from its locally excited state (Scheme 1a,b) is followed. As evident from the lifetime values, the short component may be due to either rotation of the hydrocarbon chain resulting in structural reorganization or excited-state tautomerisation or both, and the 70 ps component may arise due to flexing of the ring system (Scheme 1). In the butylamine adduct, these processes also take place but before the formation of the emissive species, which has a lifetime of 1.3 ns, eventually resulting in a higher quantum yield (Scheme 1).

However, the decay slows markedly in *tert*-butanol solution (Figure 3a,c, Table 1). This observation brings out the marked dependence of the ultrafast dynamics of epicocconone on viscosity, since acetonitrile and *tert*-butanol have comparable micropolarities,<sup>12</sup> but the latter is 10 times more viscous than the former.<sup>13</sup> The results are now in complete agreement with the steady-state trends, where almost three times higher fluorescence quantum yield is observed in *tert*-butanol solutions of epicocconone (Figure S3 and Table S1 of the Supporting Information). The earlier picosecond–nanosecond studies were not consistent with the steady-state data,<sup>2</sup> because the decay in acetonitrile is complete, to a large extent, within 7 ps. The picosecond–nanosecond experiments performed earlier missed this rather major component and therefrom arose the apparent disagreement between the steady-state and time-resolved data. This apparent anomaly now stands resolved. The viscosity dependence is also an indication of the ultrafast component being associated with a long-range molecular motion such as photo-isomerization. The apparent mismatch in the steady-state and picosecond–nanosecond fluorescence decay of epicocconone in acetonitrile and water is also resolved after the upconversion experiment. Epicocconone has even lower quantum yield in

**Scheme 1.** Probable Excited-State Dynamics of (a) Epicocconone and (b) Butylamine Adduct of Epicocconone



water than acetonitrile but shows slower decay in water (Figure S3 and S4 and Table S2 of the Supporting Information). This anomaly is also resolved and proven to be in accordance with the early time decay of epicocconone in water, which is found to be faster than that in acetonitrile (Figure 4, Table 1).

To investigate further the dependence of excited-state dynamics on the solvent viscosity, successive additions of sucrose to an aqueous solution of epicocconone were undertaken. In the presence of 35% sucrose, the dielectric constant of the solution changes from 80 to 72, but the viscosity increases four times and that is almost equal to the viscosity of *tert*-butanol (Table 2).<sup>14</sup> In steady-state absorption, the absorbance of epicocconone decreased with the addition of sucrose while its quantum yield increased 2-fold at 35% sucrose (Figure 5a,b, Table 3). As observed previously with cyclodextrins,<sup>10</sup> epicocconone can be

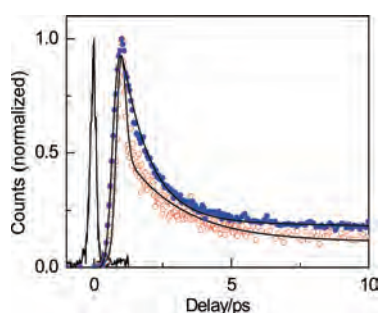


**Figure 4.** Femtosecond fluorescence transients of epicocconone in water (red open circles) and CH<sub>3</sub>CN (blue solid circles).  $\lambda_{\text{ex}} = 430$  nm and  $\lambda_{\text{em}} = 530$  nm for CH<sub>3</sub>CN and water. The solid black lines denote the lines of best fit. The fitting parameters are provided in Table 1. The cross-correlation function of the laser pulse is shifted to the left, for the sake of clarity.

**Table 2.** Effect of Varying Dielectric Constant and Viscosity on Epicocconone Absorption and Emission

% of sucrose by w/v	dielectric constant	viscosity (mPa.s)	epi abs (430 nm)	$\phi_f$
0	80.4	1.00	0.10	0.009
10	78.0	1.35	0.06	0.016
20	75.4	1.95	0.05	0.018
35	71.8	4.31	0.04	0.020

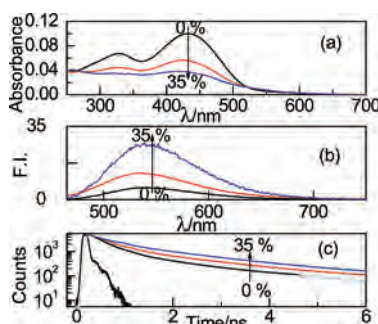


**Figure 5.** (a) Absorption spectra, (b) emission spectra at  $\lambda_{\text{ex}} = 410$  nm, and (c) fluorescence decay traces of epicocconone at  $\lambda_{\text{ex}} = 406$  nm and  $\lambda_{\text{em}} = 530$  nm in water with varying concentration of sucrose from 0 (black), 10 (red), and 35% (w/v) (blue). The fitting parameters are provided in Table 3.

surrounded by sucrose molecules, resulting in a different molar absorptivity. At the same time, a more viscous medium leads to restriction of the conformational relaxation process, thereby reducing nonradiative decay, which in turn results in higher quantum yield. In picosecond–nanosecond fluorescent decays the same trend was observed as the decay slowed upon successive additions of sucrose (Figure 5c, Table 3), but there was no change in upconversion decay profile and the femtosecond fluorescence transients were superimposable with each other (Figure S5 of the Supporting Information). This observation suggests that in sucrose–water solution the ultrafast process, which may be due to the rotation of the hydrocarbon chain or excited-state tautomerization or both, is unchanged, while the solvent-induced relaxation of epicocconone is restricted in the

**Table 3.** Fluorescence Decay Parameters of Aqueous Solutions of Epicocconone with Varying Concentration of Sucrose

% of sucrose by w/v	$\chi^2$	$\tau_1$ (ns)	$a_1$	$\tau_2$ (ns)	$a_2$
0	1.11	0.20	0.85	1.20	0.15
10	1.17	0.26	0.80	1.60	0.20
20	1.15	0.30	0.77	1.70	0.23
35	1.20	0.33	0.75	1.80	0.25

excited state and thus a higher quantum yield is observed. This, in turn, leads us to consider the solvent polarity as a key factor in deciding dynamics of epicocconone in the excited state because in sucrose–water solution the dielectric constant changes negligibly whereas the bulk polarities of acetonitrile and *tert*-butanol are different. Another possible factor may be the H-bonding ability of the solvent, which can alter the possible tautomerization of the keto–enol moiety.

This explains why epicocconone (deep purple total protein stain) is such a good protein stain for 2D gel electrophoresis. In this technique, proteins are separated on the basis of the mass of anionic detergent (sodium dodecyl sulfate, SDS) they accumulate and thus uniformly migrate toward the positive anode at their mass to charge ratio. The lysine adduct is thus surrounded by the viscous and nonpolar SDS shell accumulated around the protein, leading to a substantial increase in fluorescence as we have observed here for epicocconone in viscous sucrose.

## CONCLUSION

A major finding of this work is that there is an ultrafast component associated with the deactivation pathway of epicocconone, which explains its relatively low quantum yield of the natural product. Surprisingly, the ultrafast component is only a minor contributor to the relaxation of the butylamine adduct of epicocconone. The decay of epicocconone is accompanied by a rise time in its butylamine adduct that extends the fluorescence decay to well over 2 ns, explaining the dramatic increase in quantum yield observed when epicocconone binds to proteins. In more viscous solvent such as *tert*-butanol, the contribution of the ultrafast component is reduced further, with a concomitant increase in lifetime and fluorescence. These observations, along with the steady-state experiments and quantum chemical calculations reported earlier,<sup>2</sup> lend support to the conclusion that the ultrafast component is associated with either photoisomerization or excited-state tautomerization and that the longer component (that involves the observed rise time) is associated with a rearrangement in the excited state. In water the photoisomerization process is even faster. Addition of sucrose in aqueous solution does not alter the ultrafast process but stabilizes the emissive species overall, leading to higher quantum yields. Since the polarity does not change appreciably with the addition of sucrose to water, the effect of polarity difference between water and *tert*-butanol to decide the fate of the ultrafast pathway cannot be ruled out. At the same time the effect of H-bonding ability of the solvent must be considered. Further detailed studies, including solvent variation and synthetic epicocconone analogues, are required before this scheme can be confirmed.

## ASSOCIATED CONTENT

**S Supporting Information.** Figures showing reaction mechanism, additional absorption spectra, fluorescence spectra, and

time-resolved decays and table listing absorption and emission characteristics and decay parameters. This material is available free of charge via the Internet at <http://pubs.acs.org>.

## AUTHOR INFORMATION

### Corresponding Author

\*E-mail: [anindya@chem.iitb.ac.in](mailto:anindya@chem.iitb.ac.in) (A.D.); [peter.karuso@mw.edu.au](mailto:peter.karuso@mw.edu.au) (P.K.). Phone: +91 22 2576 7149 (A.D.); +612 9850 8290 (P.K.), Fax: +91 22 2570 3480 (A.D.); +612 9850 8313 (P.K.).

## ACKNOWLEDGMENT

This research is supported by the Australian Research Council (Grant DP0877999) to P.K. and A.D. and a SERC DST grant to A.D. Support from a FIST grant to the Department of Chemistry, IIT Bombay, is acknowledged gratefully. S.C. thanks Macquarie University for the Protein Stains Ph.D. Scholarship. T.N.B. thanks CSIR, New Delhi, India, for a Senior Research Fellowship.

## REFERENCES

- (1) Bell, P. J. L.; Karuso, P. *J. Am. Chem. Soc.* **2003**, *125*, 9304.
- (2) Panda, D.; Khatua, S.; Datta, A. *J. Phys. Chem. B* **2007**, *111*, 1648.
- (3) Coghlan, D. R.; Mackintosh, J. A.; Karuso, P. *Org. Lett.* **2005**, *7*, 2401.
- (4) Mackintosh, J. A.; Choi, H.-Y.; Bae, S.-H.; Veal, D. A.; Bell, P. J.; Ferrari, B. C.; van Dyk, D.; Verrills, N. M.; Paik, Y.-K.; Karuso, P. *Proteomics* **2003**, *3*, 2273.
- (5) Mackintosh, J. A.; Veal, D. A.; Karuso, P. *Proteomics* **2005**, *5*, 4673.
- (6) Cleeman, F.; Karuso, P. *Anal. Chem.* **2008**, *80*, 4170.
- (7) Espagne, A.; Paik, H. D.; Changenet-Barret, P.; Martin, M. M.; Zewail, H. A. *Chem. Phys. Chem.* **2006**, *7*, 1717.
- (8) Sun, Y. P.; Saltiel, J.; Park, N. S.; Hoburg, E. A.; Waldeck, D. H. *J. Phys. Chem.* **1991**, *95*, 10336.
- (9) Mali, K. S.; Dutt, G. B.; Mukherjee, T. *J. Chem. Phys.* **2008**, *128*, 124515.
- (10) Burai, T. N.; Panda, D.; Datta, A. *Chem. Phys. Lett.* **2008**, *455*, 42.
- (11) Burai, T. N.; Mukherjee, T. K.; Lahiri, P.; Panda, D.; Datta, A. *J. Chem. Phys.* **2009**, *131*, No. 034504.
- (12) Reichardt, C. *Chem. Rev.* **1994**, *94*, 2319.
- (13) Dean, J. A., Ed. *Lange's Handbook of Chemistry*, 163th ed.; McGraw-Hill: New York, 1987.
- (14) Åkerlöf, G. *J. Am. Chem. Soc.* **1932**, *54*, 4125.

Supporting Information  
for  
Ultrafast Dynamics of Epicocconone, a Second  
Generation Fluorescent Protein Stain

Department of Chemistry and Biomolecular Sciences

Macquarie University, Sydney, NSW 2109, Australia

and

Department of Chemistry

Indian Institute of Technology Bombay, Powai, Mumbai 400076, India

<sup>†</sup> Department of Chemistry and Biomolecular Sciences. Macquarie University, Sydney, NSW 2109, Australia.

<sup>‡</sup> Department of Chemistry. Indian Institute of Technology Bombay, Powai, Mumbai 400076, India.

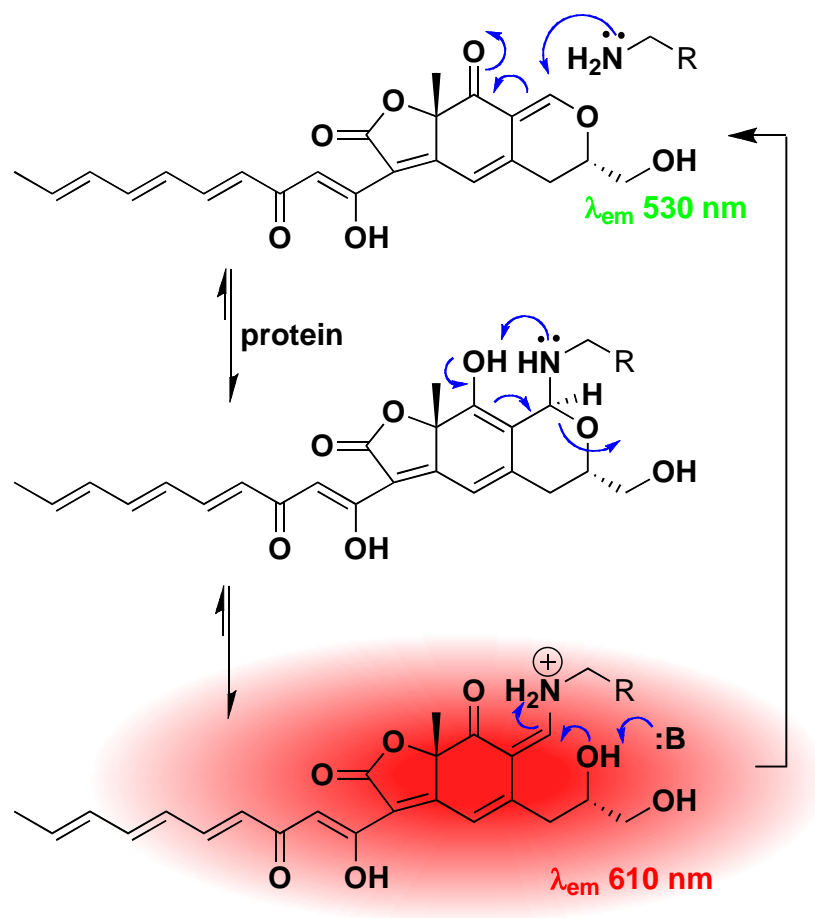
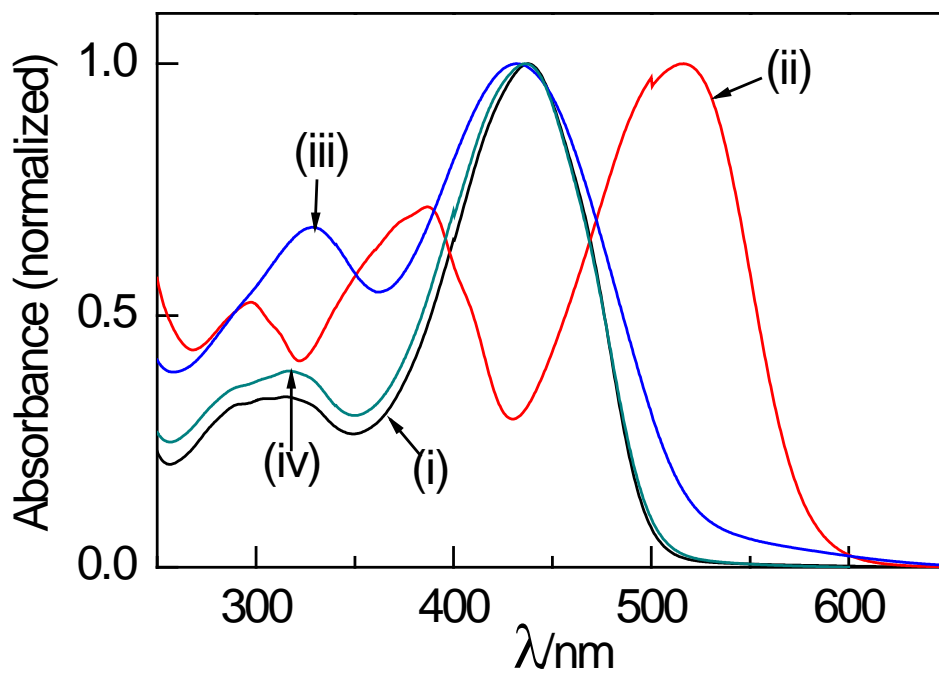
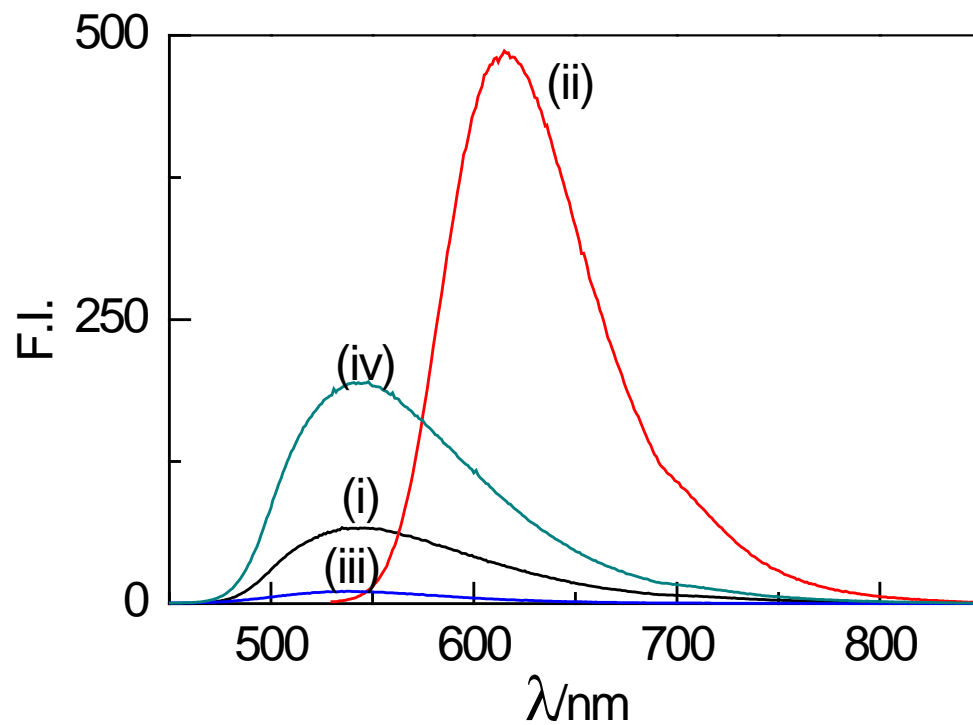


Figure S1. Mechanism of reaction between epicocconone and amine



**Figure S2.** Normalized absorption spectra of epicocconone in (i) acetonitrile (black), (ii) butylamine adduct (red), (iii) water (blue) and (iv) *tert*-butanol (dark cyan).



**Figure S3.** Emission spectra of 20  $\mu$ M epicocconone at  $\lambda_{\text{ex}} = 430$  nm in (i) acetonitrile (black), (ii) butylamine adduct (red), (iii) water (blue) and (iv) *tert*-butanol (dark cyan).

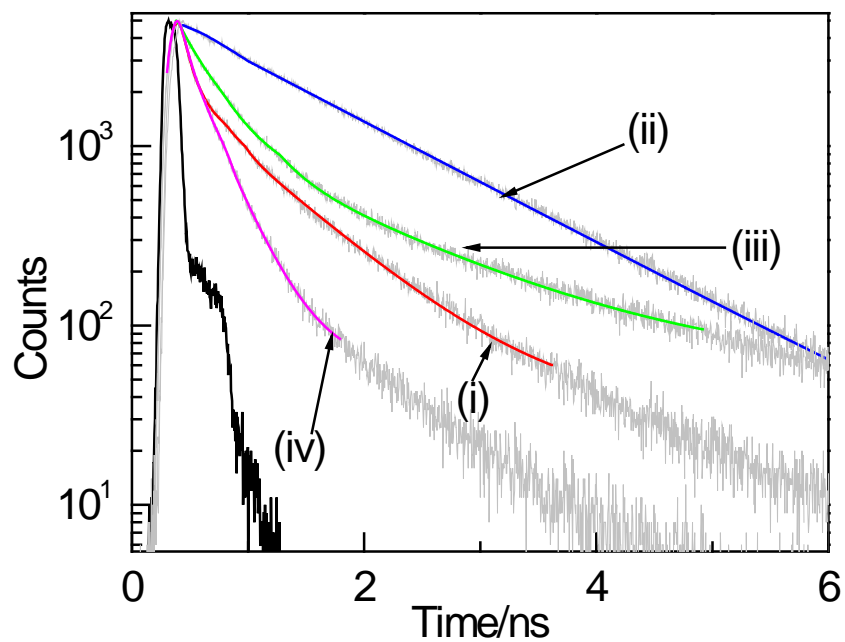


**Figure S4.** Fluorescence decay traces of epicocconone in (i) acetonitrile (red), (ii) butylamine adduct (blue), (iii) water (green) and (iv) *tert*-butanol (magenta) at  $\lambda_{\text{ex}} = 406$  nm and  $\lambda_{\text{em}} = 530$  nm for acetonitrile, water and *tert*-butanol and  $\lambda_{\text{em}} = 610$  nm for butylamine adduct.



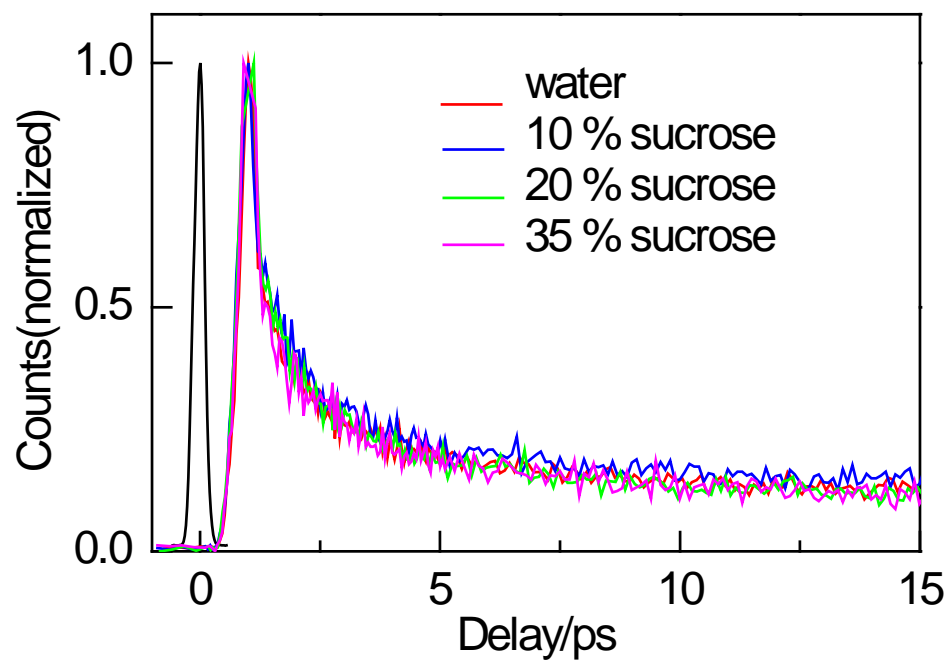


**Figure S5.** Femtosecond fluorescence transients of epicocconone in water with varying concentration of sucrose at  $\lambda_{\text{ex}} = 430$  nm and  $\lambda_{\text{em}} = 530$  nm. The cross-correlation function of the laser pulse is shifted, for the sake of clarity.

**Table S1.** Steady State Absorption and Emission Characteristics of Epicocconone.

Solvent	$\epsilon$ (L mol <sup>-1</sup> cm <sup>-1</sup> ) at $\lambda_{\text{max1}}$ and $\lambda_{\text{max2}}$	$\phi_f$
Acetonitrile	13431 (437 nm) 4998 (316 nm)	0.026
Water	11442 (433 nm) 8440 (328 nm)	0.009
<i>tert</i> -butanol	15648 (436 nm) 6253 (314 nm)	0.068

**Table S2.** Fluorescence Decay Parameters of Epicocconone in Different Media.

Medium	$\chi^2$	$\tau_1$ (ns)	$a_1$	$\tau_2$ (ns)	$a_2$
Acetonitrile	1.10	0.09	0.83	0.77	0.17
Acetonitrile + butylamine	1.00	1.30			
Water	1.11	0.24	0.86	1.34	0.14
<i>tert</i> -butanol	1.02	0.08	0.60	0.28	0.40

# The Role of Different Structural Motifs in the Ultrafast Dynamics of Second Generation Protein Stains

Soumit Chatterjee,<sup>†</sup> Peter Karuso,<sup>\*,†</sup> Agathe Boulangé,<sup>§</sup> Philippe A. Peixoto,<sup>§</sup> Xavier Franck,<sup>§</sup> and Anindya Datta<sup>\*,‡</sup>

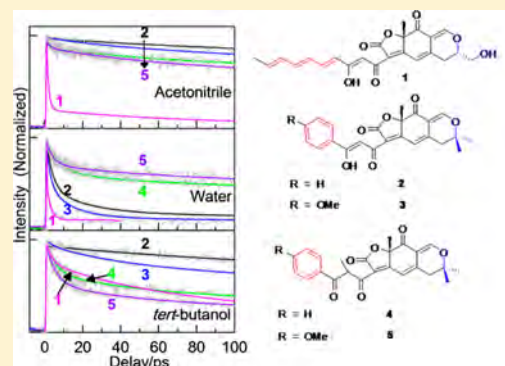
<sup>†</sup>Department of Chemistry and Biomolecular Sciences Macquarie University, Sydney, NSW 2109, Australia

<sup>‡</sup>Department of Chemistry Indian Institute of Technology Bombay, Powai, Mumbai 400076, India

<sup>§</sup>Normandie Univ, COBRA, UMR 6014 et FR 3038; CNRS; Univ Rouen; INSA Rouen, 1 rue Tesnières, 76821 Mont-Saint-Aignan Cedex, France

## S Supporting Information

**ABSTRACT:** Engineering the properties of fluorescent probes through modifications of the fluorophore structure has become a subject of interest in recent times. By doing this, the photophysical and photochemical properties of the modified fluorophore can be understood and this can guide the design and synthesis of better fluorophores for use in biotechnology. In this work, the electronic spectra and fluorescence decay kinetics of four analogues of the fluorescent natural product epicocconone were investigated. Epicocconone is unique in that the native state is weakly green fluorescent, whereas the enamine formed reversibly with proteins is highly emissive in the red. It was found that the ultrafast dynamics of the analogues depends profoundly on the H-bonding effect of solvents and solvent viscosity though solvent polarity also plays a role. Comparing the steady state and time-resolved data, the weak fluorescence of epicocconone in its native state is most likely due to the photoisomerization of the hydrocarbon side chain, while the keto enol moiety also has a role to play in determining the fluorescence quantum yield. This understanding is expected to aid the design of better protein stains from the same family.



## INTRODUCTION

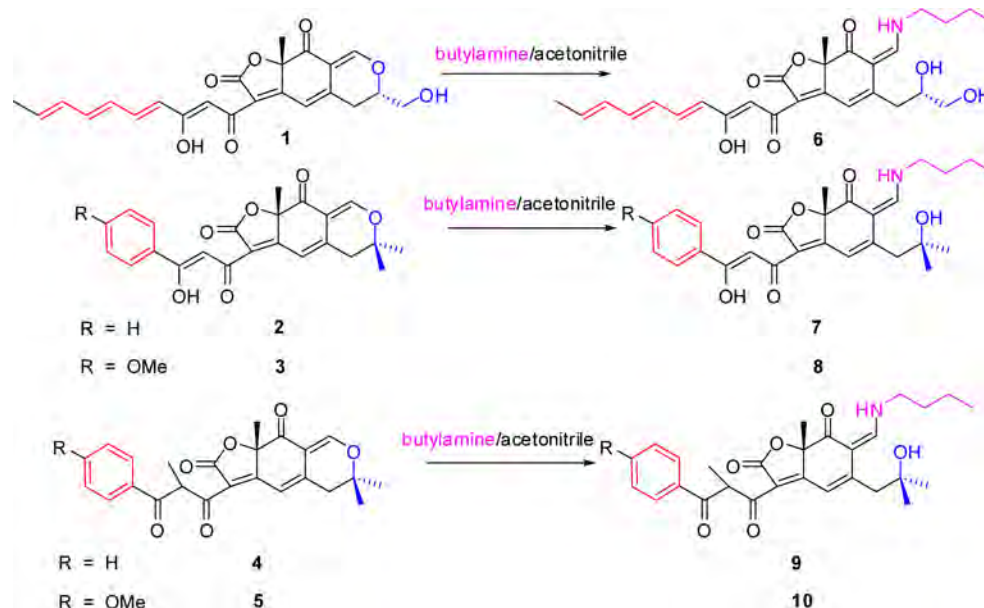
Epicocconone (**1**, Scheme 1) is a fluorescent, cell permeable natural product isolated from the fungus *Epicoccum nigrum*.<sup>1</sup> Its enamine (**6**) is characterized by a high molar absorptivity ( $\sim 10^4$ ) at wavelengths provided by common lasers (488, 532 nm), strong fluorescence under specific conditions, a Stokes shift of  $\sim 100$  nm, and a low cytotoxicity coupled with cell permeability.<sup>2</sup> These properties make it a potentially good fluorescent probe for biotechnological applications such as cell tracking and two-color staining, when multiplexed with other fluorescent probes which have similar absorbancies but different regions of emission. The conjugated  $\beta$ -diketone moiety in epicocconone is reminiscent of a similar structure in curcumin, a medicinal pigment from turmeric (*Cucuma longa* L).<sup>3,4</sup> The steady state behavior of both was found to be similar. The absorption maximum of curcumin is  $\sim 408$ – $430$  nm in most organic solvents, while the emission maximum is very sensitive to the solvent medium (460–560 nm). The fluorescence quantum yield of curcumin is low, and reduced significantly, in the presence of water, similar to epicocconone. The fluorescence lifetime is short ( $< 1$  ns) and the fluorescence decays are multiexponential, with contributions from ultrafast components of 10 and 70 ps. It was reported that solvation and excited state intramolecular proton transfer (ESIPT) are the

main non-radiative pathways and the reasons for the low quantum yield of curcumin.<sup>5,6</sup> The structural similarity between the two fluorophores makes it tempting to rationalize the excited state dynamics responsible for the low fluorescence quantum yield of epicocconone on the basis of analogy with the photophysics of curcumin. Notably, epicocconone also is only weakly fluorescent at 530 nm in aqueous solutions but becomes strongly fluorescent with an emission maximum at 610 nm upon addition of proteins. This makes it an attractive fluorescent sensor for proteins, especially as it allows for the detection of proteins in gel electrophoresis down to  $< 100$  pg/band.<sup>7,8</sup> The enhancement of fluorescence of epicocconone in the presence of proteins has been shown to be due to reversible enamine formation with lysine residues.<sup>9</sup> This unique mechanism makes epicocconone the first reversible-covalent latent fluorophore to be discovered and has been used to develop novel enzyme assays based on fluorescence<sup>10</sup> and fluorescence anisotropy.<sup>11</sup> It has also been established that epicocconone is incorporated non-covalently into micelles and cyclodextrins and results in an increase in its green emission at

**Received:** September 17, 2013

**Revised:** October 22, 2013

**Published:** October 29, 2013

Scheme 1. Reaction of Epicoconone (1) and Analogues 2–5 with Butylamine (Magenta)<sup>a</sup>

<sup>a</sup>The analogues 2 and 3 substitute the heptatriene side chain of epicoconone with an isoelectronic phenyl ring (red), the ethanol side chain (blue) is replaced with a *gem*-dimethyl, and the analogues 4 and 5 respectively substitute the keto-enol of 2 and 3 with a  $\beta$ -diketo group.

530 nm.<sup>12,13</sup> It has been proposed that photoisomerization, unlike solvation and excited state intramolecular proton transfer (ESIPT), which may be the primary non-radiative deactivation channel for this fluorophore, is suppressed in heterogeneous media, leading to the observed increases in quantum yield.<sup>12</sup> Using epicoconone butylamine adduct as a model of the protein adduct and assuming it underwent similar excited state dynamics, we proposed that the non-radiative process was due to either photoisomerization or excited state tautomerization which can be altered by solvent viscosity, solvent polarity, or H-bonding effects. To differentiate these alternative mechanisms and to understand the excited state dynamics of epicoconone, we synthesized epicoconone analogues that replaced the heptatriene tail with the homologous but unisomerizable phenyl (2) or anisyl (3) groups. The anisyl group additionally was designed to investigate the effect of resonance on the keto-enol. The keto-enol moiety was further substituted with a methyl, forcing a  $\beta$ -diketone in compounds 4 and 5. These compounds all reacted with amines to form enamines in a similar fashion to 1 (Scheme 1).<sup>9,14</sup> The present study comprises the ultrafast dynamics of these epicoconone derivatives to understand the non-fluorescing behavior of epicoconone in solution.

In our earlier study, it was shown that both 1 and its butylamine adduct (6) undergo similar excited state processes. The predominant ultrafast component of 1 ps remained unchanged upon formation of the enamine. A slower component of 70 ps led to a population buildup of the actual emissive state. Rapid internal conversion (IC) provided a facile non-radiative channel of depopulation of this state, causing the fluorescence quantum yield of 1 to be rather small. The 1 ps component was tentatively assigned to photoisomerization of the heptatriene chain present in epicoconone, but excited state tautomerism could not be ruled out. Notably, the 1 ps component remained unchanged upon enamine formation of 1. The 70 ps component, on the other hand, contributed to a greater extent in the enamine and was assigned to the flexing

motion of the heteronuclear ring system, leading to the conformationally relaxed emissive state.<sup>14</sup>

## MATERIALS AND METHODS

The synthesis of 2–5 is described elsewhere.<sup>15</sup> A solution of each compound in DMSO (1 mg/mL) was used as the stock solution for each experiment. Spectroscopy grade acetonitrile (Spectrochem, Mumbai, India) was distilled over CaH<sub>2</sub> and the distillate passed over activated neutral alumina prior to each experiment. Butylamine (Qualigens, Mumbai, India) and *tert*-butanol (spectroscopy grade, Spectrochem, Mumbai, India) were used as received. The absorption and fluorescence spectra have been recorded on a JASCO V 530 spectrophotometer and a Varian Cary Eclipse spectrofluorimeter, respectively. The emission spectra were recorded exciting at 410/400 nm with 5 nm of excitation and emission slit width and at 500 nm excitation for the butylamine adducts. The absorbancies of the solutions were kept below 0.1 to prevent inner filter effects for steady state measurements and for picosecond–nanosecond time-resolved experiments. The absorbancies of the solutions were kept at  $\sim 1.0$  for the upconversion experiments. The absorption and emission spectra were recorded before and after the femtosecond fluorescence decays in order to verify that the samples do not photodegrade. Fluorescence quantum yields of 1–5 ( $\phi_f$ ) were calculated after correction for changes in absorbance using Lucifer Yellow CH ( $\phi_f = 0.21$ ) as the reference.<sup>16</sup> Fluorescence quantum yields of 6–10 ( $\phi_f$ ) were calculated after correction for changes in absorbance using rhodamine 6G ( $\phi_f = 0.94$ ) as the reference.<sup>17</sup> Time-resolved fluorescence data were obtained using a picosecond pulsed diode laser based time-correlated single photon counting (TCSPC) instrument (IBH, United Kingdom) set at the magic angle with  $\lambda_{ex} = 406$  nm. The full width at half-maximum (fwhm) of the instrumental response at this wavelength was found to be 250 ps with a resolution of 7 ps/channel. The decay traces, thus obtained, were fitted to multiexponential decays using IBH DAS 6.2 data analysis software. The output of

a femtosecond pulsed oscillator from a mode-locked Ti:sapphire laser (Tsunami, Spectra Physics, USA) pumped by a 5 W DPSS laser (Millennia, Spectra Physics), centered at 800 nm and with a repetition rate of 80 MHz, was used as the gate pulse for the femtosecond fluorescence upconversion experiments. The second harmonic (400 nm) of this pulse was used as the source of excitation for the sample placed in a rotating cell. The power of the second harmonic light is restricted to 5 mW at the sample in order to minimize photobleaching. The fluorescence from the sample is upconverted in a nonlinear crystal (0.5 mm BBO,  $\theta = 38^\circ$ ,  $\phi = 90^\circ$ ) by mixing with the gate pulse, which consists of a portion of the fundamental beam. The upconverted light is dispersed in a monochromator and detected using photon counting electronics. A cross-correlation function obtained using the Raman scattering from ethanol has a fwhm of 300 fs. The femtosecond fluorescence decays have been fitted using a Gaussian function of the same fwhm as the excitation pulse. The fluorescence decays were recorded at the magic angle polarization with respect to the excitation pulse on an FOG 100 fluorescence optically gated upconversion spectrometer (CDP Systems Corp., Russia). The resolution was in appropriate multiples of the minimum step size of the instrument, i.e., 0.78 fs/step. The decays were analyzed by iterative reconvolution using a homemade program.<sup>18</sup> The lifetime found from the TCSPC was fixed to the longest component while fitting the fluorescence decay.

Computational results were generated using Turbomole (COSMOlogic).<sup>19</sup> Exhaustive conformational searches for the native and enamine adducts were performed with DFT-D3<sup>20</sup> calculations with the B88/P86<sup>21</sup> exchange-correlation functional using the TZVPP basis set<sup>22</sup> and a continuum solvent model for acetonitrile (COSMO).<sup>23</sup> Vertical excitations were calculated using time dependent density functional theory (TD-DFT), taking into account the 25 lowest excited states. The level of theory required to predict the actual UV spectra generally corresponded to the PBE0/TZVP level of theory.<sup>24</sup> Ground states were confirmed through frequency analyses.

## RESULTS AND DISCUSSION

Epicocconone (**1**) and its butylamine adduct (**6**) showed absorption maxima at 435 and 520 nm, respectively, while their emission maxima appeared at 535 and 615 nm, respectively.<sup>9,14</sup>

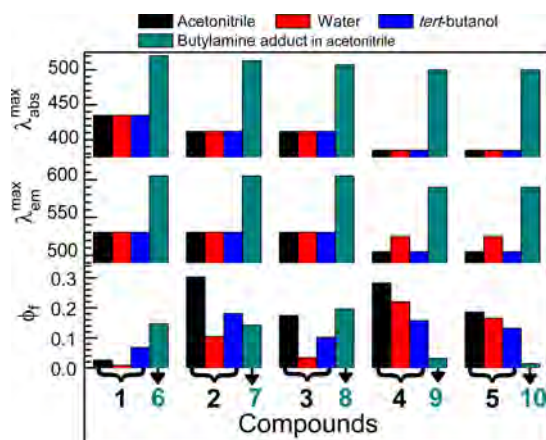


**Figure 1.** Summary of the spectral parameters of the fluorophores studied (**1–5**), in three solvents. The data for their butylamine adducts (**6–10**) in acetonitrile show the changes in spectral parameters upon enamine formation.

In the present study, we found the absorption maxima of compounds **2** and **3** (Scheme 1) to occur at 412–413 nm, while those of their butylamine adducts (**7** and **8**) were red-shifted to 513 and 507 nm, respectively (Figures 1, S1a and S1b, Supporting Information). The emission maxima were found at 530 nm for **2** and **3** and at 605 nm for **7** and **8** (Figures 1, S1a and S1b, Supporting Information). Thus, the trends in the spectral shifts upon enamine formation were quite similar to that seen for **1**. These data suggest that the aromatic ring is not involved in the lowest  $\pi \rightarrow \pi^*$  transition, as the absorption and emission spectra of an anisole derivative would be expected to have a red shift of  $\sim 20$  nm compared to that of the benzene analogue due to the extra conjugation.<sup>25–27</sup> Hence, **2** and **3** were found to be excellent models to study the effect of the heptatriene chain of **1**, as no additional photophysics seemed to complicate the situation and the keto–enol moiety, present in **1**, was conserved in **2** and **3**. In the three solvents studied, the fluorescence quantum yields of **2** and **3** were always much larger than that of **1** (Figure 1, Table 1). This may be ascribed to the absence of the non-radiative decay channel provided by photoisomerization in the heptatriene chain in **2** and **3**. However, the quantum yield of **3** was lower than that of **2** in each of the three solvents, suggesting an additional non-radiative process in **3** associated with the methoxy group. This non-radiative process could be an ICT from the *p*-methoxyphenyl group. Thus, the heptatriene group was found to be a major contributor to the non-radiative process in **1**, leading to its very low quantum yield, especially in water. This feature is very useful when formation of the enamine is the species of interest.

Compounds **4** and **5** differed from **2** and **3** in that there was an extra methyl group between the two keto groups. The effect of this is to make keto–enol tautomerism impossible due to steric requirements of the methyl. This was evident experimentally from the NMR spectra of **4** and **5** (Supporting Information), which show a quartet, integrating for one proton at  $\delta$  5.5. In contrast, this proton appears at  $\delta$  7.1 as a singlet in **2** and **3** (cf. 6.8 ppm for **1**). Similarly, in the <sup>13</sup>C NMR spectrum of **2** and **3** (Supporting Information), the carbon between the two carbonyls resonates at 97 ppm (cf. 101 ppm for **1**), while for **4** and **5** this carbon resonates at  $\sim 52.5$  ppm. These data indicated that substituting C2' with a methyl effectively inhibits keto–enol tautomerism in the ground state and these compounds could be used to look at the role of keto–enol tautomerism in the fluorescent properties of epicocconone. Computational results indicated compound **4** is 2.7 kcal/mol higher in energy in the keto–enol form (DFT//PBE0/TZVPP) than in the diketo form and that in the ground state the two keto groups are orthogonal in **4** and **5** in agreement with previous results.<sup>24</sup> Compounds **4** and **5** consequently show blue-shifted electronic absorption spectra, with maxima at  $\sim 385$  nm, compared to the maximum at  $\sim 412$  nm for **2** and **3**. The quantum yield of **4** is comparable with that of **2** in acetonitrile and *tert*-butanol but in water is 2 times higher (Figure 1, Table 1). Thus, the keto–enol group did not appear to play a major role in the non-radiative depopulation of the excited state of **1** and its analogues, in non-aqueous solvents. The quantum yield of **5** is lower than that of **4** in all three solvents—further evidence of an ICT in the *p*-methoxyphenyl derivatives. Hence, a unified picture of fluorophores **1–5** begins to emerge.

DFT calculations were used to investigate these four analogues more closely. A conformational search using



Table 1. Molar Extinction Coefficients and Quantum Yields of Compounds 1–5 in Different Solvents

solvent	$\epsilon$ (Lit.M <sup>-1</sup> cm <sup>-1</sup> )					$\phi_f$				
	1 <sup>a</sup>	2 <sup>c</sup>	3 <sup>c</sup>	4 <sup>c</sup>	5 <sup>c</sup>	1 <sup>b</sup>	2 <sup>d</sup>	3 <sup>d</sup>	4 <sup>f</sup>	5 <sup>f</sup>
acetonitrile	13400	17600	11800	750	1400	0.026	0.303	0.175	0.283	0.186
water	11400	11100	1500	1160	1020	0.009	0.105	0.034	0.221 <sup>g</sup>	0.166 <sup>g</sup>
<i>tert</i> -butanol	15600	16200	3100	1270	840	0.068	0.181	0.102	0.157	0.132

<sup>a</sup>At  $\lambda = 435$  nm. <sup>b</sup>At  $\lambda = 520$  nm. <sup>c</sup>At  $\lambda = 410$  nm. <sup>d</sup>At  $\lambda = 530$  nm. <sup>e</sup>At  $\lambda = 385$  nm. <sup>f</sup>At  $\lambda = 505$  nm. <sup>g</sup>At  $\lambda = 525$  nm.

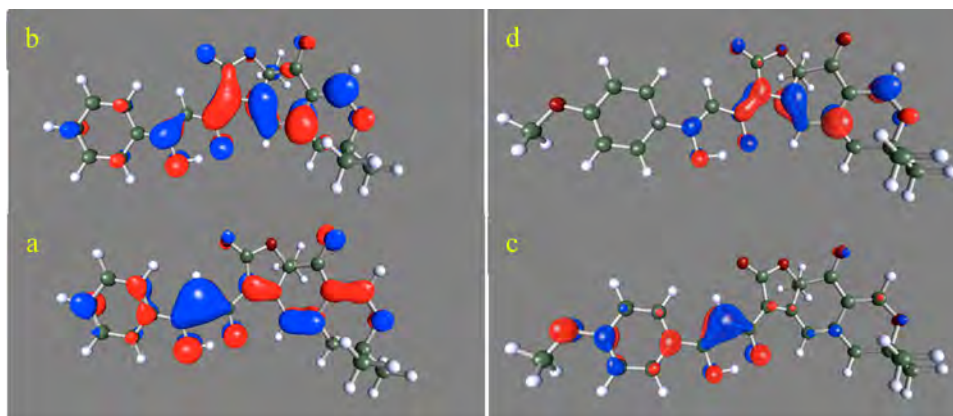


Figure 2. (a and c) HOMO (lower) and (b and d) LUMO (upper) calculated from geometry optimized 2 (left, a and b) and 3 (right, c and d) using the DFT-D3/BP86/TZVP basis set.

Table 2. Molar Extinction Coefficients and Quantum Yields of Compounds 6–10 in Acetonitrile

$\epsilon$ (Lit.M <sup>-1</sup> cm <sup>-1</sup> )					$\phi_f$				
6 <sup>a</sup>	7 <sup>c</sup>	8 <sup>e</sup>	9 <sup>g</sup>	10 <sup>g</sup>	6 <sup>b</sup>	7 <sup>d</sup>	8 <sup>f</sup>	9 <sup>h</sup>	10 <sup>h</sup>
13000	12630	9300	1645	2540	0.147	0.142	0.197	0.031	0.014

<sup>a</sup>At  $\lambda_{\text{ex}} = 520$  nm. <sup>b</sup>At  $\lambda_{\text{em}} = 615$  nm. <sup>c</sup>At  $\lambda_{\text{ex}} = 513$  nm. <sup>d</sup>At  $\lambda_{\text{em}} = 605$  nm. <sup>e</sup>At  $\lambda_{\text{ex}} = 507$  nm. <sup>f</sup>At  $\lambda_{\text{em}} = 605$  nm. <sup>g</sup>At  $\lambda_{\text{ex}} = 500$  nm. <sup>h</sup>At  $\lambda_{\text{em}} = 590$  nm.

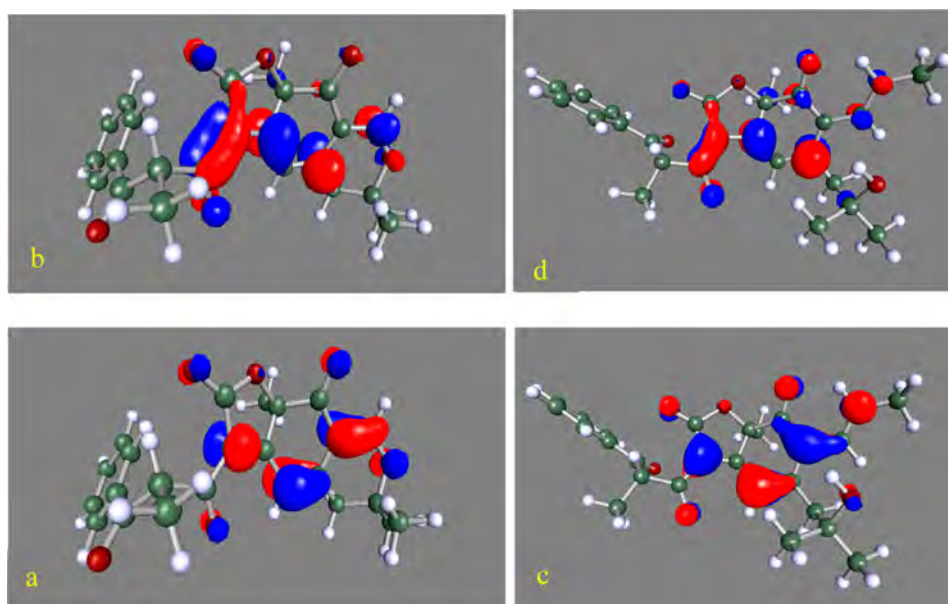
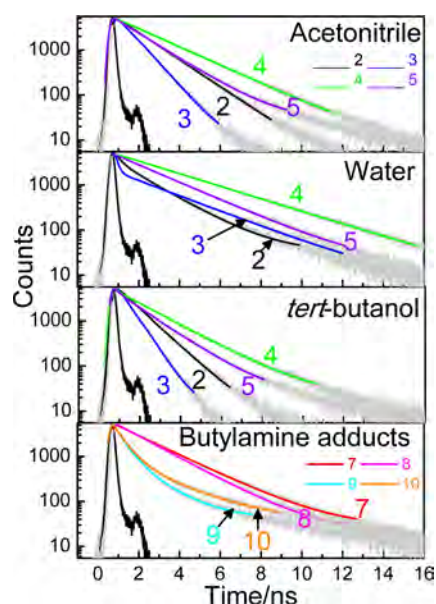


Figure 3. (a and c) HOMO (lower) and (b and d) LUMO (upper) of 4 (left, a and b) and 9 (right, c and d) showing that the two carbonyls are no longer coplanar and that the side chain (phenyl) is not involved in the photophysics.

DFT//B88-P86/S(V)P found 10 possible ground state conformers of 2. The structures within 5 kcal/mol of the lowest energy were further geometry optimized (DFT-D3//B88-P86/TZVPP) using a continuum solvent model (COSMO) for water. For the  $\beta$ -diketone, enolization of the outer ketone was

favoured but only by about 1.4 kJ/mol (Figure S6, Supporting Information). The optimum length of the O–H was found to be 1.09 Å when on the outer oxygen and 1.12 Å when on the inner oxygen with an almost barrierless (0.03 kcal/mol) transition from the higher energy tautomer to the lower



**Figure 4.** Nanosecond fluorescence decay traces of 2–5 in different solvents and the respective butylamine adducts, 7–10 in acetonitrile;  $\lambda_{\text{ex}} = 406$  nm and  $\lambda_{\text{em}} = 530$  nm for 2 and 3 in all solvents.  $\lambda_{\text{em}} = 505$  nm for 4 and 5 in acetonitrile and *tert*-butanol,  $\lambda_{\text{em}} = 525$  nm for 4 and 5 in water,  $\lambda_{\text{em}} = 605$  nm for 7 and 8, and  $\lambda_{\text{em}} = 590$  nm for 9 and 10.

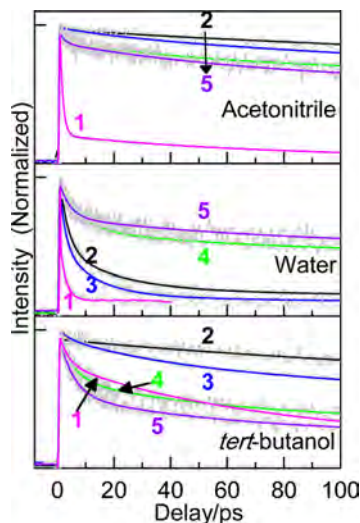


**Figure 5.** Femtosecond fluorescence transients of 1–5 in different solvents in 100 ps scale.  $\lambda_{\text{ex}} = 400$  nm and  $\lambda_{\text{em}} = 530$  nm for 2 and 3 in all solvents.  $\lambda_{\text{em}} = 505$  nm for 4 and 5 in acetonitrile and *tert*-butanol and  $\lambda_{\text{em}} = 525$  nm for 4 and 5 in water. The fitting parameters are provided in Tables S3–S6 (Supporting Information).

(Figure S6, Supporting Information). Other conformers and tautomers were of higher energy and not further considered. These results correlated well with those recently published except that we found that the second carbonyl is enolized for all the analogues.<sup>28</sup> The steady state UV spectra of 2 and 3 were calculated from the lowest energy structures (TD-DFT//pbe0/TZVP) and matched reasonably well with the actual spectra in acetonitrile (Figure S7, Supporting Information). We thus had confidence that the molecular orbitals would be well described at this level of theory. Plotting the HOMO and LUMO of 2 and 3 (Figure 2) revealed that 3 did in fact form an intramolecular ICT that was not as obvious in 2. The

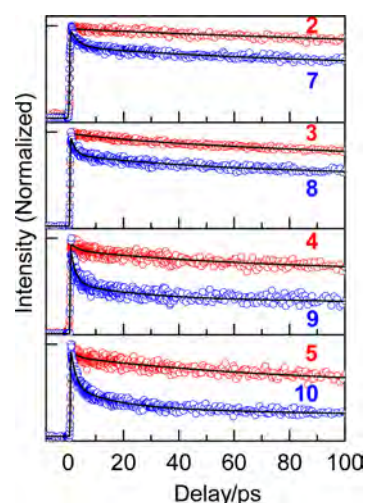


**Figure 6.** Femtosecond fluorescence transients of 2–5 (red  $\circ$ ) and 7–10 (blue  $\circ$ ) in acetonitrile in 100 ps scale.  $\lambda_{\text{ex}} = 400$  nm and  $\lambda_{\text{em}} = 530$  nm for 2 and 3,  $\lambda_{\text{em}} = 530$  nm for 4 and 5,  $\lambda_{\text{em}} = 605$  nm for 7 and 8, and  $\lambda_{\text{em}} = 590$  nm for 9 and 10. The fitting parameters are provided in Tables S3–S6 (Supporting Information).

HOMO of 3 is associated with the anisyl-keto-enol, while the LUMO is associated more with the tricyclic nucleus common to 1–5.

For complicated fluorophores like epicocconone, one needs to consider additional possibilities of excited state tautomerism, H-bonding with solvent, or changes in  $\text{pK}_{\text{a}}$  in the excited state. The  $\text{pK}_{\text{a}}$ 's of 1–5 in the ground state (absorption at 406 nm) were all about the same ( $5.7 \pm 0.1$ ) but in the excited state increased for 1–3 but not 4 and 5 (Figures S2–S5, Table S1, Supporting Information). This suggests that in the excited state for compounds 1–3 the enol proton is more tightly held in the excited state, leading to an increase in  $\text{pK}_{\text{a}}$ , and that there is no effect of the methoxy group on the  $\text{pK}_{\text{a}}$ , indicating that there is little, if any, inductive effect on the keto-enol moiety. This supports the steady-state UV-vis absorptions where no bathochromic shift is observed for 3 over 1 or 2 and the computational results. Hence, the possibility of tautomerism or change in  $\text{pK}_{\text{a}}$  of the keto-enol to alter the dynamics of epicocconone can be ruled out.

Because of the utility of epicocconone in biotechnological applications, which rely on its conversion to a highly emissive enamine, a more pertinent question is the difference in photophysics brought about by enamine formation of our analogues. Upon formation of the butylamine adduct 6, the quantum yield increases 6.5 times in acetonitrile compared to 1 but 7 decreases 2-fold with respect to 2, while 8 shows a similar quantum yield to 3 (Figure 1, Table 2). Large Stokes shifts were observed in all cases, in accordance with the postulated enamine formation.<sup>9</sup> Enamines 6–8 all have quite similar quantum yields, absorption spectra, and Stokes shifts suggesting that enamine formation trumps any effects of the side chain.

In compounds 4 and 5, the HOMO and LUMO orbitals do not involve the side chain, which explains their almost identical steady state behavior. This trend is also seen in the enamines 9 and 10 (Figure 3).

8 has a larger quantum yield than 7, despite having the *p*-methoxy group which appears to be responsible for a lower quantum yield of 3 than 2. The reason for this apparent anomaly is not very clear at this point, but it is possible that a charge transfer from the nitrogen atom in the enamine moiety

Table 3. Average Lifetimes, Quantum Yields, and Radiative and Non-Radiative Rate Constants for Compounds 2–5

solvent	2			3			4			5		
	$\langle\tau\rangle$ (ns)	$\phi_f$	$k_R \times 10^9 \text{ s}^{-1}$	$k_{NR} \times 10^9 \text{ s}^{-1}$	$\langle\tau\rangle$ (ns)	$\phi_f$	$k_R \times 10^9 \text{ s}^{-1}$	$k_{NR} \times 10^9 \text{ s}^{-1}$	$\langle\tau\rangle$ (ns)	$\phi_f$	$k_R \times 10^9 \text{ s}^{-1}$	$k_{NR} \times 10^9 \text{ s}^{-1}$
CH <sub>3</sub> CN	0.86	0.30	0.35	0.81	0.68	0.18	0.26	1.21	1.14	0.28	0.25	0.63
water	0.11	0.11	1.00	8.09	0.04	0.03	0.75	24.25	0.96	0.22	0.23	0.81
<i>tert</i> -BuOH	0.82	0.18	0.22	1.00	0.39	0.10	0.26	2.30	0.42	0.16	0.38	2.00
												0.96
												1.00
												3.48

Table 4. Average Lifetimes, Quantum Yields, and Radiative and Non-Radiative Rate Constants for Compounds 7–10 in Acetonitrile

solvent	7			8			9			10		
	$\langle\tau\rangle$ (ns)	$\phi_f$	$k_R \times 10^9 \text{ s}^{-1}$	$k_{NR} \times 10^9 \text{ s}^{-1}$	$\langle\tau\rangle$ (ns)	$\phi_f$	$k_R \times 10^9 \text{ s}^{-1}$	$k_{NR} \times 10^9 \text{ s}^{-1}$	$\langle\tau\rangle$ (ns)	$\phi_f$	$k_R \times 10^9 \text{ s}^{-1}$	$k_{NR} \times 10^9 \text{ s}^{-1}$
CH <sub>3</sub> CN	0.81	0.14	0.17	1.06	0.92	0.20	0.22	0.87	0.20	0.03	0.15	4.85
												6.19
												0.06
												0.16



is hindered by charge transfer in the opposite direction in the presence of the *p*-OMe group, somewhat like the hindrance of the more efficient flip-flop motion of the dimethylamino group in 3-aminoquinoline,<sup>29</sup> by an intramolecular charge transfer process. This argument gains some credence from the fact that this anomalous behavior was not observed while comparing **9** with **10**. Clearly, charge transfer from the anisyl group to the rest of the molecule is hindered in **10** because it is not actually conjugated with the fluorescent core and so the two charge transfer processes are not coupled in **10**, unlike in **8**. Another intriguing observation in this regard was the miniscule quantum yields of **9** and **10** (Figure 1, Table 2). This might also be explained in the light of a more efficient ICT from the enamine group in these adducts and a decrease in the efficiency of the non-radiative process due to an opposing ICT in **7** and **8**.

The fluorescence decays in the nanosecond time regime follow the same trend in the three solvents (Figure 4). The decays of **2** are slower than those of **3**, while the decays of **4** are slower than those of **5**. This observation was in line with the contention about a more efficient non-radiative deactivation by ICT in the presence of anisyl groups. Moreover, the decays of **4** were slower than those of **2** and the decays of **5** were slower than those of **3**, indicating that the keto–enol group did have a role to play in the excited state dynamics. However, the possibility of faster dynamics in the picosecond regime, analogous to that observed for **1**, needs to be considered before drawing an inference from the time-resolved data, as such ultrafast dynamics is capable of affecting the photophysics of these molecules rather drastically. Indeed, an ultrafast component of 2–3 ps was observed for **2** and **3** in water, with a contribution of 50%. This component was not obtained in acetonitrile or *tert*-butanol (Figure 5, Tables S6 and S7, Supporting Information). Thus, the picosecond dynamics of **2** and **3** was found to be slower than that in **1**. It may be recalled that, for **1**, a sub-picosecond ultrafast component was predominant in water as well as in acetonitrile and this component was assigned to the photoisomerization of the heptatriene chain.<sup>13</sup> Absence of the sub-picosecond component for **2** and **3**, which have the heptatriene replaced with an isoelectronic phenyl group, supports our assignment of this component to photoisomerization.<sup>12,14</sup> The 2–3 ps component observed for **2** and **3** can be assigned to intramolecular charge transfer (ICT), as its contribution was more prominent in water, indicating the involvement of a polar excited state. Faster decays in **3** can be rationalized in terms of more facile ICT, due to the presence of the anisyl group, as predicted by DFT calculations. Thus, it appears that, in the absence of photoisomerization, ICT plays a dominating role in the photophysics of epiconone derivatives. Since the ICT in **2** was suppressed in the more viscous *tert*-butanol, it is likely to be associated with some bond twisting as well. A relatively slower component of 20–80 ps was found for **2** as well as **3** in all three solvents. This component may be assigned to the flexing of the tricyclic system to populate the emissive state, as was shown for **1**.<sup>14</sup> Compounds **4** and **5** had almost identical picosecond decay profiles in acetonitrile, with a 10% contribution of a 2 ps component. In water and *tert*-butanol, relatively slower components (4–7 ps) were observed (Figure 5, Tables S8 and S9, Supporting Information). Unlike in **2** and **3**, the slower components were ca. 50 ps in all three solvents. The slightly lower quantum yield of **4** ( $\phi_f = 0.283$ , Table 1) than **2** ( $\phi_f = 0.303$ , Table 1) in acetonitrile can be rationalized by the ultrafast component present in **4**. The difference in quantum

yields of **3** and **5** can only be explained on the basis of their longer average lifetime. Radiative and non-radiative decay rates of these compounds in different solvents have been calculated in an attempt to generate a more quantitative understanding of the quantum yields.

So far, a comparison has been made between the temporal profiles of **2** and **3** and between those of **4** and **5** in acetonitrile, in an attempt to understand the role of ICT in these molecules. Upon a similar comparison for the other two solvents studied, it appears that qualitatively, the trends are similar. Decays for **3** are faster than **2**, while **5** has faster decays than **4** (Figures 4 and 5), suggesting that ICT plays an important role in the photophysics of **2**–**5**. The next question to address is the role of the keto–enol group in this ICT process. DFT calculations indicate that the two carbon–oxygen bonds are coplanar in **2** and **3** but not in **4** or **5**.<sup>28</sup> This may be rationalized in the light of the intramolecular hydrogen bond between the keto and enol groups in **2** and **3** and lack thereof between the two keto groups in **4** and **5**. It is possible that such coplanarity, or lack thereof, can favor (or hinder) ICT in these molecules. A comparison between the fluorescence decays of **2** and **4** and that between **3** with **5** is thus required. The nanosecond lifetimes of **4** were longer than those of **2** in all three solvents, while those of **5** were longer than those of **3** (Figure 4, Tables S2–S5, Supporting Information). Surprisingly, this trend was qualitatively opposite to that of fluorescence quantum yields (Figure 1, Table 1). For the picosecond components, this anomaly persists in acetonitrile and *tert*-butanol (Figure 5, Tables S6–S9, Supporting Information). In water, however, the fastest component in the keto–enol molecules (**2**, **3**) was of 2–3 ps, while that for the diketones (**4**, **5**) was 4–7 ps, with a decrease in their relative contribution. The slower picosecond component was ca. 15–20 ps in **2** and **3** but ca. 50 ps in **4** and **5**. This was in agreement with the order of quantum yields (**4** > **2** and **5** > **3**). Hence, we can infer that the diketone group does have a role to play in the photophysics of these compounds. The shorter picosecond components of the diketones compared to corresponding keto–enols indicate the occurrence of a more efficient non-radiative decay pathway in the diketones in acetonitrile and *tert*-butanol. This pathway is likely to be associated with the movement of the two carbonyl groups with respect to each other, which would be restricted in the intramolecularly hydrogen bonded keto–enol compounds. The anomalous observations in water are likely to arise from the competition to intramolecular hydrogen bond formation, offered by the solvent, which would tend to form intermolecular solute–solvent hydrogen bonds. The interplay of different factors that affect the non-radiative processes is best monitored by studying the non-radiative rates. This has been presented later in the manuscript, after a discussion of the temporal properties of the butylamine adducts.

The nanosecond lifetimes of butylamine adducts **8**, **9**, and **10** followed the same qualitative trends as quantum yields, when compared with their parent compounds **3**, **4**, and **5**, respectively. However, these trends are not quantitative. Upon going from **3** to **8**, the lifetime doubles, while the quantum yield increases by only 13%. Upon formation of the enamines of **4** and **5**, the lifetimes decrease to one-third and half of the lifetimes of the parent compounds, while the quantum yields decrease by an order of magnitude (Figure 1, Tables 1 and 2). This was an indication that, even in the enamines, picosecond dynamics plays an important role.

Indeed, an ultrafast component of 2–3 ps, which was not observed in **2** and contributed little in **3**, was present to a significant extent (ca. 20%) for **7** and **8** in acetonitrile. The contribution of this component increased from ca. 10% in **4** and **5** to ca. 50% in **9** and **10** (Figure 6, Tables S8 and S9, Supporting Information). This component persisted in **9** and **10**, with an even greater contribution of ca. 50%. Thus, the contribution of the diketo moiety to the ultrafast non-radiative deactivation of the excited state appeared to be present in the enamines. On the other hand, the slower time constant was 20 ps in **7** and **8** (i.e., the enamines with the keto–enol moiety), while its value was 50 ps in **9** and **10** (i.e., the diketonic enamines). Thus, it appears that the conformational relaxation in enamines becomes faster in the diketo compounds. In addition, we found that the *p*-OMe had no role in the excited state dynamics of the butylamine adducts, as its presence did not lead to any change in the decay characteristics. Therefore, we can conclude that the nature of the  $\beta$ -diketone is the key factor guiding the excited state dynamics of the butylamine adducts while the side group remains inactive, which in turn supports and explains the dramatic increase in the quantum yield of **6**.<sup>1,9,14</sup>

The variation in fluorescence quantum yields between the four analogues in different solvents was investigated to understand the effects of hydrogen bonding on radiative and non-radiative decay rates (Table 3). Compounds **2** and **3** in acetonitrile showed similar radiative rate constants, while the non-radiative rate constant in **3** was ca. 1.5-fold higher than that of **2**, resulting in a higher quantum yield of **2** (Table 3). Similarly, in water and *tert*-butanol, a higher quantum yield of **2** than **3** can be ascribed to a lower non-radiative rate with respect to **3**. In water, the non-radiative rate constant was almost 3 times higher in **3** than that in **2**, thus accounting for the 3 times less quantum yield in **3** (Table 3). Similarly, a comparison between **4** and **5** in acetonitrile, water, and *tert*-butanol brings out the role of the non-radiative rates in the quantum yields. In **4** and **5**, non-radiative rates were found to be much slower in water, causing higher quantum yields in these compounds. We might therefore consider that the *p*-OMe causes an increase in the non-radiative rate for compounds while considering compounds of similar functional groups, i.e., for keto–enol bearing compounds like **2** and **3** or diketo compounds like **4** and **5**.

A comparison between **2** and **4**, in acetonitrile and *tert*-butanol, hints at the interplay of the radiative and non-radiative decay rates to elucidate the difference in their quantum yields. It can be found that **2**, having the keto–enol moiety, showed higher radiative and non-radiative decay rates simultaneously, but the radiative decay rate was found to be the key factor to explain the higher quantum yield of **2** over **4** (Table 3). This was not seen if **3** and **5** were compared in these solvents and the quantum yield was found to be a function of non-radiative decay rate, where **5**, having the diketo moiety, showed higher quantum yield than **3** (Table 3). In water, molecules having a keto–enol moiety had an almost 4-fold higher radiative rate constant with respect to the diketo counterpart, but it was the huge suppression of the non-radiative decay of the diketo compounds that led to a leap in their quantum yield (Table 3). We can conclude that the presence of a *p*-OMe group leads to an increase in the non-radiative rate in polar protic solvent for the keto–enol moiety bearing fluorophores. This could indicate the stabilization of a charge transfer state by the participation of hydrogen bonding with solvent molecules.

Comparing **7** and **8** (Table 4), a little lower quantum yield of **7** was found to be a result of the higher radiative rate constant of **7**. In the cases of **9** and **10** (Table 4), a similar trend was observed. Therefore, for the butylamine adducts, compounds having the *p*-OMe showed slightly higher radiative decay for keto–enol moieties but behaved oppositely for the diketo. In between **7** and **9**, it was found that the diketo group caused instability, resulting in an increase in non-radiative rate. This may be rationalized by the ICT from the enamine, which is less favorable in the case of diketo. The presence of *p*-OMe makes this process even unfavorable which is evident from the fact that, in between **8** and **10**, **10** not only showed a 7 times increase in the non-radiative rate, but also its radiative decay rate became faster by 2-fold, making it a very poor emitter in water.

## ■ CONCLUSION

In our earlier study, we postulated that photoisomerization or tautomerism of the  $\beta$ -diketone may be responsible for the non-fluorescing nature of epicocconone.<sup>14</sup> The present study, on four epicocconone analogues, establishes the involvement of photoisomerization of the heptatriene side chain, rather than the tautomerism of the  $\beta$ -diketone, as the major non-radiative process in epicocconone. This is manifested in the significantly higher fluorescence observed in the analogues that lack the conjugated chain. The corresponding butylamine adducts of the analogues showed a similar kind of reversible enamine formation with butylamine, as was evident from the red-shifted absorption and emission spectra. However, unlike epicocconone, they did not show the characteristic increase in quantum yield, suggesting that the heptatriene photoisomerization was not a significant relaxation pathway for the enamine of epicocconone. All the butylamine adducts (**6**–**8**) having a keto–enol moiety had comparable fluorescence intensities, indicating that intramolecular H-bonding helped stabilize the excited state. Compounds with a  $\beta$ -diketo group (**9**, **10**) had much lower quantum yields. This process can be affected by the intermolecular H-bonding with solvents, as found from the variation of the quantum yields of the analogues with different solvents. Other parameters like solvent polarity and viscosity can also play a crucial role in determining the fate of the excited state dynamics of these molecules. From our results, factors that increased quantum yield include photoisomerism in the heptatriene chain, flexing of the fused ring system, and a possible charge transfer involving the diketo group. This inference points the way to the design and synthesis of analogues with higher quantum yields. In order to obtain higher quantum yields, the heptatriene chain needs to be engineered so as to eliminate photoisomerization, while the keto enol moiety needs to be conserved in order to obtain a higher quantum yield for the butylamine adducts.

## ■ ASSOCIATED CONTENT

### ■ Supporting Information

Additional time-resolved decays,  $pK_a$  plots, computational data, and tables of decay parameters. This material is available free of charge via the Internet at <http://pubs.acs.org>.

## ■ AUTHOR INFORMATION

### Corresponding Authors

\*E-mail: [peter.karuso@mq.edu.au](mailto:peter.karuso@mq.edu.au). Phone: +612 9850 8290. Fax: +612 9850 8313.

\*E-mail: anindya@chem.iitb.ac.in. Phone: +91 22 2576 7149. Fax: +91 22 2570.

## Notes

The authors declare no competing financial interest.

## ACKNOWLEDGMENTS

This research is supported by the Australian Research Council (DP0877999) to P.K. and A.D. and a SERC DST grant to A.D. Support from a FIST grant to the Department of Chemistry, IIT Bombay, is gratefully acknowledged. We gratefully acknowledge the Région Haute Normandie for financial support to P.A.P. and A.B. and the Australian Research Council for support of P.K. and S.C. We thank the Ministère des Affaires Étrangères (France) and the Department of Innovation, Industry, Science and Research (Australia) for FAST grants (P.K. and X.F.).

## REFERENCES

- (1) Bell, P. J. L.; Karuso, P. Epicocconone, a Novel Fluorescent Compound from the Fungus *Epicoccum nigrum*. *J. Am. Chem. Soc.* **2003**, *125*, 9304–9305.
- (2) Choi, H.-Y.; Veal, D. A.; Karuso, P. Epicocconone, a New Cell-Permeable Long Stokes' Shift Fluorescent Stain for Live Cell Imaging and Multiplexing. *J. Fluoresc.* **2006**, *16*, 475–482.
- (3) Chignell, C. F.; Bilski, P.; Reszka, K. J.; Motten, A. G.; Sik, R. H.; Dahl, T. A. Spectral and Photochemical Properties of Curcumin. *Photochem. Photobiol.* **1994**, *59*, 295–302.
- (4) Dahl, T. A.; Bilski, P.; Reszka, K. J.; Chignell, C. F. Photocytotoxicity of Curcumin. *Photochem. Photobiol.* **1994**, *59*, 290–294.
- (5) Priyadarsini, K. I. Photophysics, Photochemistry and Photobiology of Curcumin: Studies from Organic Solutions, Bio-Mimetics and Living Cells. *J. Photochem. Photobiol., C* **2009**, *10*, 81–95.
- (6) Adhikary, R.; Mukherjee, P.; Kee, T. W.; Petrich, J. W. Excited-State Intramolecular Hydrogen Atom Transfer and Solvation Dynamics of the Medicinal Pigment Curcumin. *J. Phys. Chem. B* **2009**, *113*, 5255–5261.
- (7) Mackintosh, J. A.; Choi, H. Y.; Bae, S. H.; Veal, D. A.; Bell, P. J.; Ferrari, B. C.; Van Dyk, D. D.; Verrills, N. M.; Paik, Y. K.; Karuso, P. A Fluorescent Natural Product for Ultra Sensitive Detection of Proteins in One-Dimensional and Two-Dimensional Gel Electrophoresis. *Proteomics* **2003**, *3*, 2273–2288.
- (8) Ball, M. S.; Karuso, P. Mass Spectral Compatibility of Four Proteomics Stains. *J. Proteome Res.* **2007**, *6*, 4313–4320.
- (9) Coghlan, D. R.; Mackintosh, J. A.; Karuso, P. Mechanism of Reversible Fluorescent Staining of Protein with Epicocconone. *Org. Lett.* **2005**, *7*, 2401–2404.
- (10) Karuso, P.; Crawford, A. S.; Veal, D. A.; Scott, G. B. I.; Choi, Y.-H. Real-Time Fluorescence Monitoring of Proteolysis. *J. Proteome Res.* **2008**, *7*, 361–366.
- (11) Cleemann, F.; Karuso, P. A Fluorescence Anisotropy Assay for the Traceless Kinetic Analysis of Protein Digestion. *Anal. Chem.* **2008**, *80*, 4170–4174.
- (12) Panda, D.; Khatua, S.; Datta, A. Enhanced Fluorescence of Epicocconone in Surfactant Assemblies as Consequence of Depth-Dependent Microviscosity. *J. Phys. Chem. B* **2007**, *111*, 1648–1656.
- (13) Burai, T. N.; Panda, D.; Datta, A. Fluorescence Enhancement of Epicocconone in Its Complex with Cyclodextrins. *Chem. Phys. Lett.* **2008**, *455*, 42–46.
- (14) Chatterjee, S.; Burai, T. N.; Karuso, P.; Datta, A. Ultrafast Dynamics of Epicocconone, A Second Generation Fluorescent Protein Stain. *J. Phys. Chem. A* **2011**, *115*, 10154–10158.
- (15) Boulangé, A.; Peixoto, P. A.; Franck, X. Diastereoselective IBX Oxidative Dearomatization of Phenols by Remote Induction: Towards the Epicocconone Core Framework. *Chem.—Eur. J.* **2011**, *17*, 10241–10245.
- (16) Stewart, W. W. Synthesis of 3, 6-disulfonated 4-amino-naphthalimides. *J. Am. Chem. Soc.* **1981**, *103*, 7615–7620.
- (17) Fischer, M.; Georges, J. Fluorescence Quantum Yield of Rhodamine 6G in Ethanol as a Function of Concentration Using Thermal Lens Spectrometry. *Chem. Phys. Lett.* **1996**, *260*, 115–118.
- (18) Burai, T. N.; Mukherjee, T. K.; Lahiri, P.; Panda, D.; Datta, A. Early Events Associated with the Excited State Proton Transfer in 2-(2'-pyridyl)benzimidazole. *J. Chem. Phys.* **2009**, *131*, 034504–034508.
- (19) TURBOMOLE V6.3 2011, A Development of University of Karlsruhe and Forschungszentrum GmbH.
- (20) Grimme, S.; Antony, J.; Ehrlich, S.; Krieg, H. A Consistent and Accurate ab initio Parametrization of Density Functional Dispersion Correction (DFT-D) for the 94 Elements H–Pu. *J. Chem. Phys.* **2010**, *132*, 154104–154119.
- (21) Becke, A. D. Density-Functional Exchange-Energy Approximation with Correct Asymptotic Behavior. *Phys. Rev. A* **1988**, *38*, 3098–3100.
- (22) Weigend, F.; Häser, M.; Patzelt, H.; Ahlrichs, R. RI-MP2: Optimized Auxiliary Basis Sets and Demonstration of Efficiency. *Chem. Phys. Lett.* **1998**, *294*, 143–152.
- (23) Klamt, A.; Schürmann, G. COSMO: A New Approach to Dielectric Screening in Solvents with Explicit Expressions for the Screening Energy and Its Gradient. *J. Chem. Soc., Perkin Trans.2* **1993**, *5*, 799–805.
- (24) Schäfer, A.; Huber, C.; Ahlrichs, R. Fully Optimized Contracted Gaussian Basis Sets of Triple Zeta Valence Quality for Atoms Li to Kr. *J. Chem. Phys.* **1994**, *100*, 5829–5835.
- (25) Ma, M.; Johnson, K. E. Carbocation Formation by Selected Hydrocarbons in trimethylsulfonium bromide-AlCl<sub>3</sub>/AlBr<sub>3</sub>-HBr Ambient Temperature Molten Salts. *J. Am. Chem. Soc.* **1995**, *117*, 1508–1513.
- (26) van Walree, C. A.; Roest, M. R.; Schuddeboom, W.; Jenneskens, L. W.; Verhoeven, J. W.; Warman, J. M.; Kooijman, H.; Spek, A. L. Comparison between SiMe<sub>2</sub> and CMe<sub>2</sub> Spacers as  $\sigma$ -Bridges for Ohotoinduced Charge Transfer. *J. Am. Chem. Soc.* **1996**, *118*, 8395–8407.
- (27) Moss, D. B.; Parmenter, C. S. A Time-Resolved Fluorescence Observation of Intramolecular Vibronic Redistribution within the Channel Three Region of S1 Benzene. *J. Phys. Chem.* **1986**, *90*, 1011–1014.
- (28) Syzgantseva, O. A.; Tognetti, V.; Joubert, L.; Boulangé, A.; Peixoto, P. A.; Leleu, A.; Franck, X. Electronic Excitations of Epicocconone Analogues: TDDFT Methodological Assessment Guided by Experiment. *J. Phys. Chem. A* **2012**, *116*, 8634–8643.
- (29) Panda, D.; Datta, A. The Role of the Ring Nitrogen and the Amino Group in the Solvent Dependence of The Excited-State Dynamics of 3-aminoquinoline. *J. Chem. Phys.* **2006**, *125*, 054513–054519.

Supporting Information

for

# The Role of Different Structural Motifs in the Ultrafast Dynamics of Second Generation Protein Stains

*Soumit Chatterjee,<sup>†</sup> Peter Karuso,<sup>\*,†</sup> Agathe Boulangé,<sup>§</sup> Philippe A. Peixoto,<sup>§</sup> Xavier Franck<sup>§</sup> and Anindya Datta<sup>\*,‡</sup>*

Department of Chemistry and Biomolecular Sciences

Macquarie University, Sydney, NSW 2109, Australia

Department of Chemistry

Indian Institute of Technology Bombay,

Powai, Mumbai 400076, India

and

Normandie Univ, COBRA, UMR 6014 et FR 3038; CNRS ; Univ Rouen; INSA Rouen, 1 rue Tesnières, 76821 Mont-Saint-Aignan, Cedex, France

---

\* To whom correspondence should be addressed. Email: [anindya@chem.iitb.ac.in](mailto:anindya@chem.iitb.ac.in) (A.D.) Phone: +91 22 2576 7149, Fax: +91 22 2570 and Email: [peter.karuso@mq.edu.au](mailto:peter.karuso@mq.edu.au) (P.K.) Phone: +612 9850 8290, Fax: +612 9850 8313.

<sup>†</sup>Department of Chemistry and Biomolecular Sciences, Macquarie University.

<sup>‡</sup> Department of Chemistry, Indian Institute of Technology Bombay.

<sup>§</sup> CNRS UMR 6014, C.O.B.R.A. & FR 3038, Université de Rouen, 76131 Mont-Saint-Aignan cedex, France



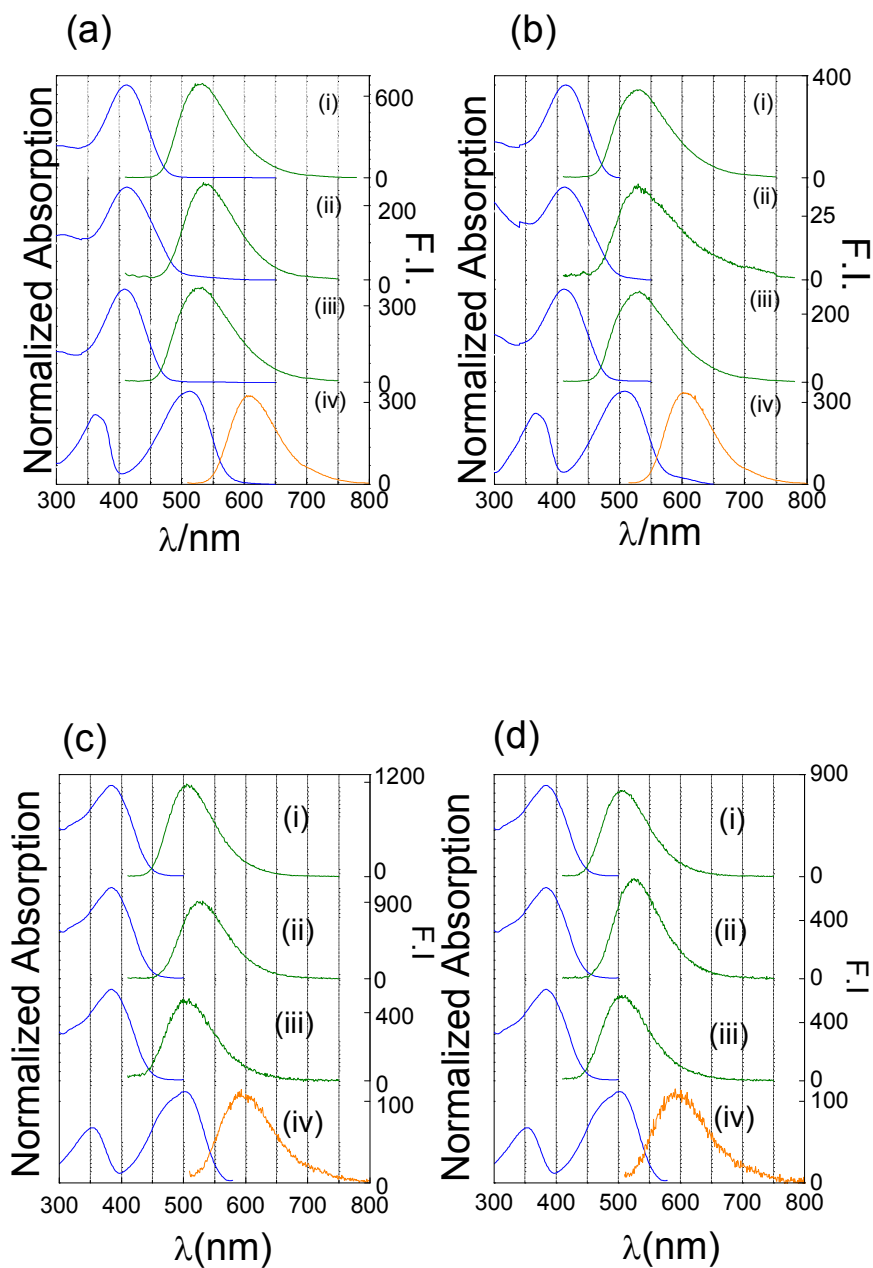


**Figure S1.** Normalized absorption spectra and emission spectra in (i) acetonitrile, (ii) water, (iii) *tert*-butanol of (a) 2, (b) 3 (c) 4 and (d) 5 and normalized absorption spectra and emission spectra in (iv) acetonitrile of (a) 7, (b) 8 (c) 9 and (d) For 2 and 3,  $\lambda_{\text{ex}} = 410$  nm and for 7 and 8  $\lambda_{\text{ex}} = 500$  nm in neat solvents. For 4 and 5,  $\lambda_{\text{ex}} = 400$  nm and for 9 and 10  $\lambda_{\text{ex}} = 500$  nm. The blue lines correspond to the absorption spectra and the green and orange lines correspond to the emission spectra respectively.

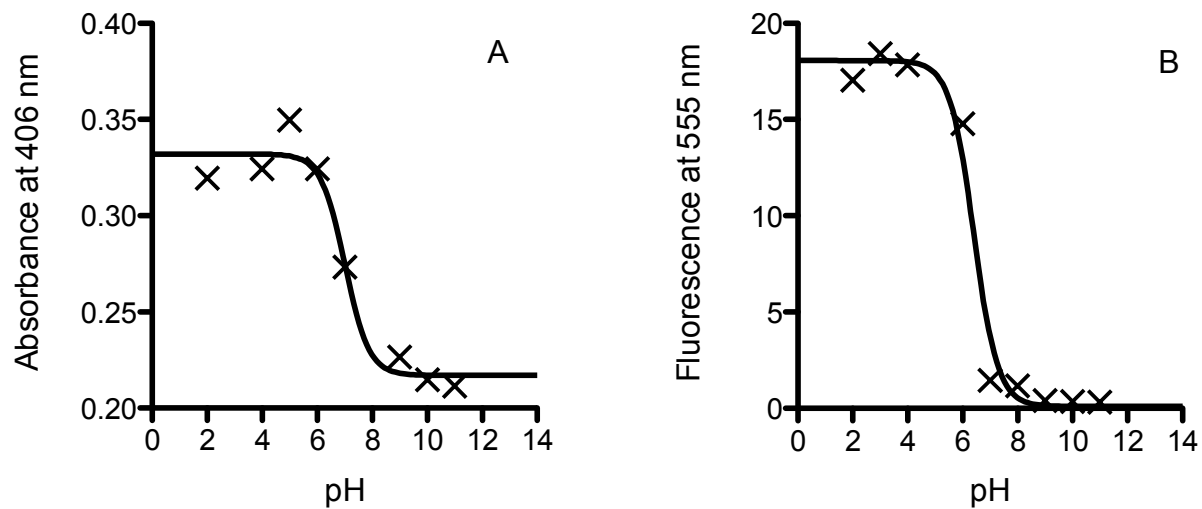


**Figure S2:**  $pK_a$  of **2** in the ground state (A) and excited state (B).

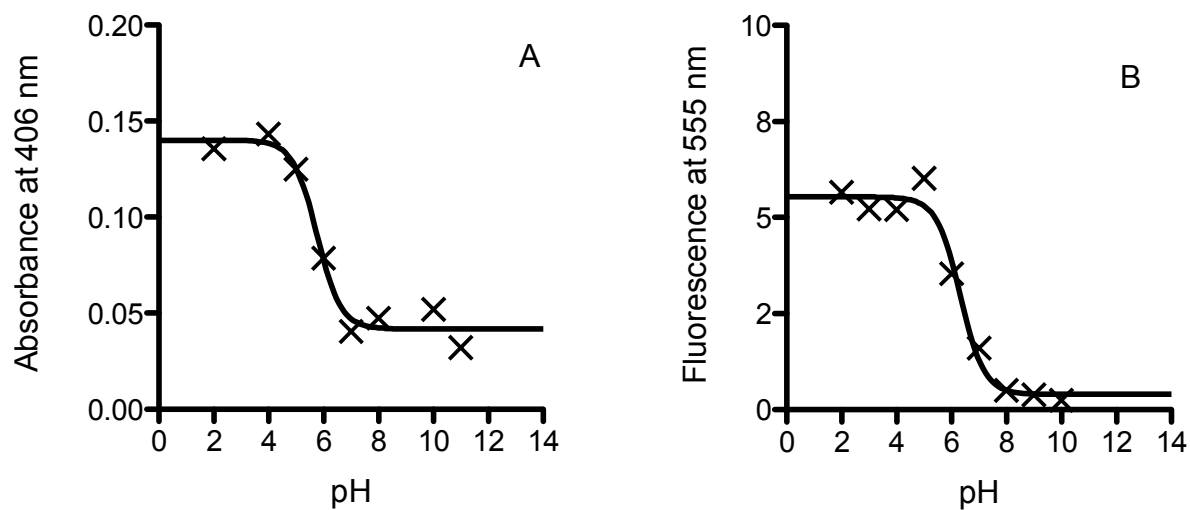


**Figure S3:**  $pK_a$  of **3** in the ground state (A) and excited state (B).

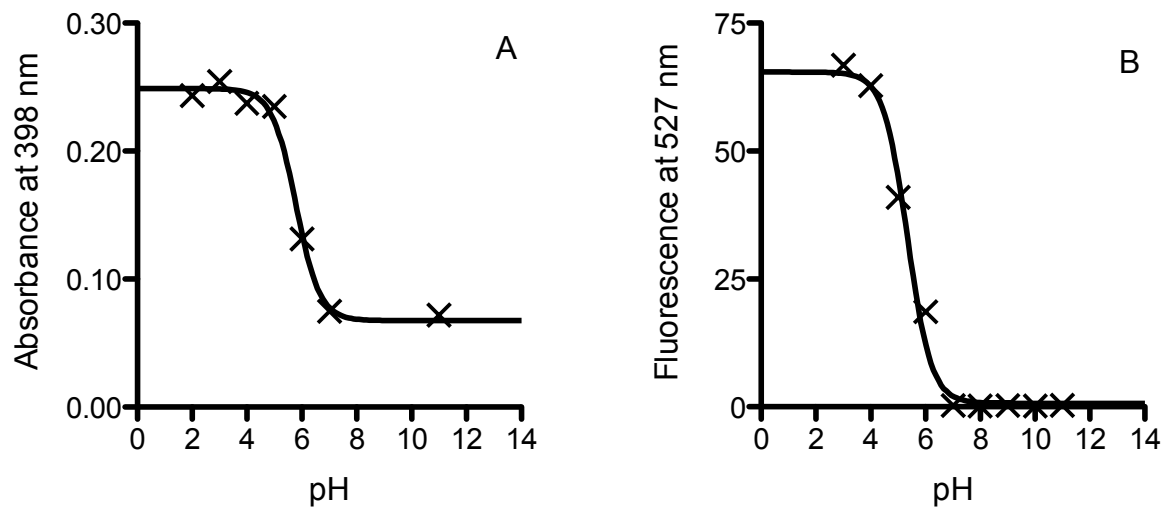


**Figure S4:**  $pK_a$  of **4** in the ground state (A) and excited state (B).

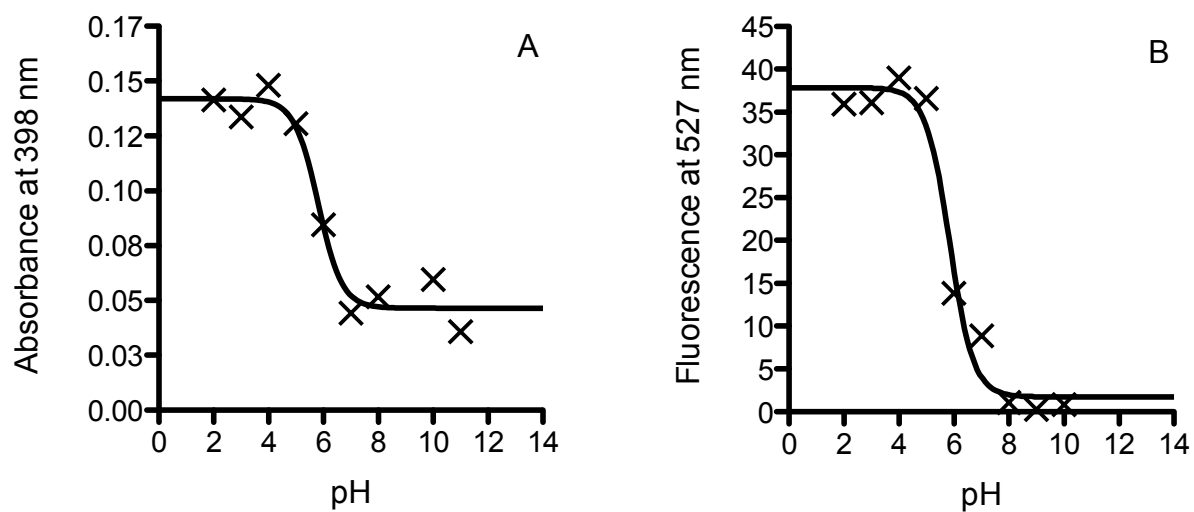


**Figure S5:**  $pK_a$  of **5** in the ground state (A) and excited state (B).

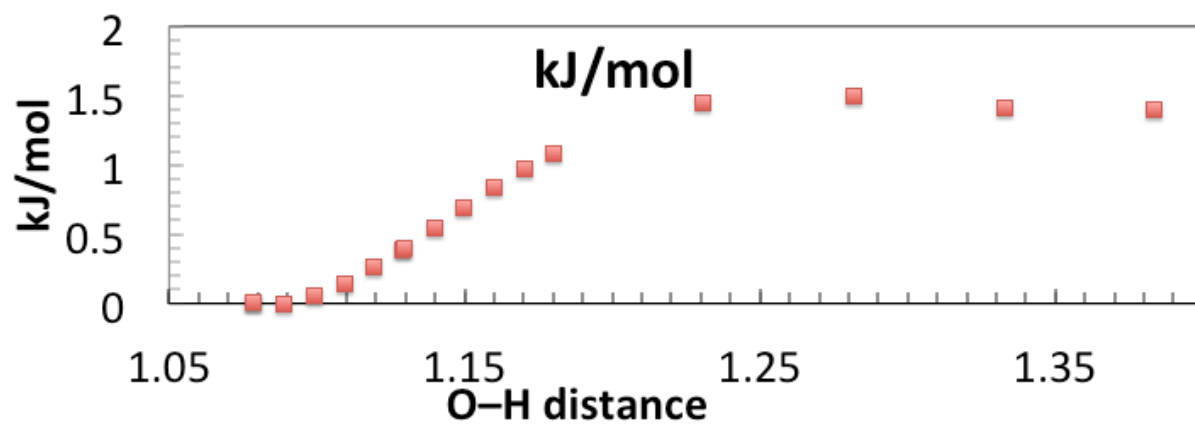


**Figure S6:** DFT//B88-P86/SV(P) bond scan calculation of tautomerisation of the  $\beta$ -diketone in **2**. The x-axis measures distance of the proton from the outer carbonyl.

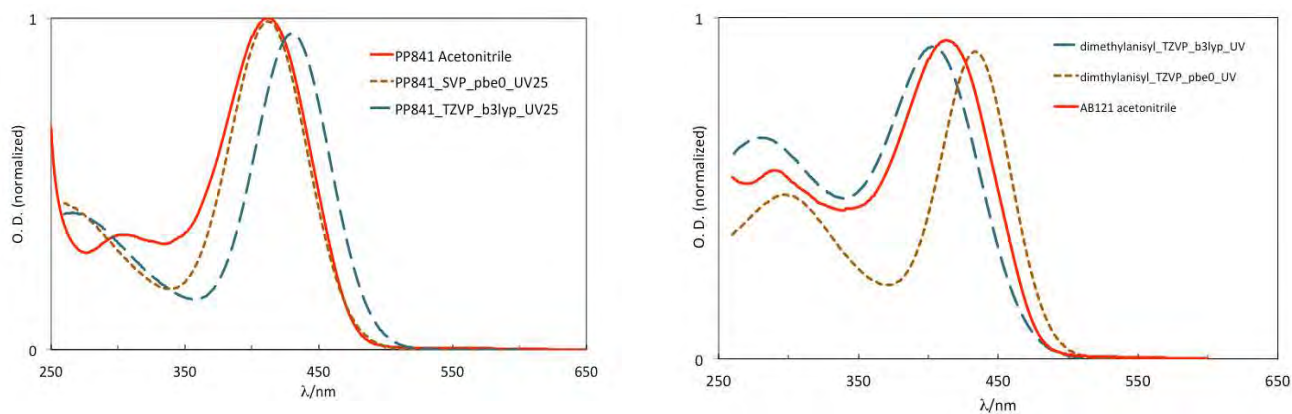


**Figure S7.** Calculated absorption spectra for **2** (left) and **3** (right) using TDDFT/b3lyp/TZVP (blue), TDDFT/pbe0/TZVP (brown) compared to the actual spectrum in acetonitrile (red).



**Table S1:** pK<sub>a</sub> values calculated from Figures S2-S5 in the ground state and excited state\*

	<b>2</b>	<b>3</b>	<b>4</b>	<b>5</b>	<b>2*</b>	<b>3*</b>	<b>4*</b>	<b>5*</b>
pK <sub>a</sub>	— <sup>§</sup>	5.7	5.6	5.8	6.4	6.3	5.3	5.8
R <sup>2</sup>	—	0.9785	0.9555	0.9709	0.983	0.983	0.9901	0.9777

\* Indicates excited state pK<sub>a</sub> calculated by changes in fluorescence

§ Due to overlapping absorptions this number is not reliable.

**Table S2.** Fluorescence Decay Parameters for **2** and **7** in Different Media.

Medium	$\chi^2$	$\tau_1$ (ns)	a <sub>1</sub>	$\tau_2$ (ns)	a <sub>2</sub>
Acetonitrile	1.07	1.40			
<b>7</b> (CH <sub>3</sub> CN)	1.20	1.80			
Water	1.16	1.1	0.71	2.4	0.29
<i>tert</i> -butanol	1.15	1.00			

**Table S3.** Fluorescence Decay Parameters for **3** and **8** in Different Media.

Medium	$\chi^2$	$\tau_1$ (ns)	a <sub>1</sub>	$\tau_2$ (ns)	a <sub>2</sub>
Acetonitrile	1.18	0.90			
<b>8</b> (CH <sub>3</sub> CN)	1.20	1.80			
Water	1.10	0.11	0.85	2.55	0.15
<i>tert</i> -butanol	1.20	0.61			

**Table S4.** Fluorescence Decay Parameters for **4** and **9** in Different Media.

Medium	$\chi^2$	$\tau_1$ (ns)	$a_1$	$\tau_2$ (ns)	$a_2$
Acetonitrile	1.02	2.1			
<b>9</b> (CH <sub>3</sub> CN)	1.20	0.47	0.83	1.42	0.17
Water	1.07	3.1			
<i>tert</i> -butanol	1.00	0.17	0.35	1.8	0.65

**Table S5.** Fluorescence Decay Parameters for **5** and **10** in Different Media.

Medium	$\chi^2$	$\tau_1$ (ns)	$a_1$	$\tau_2$ (ns)	$a_2$
Acetonitrile	1.06	1.54			
<b>10</b> (CH <sub>3</sub> CN)	1.18	0.55	0.85	2.1	0.15
Water	1.04	2.23			
<i>tert</i> -butanol	1.12	0.32	0.20	1.5	0.80

**Table S6.** Temporal Parameters of **2** and **7** in Different Media from Upconversion Experiments.

Medium	$\tau_1$ (ps)	$a_1$	$\tau_2$ (ps)	$a_2$	$\tau_3$ (ps)	$a_3$
CH <sub>3</sub> CN			30	0.05	900	0.95
<b>7</b> (CH <sub>3</sub> CN)	3	0.20	55	0.10	1150	0.70
Water	3	0.55	20	0.30	700	0.15
<i>tert</i> -butanol			80	0.10	900	0.90

**Table S7.** Temporal Parameters of **3** and **8** in Different Media from Upconversion Experiments.

Medium	$\tau_1$ (ps)	$a_1$	$\tau_2$ (ps)	$a_2$	$\tau_3$ (ps)	$a_3$
CH <sub>3</sub> CN	2	0.02	30	0.08	750	0.90
<b>8</b> (CH <sub>3</sub> CN)	2	0.20	50	0.15	1400	0.65
Water	2	0.50	13	0.40	350	0.10
<i>tert</i> -butanol	3	0.10	35	0.20	550	0.70

**Table S8.** Temporal Parameters of **4** and **9** in Different Media from Upconversion Experiments.

Medium	$\tau_1$ (ps)	$a_1$	$\tau_2$ (ps)	$a_2$	$\tau_3$ (ps)	$a_3$
CH <sub>3</sub> CN	2.5	0.10	55	0.15	1500	0.75
<b>9</b> (CH <sub>3</sub> CN)	2	0.50	25	0.20	650	0.30
Water	7	0.35	50	0.15	1900	0.50
<i>tert</i> -butanol	5	0.35	55	0.25	1000	0.40

**Table S9.** Temporal Parameters of **5** and **10** in Different Media from Upconversion Experiments.

Medium	$\tau_1$ (ps)	$a_1$	$\tau_2$ (ps)	$a_2$	$\tau_3$ (ps)	$a_3$
CH <sub>3</sub> CN	2	0.05	50	0.20	1100	0.75
<b>10</b> (CH <sub>3</sub> CN)	2	0.45	20	0.25	500	0.30
Water	4	0.30	60	0.15	1500	0.55
<i>tert</i> -butanol	5	0.45	50	0.25	800	0.30

## NMR spectra for compound 2, 3, 4 and 5

### Compound 2:

**$^1\text{H}$  NMR (300 MHz,  $\text{CDCl}_3$ )  $\delta$  ppm :** 1.40 (s, 3H,  $\text{CH}_3$ ), 1.46 (s, 3H,  $\text{CH}_3$ ), 1.73 (s, 3H,  $\text{CH}_3$ ), 2.71 (d,  $J = 16.6$  Hz, 1H, CH), 2.78 (d,  $J = 16.6$  Hz, 1H, CH), 7.11 (s, 1H, CH), 7.46 (t,  $J = 7.2$  Hz, 2H,  $\text{CH}_{\text{ar}}$ ), 7.50 (s, 1H, CH), 7.55 (t,  $J = 7.2$  Hz, 1H,  $\text{CH}_{\text{ar}}$ ), 7.76 (s, 1H, CH), 8.00 (d,  $J = 7.4$  Hz, 2H,  $\text{CH}_{\text{ar}}$ ).

**$^{13}\text{C}$  NMR (75 MHz,  $\text{CDCl}_3$ )  $\delta$  ppm :** 26.2, 26.5, 28.0, 40.1, 81.4, 86.5, 97.3, 110.7, 113.5, 114.6, 127.9, 128.8, 133.2, 135.2, 141.4, 159.0, 168.1, 168.3, 174.4, 189.8, 190.5.

### Compound 3:

**$^1\text{H}$  NMR (300 MHz,  $\text{CDCl}_3$ )  $\delta$  ppm :** 1.39 (s, 3H,  $\text{CH}_3$ ), 1.42 (s, 3H,  $\text{CH}_3$ ), 1.72 (s, 3H,  $\text{CH}_3$ ), 2.73 (d,  $J = 6.78$  Hz, 2H,  $\text{CH}_2$ ), 3.88 (s, 3H,  $\text{CH}_3$ ), 6.94 (d,  $J = 9.03$  Hz, 2H,  $\text{CH}_{\text{ar}}$ ), 7.10 (s, 1H, CH), 7.45 (s, 1H, CH), 7.75 (s, 1H, CH), 7.99 (d,  $J = 8.85$  Hz, 2H,  $\text{CH}_{\text{ar}}$ ).

**$^{13}\text{C}$  NMR (75 MHz,  $\text{CDCl}_3$ )  $\delta$  ppm :** 26.2, 26.6, 28.0, 40.1, 55.7, 81.3, 86.5, 96.9, 110.7, 113.6, 114.1, 114.7, 128.6, 130.2, 140.9, 158.8, 163.9, 167.3, 168.5, 172.6, 189.9, 190.4.

### Compound 4:

**$^1\text{H}$  NMR (300 MHz,  $\text{CDCl}_3$ )  $\delta$  ppm :** 1.40 (m, 9H, 3 x  $\text{CH}_3$ ), 1.69 (s, 3H,  $\text{CH}_3$ ), 2.70 (d,  $J = 3.2$  Hz, 2H,  $\text{CH}_2$ ), 3.86 (s, 3H,  $\text{CH}_3$ ), 5.47 (q,  $J = 7.0$  et 13.7 Hz, 1H, CH), 6.92 (d,  $J = 8.9$  Hz, 2H,  $\text{CH}_{\text{ar}}$ ), 7.09 (s, 1H, CH), 7.76 (s, 1H, CH), 7.93 (d,  $J = 8.9$  Hz, 2H,  $\text{CH}_{\text{ar}}$ ).

**$^{13}\text{C}$  NMR (75 MHz,  $\text{CDCl}_3$ )  $\delta$  ppm :** 13.5, 26.3, 26.6, 28.4, 40.0, 52.3, 55.6, 81.6, 86.6, 110.8, 112.8, 114.1, 115.9, 128.7, 131.2, 144.4, 159.7, 163.8, 169.1, 172.9, 189.5, 193.7, 197.1.

### Compound 5:

**$^1\text{H}$  NMR (300 MHz,  $\text{CDCl}_3$ )  $\delta$  ppm :** 1.40-1.45 (m, 9H,  $\text{CH}_3$ ), 1.69 (d,  $J = 3.21$  Hz, 3H,  $\text{CH}_3$ ), 2.72 (s, 2H,  $\text{CH}_2$ ), 5.45-5.61 (m, 1H, CH), 7.09 (s, 1H, CH), 7.45-7.57 (m, 3H,  $\text{CH}_{\text{ar}}$ ), 7.76 (s, 1H,  $\text{CH}_{\text{ar}}$ ), 7.95-8.00 (m, 2H,  $\text{CH}_{\text{ar}}$ ).

**$^{13}\text{C}$  NMR (75 MHz,  $\text{CDCl}_3$ )  $\delta$  ppm :** 13.3, 26.3, 26.5, 28.4, 40.0, 52.6, 52.7, 81.6, 86.8, 110.6, 112.8, 115.6, 128.9, 133.4, 135.8, 144.6, 159.8, 169.2, 173.1, 189.7, 193.6, 198.7.

# Excited State Dynamics of Brightly Fluorescent Second Generation Epicocconone Analogs

*Soumit Chatterjee,<sup>†</sup> Peter Karuso,<sup>\*†</sup> Agathe Boulangé,<sup>§</sup> Xavier Franck<sup>§</sup> and Anindya Datta<sup>\*,‡</sup>*

<sup>†</sup> Department of Chemistry & Biomolecular Sciences, Macquarie University, Sydney 2109, Australia

<sup>§</sup> CNRS UMR 6014, C.O.B.R.A. 1, rue Tesnière, 76131 Mont Saint Aignan cedex, Université de Rouen, France

<sup>‡</sup> Department of Chemistry, Indian Institute of Technology Bombay, Mumbai 400076. India

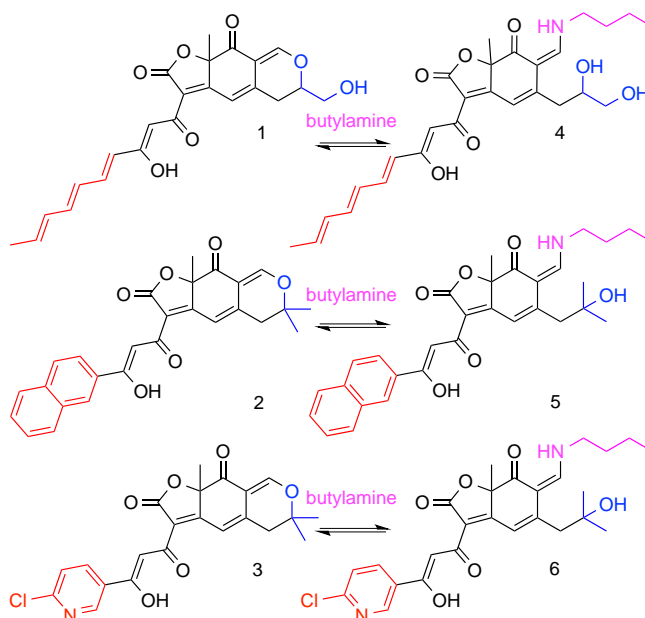
**KEYWORDS:** fluorescence, proteomics, femtochemistry, epicocconone, fluorescent probes.

**ABSTRACT:** The natural product epicocconone, owing to its unique fluorescence properties, has been development into a range of products used in biotechnology, especially proteomics. However, its weak green fluorescence in its native state, while advantageous for proteomics applications, is a disadvantage in other applications that require two-color readouts. Here we report, the photophysical characterization of two brightly fluorescent analogs of epicocconone. These analogs, with naphthyl or pyridyl groups replacing the heptatriene chain, resulted in bright fluorescence in both the native state as well as the long Stokes' shifted enamine. Time-resolved fluorescence studies and DFT calculations were carried out to understand the excited state

processes involved in fluorescence. Results showed the *p*-chloro group on the pyridyl is responsible for the high fluorescence of the native fluorophore. The application of one of these compounds to staining electrophoresis gels is exemplified.

## 1. Introduction

Fluorescence based biological assays require large extinction coefficients and quantum yields in order to achieve the best possible sensitivity. In addition, a large Stokes' shift is desirable, to avoid interference from Rayleigh scattering and minimize inner filter effects.<sup>1</sup> Design and elucidation of the photophysics of new fluorescent probes is an area which continues to be of considerable interest, as the discovery of new fluorescent frameworks has the potential of broadening the range of utility of application of small molecules in biology.<sup>2-6</sup> One approach, in this context, is the discovery of new fluorophores from nature.<sup>7</sup> Epicocconone (**1**) is an example of a cell-permeable latent fluorophore isolated from the fungus *Epicoccum nigrum* using bioassay directed procedures.<sup>8</sup> It fluoresces feebly at 530 nm in aqueous solutions, but reacts reversibly with lysine residues of proteins to yield highly emissive enamines ( $\lambda_{\text{em}} = 610$  nm)<sup>9</sup> that are characterized by high molar absorptivity ( $\sim 10^4$ ), strong orange-red fluorescence ( $\sim 100$  nm Stokes' shift), and low cytotoxicity.<sup>10</sup> These properties have led to a range of commercial applications including cell tracking and two-colour staining<sup>10,11</sup> when multiplexed with other fluorescent probes,<sup>12</sup> detection of proteins in 2D gel electrophoresis (Deep Purple Total Protein Stain™; GE Healthcare),<sup>13</sup> protein quantification in solution (FluoroProfile™; Sigma-Aldrich),<sup>15</sup> live cell imaging (LavaCell™; Fluorotechnics) as well as in kinetic assays for enzymatic digestion.<sup>16</sup>



**Scheme 1.** Reaction of epicocconone (**1**) and analogs **2**, **3** with butylamine (magenta). Replacement of the triene sidechain (red) with naphthyl (**2**) or pyridyl (**3**) increases the quantum yield and replacement of the methanol sidechain (blue) with a gem-dimethyl increases stability.

In our earlier studies with epicocconone and its analogs, we elucidated the nonradiative pathways responsible for the poor fluorescence of **1** compared to **4**. We found that the green emission of **1** is enhanced in the presence of surfactants such as SDS, CTAB and Triton X100 and with  $\alpha$ - and  $\beta$ -cyclodextrins due to the rigidity provided by the micelles and cyclodextrin cavity, restricting photoisomerization thus enhancing fluorescence.<sup>19</sup> In addition, by comparing analogs with an enolizable and unenolizable  $\beta$ -diketone, it was established that photoisomerization of the heptatriene side chain, not the tautomerism of the  $\beta$ -diketone, was the major nonradiative process in **1**.<sup>20,21</sup> Thus analogs where the triene sidechain of **1** was replaced by the isosteric phenyl or anisyl residue possess significantly higher quantum yields.<sup>21</sup> The corresponding butylamine adducts showed similar reversible enamine formation with butylamine, as was evident from the red shifted absorption and emission spectra. However, unlike **1**, they did not show the characteristic increase in quantum yield upon reaction with

amines suggesting that heptatriene photoisomerization was not a significant relaxation pathway for the enamine of epicocconone (**4**). It was also found that intramolecular H-bonding of the enolized  $\beta$ -diketone helped stabilize the excited state of the butylamine adducts.<sup>21</sup> Photobleaching, a major issue with **1**,<sup>14</sup> can be attributed to photoisomerization of the heptatriene chain and/or photooxidation of the alcohol. By replacing the triene with more stable aromatic rings and the diol of **4** with a tertiary alcohol (as in **5** and **6**) it was envisaged that photobleaching and stability would be increased.

The present study is focused on the excited state dynamics of two new epicocconone analogs. In these compounds, the isomerizable heptatriene chain of **1** (Scheme 1, red) is replaced with a naphthyl (**2**) or *p*-chloropyridyl group (**3**). In addition, the oxidizable CH<sub>2</sub>OH group (Scheme 1, blue) is replaced by a gem-dimethyl group. These compounds all reacted with amines, such as butylamine (Scheme 1, magenta) to form enamines (**5**, **6**) in a similar fashion to **1**.

## 2. Results and Discussion

Epicocconone (**1**) and its butylamine adduct (**4**), in acetonitrile, showed absorption maxima at 435 nm and 520 nm respectively, while their emission maxima appear at 535 nm and 615 nm respectively.<sup>21</sup> The absorption maxima at 415 nm of compounds **2** and **3** were blue shifted relative to **1** by 20 nm in acetonitrile. In contrast the butylamine adducts (**5** and **6**), absorbed at 515 and 520 nm respectively (Figure 1), similar to **1**. The emission maxima were found to be very similar to **1** at 530 nm for **2**, at 535 nm for **3**, 610 nm for **5** and 615 nm for **6** respectively in acetonitrile (Figure 1). These data suggested that the side chain (red in Scheme 1) has little effect on the chromophore.



In spite of having very similar absorption and emission wavelengths to **1**, the fluorescence quantum yields of **2** and **3** were quite different (Figure 2, Table 1a) and must be a result of the sidechains. This could be ascribed to the absence of the nonradiative decay pathways resulting from photoisomerization in the heptatriene chain of **1**. The quantum yields of **2** and **3** were found to be 15× and 21× higher than **1** in acetonitrile respectively, while quantum yields of **2** and **3** were 3× and 5× higher than of **1** in *tert*-butanol and 10× and 20× higher in 20 mM SDS solution. In water, quantum yields were found to be 4× and 5× higher for **2** and **3** respectively than **1** (Table 1a, Figure 2).

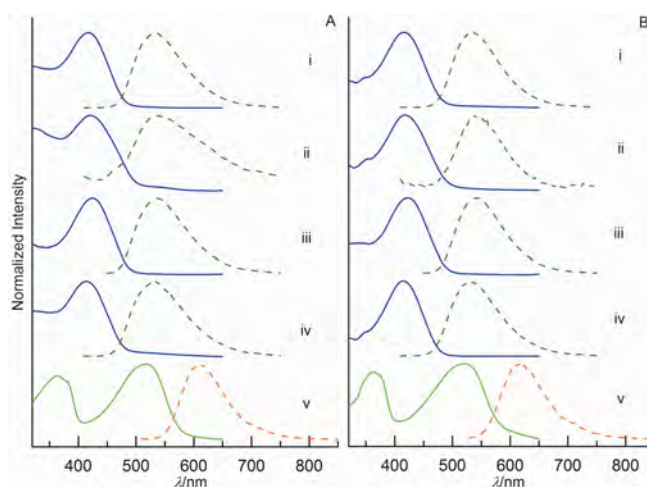


**Figure 1.** A) Normalized absorption (solid) and emission spectra (hashed) of **2** in; i) acetonitrile, ii) water, iii) 20 mM SDS, iv) *tert*-butanol and v) **5** in acetonitrile. B) Normalized absorption and emission spectra of **3** in; i) acetonitrile, ii) water, iii) 20 mM SDS, iv) *tert*-butanol and v) **6** in acetonitrile.

Upon formation of the butylamine adduct of **1** (**4**), the quantum yield increased 5.6× in acetonitrile compared to **1** but quantum yield of **5** decreased almost 1.7× with respect to **2**, while **6** showed almost 3× lower quantum yield with respect to **3** (Table 1b, Figure 2). Large Stokes' shifts were observed in all cases, in accordance with putative enamine formation. All the

enamines (**4-6**) actually had quite similar quantum yields, absorption spectra and Stokes' shifts (Figure 2). This observation confirmed that the photophysics/excited state dynamics of the enamines is also dominated by the bicyclic core (Figure 1; in black) and that the side chain has little if any affect.

**Table 1a.** Molar extinction coefficients and quantum yields of compounds **1-3** in different solvents.

solvent	$\epsilon$ (Lit.M <sup>-1</sup> cm <sup>-1</sup> )			$\phi_f$		
	<b>1</b> <sup>a</sup>	<b>2</b> <sup>b</sup>	<b>3</b> <sup>b</sup>	<b>1</b>	<b>2</b>	<b>3</b>
Acetonitrile	13400	14575	27610	0.026	0.386	0.557
Water	11400	1200	15650	0.009	0.034	0.047
20 mM SDS	11500	2500	20400	0.023	0.255	0.471
<i>tert</i> -butanol	15600	5670	16830	0.068	0.221	0.338

<sup>a</sup> at  $\lambda = 435$  nm; <sup>b</sup> at  $\lambda = 415$  nm

**Table 1b.** Molar extinction coefficients and quantum yields of compounds **4-6**.

solvent	$\epsilon$ (Lit.M <sup>-1</sup> cm <sup>-1</sup> )			$\phi_f$		
	<b>4</b> <sup>a</sup>	<b>5</b> <sup>b</sup>	<b>6</b> <sup>b</sup>	<b>4</b>	<b>5</b>	<b>6</b>
Acetonitrile	13000	17546	24850	0.147	0.225	0.170

<sup>a</sup> at  $\lambda = 435$  nm; <sup>b</sup> at  $\lambda = 415$  nm

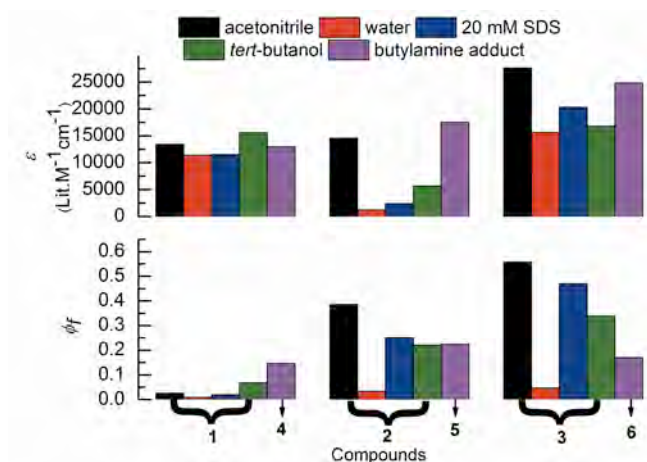


**Figure 2.** Comparison of molar absorptivity coefficients and quantum yields of epicocconone (**1**) with **2** and **3** in acetonitrile (black), water (red), 20 mM SDS (blue), *tert*-butanol (green) and their respective butylamine adducts (**4-6**) in acetonitrile (purple).

The high quantum yield of **3** (>55% *c.f.* epicocconone; <3%) was accompanied by a 2× high molar absorptivity (Figure 2) in acetonitrile (Table 1a). This represents a dramatic improvement in photophysical characteristics (brightness) over **1**. However, the butylamine adduct (**6**) did not maintain these impressive characteristics, with the quantum yield dropping to 17%, quite similar to **4**. To better understand these potentially useful photophysical characteristics, we undertook nanosecond and femtosecond decay studies.

The fluorescence decays in nanosecond time regime were in line with the corresponding quantum yields of **2** and **3** in different solvents. Decays were found to be a single exponential for **2** in acetonitrile and in *tert*-butanol, while in water, a bimodal decay was observed (Figure 3A, Table 2a). In the case of **3**, similar observations were made (Figure 3B, Table 2b). A slower decay of **2** in acetonitrile than in *tert*-butanol was in accordance with the observed higher quantum yield of **2** in acetonitrile. Similar observations were recorded for **3**. A dominant faster component in water for **2** was in agreement with its lower quantum yields in this solvent. This

faster component disappeared in 20 mM SDS. However, there was an apparent anomaly in water. The dominant decay with a  $t$  of 1.1 ns (Table 2b) implied that **3** should have a higher quantum yield in water than in organic solvent, which was not the case. This observation suggested there might be an ultrafast relaxation pathway that is missed by time-correlated single-photon counting experiments on the nanosecond timescale.

The enamine of **3** (**5**) exhibited a bimodal decay and had a faster component similar to **2** in water, but with a significantly lower relative contribution, which explained the higher quantum yield of **5** over **2** in water. The fluorescence decay of **6**, on the other hand, was a single exponential with a lifetime comparable with that of **3** in *tert*-butanol and slightly lower than the average lifetime of **3** in water. Again, the trend in quantum yields did not match with the observed trend in average lifetimes calculated from the nanosecond time resolved fluorescence experiments of **3** or **6** (Table 2a) where **6** showed much lower quantum yield than **3** in *tert*-butanol yet had 4× higher quantum yield than **3** in water (Table 1a).

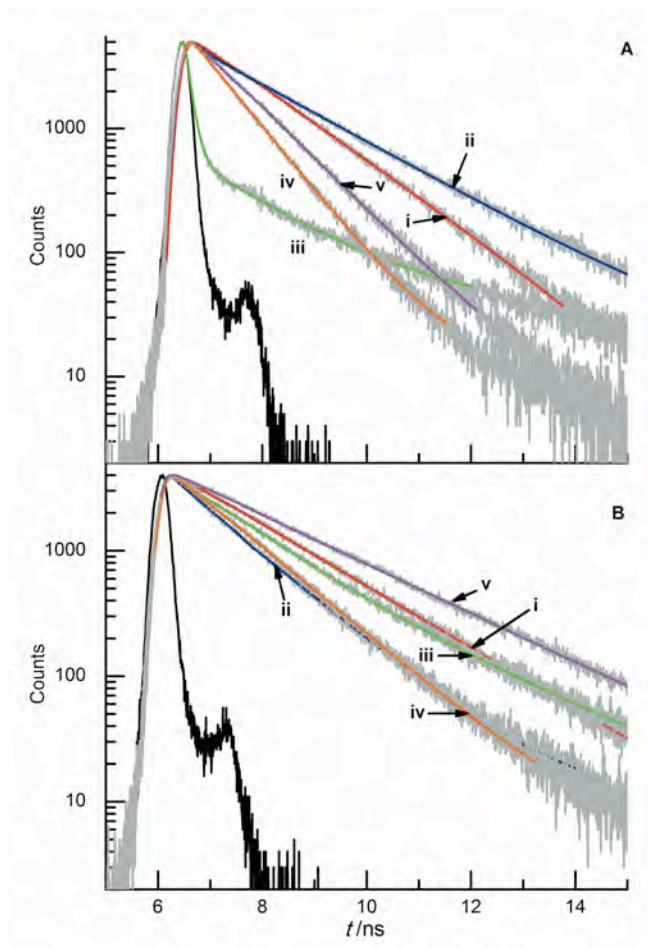


**Figure 3.** Nanosecond fluorescence decay traces of A) **2** and B) **3** in; i) acetoneitrile, ii) acetoneitrile with butylamine, iii) water, iv) *tert*-butanol, v) 20 mM SDS;  $\lambda_{\text{ex}} = 406$  nm and  $\lambda_{\text{em}} = 530$  nm for **2** and  $\lambda_{\text{em}} = 535$  nm for **3** in all solvents.  $\lambda_{\text{em}} = 615$  nm for **5** and  $\lambda_{\text{em}} = 620$  nm for **6** in acetoneitrile.

**Table 2a.** Fluorescence Decay Parameters for **2** and **5** in Different Solvents

solvent	$\chi^2$	$\tau_1$ (ns)	$a_1$	$\tau_2$ (ns)	$a_2$	$\langle\tau\rangle$ (ns)
Acetonitrile	1.01	1.46	1.00			1.46
<b>5</b> (CH <sub>3</sub> CN)	1.03	1.87	0.70	0.17	0.30	1.36
Water	1.20	1.63	0.05	0.12	0.95	0.20
20 mM SDS	1.02	0.84	1.00			0.84
<i>tert</i> -butanol	1.10	1.04	1.00			1.04

$\tau_i$  is the fluorescence lifetime and  $a_i$  the relative amplitude.  $\langle\tau\rangle$  is the average lifetime ( $\sum a_i\tau_i$ ).  $\chi^2$  is the ratio of experimental and model standard deviations.

**Table 2b.** Fluorescence Decay Parameters for **3** and **6** in Different Solvents

solvent	$\chi^2$	$\tau_1$ (ns)	$a_1$	$\tau_2$ (ns)	$a_2$	$\langle\tau\rangle$ (ns)
Acetonitrile	1.08	1.76	1.00			1.76
<b>6</b> (CH <sub>3</sub> CN)	1.05	1.28	1.00			1.28
Water	1.07	1.10	0.67	2.27	0.33	1.49
20 mM SDS	1.13			2.20	1.00	2.20
<i>tert</i> -butanol	1.02	1.24	1.00			1.24

$\tau_i$  is the fluorescence lifetime and  $a_i$  the relative amplitude.  $\langle\tau\rangle$  is the average lifetime ( $\sum a_i\tau_i$ ).  $\chi^2$  is the ratio of experimental and model standard deviations.

In order to rationalize this anomaly, the dynamics were studied in the femtosecond-picosecond time domain (Figures 4 and 5). In acetonitrile, **2** had the slowest decay (Figure 4A and 4C, Table 3a) but the corresponding enamine (**5**) showed an ultrafast component of 2-3 ps that made a 20% contribution to the decay. The slower (ns) component was found to be similar

to that for **2** and thus the ultrafast component could be held responsible for the lower quantum yield of **5** compared to **2** in acetonitrile.

In *tert*-butanol (Figure 4B and 4D, Table 3a), the ultrafast component was not present and could not account for the similar quantum yields of **2** in *tert*-butanol and **5** in acetonitrile. As stated above, **2** and **3** possess different excited state dynamics compared to their butylamine adducts (**5** and **6**) and that the aryl group does not appear to participate in the excited state dynamics of the chromophore. However, a sub-picosecond component of ~600 fs is a significant contributor to the overall decay for **2** in water (Figure 4B and 4D, Table 3a). It was found that the decay of **2** in water was complete within 30 ps (Figure 4B). The origin of this fast decay is yet to be understood clearly, but our earlier experiments with different analogs of **1** indicated that intramolecular H-bonding of the diketone is affected by the intermolecular H-bonding with water and destabilisation of the excited state.<sup>21</sup> This may be the case with these compounds as well.

In 20 mM SDS, the ultrafast decay of **2** was quite similar to that in *tert*-butanol (Figure 4B and 4D), which might be expected considering the similarities in viscosity and dielectric of these two solvents.

Decay of **3** was found to be much faster than **2** in acetonitrile primarily due to an ultrafast component with a 3 ps lifetime (Figure 5A and 5C, Table 3b). However, the quantum yield of **3** was higher than **2** (Figure 2, Table 1a). This anomaly could not be explained from the temporal parameters but could arise from an internal charge transfer, for example. Compound **6** had similar lifetimes and respective contributions to **5** and a comparison between the temporal parameters of the two accounted for the slightly lower quantum yield of **6** in acetonitrile (Tables 2 and 3). The comparison of quantum yields and the lifetime parameters of **5** and **6** with **2** and **3**

supports our hypothesis of distinct excited state dynamics of the amine adducts compared to the native compounds. It is also clear that the side chain of the diketo moiety does not contribute to the excited state dynamics to any major degree with the possible exception of the anomaly noted above for **3**.

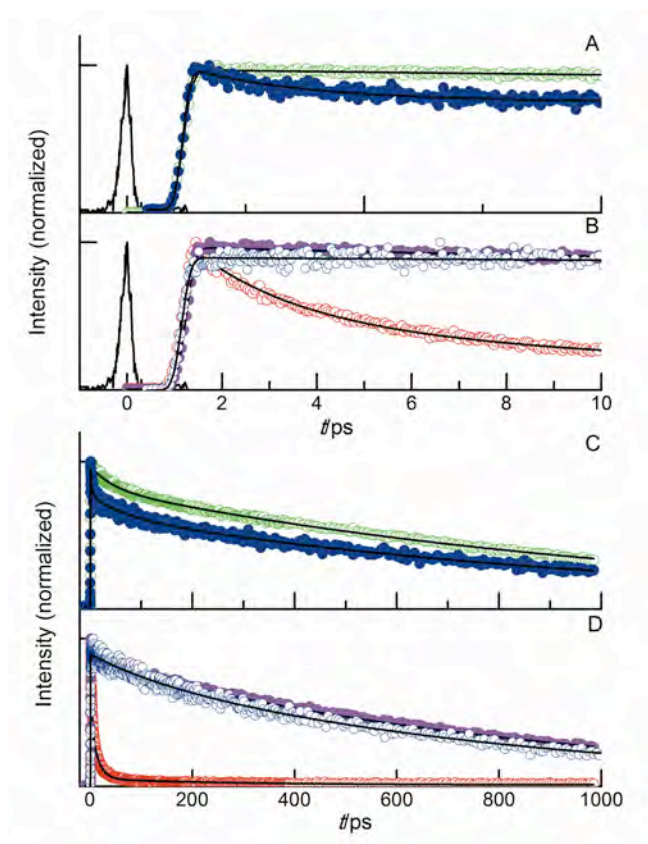


**Figure 4.** Femtosecond fluorescence transients of; A) **2** (○) and **5** (●) in CH<sub>3</sub>CN, B) **2** in water (○), 20 mM SDS (○) and in *tert*-butanol (●); C) **2** (○) and **5** (●) in CH<sub>3</sub>CN and D) **2** in water (○), 20 mM SDS (○) and in *tert*-butanol (●).  $\lambda_{\text{ex}} = 400$  nm and  $\lambda_{\text{em}} = 530$  nm for **2** in all solvents and  $\lambda_{\text{em}} = 610$  nm for **5** in acetonitrile. The solid black lines denote the lines of best fit. The fitting parameters are provided in Table 3a. The cross-correlation function of the laser pulse in A and B is shifted, for the sake of clarity.



**Table 3a.** Temporal Parameters for **2** and **5** Derived from Upconversion Experiments.

solvent	$\tau_1$ (ps)	$a_1$	$\tau_2$ (ps)	$a_2$	$\tau_3$ (ps)	$a_3$
CH <sub>3</sub> CN			45	0.15	1120	0.85
<b>5</b> (CH <sub>3</sub> CN)	2.3	0.20	65	0.15	1050	0.65
Water	0.6	0.30	5	0.50	30	0.20
20 mM SDS			140	0.15	810	0.85
<i>tert</i> - butanol			15	0.15	850	0.85

$\tau_i$  is the fluorescence lifetime and  $a_i$  the relative amplitude.

**Table 3b.** Temporal Parameters for **3** and **6** Derived from Upconversion Experiments

solvent	$\tau_1$ (ps)	$a_1$	$\tau_2$ (ps)	$a_2$	$\tau_3$ (ps)	$a_3$
CH <sub>3</sub> CN	3.2	0.45	40	0.20	970	0.35
<b>6</b> (CH <sub>3</sub> CN)	2.5	0.15	60	0.10	840	0.75
Water	2.4	0.45	30	0.30	730	0.25
20 mM SDS	2.0	-0.15			3300	1.15
<i>tert</i> - butanol			33	0.10	1100	0.90

$\tau_i$  is the fluorescence lifetime and  $a_i$  the relative amplitude.

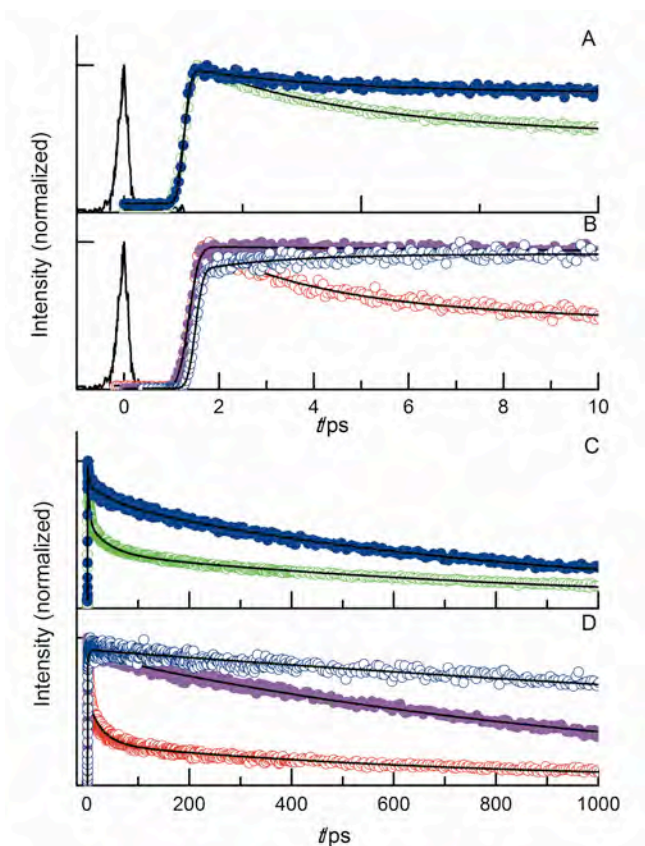


**Figure 5.** Femtosecond fluorescence transients of; A) **3** (○) and **6** (●) in CH<sub>3</sub>CN; B) **3** in water (○), 20 mM SDS (○) and in *tert*-butanol (●); C) **3** (○) and **6** (●) in CH<sub>3</sub>CN in a full scale of 1 ns and; D) **3** in water (○), 20 mM SDS (○) and in *tert*-butanol (●).  $\lambda_{\text{ex}} = 400$  nm and  $\lambda_{\text{em}} = 535$  nm for **3** in all four solvents and  $\lambda_{\text{em}} = 615$  nm for **6** in acetonitrile. The solid black lines denote the lines of best fit. The fitting parameters are provided in Table 3a. The cross-correlation function of the laser pulse in A and B is shifted, for the sake of clarity.

In water and *tert*-butanol, the fluorescence decay for **3** was found to be slower than **2**, which falls in line with higher quantum yield of **3** over **2** in these solvents. However, in 20 mM SDS, **3** displayed a risetime of 2 ps, the magnitude of which was almost the same with the ultrafast decay found for **3** in water (Figure 5B). This suggests an internal charge transfer (ICT) from the chloro-pyridyl group to the epicoconone nucleus that remains unaffected by the

hydrophobic environment of SDS micelles. The suppression of the ultrafast deactivation process for **3** leads to an increase in the fluorescence lifetime to 3.3 ns (Table 3b) in SDS solution and explains the higher quantum yield of **3**.

Both **2** and **3** exhibited slower decays in all the solvents studied (Figure 6) with respect to **1**. In particular, the ultrafast decay in water, characteristic of epicocconone, was absent in **3** altogether (Figure 6A). This explains the high quantum yield of **3** in water compared to **1**. However, the ultrafast dynamics alone is not adequate to explain the higher quantum yield of **3** over **2** in acetonitrile. In polar solvents like water and *tert*-butanol though, in the relative quantum yields of **1**, **2** and **3** were in line with their picosecond lifetimes.

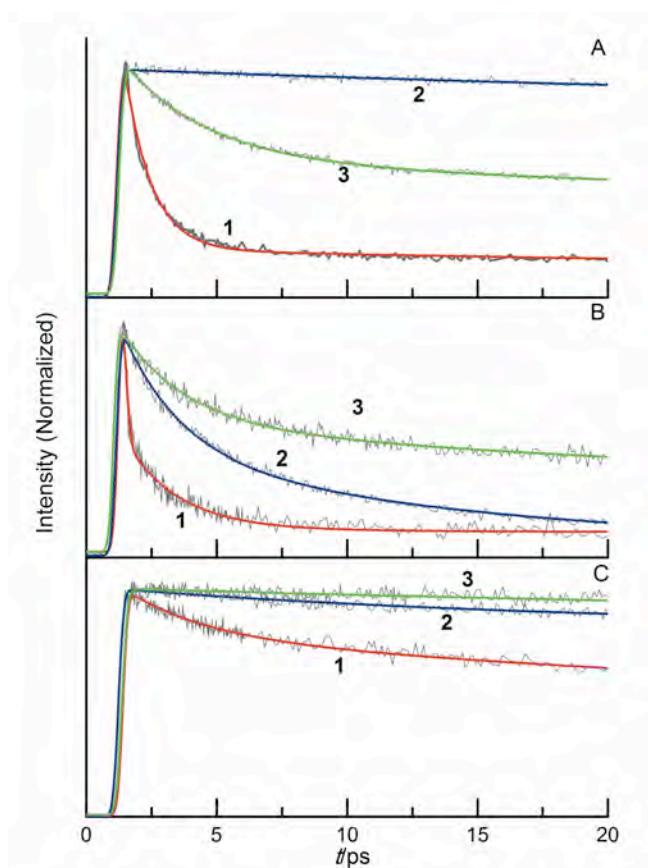


**Figure 6.** Comparison of femtosecond-picosecond decay traces between **1** (red), **2** (blue) and **3** (green) in A) acetonitrile, B) water and C) *tert*-butanol.

These data can be rationalized further by comparison with other fluorophores with related functional groups. For example, 1-aminofluorenone, where there is an intramolecular H-bonding network, there is a 7.5-9 ps Excited State Intramolecular Proton Transfer (ESIPT). In polar protic solvents, the intramolecular H-bonding network between amino and ketone is disrupted by solvent H-bonding leading to destabilization of the excited state.<sup>22,23</sup> The role of hydrogen bonding networks in ESIPT processes has also been established in *N,N*-dimethylanilino-1,3-diketone and curcumin, both contain a b-keto-enol group similar to **1-6** and a propensity for charge transfer mediated ESIPT, that is on the 4-5 ps timescale.<sup>24,25</sup> From these studies, and comparing with our data, it appears that the shorter components ( $\tau_1$ ) in the 2-3 picosecond regime for **3** in acetonitrile and 20 mM SDS (Table 3b) can be associated with its internal charge transfer, while in water this ubiquitous short component in **2** and **3** (0.6/2 ps) is most likely due to intermolecular proton transfer with solvent. Desolvation of water, which takes place in sub-picosecond time scale,<sup>26</sup> is unlikely but cannot be ruled out. The slower process ( $\tau_2$ ), which ranges from 15-50 ps, can then be ascribed to the conformational relaxation of the intramolecular b-diketo H-bond in aprotic solvents or intermolecular H-bonded species with polar protic solvents. The longest lifetime decays ( $\tau_3$ ) can be assigned to the emissive  $S_1$  state.

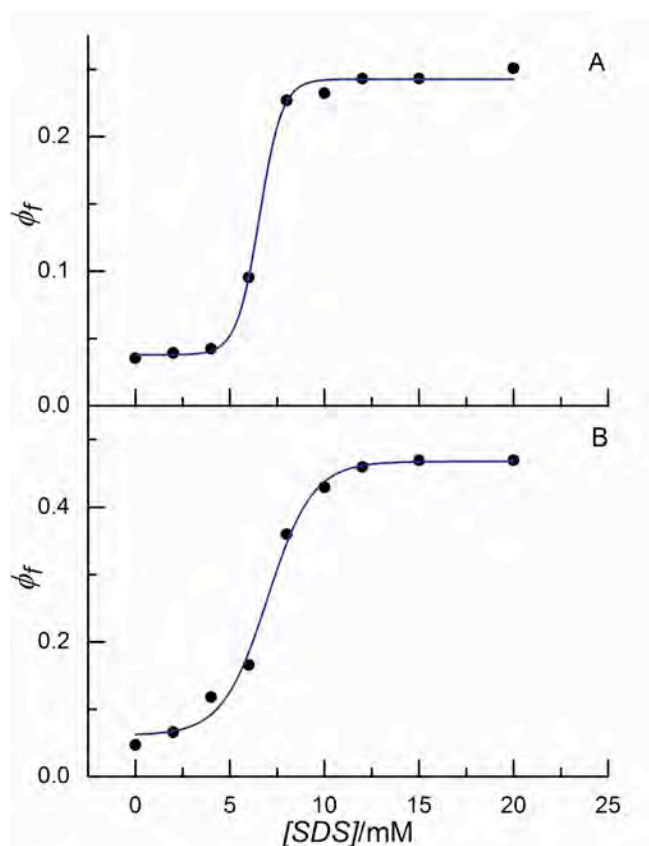


**Figure 7.** Quantum yield of (A) **2** and (B) **3** in response to SDS concentration. The CMC for SDS is 8.2 mM.

The difference in fluorescence quantum yields between the two analogs in different solvents can also be explained by the interplay between radiative and non-radiative decay rates. In acetonitrile, compound **3** had 4× higher radiative and 2× higher non-radiative rate constant than **2**. The higher quantum yield of **3** in acetonitrile (Figure 2, Table 1a) could thus be rationalized by the higher radiative rate of **3**. Similarly, in water, the non-radiative rate constant was ~19× faster for **2** than for **3** while the radiative rate constant for **2** is ~14× times faster than for **3** (Table 4a) resulting in the dominance of non-radiative decays leading to a lower quantum yield for **2** (Table 1a). Suppression of radiative as well as nonradiative rate was observed for both **2** and **3** in 20 mM SDS with respect to that in water. This effect was strongest for the non-

radiative decays and was in line with these molecules being incorporated inside the SDS micelles, that have a higher viscosity and lower dielectric, resulting in higher quantum yields.

Titration of **2** and **3** with SDS (Figure 7) showed an increase in quantum yield above the critical micelle concentration (CMC) confirming that these molecules are readily incorporated into micelles. The increase in quantum yield was also reflected in an increase in decay lifetimes with increasing SDS, indicating that the excited state is also more stable inside the hydrophobic and/or viscous environment of the micelle.

**Table 4a.** Average lifetimes, radiative and nonradiative rate constants for compounds **2** and **3**.

	<b>2</b>			<b>3</b>		
solvent	$\langle \tau \rangle^a$	$k_R$ (ns <sup>-1</sup> ) <sup>b</sup>	$k_{NR}$ (ns <sup>-1</sup> ) <sup>c</sup>	$\langle \tau \rangle^a$	$k_R$ (ns <sup>-1</sup> ) <sup>b</sup>	$k_{NR}$ (ns <sup>-1</sup> ) <sup>c</sup>
CH <sub>3</sub> CN	0.96	0.40	0.64	0.35	1.60	1.27
Water	0.01	3.40	96.6	0.19	0.25	5.01
20 mM SDS	0.71	0.36	1.05	3.79	0.12	0.14
<i>tert</i> -butanol	0.72	0.30	1.08	0.99	0.34	0.67

<sup>a</sup>  $\langle \tau \rangle = \sum a_i \tau_i$  from upconversion experiments.

$$^b k_R = \frac{\varphi_f}{\tau}, \quad ^c k_{NR} = \frac{1-\varphi_f}{\tau}$$

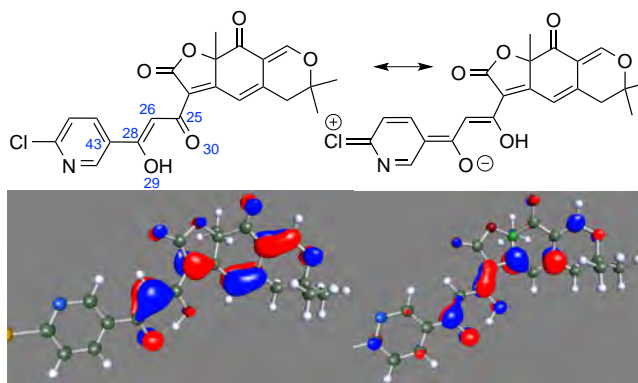
**Table 4b.** Average lifetimes, radiative and nonradiative rate constants for compounds **5** and **6**.

	<b>5</b>			<b>6</b>		
solvent	$\langle \tau \rangle^a$	$k_R$	$k_{NR}$	$\langle \tau \rangle^a$	$k_R$	$k_{NR}$
		(ns <sup>-1</sup> ) <sup>b</sup>	(ns <sup>-1</sup> ) <sup>c</sup>		(ns <sup>-1</sup> ) <sup>b</sup>	(ns <sup>-1</sup> ) <sup>c</sup>
CH <sub>3</sub> CN	0.69	0.33	1.12	0.64	0.27	1.30

<sup>a</sup>  $\langle \tau \rangle = \sum a_i \tau_i$  from upconversion experiments.

$$^b k_R = \frac{\varphi_f}{\tau}, \quad ^c k_{NR} = \frac{1-\varphi_f}{\tau}$$

In case of **3**, a charge transfer from the pyridyl group could play a stabilizing role in acetonitrile by providing more of a double bond character to the C43-C28 bond (Scheme 2) while keeping the intramolecular H-bonding of the b-diketone system intact. This would lead to higher radiative rate in acetonitrile where intramolecular H-bonding is not affected and explains the higher quantum yield of **3** in acetonitrile over *tert*-butanol.



**Scheme 2.** Resonance hybrids of **3** for HOMO (left) and LUMO (right) orbitals below.

To test this theory, high level DFT calculations (RI-DFT-D3//BP86/TZVPP) using a continuum solvent model (COSMO) for acetonitrile were carried out on **3**. The HOMO and the LUMO of the ground state supported an ICT where the HOMO does not involve the pyridine group but the LUMO does (Scheme 2). Furthermore, bond lengths were measured for the ground state ( $S_0$ ) and the geometry optimized singlet first excited state ( $S_1$ ) (Tables S4 and S5;

Supporting Information). It was found that removing either the chlorine or nitrogen had little effect on the bond lengths in  $S_0$  ( $\Delta r \leq 0.3$  pm). However, in  $S_1$  the C43-C28 bond length was ~4.8 pm shorter for **3** compared to **3** with no chlorine. In compensation, C26-C28 is longer by ~4.2 pm suggesting that C43-C28 has more of a double bond character in the excited state when a chlorine is present (Scheme 2) that would inhibit rotation around C43-C28. This could explain the higher quantum yield of **3** in all solvents compared to **1**.<sup>20</sup> Replacement of the nitrogen with CH had less of an effect.

A similar inference can be drawn between **5** and **6** (Table 4b), where a somewhat higher quantum yield for **5** was found to be a result of the interplay between the higher radiative rate constant and lower non-radiative rate constant for **5**. Similar radiative and non-radiative rates for **5** and **6** suggest that the excited state dynamics of the butylamine adducts is not a function of the substituent on the acyl sidechain but depends on the heteronuclear ring system that is ubiquitous in all epicocconone analogs.

The increase in fluorescence associated with increasing SDS and the marked shift in fluorescence emission upon enamine formation suggested that these compounds could be used to stain proteins in SDS polyacrylamide electrophoresis (PAGE). Comparison of the protein staining ability in 1D protein gel electrophoresis (Figure 8), shows comparable results between **1** and **3**. Specifically, both dyes stained  $\alpha$ -lactoglobulin (lowest band) the best and soybean trypsin inhibitor (second last band) the least. The limits of detection for the 6 proteins are quite similar and in the range of 0.4-1.5 ng/band. However, **3** was not as sensitive as the natural product **1** for 1D PAGE staining but this may be due to other factors than just photophysical characteristics. For example in the gel after fixation there is a high concentration of SDS around the proteins and



the pH is around 2.5, which may suit **1** more than **3**. In addition, the higher background of gels stained with **3** is a result of **3** being an order of magnitude more fluorescent than **1** (Table 1a).

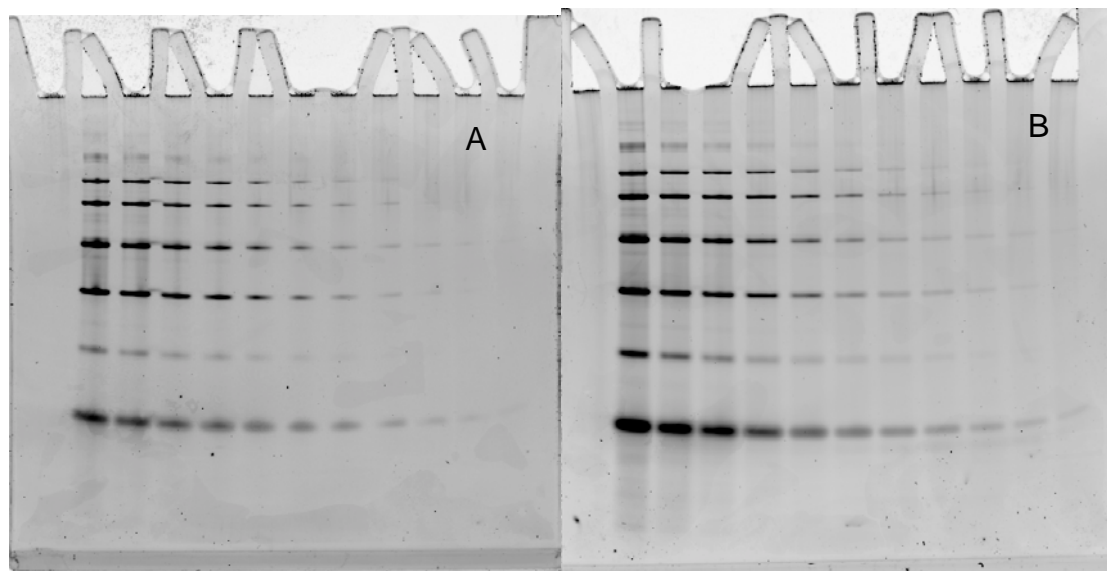


**Figure 8.** Serial dilution of 6 proteins from 128 ng to 128 pg/spot and stained with 1 mg/mL (100 mL) of **3** (A) and Deep Purple (B) that contains **1** at ~1 mg/mL. Gels were scanned together on a Typhoon laser scanner (532 nm) and contrast and brightness optimized automatically (ImageQuant).

### 3. Conclusions

In our previous studies we established photoisomerization of the heptatriene side chain as the major nonradiative process in epicocconone (**1**), resulting in low to very low quantum yields.<sup>19-21</sup> In order to design and synthesize analogs with higher quantum yields, the heptatriene chain needed to be reengineered to eliminate photoisomerization, while the keto-enol moiety needed to be conserved the large Stokes' shift for the butylamine adducts.<sup>27</sup> This was achieved in

the design and synthesis of **2** and **3** that had significantly higher fluorescence in their native states than epicocconone with quantum yields up to 56% for **3** compared to <3% for epicocconone (**1**) under the same conditions. The analogs retained the characteristic reaction with amines of **1** to form red fluorescent enamines. The fact replacement of the isomerizable heptatriene with unisomerizable and bulky naphthyl and *p*-chloropyridyl groups increased quantum yields demonstrated the importance of photoisomerization in the non-radiative pathways for this class of fluorophore. In addition, we have demonstrated the importance of intramolecular H-bonding in the  $\beta$ -keto-enol group, which helps stabilize the excited states and thus leads to large increases in quantum yields in hydrophobic and viscous environments such as in cellular membranes or around proteins in SDS-PAGE. This keto-enol internal H-bond becomes less important in water, resulting in an order of magnitude lower quantum yields, which is recovered in 20 mM SDS. DFT calculations showed that in the excited state, the chloro group of **3** was critical for stabilizing the  $\beta$ -keto-enol by inhibiting rotation of the pyridyl group; another potential source of non-radiative decay of the excited state.

The butylamine adducts (**4-6**) display similar dynamics that is quite different to the native fluorophores (**1-3**). The pyridyl analog (**3**) is much more fluorescent than the others, due to hyperconjugation to the Cl atom. This was particularly evident from our computational studies and is supported by experimental results presented here. These results and titrations with SDS suggested **2** and **3** could be useful synthetic alternatives to epicocconone for protein staining and as dual-stains in biotechnology; emitting strongly in the green in their native states and equally strongly in the red once conjugated to amines such as lysine residues in proteins. This is quite unlike the natural product that is essentially non-fluorescent in its native state. The pyridyl analog (**3**) in particular is highly fluorescent in both the native and conjugated forms but

fluoresces different colors (green and red respectively) making this compound potentially useful in tw-color or turn-on/turn-off applications.

Staining of proteins in electrophoresis gels showed comparable performance between the commercial product (Deep Purple<sup>®</sup>; containing **1**) and analog **3** without protocol optimization. This study points the way to the design of improved analogs with electron donating groups that are currently underway and will be reported in due course.

## 4. Experimental Section

The synthesis of the compounds (**2**, **3**) is described elsewhere.<sup>27</sup> A solution of each compound in DMSO (1 mg/mL) was used as the stock solution for each experiment. Spectroscopy grade acetonitrile (Spectrochem, Mumbai, India) was distilled over CaH<sub>2</sub> and the distillate passed over activated neutral alumina prior to each experiment. *tert*-Butanol (spectroscopy grade, Spectrochem, Mumbai, India) was used as received. *n*-Butylamine (Qualigens, Mumbai, India) is dried with solid KOH and then refluxed with and distilled from P<sub>2</sub>O<sub>5</sub>.

The absorption and fluorescence spectra have been recorded on JASCO V 530 spectrophotometer and Varian Cary Eclipse fluorimeter, respectively. The emission spectra were recorded with excitation at 400 nm with excitation and emission slit widths of 5 nm and at 500 nm excitation for the butylamine adducts. The absorbencies of the solutions were kept below 0.1 to prevent inner filter effects for steady state measurements and for picosecond-nanosecond time-resolved experiments. The absorbencies of the solutions were kept at ~1.0 for the upconversion experiments. The absorption and emission spectra were recorded before and after the femtosecond fluorescence decays in order to verify that the samples do not photodegrade.

Fluorescence quantum yields ( $\phi_f$ ) of the compounds in neat solutions were calculated after correction for changes in absorbance using Lucifer Yellow CH ( $f_f = 0.21$ ) as the reference.<sup>28</sup> Fluorescence quantum yields ( $\phi_f$ ) of the butylamine adducts were calculated after correction for changes in absorbance using rhodamine 6G ( $\phi_f = 0.94$ ) as the reference.<sup>29</sup> Time-resolved fluorescence in picoseconds-nanosecond time regime were measured using a picosecond pulsed diode laser based time-correlated single photon counting (TCSPC) instrument (IBH, United Kingdom) set at the magic angle with  $\lambda_{ex} = 406$  nm.<sup>30</sup>

In our femtosecond upconversion setup (FOG 100, CDP), the sample was excited at 400 nm using the second harmonic of a mode-locked Ti-sapphire laser (Tsunami, Spectra Physics) pumped by a 5W Millennia (Spectra Physics) laser. The fundamental beam (800 nm) was frequency doubled in a nonlinear crystal (1 mm BBO,  $\theta = 25^\circ$ ,  $\phi = 90^\circ$ ). The fluorescence emitted from the sample was upconverted in a nonlinear crystal (0.5 mm BBO,  $\theta = 38^\circ$ ,  $\phi = 90^\circ$ ) using the fundamental beam as a gate pulse. The upconverted light is dispersed in a monochromator and detected using photon counting electronics. A cross-correlation function obtained using the Raman scattering from ethanol displayed a full width at half-maximum (fwhm) of 300 fs. The femtosecond fluorescence decays were fitted using a Gaussian function of the same FWHM as the excitation pulse. The fluorescence decays were recorded at the magic angle polarization with respect to the excitation pulse on a FOG 100 fluorescence optically gated upconversion spectrometer. The resolution was in appropriate multiples of the minimum step size of the instrument, i.e. 0.78 fs/step. The decays were analyzed by iterative reconvolution using a homemade program.<sup>31</sup>

Compound **3** was dissolved in DMSO (10 mg/mL) and diluted to 1 mg/mL with water. One vial of GE low molecular weight markers (GE Healthcare; 17-0446-01, 575 mg of total

protein) was diluted with 1× LDS buffer (250 mL Invitrogen 4× LDS buffer (NP0008), 100 mL 1M DTT, 650 mL water) to achieve a final concentration of 51.2 µg/mL of soybean trypsin inhibitor (STI). The stock solution was serially diluted (2×) from 12.8 µg/mL to 0.125 µg/mL (based on STI). Protein solutions (10 µL) and loading buffer (10 µL) were mixed.

12% Bis-Tris Novex NuPage (Invitrogen NP0342BOX), 1 mm thick gels were loaded with the dilution series (20 µL of each dilution) and run in Xcell SureLock minigel systems (Invitrogen, EI0001) at 150 V for approximately 65 min (buffer front just off gel) using MES buffer (50 mM MES, 50 mM Tris, 1 mM EDTA, 0.1% SDS, pH 7.3). The gels were then removed and fixed in 15% ethanol (v/v), 1% citric acid (100 mL) on a rocker for 1 h and then with fresh fixative overnight. The next day, the fixative (100 mL) was replaced and after 1 hr, drained and stained with either Deep Purple Total Protein Stain (GE Healthcare, RPN6306) or **3** (50 µL of a 1 mg/mL solution in DMSO) in sodium borate buffer (50 mL; 100 mM, pH 10.9). These concentrations resulted in approximately 1 µg/mL active fluorophore in each case. After 1 h staining the gels were de-stained in 15% ethanol (100 mL) for 30 minutes and transferred to fixative (100 mL; 15% ethanol (v/v), 1% citric acid (w/v)) for 30 minutes. All gels were imaged using a Typhoon Trio (GE, 63-0055-87) using the 532 nm Nd-YAG laser, 540 PMT, 610BP30 filter, 100 µm resolution and normal sensitivity.

Density Functional Theory (DFT) calculations were run using Turbomole 6.5 (Cosmologic, GmbH & Co). Theoretical ground state geometries for all conformations were calculated (RI-DFT-D3//BP86/TZVPP)<sup>32</sup> in continuum solvent model for acetonitrile (COSMO).<sup>33</sup> Ground state and the singlet first excited state geometries and energies were compared using RI-DFT//BP86/TZVPP calculations in vacuum (see Supporting Information) using the default parameters except a finer gridsize of m5<sup>34</sup> was used throughout.

## ASSOCIATED CONTENT

**Supporting Information.** Computational results, compound coordinates, steady state spectra and fluorescence decay data. This material is available free of charge via the Internet at <http://pubs.acs.org>.

## AUTHOR INFORMATION

### Corresponding Authors

<sup>\*,†</sup> Department of Chemistry & Biomolecular Sciences Macquarie University, Sydney NSW, 2109, Australia Fax: (+612-9850-8313) E-mail: [peter.karuso@mq.edu.au](mailto:peter.karuso@mq.edu.au).

<sup>\*,‡</sup> Department of Chemistry, Indian Institute of Technology Bombay, Mumbai 400076, India. Fax: (+9122-2576-7152) E-mail: [adutta@iitb.ac.in](mailto:adutta@iitb.ac.in)

### Author Contributions

The manuscript was written through contributions of all authors. All authors have given approval to the final version of the manuscript.

### Funding Sources

This research is supported by the Australian Research Council (DP0877999) to P.K. and A.D. and a SERC DST grant to A.D. Support from a FIST grant to the Department of Chemistry, IIT Bombay, is gratefully acknowledged. We gratefully acknowledge the Region Haute Normandie for financial support to A.B. and the Australian Research Council for support of S.C. We thank the Ministere des Affaires Etrangeres (France) and the Department of Innovation, Industry, Science and Research (Australia) for FAST grants (P.K. and X.F.)

## ACKNOWLEDGMENT

We would like to acknowledge our thanks and gratitude to Kent Taylor and Malcolm Ball (Gratuk Enterprises) and the Australian Proteome Analysis Facility (APAF) for running the protein gel electrophoresis.

## 5. REFERENCES

- (1) J. R. Lakowicz, *Principles of Fluorescence Spectroscopy*, 3rd ed.; Springer: New York, **2006**.
- (2) M. F. Lopez, K. Berggren, E. Chernokalskaya, A. Lazarev, M. Robinson, W. F. Patton, *Electrophoresis* **2000**, *21*, 3673–3683.
- (3) R. P. Haugland, *Handbook of Fluorescent Probes and Research Products*, 11th ed.; Molecular Probes: Eugene OR USA, **2010**.
- (4) M. Waldstrøm, R. K. Christensen, D. Ørnskov, *Cancer Cytopathol.* **2013**, *121*, 136–145.
- (5) P. Samarawardana, M. Singh, K. R. Shroyer, *Appl. Immunohistochem.* **2011**, *19*, 514–518.
- (6) N. S. Tannu, G. S. Sanchez Brambila, P. Kirby, T. M. Andacht, *Electrophoresis* **2006**, *27*, 3136–3143.
- (7) P. Mukherjee, D. B. Fulton, M. Halder, X. Han, D. W. Armstrong, J. W. Petrich, C. S. Lobban, *J. Phys. Chem. B* **2006**, *110*, 6359–6364.
- (8) P. J. L. Bell, P. Karuso, *J. Am. Chem. Soc.* **2003**, *125*, 9304–9305.

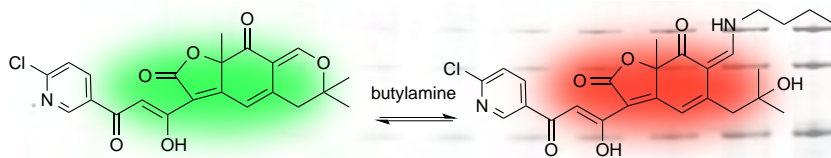
- (9) a) D. R. Coghlan, J. A. Mackintosh, P. Karuso, *Org. Lett.* **2005**, 7, 2401–2404; b) D. Panda, S. Khatua, A. Datta, *J. Phys. Chem. B* **2007**, 111, 1648–1656.
- (10) H.–Y. Choi, D. A. Veal, P. Karuso, *J. Fluorescence* **2006**, 16, 475–482.
- (11) a) Y. Zhao, Q. Zheng,; K. Dakin, K. Xu, M. L. Martinez, W.–H. Li, *J. Am. Chem. Soc.* **2004**, 126, 4653–4663; b) C. P. Moritz, S. X. Marz, R. Reiss, T. Schulenburg, E. Friauf, *Proteomics* **2014**, 14, 162–168.
- (12) L. Wang, K. D. Cole, A. K. Gaigalas, Y.–Z. Zhang, *Bioconjugate Chem.* **2005**, 16, 194–199.
- (13) J. A. Mackintosh, H.–Y. Choi, S. H. Bae, D. A. Veal, P. J. Bell, B. C. Ferrari, D. D. Van Dyk, N. M. Verrills, Y. K. Paik, P. Karuso, *Proteomics* **2003**, 3, 2273–2288.
- (14) G. B. Smejkal, M. H. Robinson, A. Lazarev, *Electrophoresis* **2004**, 25, 2511–2519.
- (15) J. A. Mackintosh, D. A. Veal, P. Karuso, *Proteomics* **2005**, 5, 4673–4677.
- (16) F. Cleeman, P. Karuso, *Anal. Chem.* **2008**, 80, 4170–4174.
- (17) A. P. Goodwin, J. L. Mynar, Y. Z. Ma, G. R. Fleming, J. M. J. Frechet. *J. Am. Chem. Soc.* **2005**, 127, 9952–9953.
- (18) R. Badugu, K. Sakamoto. *Chem. Commun.* **2003**, 12, 1368–1369.
- (19) T. N. Burai, D. Panda, A. Datta, *Chem. Phys. Lett.* **2008**, 455, 42–46.
- (20) S. Chatterjee, T. N. Burai, P. Karuso, A. Datta, *J. Phys. Chem. A* **2011**, 115, 10154–10158.



- (21) a) S. Chatterjee, P. Karuso, A. Boulangé, P. A. Peixoto, X. Franck, A. Datta, *J. Phys. Chem. B* **2013**, *117*, 14951–14959; b) O. A. Syzgantseva, V. Tognetti, A. Boulangé, P. A. Peixoto, S. Leleu, X. Franck, L. Joubert, *J. Phys. Chem. A* **2014**, *118*, 757–764.
- (22) M. Varne, V. Samant, J. A. Mondal, S. K. Nayak, H. N. Ghosh, D. K. Palit, *ChemPhysChem*. **2009**, *10*, 2979–2994.
- (23) V. Samant, A. K. Singh, G. Ramakrishna, H. N. Ghosh, T. K. Ghanty, D. K. Palit, *J. Phys. Chem. A* **2005**, *109*, 8693–8704.
- (24) R. Ghosh, D. K. Palit, *Photochem. Photobiol. Sci.* **2013**, *12*, 987–995.
- (25) R. Ghosh, J. A. Mondal, D. K. Palit, *J. Phys. Chem. B* **2010**, *114*, 12129–12143.
- (26) T. Steinel, J. B. Asbury, J. Zheng, M. D. Fayer, *J. Phys. Chem. A* **2004**, *108*, 10957–10964.
- (27) P. A. Peixoto, A. Boulangé, M. Ball, B. Naudin, T. Alle, P. Cosette, P. Karuso, X. Franck, *J. Am. Chem. Soc.* **2014**, *136*, 15248–15256.
- (28) W. W. Stewart, *J. Am. Chem. Soc.* **1981**, *103*, 7615–7620.
- (29) M. Fischer, J. Georges, *Chem. Phys. Lett.* **1996**, *260*, 115–118.
- (30) P. P. Mishra, J. Bhatnagar, A. Datta, *Chem. Phys. Lett.* **2004**, *386*, 156–161.
- (31) T. N. Burai, T. K. Mukherjee, P. Lahiri, D. Panda, A. Datta, *J. Chem. Phys.* **2009**, *131*, 034504–034508.

- (32) a) S. Grimme, J. Antony, S. Ehrlich, H. Krieg, *J. Chem. Phys.* **2010**, 132, 154104; b) F. Weigend, R. Ahlrichs, *Phys. Chem. Chem. Phys.* **2005**, 7, 3297–3305; c) R. Bauernschmitt, M. Häser, O. Treutler, R. Ahlrichs, *Chem. Phys. Lett.* **1997**, 264, 573–578; d) O. Treutler, R. Ahlrichs, *J. Chem. Phys.* **1995**, 102, 346–354.
- (33) A. Klamt, G. Schüürmann, *J. Chem. Soc. Perkin Trans. 2* **1993**, (5), 799–805.
- (34) K. Eichkorn, F. Weigend, O. Treutler, R. Ahlrichs, *Theor. Chem. Acc.* **1997**, 97, 119–124.

### Table of Contents Graphic



Improving on Nature has yielded fluorophores based on epicoconone that are more fluorescent than the natural product. In particular the 2-chloropyridyl analog stabilizes the  $\beta$ -ketoenol to such an extent that a 20 $\times$  increase in fluorescence is achieved.

## Supporting information

### Excited State Dynamics of Brightly Fluorescent Second Generation Epicocconone Analogues

Soumit Chatterjee, Peter Karuso,\* Agathe Boulang , Xavier Franck and Anindya Datta\*

#### Computational results

All computations were carried out using Turbomole 6.5 on an 8 core Powermac computer using DFT calculations as indicated. All ground states were confirmed by frequency analysis.

**Table S1:** Relative calculated energies (kcal/mol) for 2 tautomers and 2 conformers of compound **3** in a continuum dielectric equivalent to acetonitrile.

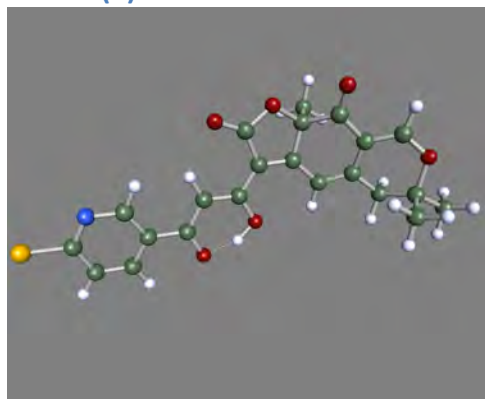
kcal/mol relative to AB183_1a	RI- DFT// BP86/ SVP	RI-DFT-D3 //BP86/TZV PP + COSMO	RI-DFT //BP86/TZV PP Ground state	RI-DFT //BP86/TZV PP 1st excited state	RI-DFT //BP86/TZV PP GS at 1st ES geometry
AB183_1a	0.00	0.00	0.00	51.54	6.57
AB183_1b	0.32	0.55	0.32	51.55	6.68
AB183_2a	0.10	0.14	0.13	51.65	6.64
AB183_2b	0.31	0.53	0.21	51.65	6.60
AB183_2zw*		19.53	41.94	50.23	48.79
AB183_1zw*		19.57	40.77	53.64	49.24

\* these are the zwitter ionic forms where the keto-enol proton is on the pyridine N

Table S1 indicates that in the ground state there is little to differentiate the 4 conformations and a Boltzmann distribution is expected. The last three columns are in the gas phase. In all cases the  $S_1$  state is about 51.5 kcal/mol higher in energy than the ground state and about 6.6 kcal/mol lower than the  $S_1^*$  state. This corresponds to a predicted emission of ~635 nm. The zwitter ionic form (H on N) is ~20 kcal/mol higher in energy is acetonitrile and thus unlikely to be a major contributor to the ground state. The higher energies in the gas phase (last three columns) for the zwitter ion is not surprising but it is interesting that in the gas phase, at least, the zwitterion forms are more stable than the other tautomers in the excited state.

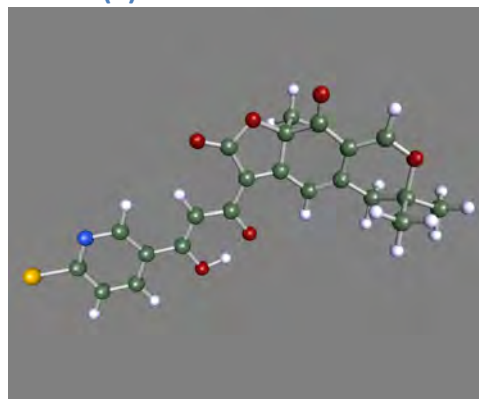
Coordinates of geometry optimized structures (RIDFT//BP86/TZVPP –COSMO) in XYZ format.

AB183 (3) conformation 1a



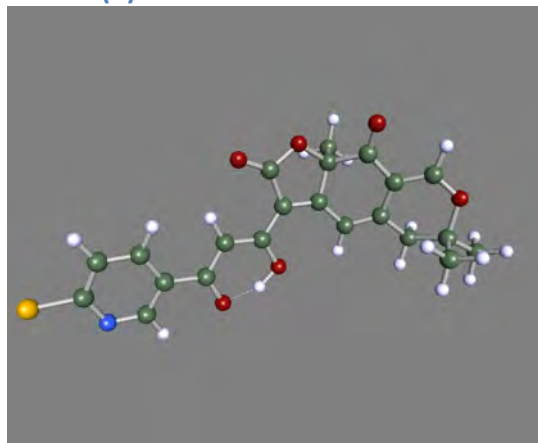
```
48
O 2.599097 0.331847 -4.571832
C 1.282445 1.059584 -4.681058
C 0.245958 0.011740 -5.075750
H -0.723552 0.504539 -5.223585
H 0.127919 -0.750832 -4.295105
H 0.537546 -0.478977 -6.011986
C 1.510956 2.089299 -5.773430
H 0.587219 2.659390 -5.934405
H 1.783225 1.595649 -6.714665
H 2.308570 2.787492 -5.490164
C 0.965015 1.715167 -3.332714
H -0.028100 2.178496 -3.385651
H 1.690022 2.527449 -3.152942
C 1.063418 0.758304 -2.180678
C 2.117352 -0.224777 -2.289491
C 2.843179 -0.328157 -3.457711
H 3.707746 -0.990739 -3.532444
C 0.209533 0.806025 -1.103826
H -0.652573 1.467622 -1.110721
C 0.419535 -0.098949 -0.028365
C 1.795393 -0.686111 0.148527
C 2.418940 -1.140329 -1.184026
O 3.139718 -2.131567 -1.254632
C -0.402964 -0.650295 0.932772
C -1.790352 -0.332292 1.194245
C -2.576225 -0.998946 2.133025
H -2.121315 -1.800091 2.703295
C -3.935485 -0.612311 2.325505
O -4.454258 0.342275 1.652235
O -2.299607 0.667823 0.475552
H -3.287636 0.737128 0.811750
C 0.357240 -1.715561 1.618123
O 0.029527 -2.497205 2.493922
O 1.632479 -1.766165 1.085759
C 2.767056 0.346047 0.764986
H 3.736299 -0.136405 0.938487
H 2.352838 0.698302 1.717617
H 2.900305 1.201436 0.092594
C -6.362292 -2.590811 5.147592
N -5.149997 -3.084768 4.929506
C -4.381038 -2.448235 4.030871
H -3.395445 -2.887006 3.873785
C -4.793939 -1.307968 3.324479
C -6.088606 -0.822507 3.581899
H -6.448097 0.058143 3.051582
C -6.896545 -1.465823 4.509567
H -7.901211 -1.116079 4.735852
Cl -7.344773 -3.435918 6.330266
```

AB183 (3) conformation 1b



```
48
O 2.595335 0.344326 -4.577371
C 1.282260 1.079573 -4.679407
C 0.240834 0.040909 -5.085173
H -0.726210 0.539895 -5.228535
H 0.118542 -0.728842 -4.312243
H 0.530590 -0.441841 -6.026118
C 1.516332 2.119338 -5.761027
H 0.595497 2.695614 -5.916561
H 1.786721 1.634131 -6.707188
H 2.317201 2.810655 -5.470136
C 0.967457 1.722754 -3.324586
H -0.023678 2.190805 -3.372653
H 1.695778 2.530188 -3.136407
C 1.062482 0.755278 -2.181209
C 2.110471 -0.233364 -2.300878
C 2.835536 -0.328655 -3.470049
H 3.696470 -0.995193 -3.551592
C 0.212862 0.799366 -1.100907
H -0.649239 1.461227 -1.094179
C 0.423350 -0.115770 -0.034274
C 1.795726 -0.711453 0.134854
C 2.409992 -1.160095 -1.203573
O 3.122989 -2.156042 -1.286035
C -0.403169 -0.665659 0.922216
C -1.802880 -0.315513 1.164161
C -2.569593 -1.014806 2.148968
H -2.097236 -1.811851 2.711091
C -3.895141 -0.661017 2.366931
O -4.452019 0.319621 1.665308
O -2.323646 0.636868 0.478989
H -3.668168 0.644423 1.029964
C 0.351357 -1.738334 1.601056
O 0.024223 -2.525804 2.472942
O 1.627860 -1.795293 1.066315
C 2.776089 0.311094 0.753684
H 3.742468 -0.178909 0.922010
H 2.366713 0.660819 1.709336
H 2.913322 1.169208 0.085574
C -6.369036 -2.544121 5.189247
N -5.114995 -2.968877 5.080983
C -4.335855 -2.359280 4.176400
H -3.313670 -2.734099 4.116325
C -4.776605 -1.310254 3.351673
C -6.112027 -0.890399 3.498549
H -6.501384 -0.081621 2.883052
C -6.931468 -1.512249 4.431715
H -7.967695 -1.213105 4.571241
Cl -7.365194 -3.359249 6.379921
```

### AB183 (3) conformation 2a

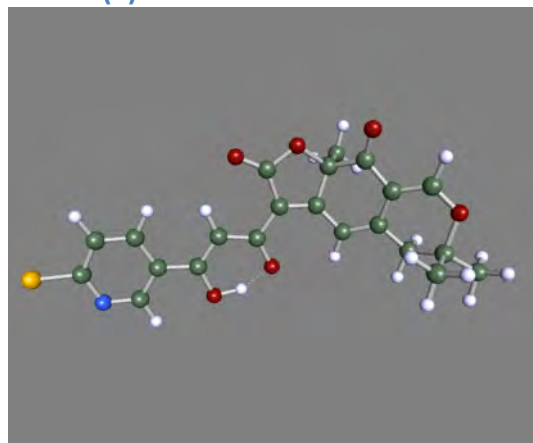


48

```
O 2.589900 0.361038 -4.586417
C 1.267143 1.079418 -4.685030
C 0.237202 0.026252 -5.082634
H -0.736717 0.512484 -5.223111
H 0.128321 -0.742537 -4.306769
H 0.528709 -0.455733 -6.023423
C 1.483150 2.118340 -5.771188
H 0.554307 2.682215 -5.924563
H 1.755479 1.633309 -6.716877
H 2.276365 2.820864 -5.486281
C 0.950487 1.723247 -3.330889
H -0.046709 2.178570 -3.376249
H 1.669375 2.540466 -3.148922
C 1.062276 0.760105 -2.185319
C 2.121790 -0.215389 -2.306233
C 2.843199 -0.305438 -3.478354
H 3.712067 -0.961398 -3.561427
C 0.214937 0.796396 -1.102704
H -0.651592 1.452262 -1.100622
C 0.437907 -0.112477 -0.033372
C 1.818124 -0.693075 0.130704
C 2.435032 -1.136331 -1.208493
O 3.160132 -2.123540 -1.289969
C -0.374261 -0.672282 0.931777
C -1.760964 -0.362209 1.206049
C -2.534797 -1.034877 2.151041
H -2.070981 -1.834608 2.716060
C -3.894357 -0.656702 2.355074
O -4.424425 0.295882 1.686616
O -2.283063 0.635593 0.494319
H -3.269706 0.697660 0.840695
C 0.396451 -1.737103 1.605922
O 0.079483 -2.524871 2.480272
O 1.667660 -1.778954 1.063255
C 2.788280 0.341235 0.746082
H 3.761347 -0.136764 0.910286
H 2.378639 0.685956 1.703435
H 2.912139 1.200989 0.077478
C -6.427517 -2.517018 5.160936
N -6.862027 -1.438791 4.519649
C -6.024047 -0.876592 3.634270
H -6.390659 0.008766 3.114259
C -4.734677 -1.362943 3.361737
C -4.314657 -2.505082 4.065346
H -3.331237 -2.942132 3.901345
C -5.169671 -3.102086 4.983892
H -4.878381 -3.988669 5.542150
```

C1 -7.539615 -3.240168 6.309396

### AB183 (3) conformation 2b



48

```
O 2.586362 0.347961 -4.583986
C 1.267420 1.073235 -4.682370
C 0.231019 0.024820 -5.075783
H -0.740462 0.516060 -5.215670
H 0.119260 -0.741562 -4.297954
H 0.518224 -0.460939 -6.015954
C 1.487477 2.108232 -5.771475
H 0.561648 2.677066 -5.924679
H 1.755426 1.619318 -6.716417
H 2.285214 2.806871 -5.489653
C 0.956443 1.722046 -3.329358
H -0.038035 2.183258 -3.374118
H 1.680607 2.535195 -3.150087
C 1.064333 0.761346 -2.181398
C 2.118270 -0.220853 -2.301753
C 2.837413 -0.317406 -3.474598
H 3.702458 -0.978426 -3.557468
C 0.219485 0.804816 -1.097300
H -0.646472 1.461580 -1.089172
C 0.439095 -0.106199 -0.029083
C 1.814934 -0.694576 0.136335
C 2.427964 -1.142270 -1.202890
O 3.147518 -2.133566 -1.284995
C -0.381204 -0.658136 0.931670
C -1.782223 -0.314517 1.177408
C -2.544256 -1.024448 2.159470
H -2.066558 -1.822046 2.716343
C -3.871313 -0.682647 2.381232
O -4.438212 0.299356 1.687381
O -2.308534 0.638036 0.498727
H -3.661965 0.634741 1.054814
C 0.381333 -1.725317 1.610161
O 0.061832 -2.512031 2.485665
O 1.656076 -1.777159 1.070804
C 2.791841 0.334756 0.749700
H 3.761512 -0.149503 0.915683
H 2.383945 0.684292 1.706049
H 2.921993 1.192222 0.079336
C -6.470535 -2.481466 5.143103
N -6.926335 -1.481251 4.400563
C -6.071030 -0.926698 3.526559
H -6.463928 -0.106784 2.925934
C -4.739727 -1.349297 3.365447
C -4.297985 -2.413243 4.173689
```

H -3.280073 -2.792491 4.101950 Cl -7.605106 -3.191239 6.276530  
 C -5.170420 -2.996497 5.081513  
 H -4.861168 -3.820311 5.720305

**Table S2:** Relative calculated energies (kcal/mol) for compound **3** where the Cl or N are removed and geometry reoptimized.

kcal/mol* relative to AB183_1a	RI-DFT- D3//BP86/ TZVPP - COSMO	RI-DFT //BP86/TZVPP gas phase	RI-DFT //BP86/TZVPP 1st excited state gas phase	RI-DFT- //BP86/TZVPP GS at 1st ES geometry
AB183_1a_ TZVPP_noCl	0.00	0.00	36.00	16.29
AB183_1b_ TZVPP_noCl	0.46	0.19	35.99	16.25 <sup>‡</sup>
AB183_2a_ TZVPP_noCl	0.12	0.13	34.34	16.67
AB183_2b_ TZVPP_noCl	0.51	0.13	34.34	16.68 <sup>‡</sup>
AB183_1a_ TZVPP_noN <sup>‡</sup>	0.00	0.00	44.75	25.92
AB183_1b_ TZVPP_noN <sup>‡</sup>	0.31	0.11	47.91	13.79

\* energies are relative to conformation **1a** in each case.

<sup>‡</sup> same as tautomer **2a** and **2b** respectively

In the excited state, conformations 1b and 2b (noCl) change to **1a** and **2a** respectively. **There is a barrierless transition, in the non-chlorinated excited state, from one tautomer to the other.** This can explain the nanosecond decay in the aryl analogues that is not present in the chloropyridine analogue. Secondly, the analogues with no nitrogen (noN) rearrange in the excited state to have the aryl ring rotated out of plane with the  $\beta$ -keto-enol. This is another mechanism for non-radiative decay that is not observed in the pyridine analogue.

**Table S3:** Dipole moments of **3** in solvent and the gas phase.

Dipole moment (debye)	RI-DFT// BP86/SVP	RI-DFT-D3 //BP86/TZV PP - COSMO	RI-DFT//BP86 /TZVPP Ground state Gas phase	RI-DFT//BP86/ TZVPP 1st excited state gas phase
AB183_1a	15.2426	16.2979	10.7563	11.3086
AB183_1b	14.7074	15.6410	10.3737	10.8480
AB183_2a	13.4606	14.4470	9.5147	11.6153
AB183_2b	12.6058	13.3164	8.8744	9.2197
AB183_2zw		11.3946	7.7865	8.6402
AB183_1zw		9.084	5.1631	7.2134

No decrease in dipole moment is observed in the excited state

**Table S4:** Bond lengths of the keto-enol group in structure **3** expressed as a difference (pm) from the bond length in the global ground state (AB183\_1a).

distances (pm)	C28-C43	C26-C28	C25-C26	C28-O29	C25-O30
AB183_1a_TZVPP	0.000	0.000	0.000	0.000	0.000
AB183_1a_TZVPP_noCl	-0.007	0.066	-0.032	0.025	0.016
AB183_1a_TZVPP_noN	-0.077	0.283	-0.145	0.164	0.066
AB183_1b_TZVPP	0.000	0.000	0.000	0.000	0.000
AB183_1b_TZVPP_noCl	0.115	0.029	-0.026	0.055	-0.022
AB183_1b_TZVPP_noN	0.007	0.243	-0.229	0.121	0.072
AB183_2a_TZVPP	0.000	0.000	0.000	0.000	0.000
AB183_2a_TZVPP_noCl	0.003	0.094	-0.064	-0.005	0.048
AB183_2a_TZVPP_noN	-0.059	0.321	-0.180	0.102	0.116
AB183_2b_TZVPP	0.000	0.000	0.000	0.000	0.000
AB183_2b_TZVPP_noCl	0.144	0.068	-0.078	0.001	0.032
AB183_2b_TZVPP_noN	0.040	0.339	-0.314	0.005	0.178

The results indicate that removing the Cl has little effect on the bond lengths except for conformation 2b where the length of C43-C28 increases slightly. Similarly removing the nitrogen has little effect on C28-C43 bond length. However, removing the nitrogen does increase the length of the second C-C bond by 0.24-0.34 pm and decrease the length of the next bond (C25-C26) by 0.15-0.31 pm. These increases and decreases in length are so small (femtometre range) that it can be concluded that the Cl and N have no affect on ground state geometry.

**Table S5:** Bond lengths of the keto-enol group in structure **3** (in the first excited state) expressed as a difference (pm) from the bond length in the global ground state (AB183\_1a).

distances (pm)	C28-C43	C26-C28	C25-C26	C28-O29	C25-O30
AB183_1a_TZVPP	-0.239	-0.520	0.710	0.689	0.429
AB183_1a_TZVPP_noCl	<b>4.644</b>	<b>-4.649</b>	<b>3.276</b>	0.029	0.487
AB183_1a_TZVPP_noN	1.068	<b>-6.027</b>	<b>3.337</b>	1.409	1.769
AB183_1b_TZVPP	-0.364	0.109	-0.093	0.509	0.761
AB183_1b_TZVPP_noCl	-0.364	-0.952	-0.369	-4.949	5.374
AB183_1b_TZVPP_noN	-0.746	-0.516	<b>4.993</b>	1.146	-1.146
AB183_2a_TZVPP					
AB183_2a_TZVPP_noCl	<b>4.611</b>	<b>-4.727</b>	<b>3.321</b>	0.296	0.537
AB183_2a_TZVPP_noN	-2.029	<b>-4.727</b>	<b>3.323</b>	0.301	0.537
AB183_2b_TZVPP	-0.305	-0.961	-0.386	-4.757	5.501
AB183_2b_TZVPP_noCl	<b>6.328</b>	-0.961	-0.386	<b>-4.757</b>	<b>5.501</b>
AB183_2b_TZVPP_noN	-0.713	-0.421	<b>4.908</b>	1.029	-1.040

Deviation of >3 pm are in bold

When no chlorine is present the C43-C28 bond length increases in the excited state by ~4.8 pm. In compensation the C28-C26 bond length decreases by ~4.2 pm.

## Steady State spectra

### *Experimental Procedures:*

Stock solutions of SDS (1M) and epicocconone analogue (1 mM) were prepared in water and DMSO respectively and filtered (0.22  $\mu\text{m}$ ). To a set of matched quartz cuvettes was added analogue stock solution (10  $\mu\text{L}$ ) or DMSO (10  $\mu\text{L}$ ; reference cell), made up to 2 mL with distilled water and the absorption and fluorescence spectra recorded. Successive additions of SDS stock solution (2  $\mu\text{L}$ ) to each cuvette was followed by re-measurement of absorption and fluorescence spectra (Figure S2, S3).

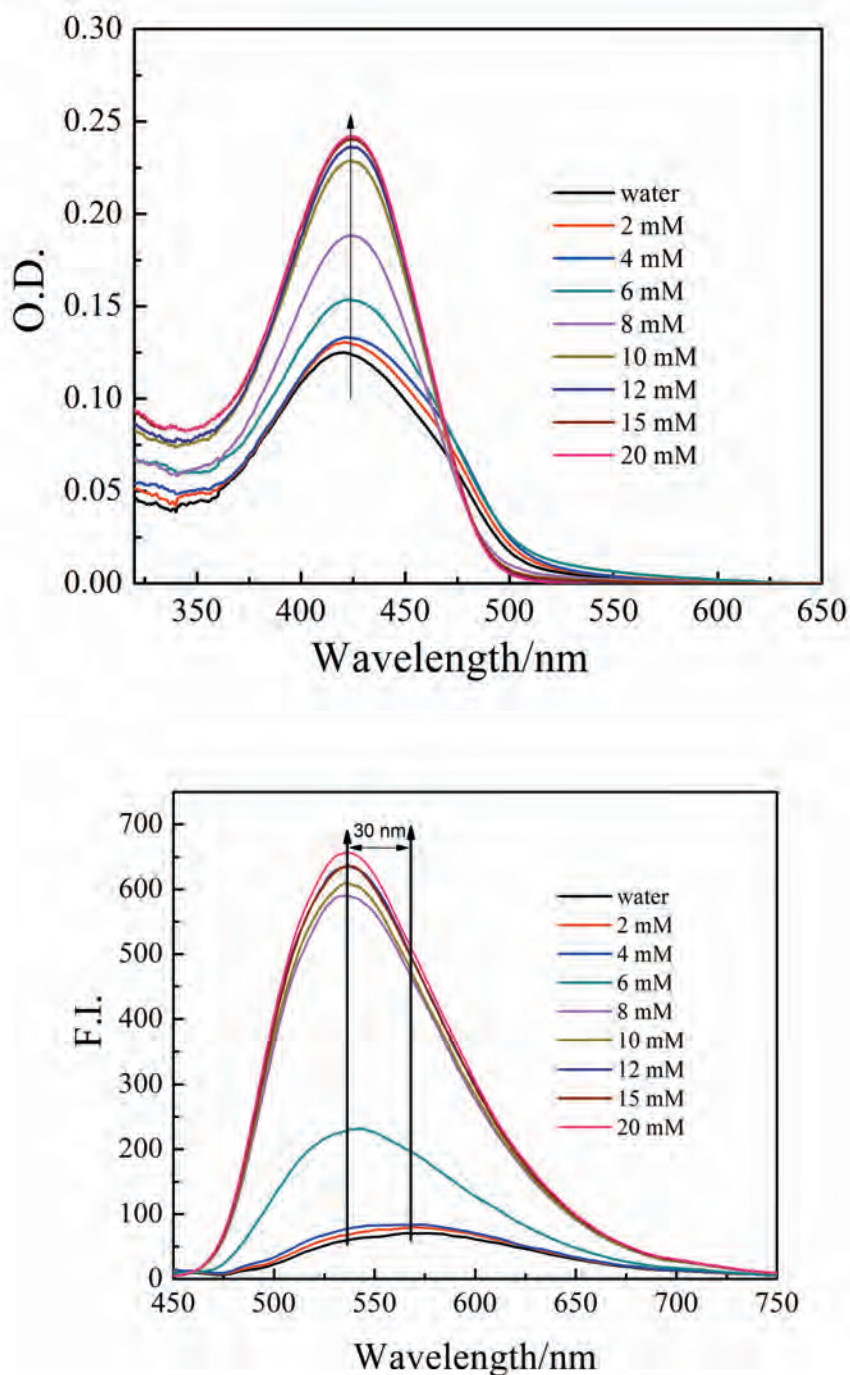


**Figure S2.** Absorption and emission spectra of **2** with varying concentration of SDS



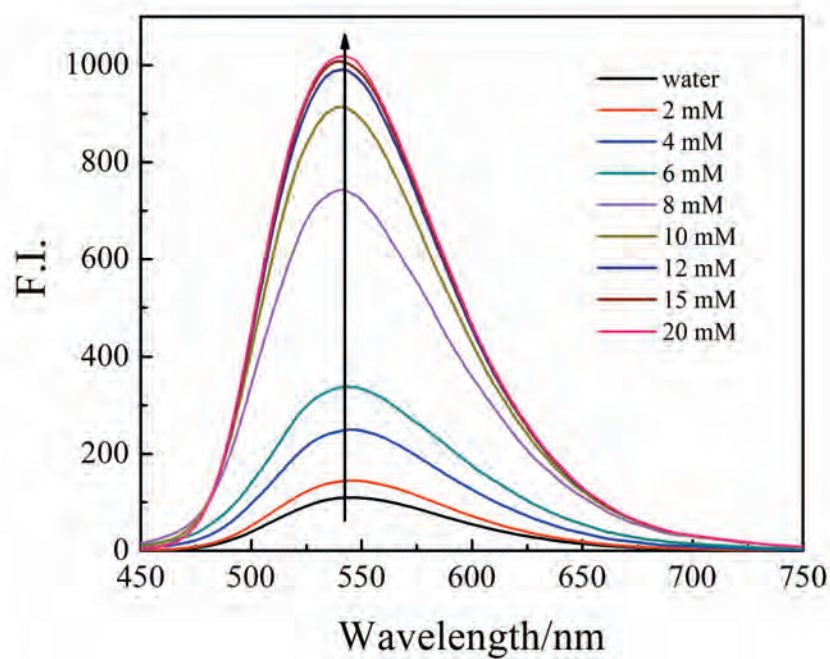
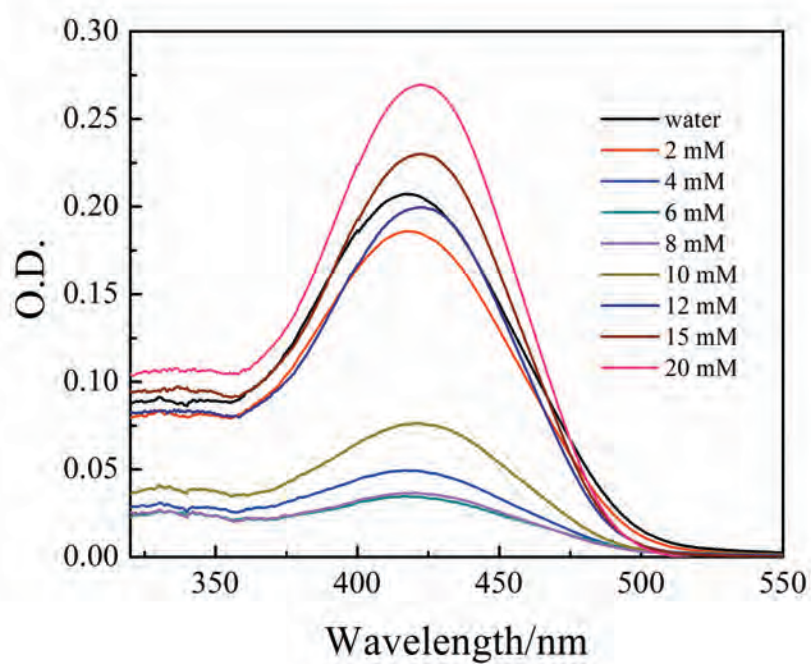


**Figure S3.** Absorption and emission spectra of **3** with varying concentration of SDS

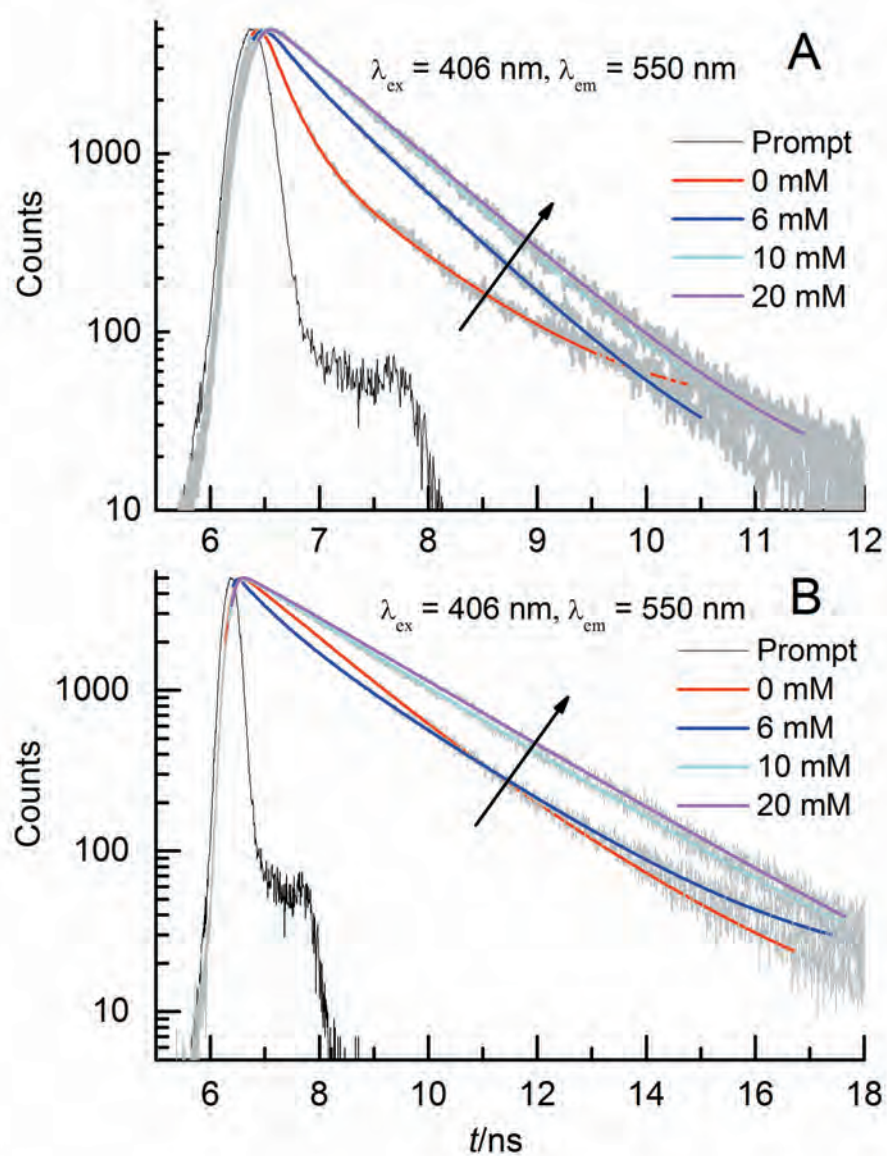


**Figure S4.** TCSPC decay traces of A) **2** and B) **3** with varying concentration of SDS

**Table S6.** Fluorescence Decay Parameters for **2** with varying concentration of SDS.

SDS (mM)	$\chi^2$	$\tau_1$ (ns)	$a_1$	$\tau_2$ (ns)	$a_2$	$\langle\tau\rangle$ (ns)
0	1.20	0.12	0.95	1.63	0.05	0.20
2	1.10	0.20	0.84	0.90	0.16	0.31
6	1.00	0.24	0.29	0.80	0.71	0.64
8	1.10			0.80	1.00	0.80
10	1.08			0.80	1.00	0.80
12	1.05			0.80	1.00	0.80
15	1.09			0.80	1.00	0.80
20	1.02			0.84	1.00	0.84

**Table S7.** Fluorescence Decay Parameters for **3** with varying concentration of SDS.

SDS (mM)	$\chi^2$	$\tau_1$ (ns)	$a_1$	$\tau_2$ (ns)	$a_2$	$\langle\tau\rangle$ (ns)
0	1.07	1.10	0.67	2.27	0.33	1.49
2	1.06	1.40	0.80	2.40	0.20	1.60
6	1.12	0.70	0.40	2.32	0.60	1.67
8	1.01			2.20	1.00	2.20
10	1.10			2.20	1.00	2.20
12	1.13			2.20	1.00	2.20
15	1.13			2.20	1.00	2.20
20	1.13			2.20	1.00	2.20

## Conclusion

We have established photoisomerization of the heptatriene side chain as the major nonradiative process in epicocconone. It is further indicated that in order to design and synthesise analogues with higher quantum yields, the heptatriene chain needs to be reengineered so as to eliminate photoisomerization, while the keto-enol moiety needs to be conserved in order to obtain a higher quantum yield for the butylamine adducts. This is successfully manifested in the significantly higher fluorescence observed in the analogues studied. This is further manifested by slower fluorescence decays with respect to epicocconone in all the three solvents studied, as photoisomerization leading to rapid internal conversion cannot take place in these compounds. This observation reinforces our postulate that the intramolecular H-bonding system of the keto-enol moiety helps stabilize the excited states of epicocconone and its analogues in aprotic solvents and substitution next to the keto-enol can alter the dynamics by virtue of steric factors or charge transfer or some local phenomenon. These compounds can be considered as synthetic alternatives to epicocconone as protein stains and can find potential use as dual-colour stains in biotechnology. Protein staining with the pyridyl-analogue shows comparable performance with respect to the commercial product without protocol optimization. Furthermore the pyridyl analogue is highly fluorescent in its native state, reaching 57% in acetonitrile (*c.f.* 2.6% for epicocconone) but is very similar to epicocconone when reacted with an amine (enamine state). This indicates that nitrogen-containing substitutes can be of particular interest in making highly fluorescent compounds. Further studies, including deuterium effect and temperature variation will be done in future to establish a clear picture of the excited state dynamics, which might originate from multiple conformers in the ground state.



## **Chapter 3: Review on Green Fluorescent Protein Chromophore**



### 3.1. Discovery and Early History of Green Fluorescent Protein (GFP)

Green Fluorescent Protein (GFP), discovered by Shimomura *et al.*, is a companion protein to aequorin, the chemiluminescent protein from *Aequorea* jellyfish.<sup>100</sup> While the chemiluminescence of pure aequorin is blue and peaks near 470 nm, the bioluminescence of living *Aequorea* is observed at 508 nm. This phenomenon has been attributed to Förster Resonance Energy Transfer (FRET) from aequorin to GFP, which then emits in the green.<sup>101</sup> Similar observations have been made in the related coelenterates like *Obelia* (a hydroid) and *Renilla* (a sea pansy).<sup>102</sup> Morise *et al.* purified and crystallized GFP, measured its absorbance spectrum and fluorescence quantum yield, and established that aequorin can efficiently transfer energy to GFP when the two are coadsorbed onto a cationic support.<sup>103</sup> Prendergast and Mann obtained the first clear estimate for the monomer molecular weight.<sup>104</sup> Shimomura proteolyzed denatured GFP, analyzed the peptide that retained visible absorbance, and correctly proposed that the chromophore is 4-(*p*-hydroxybenzylidene)imidazolidin-5-one and that it is attached to the peptide backbone through the 1- and 2-positions of the ring.<sup>105</sup> Later, Prasher *et al.*, Chalfie *et al.* and Inouye & Tsuji successfully expressed GFP in other organisms without the involvement of jellyfish-specific enzymes.<sup>106-108</sup> Henceforth, green fluorescent protein (GFP) has become a ubiquitous marker in cell biology.<sup>15,16,18,27,109-119</sup>

### 3.2. Use of GFP

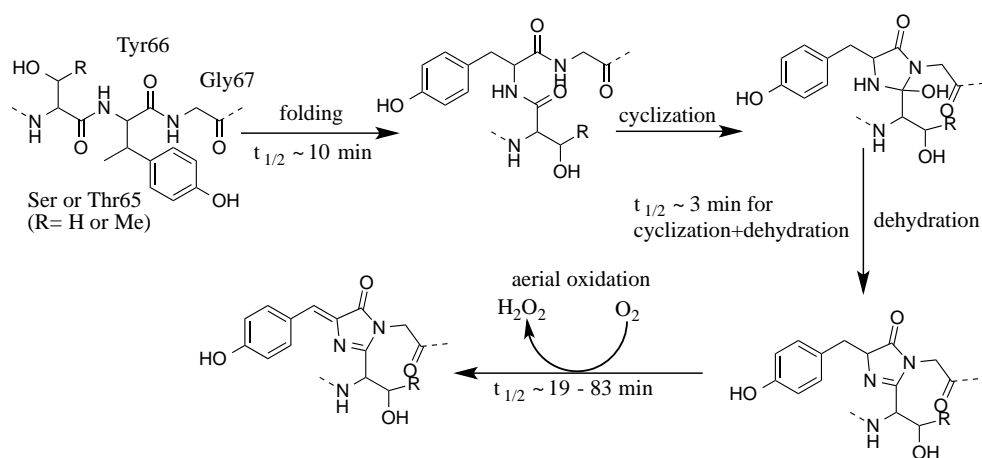
In contrast to potentially toxic fluorescent dyes, GFP can be genetically engineered into other proteins and subsequently, their distribution and movement in cells can be monitored by tracking the green emission.<sup>20,21</sup> This approach has been used successfully in a large number of bacteria, fungi, plants, insects, and nematodes.<sup>107</sup> Since active GFP can be observed when expressed in many divergent species, it requires no substrate or accessory proteins for



chromophore formation. This makes GFP an ideal reporter protein in living cells. One potential limitation of GFP as a reporter for gene expression is its relatively slow rate of onset of fluorescence *in vivo*, limiting its use to experiments exceeding the hour time scale. This slow rate is reported to be due to the oxidation step in chromophore formation, which has been estimated to occur with a time constant of 2-4 h *in vivo* and involves the production of one mole equivalent of hydrogen peroxide.<sup>24,120,121</sup>

### 3.3. The GFP Chromophore

The green fluorescent protein is composed of a total of 238 amino acids. The chromophore, *p*-hydroxybenzylideneimidazolinone (*p*-HBDI), is located inside the centre of an 11-stranded beta-barrel structure. It is held in place by covalent as well as non-covalent bonds.<sup>122</sup> The chromophore is formed by a reaction of the residues 65-67 (Ser-Tyr-Gly) in the native protein. The mechanism of formation of the GFP chromophore was been proposed by Heim *et al.*, Cubitt *et al.*, and Reid *et al.*<sup>24-26</sup> First, GFP folds into a nearly native conformation, then the imidazolinone is formed via nucleophilic attack of the amide of Gly67 on the carbonyl of Ser65, followed by dehydration. Finally, molecular oxygen dehydrogenates the  $\alpha$ - $\beta$  bond of Tyr66 leading to conjugation of the aromatic ring with the imidazolinone with the concomitant release of hydrogen peroxide.<sup>121</sup> At this stage the chromophore acquires visible absorbance and fluorescence (Scheme 3.1).<sup>27</sup> It is worth stating that there are now faster maturing mutants widely available and that wtGFP is hardly used these days.



**Scheme 3.1.** Proposed mechanism by Cubitt *et al.*<sup>26</sup> for the intramolecular biosynthesis of GFP chromophore. The scheme is adopted from ref 10.

### 3.4. Photophysics of *p*-HBDI in Protein

*p*-HBDI, in GFP, shows a major excitation peak at 395 nm which is almost three times stronger than a minor peak at 475 nm. Excitation at 395 nm gives emission at 508 nm, whereas excitation at 475 nm gives a maximum at 503 nm.<sup>24</sup> The quantum yield of GFP has been calculated to be 0.8. The excitation wavelength dependent emission maximum indicates that the population includes at least two chemically distinct species, which do not fully equilibrate within the lifetime of the excited state. At pH = 10-11, when the protein starts to unfold, the 475 nm absorbance becomes stronger at the expense of the 395 nm peak.<sup>123</sup> Hence, the 475 nm peak is assigned to GFP molecules containing deprotonated or anionic chromophores, whereas the 395 nm peak is assigned to GFP molecules with protonated or neutral chromophores.<sup>25,26,120,124-126</sup> On intense UV illumination, the characteristic 395 nm absorption of the neutral form gradually declines with the concomitant increase in the 475 nm peak of the anionic chromophore.<sup>122,127,128</sup>

The green emission is ascribed to the excited state of the anionic chromophore. The anion is formed upon excitation of the neutral chromophore by the loss of a proton from the locally excited state (ESPT).<sup>127</sup> Excited state proton transfer (ESPT), like that proposed for the GFP

chromophore, is generally a reversible process. In GFP, the process takes place in picoseconds as proton transfer occurs via the hydrogen bonds of a buried water and Ser205 to Glu222, which provides an escape channel for the transferred proton.<sup>129,130</sup> In the crystal structure of monomeric wild-type GFP, Thr203 exists in two conformations; approximately 85% with the OH facing away from the phenol oxygen, and 15% with the OH rotated toward it.<sup>129</sup> This proportion agrees well with the spectroscopic estimate for the ratio of neutral to anionic chromophores at equilibrium.<sup>127</sup> A photoisomerization process has been found to occur post ESPT, leading to the formation of the dark trans-form of the chromophore to some extent.<sup>131</sup>

### 3.5. Synthesis of *p*-HBDI

The motivation for the synthesis of the GFP chromophore (*p*-HBDI) and its derivatives stems from the need to study the fluorescence properties of model chromophores of the mutant proteins and to prepare different classes of fluorescent proteins. Niwa and co-workers first synthesized five different chromophores of this class, including *p*-HBDI, using the Erlenmeyer azalactone synthesis (Scheme 3.2).<sup>132,133 134</sup>



interaction and H-bonding, providing a chance for the ESPT from the chromophore. As a result, a strong green fluorescence from the anion is observed. The exact origin of the IC has long been a subject of debate. While some suggest a single bond rotation ( $\phi$ ),<sup>151,154,157</sup> others suggest double bond rotation ( $\tau$ )<sup>132,150,153,158-160</sup> or a simultaneous and concerted rotation of both single and double bonds known as the “hula-twist” ( $\phi, \tau$ ) (Figure 3.3).<sup>131,142,143,147,155,161-166</sup>

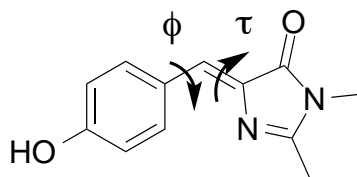


**Figure 3.1.** Hula-twisting of *p*-hydroxybenzylideneimidazolinone (*p*-HBDI)

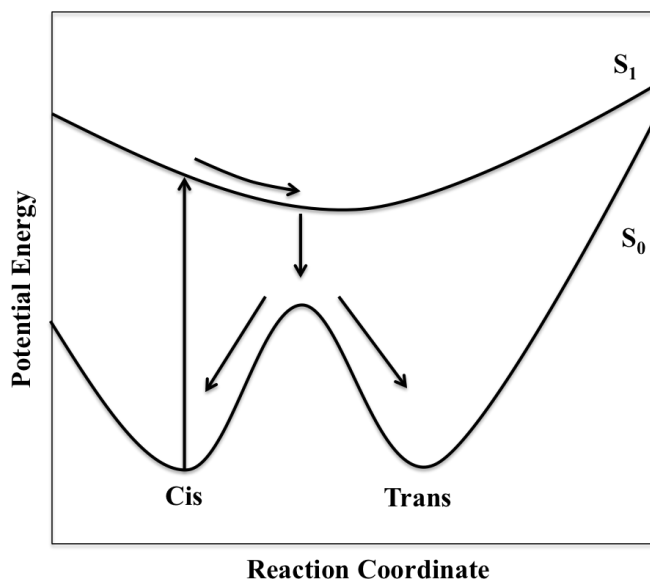


**Figure 3.2.** Proposed twisted intermediate pathway for the ultrafast relaxation of *p*-HBDI

Zimmer and co-workers have proposed that one bond flip (OBF) around  $\tau$  displaces a larger volume than both the hula-twists (HT) and the  $\phi$  OBF. However, individually HT and  $\phi$  OBF displaces the same volume, and therefore the volume conserving property of the HT cannot

be a sufficient reason for the excited chromophore to undergo a HT. From MM calculations, they also substantiated that the protein matrix of GFP forms a cavity around the chromophore that is complementary to an excited state conformation in which the phenol and imidazolidinone rings are perpendicular to each other, a conformation that can only be achieved by a concerted rotation around  $\tau$  and  $\phi$ .<sup>167</sup> The hula-twist mechanism was experimentally supported by Mandal *et al.*<sup>142,147</sup> Later, Tolbert and co-workers showed the importance of other amino acids in the vicinity of *p*-HBDI inside the protein cavity to act as additional nucleophile and help it fluoresce.<sup>168</sup> Recently, Sen and co-workers, with the help of two derivatives, proposed a multicoordinate excited state relaxation process and showed a TICT (twisted intramolecular charge transfer) mediated rotation around the exocyclic C=C bond to be the reason for fast IC of *p*-HBDI (Figure 3.3).<sup>111</sup> Thus, the jury is still out on the exact mechanistic explanation of the non-fluorescent nature of HBDI and its analogues that have been synthesized earlier.

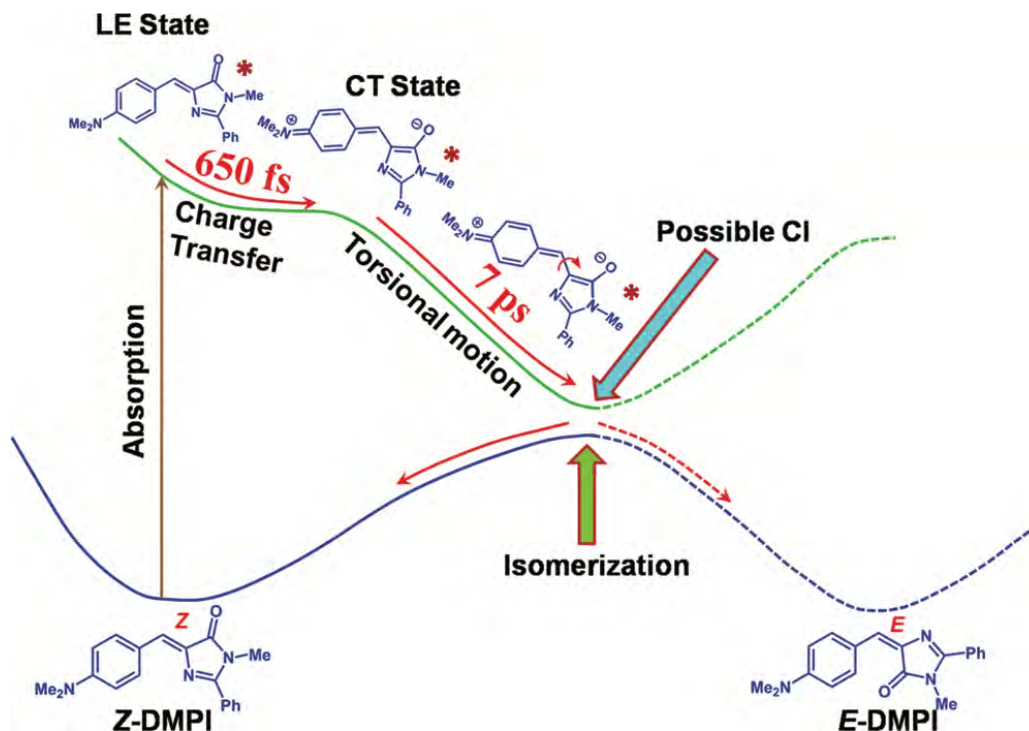


**Figure 3.3.** Schematic Excited State Dynamics of DMPI in acetonitrile.<sup>111</sup>

### 3.7. Recent Advances in Synthesis of Fluorescent HBDI Derivatives

In the last few years, a few fluorescent analogues of HBDI have been successfully synthesized. Most of the early research on the derivatized chromophore has focused on modifying the substituents at C(1), which helps tune the emission wavelength. On the other hand, efforts have been made to substitute the methyl at N(1) in order to render the compounds bulky enough to restrict the postulated relaxation process. Changing the phenyl residue from the *p*-HBDI into other substituents like substituted phenyl, pyrrole etc. has also been attempted (Figure 3.4 and 3.5). Altering the core structure of the chromophore by making them bulkier or adding push-pull electronic effect increased the quantum yield of some compounds (Figure 3.4). Yet, these compounds were found to have some disadvantages associated with their size and poor solubility.<sup>158</sup>

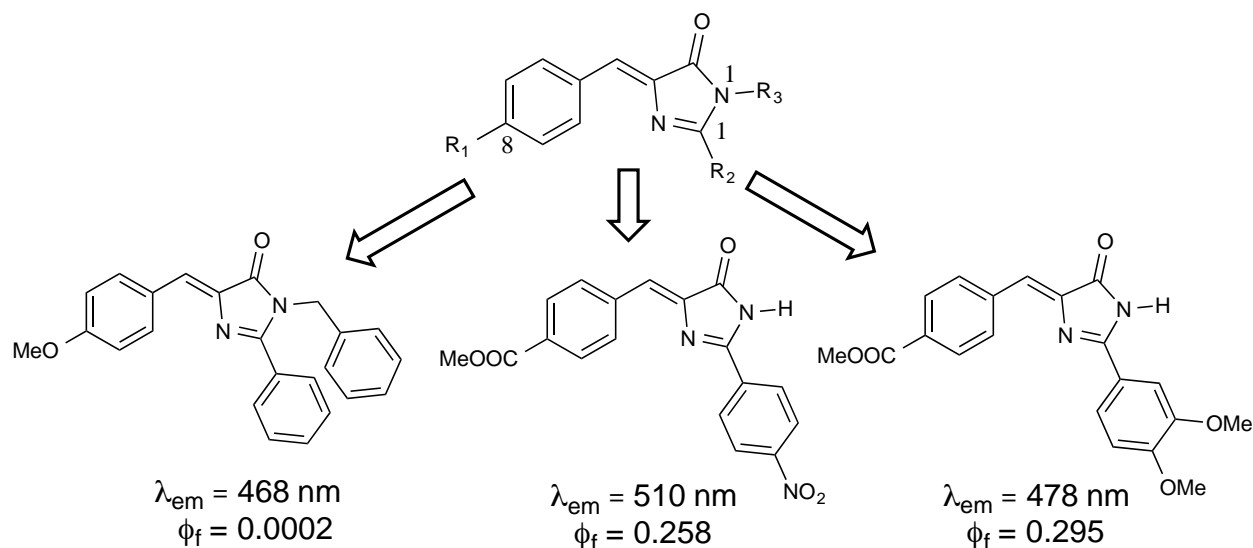


**Figure 3.4.** Fluorescent derivatives of GFP chromophore. The quantum yields are calculated in dioxane.<sup>158</sup>

Chou and co-workers first synthesized a derivatized GFP chromophore, *o*-HBDI (4-(2-hydroxybenzylidene)-1,2-dimethyl-1H-imidazol-5(4*H*)-one).<sup>135</sup> In this chromophore, a seven

membered ring could be formed by intramolecular hydrogen bonding and this could hinder the exocyclic torsional deformation, causing a decrease in the rate of radiationless decay. Additionally theoretical studies also showed that excited state intramolecular proton transfer from the hydroxyl proton to N(2) is possible, leading to the formation of a zwitterionic species. The emission was found to be red shifted to 605 nm in organic solvent unlike *wtGFP* emission at 508 nm. Due to the conformational locking, the quantum yield was found to increase by ~30 times compared to *p*-HBDI. The 605 nm emission was proposed to be due to the zwitterionic tautomer. Surprisingly, a dual emission was observed in aqueous solutions. This was ascribed to possible rupture of intramolecular hydrogen bonding of O–H $\cdots$ N, inhibiting ESIPT in protic solvent. At pH = 12, a single anionic emission at 580 nm was reported. In a later study, Yang and coworkers reported an increase in the emission quantum yield of *o*-HBDI at low temperature.<sup>169</sup> Subsequently, Chou and co-workers synthesized and studied a series of substituted *o*-HBDI analogues as well as pyrrole derivatives in an attempt to understand the photophysics of this class of molecule (Figure 3.5).<sup>170</sup> Femtosecond optical gating, transient absorption and UV/mid-IR time resolved spectroscopy revealed an instantaneous rise to a few hundred femtosecond oscillations for the tautomer emission at 605 nm for *o*-HBDI. The formation of anions in the ground state of the molecules was reported in aprotic solvent like CH<sub>3</sub>CN, due to *cis-trans* isomerization. It was established that in *o*-HBDI, a barrierless ultrafast ESIPT occurs, followed by isomerization and deprotonation, which could not take place in *p*-HBDI or *wtGFP* (Figure 3.6).<sup>170,171</sup> Tolbert and co-workers synthesized Zn<sup>2+</sup> and -BF<sub>2</sub> coordinated pyridyl derivatives of GFP chromophore, which were highly fluorescent owing to the restricted conformation.<sup>172</sup> Similar compounds were earlier synthesized by Wu *et al.*<sup>173</sup>



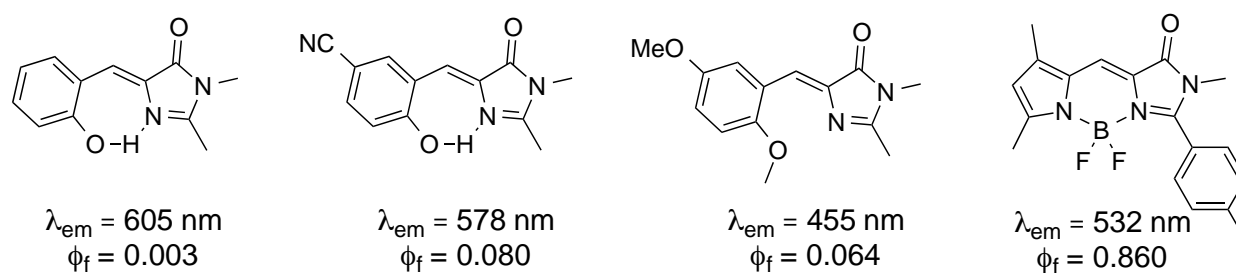


**Figure 3.5.** Examples of *o*-HBDI analogues synthesized by Chou and co-workers. The quantum yields are calculated in cyclohexane,<sup>170</sup> and methanol.<sup>173</sup>

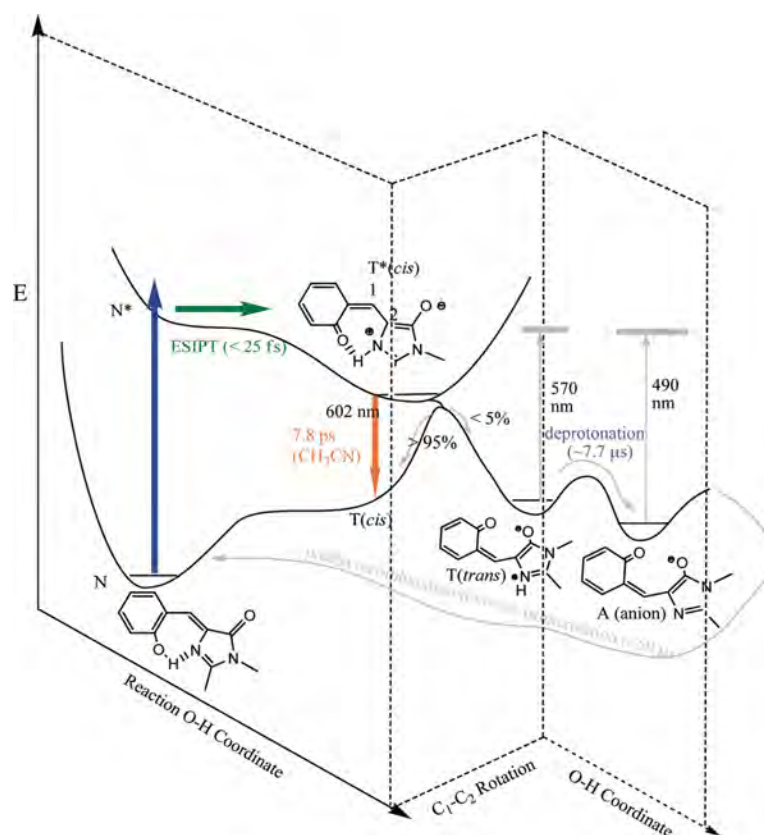


**Figure 3.6.** ESIPT and ground state reverse proton transfer mechanism of *o*-HBDI in  $\text{CH}_3\text{CN}$  as proposed by Chou and coworkers.<sup>171</sup>

Yang and co-workers focused on the synthesis of imidazole derivatives of GFP-type chromophores (Figure 3.7) where the *cis* isomer exhibited a dual emission (*ca.* 460 nm, normal and *ca.* 595 nm, tautomer) in aprotic solvents, while only the normal emission was obtained in MeOH, due to inhibited ESIPT process in protic solvent as proposed earlier for *o*-HBDI.<sup>174</sup> The larger Stokes' shifted emission was rationalized as an excited-state intramolecular proton transfer

(ESIPT) mediated by an N–H···N type of hydrogen bond (Figure 3.7). Compared to other green fluorescent protein (GFP) analogues such as o-HBDI, 2-BFP (Figure 3.7) possesses enhanced quantum yields and much slower proton-transfer rates. Fluorescence upconversion experiments revealed two rising components for the tautomer formation of 2-BFP and indicated that the proton transfer is triggered by the relaxation of the N\* state. The weaker photoacidity of N–H was proposed to play a key role for the observed photophysical and photochemical properties.

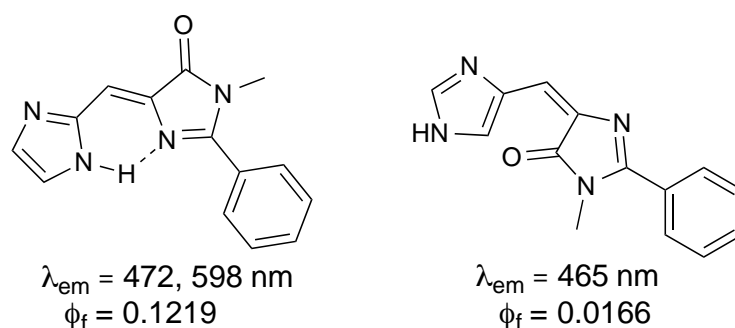


**Figure 3.7.** Examples of blue fluorescent protein chromophore (2-BFP and 4-BFP respectively) analogues. The quantum yields are calculated in *p*-xylene.<sup>174</sup>

Very recently, a different approach towards synthesizing a series of structurally locked GFP core chromophores has been developed by Chou and coworkers.<sup>175</sup> In this approach, a five membered ring stops the rotation of the C(4)-C(5) bond (Figure 3.8). Additionally, a seven membered hydrogen bonded ring allows ESIPT. Together, these modifications result in a dramatic enhancement of fluorescence of *o*-LHBDI (ortho-locked HBDI) at room temperature ( $\phi_f = 0.18$  in toluene), opening up tremendous prospects in biotechnology and in field devices like OLED (organic light emitting diodes), due to an amplified spontaneous emission. The emission peak was observed at ~585 nm and was ascribed to be originating from the tautomer formed via ESIPT.

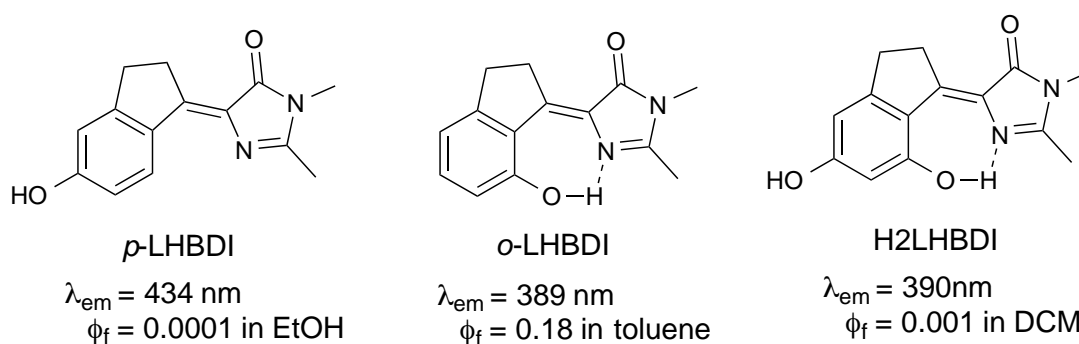


**Figure 3.8.** Example of locked GFP chromophores synthesized by Chou and coworkers.<sup>175</sup>

The high quantum yield of the GFP core chromophore can be attributed to the protein cavity conformation, which suppresses nonradiative relaxation by restricting large-amplitude motions (rotation and bending about bonds) as well as by reducing the degree of small-amplitude motions (vibration and stretching). Inhibiting the inherent rotational motion of the GFP core chromophores by cyclization of exocyclic single bond and through the intramolecular hydrogen bonding to restrict the C(3)–C(4)–C(5) motion lead to an order of magnitude increase in quantum yield.

## References

- (100) Shimomura, O.; Johnson, F. H.; Saiga, Y. *J. Cell. Comp. Physiol.* **1962**, 59, 223.
- (101) Johnson, F. H.; Shimomura, O.; Saiga, Y.; Gershman, I. C.; Reynolds, G. T.; Waters, J. *R. J. Cell. Comp. Physiol.* **1962**, 60, 85.
- (102) Morin, J. G.; Hastings, J. W. *J. Cell. Physiol.* **1971**, 77, 313.
- (103) Morise, H.; Shimomura, O.; Johnson, F. H.; Winant, J. *Biochemistry* **1974**, 13, 2656.
- (104) Prendergast, F. G.; Mann, K. G. *Biochemistry* **1978**, 17, 3448.
- (105) Shimomura, O. *FEBS Lett.* **1979**, 104, 220.
- (106) Prasher, D. C.; Eckenrode, V. K.; Ward, W. W.; Prendergast, F. G.; Cormier, M. J. *Gene*

- 1992**, *111*, 229.
- (107) Chalfie, M.; Tu, Y.; Euskirchen, G.; Ward, W. W.; Prasher, D. C. *Science* **1994**, *263*, 802.
  - (108) Inouye, S.; Tsuji, F. I. *FEBS Lett.* **1994**, *351*, 211.
  - (109) Chudakov, D. M.; Matz, M. V.; Lukyanov, S.; Lukyanov, K. A. *Physiol. Rev.* **2010**, 1103.
  - (110) Doerr, A. *Nat. Methods* **2011**, *8*, 790.
  - (111) Rafiq, S.; Rajbongshi, B. K.; Nair, N. N.; Sen, P.; Ramanathan, G. *J. Phys. Chem. A* **2011**, *115*, 13733.
  - (112) Donner, J. S.; Thompson, S. A.; Kreuzer, M. P.; Baffou, G.; Quidant, R. *Nano Lett.* **2012**, *12*, 2107.
  - (113) Losfeld, M. E.; Soncin, F.; Ng, B. G.; Singec, I.; Freeze, H. H. *FASEB* **2012**, *26*, 4210.
  - (114) Van Oort, B.; Ter Veer, M. J. T.; Groot, M. L.; Van Stokkum, I. H. M. *Phys. Chem. Chem. Phys.* **2012**, *14*, 8852.
  - (115) Addison, K.; Heisler, I. A.; Conyard, J.; Dixon, T.; Page, P. C. B.; Meech, S. R. *Faraday Discuss.* **2013**, *163*, 277.
  - (116) Cheng, P. H.; Li, C. L.; Her, L. S.; Chang, Y. F.; Chan, A. W. S.; Chen, C. M.; Yang, S. H. *Brain Struct. Funct.* **2013**, *218*, 283.
  - (117) Clark, J.; Grznarova, P.; Stansell, E.; Diehl, W.; Lipov, J.; Spearman, P.; Ruml, T.; Hunter, E. *Plos One* **2013**, *8*, e83863.
  - (118) Pan, Y.; Leifert, A.; Graf, M.; Schiefer, F.; Thoroe-Boveleth, S.; Broda, J.; Halloran, M. C.; Hollert, H.; Laaf, D.; Simon, U.; Jahn-Dechent, W. *Small* **2013**, *9*, 863.
  - (119) Saha, R.; Verma, P. K.; Rakshit, S.; Saha, S.; Mayor, S.; Pal, S. K. *Sci. Rep.* **2013**, *3*, 1580.

- (120) Heim, R.; Cubitt, A. B.; Tsien, R. Y. *Nature* **1995**, 373, 663.
- (121) Zhang, L.; Patel, H. N.; Lappe, J. W.; Wachter, R. M. *J. Am. Chem. Soc.* **2006**, 128, 4766.
- (122) Branchini, B. R.; Lusins, J. O.; Zimmer, M. *J. Biomol. Struct. Dyn.* **1997**, 14, 441.
- (123) Ward, W. W.; Prentice, H. J.; Roth, A. F.; Cody, C. W.; Reeves, S. C. *Photochem. Photobiol.* **1982**, 35, 803.
- (124) Stoner-Ma, D.; Melief, E. H.; Nappa, J.; Ronayne, K. L.; Tonge, P. J.; Meech, S. R. *J. Phys. Chem. B* **2006**, 110, 22009.
- (125) Stoner-Ma, D.; Jaye, A. A.; Ronayne, K. L.; Nappa, J.; Meech, S. R.; Tonge, P. J. *J. Am. Chem. Soc.* **2008**, 130, 1227.
- (126) Fang, C.; Frontiera, R. R.; Tran, R.; Mathies, R. A. *Nature* **2009**, 462, 200.
- (127) Chattoraj, M.; King, B. A.; Bublit, G. U.; Boxer, S. G. *Proc. Natl. Acad. Sci. U.S.A.* **1996**, 93, 8362.
- (128) Yokoe, H.; Meyer, T. *Nat. Biotechnol.* **1996**, 14, 1252.
- (129) Brejc, K.; Sixma, T. K.; Kitts, P. A.; Kain, S. R.; Tsien, R. Y.; Ormö, M.; Remington, S. *J. Proc. Natl. Acad. Sci. U.S.A.* **1997**, 94, 2306.
- (130) Palm, G. J.; Zdanov, A.; Gaitanaris, G. A.; Stauber, R.; Pavlakis, G. N.; Wlodawer, A. *Nature Struct. Biol.* **1997**, 4, 361.
- (131) Weber, W.; Helms, V.; McCammon, J. A.; Langhoff, P. W. *Proc. Natl. Acad. Sci. U.S.A.* **1999**, 96, 6177.
- (132) Niwa, H.; Ionuye, S.; Horano, T.; Matsuno, T.; Kojima, S.; Kubota, M.; Ohashi, M.; Tsuji, F. I. *Proc. Natl. Acad. Sci. U.S.A.* **1996**, 93, 13617.
- (133) Kojima, S.; Ohkawa, H.; Hirano, T.; Maki, S.; Niwa, H.; Ohashi, M.; Inouye, S.; Tsuji, F. *I. Tetrahedron Lett.* **1998**, 39, 5239.

- (134) Buck, J. S.; Ide, W. S. *Org. Synthesis* **1943**, 2, 55.
- (135) Chen, K. Y.; Cheng, Y. M.; Lai, C. H.; Hsu, C. C.; Ho, M. L.; Lee, G. H.; Chou, P. T. *J. Am. Chem. Soc.* **2007**, 129, 4534.
- (136) Hsieh, C.-C.; Chou, P.-T.; Shih, C.-W.; Chuang, W.-T.; Chung, M.-W.; Lee, J.; Joo, T. *J. Am. Chem. Soc.* **2011**, 133, 2932.
- (137) Saltiel, J.; Waller, A. S.; Sears, D. F. *J. Am. Chem. Soc.* **1993**, 115, 2453.
- (138) Todd, D. C.; Fleming, G. R. *J. Chem. Phys.* **1993**, 98, 269.
- (139) Litvinenko, K. L.; Webber, N. M.; Meech, S. R. *Chem. Phys. Lett.* **2001**, 346, 47.
- (140) Webber, N. M.; Litvinenko, K. L.; Meech, S. R. *J. Phys. Chem. B* **2001**, 105, 8036.
- (141) Kummer, A. D.; Wiehler, J.; Schüttrigkeit, T. A.; Berger, B. W.; Steipe, B.; Michel-Beyerle, M. E. *ChemBioChem* **2002**, 3, 659.
- (142) Mandal, D.; Tahara, T.; Webber, N. M.; Meech, S. R. *Chem. Phys. Lett.* **2002**, 358, 495.
- (143) Litvinenko, K. L.; Webber, N. M.; Meech, S. R. *J. Phys. Chem. A* **2003**, 107, 2616.
- (144) Mandal, D.; Tahara, T.; Meech, S. R. *J. Phys. Chem. B* **2003**, 108, 1102.
- (145) Stübner, M. R.; Schellenberg, P. *J. Phys. Chem. A* **2003**, 107, 1246.
- (146) Ishii, K.; Takeuchi, S.; Tahara, T. *Chem. Phys. Lett.* **2004**, 398, 400.
- (147) Mandal, D.; Tahara, T.; Meech, S. R. *J. Phys. Chem. B* **2004**, 108, 1102.
- (148) Vengris, M.; van Stokkum, I. H. M.; He, X.; Bell, A. F.; Tonge, P. J.; van Grondelle, R.; Larsen, D. S. *J. Phys. Chem. A* **2004**, 108, 4587.
- (149) Usman, A.; Mohammed, O. F.; Nibbering, E. T. J.; Dong, J.; Solntsev, K. M.; Tolbert, L. M. *J. Am. Chem. Soc.* **2005**, 127, 11214.
- (150) Gepshtein, R.; Huppert, D.; Agmon, N. *J. Phys. Chem. B* **2006**, 110, 4434.
- (151) Stavrov, S. S.; Solntsev, K. M.; Tolbert, L. M.; Huppert, D. *J. Am. Chem. Soc.* **2006**, 128, 1540.

- (152) Yang, J. S.; Huang, G. J.; Liu, Y. H.; Peng, S. M. *Chem. Commun.* **2008**, 1344.
- (153) Voityuk, A. A.; Michel-Beyerle, M. E.; Rösch, N. *Chem. Phys.* **1998**, *231*, 13.
- (154) Martin, M. E.; Negri, F.; Olivucci, M. *J. Am. Chem. Soc.* **2004**, *126*, 5452.
- (155) Toniolo, A.; Olsen, S.; Manohara, L.; Martínez, T. *J. Faraday Discuss.* **2004**, *127*, 149.
- (156) Sinicropi, A.; Anduniow, T.; Ferre, N.; Basosi, R.; Olivucci, M. *J. Am. Chem. Soc.* **2005**, *127*, 11534.
- (157) Rajbongshi, B. K.; Sen, P.; Ramanathan, G. *Chem. Phys. Lett.* **2010**, *494*, 295.
- (158) Follenius-Wund, A.; Bourotte, M.; Schmitt, M.; Iyice, F.; Lami, H.; Bourguignon, J. J.; Haiech, J.; Pigault, C. *Biophys. J.* **2003**, *85*, 1839.
- (159) Altoe, P.; Bernardi, F.; Garavelli, M.; Orlandi, G.; Negri, F. *J. Am. Chem. Soc.* **2005**, *127*, 3952.
- (160) Solntsev, K. M.; Poizat, O.; Dong, J.; Rehault, J.; Lou, Y. B.; Burda, C.; Tolbert, L. M. *J. Phys. Chem. B* **2008**, *112*, 2700.
- (161) Liu, R. S. H. *Acc. Chem. Res.* **2001**, *34*, 555.
- (162) Liu, R. S. H.; Hammond, G. S. *Chem.—Eur. J.* **2001**, *7*, 4536.
- (163) Webber, N. M.; Litvinenko, K. L.; Meech, S. R. *J. Phys. Chem. B* **2001**, *105*, 8036.
- (164) Litvinenko, K. L.; Webber, N. M.; Meech, S. R. *Bull. Chem. Soc. Jpn.* **2002**, *75*, 1065.
- (165) Maddalo, S. L.; Zimmer, M. *Photochem. Photobiol.* **2006**, *82*, 367.
- (166) Megley, C. M.; Dickson, L. A.; Maddalo, S. L.; Chandler, G. J.; Zimmer, M. *J. Phys. Chem. B* **2009**, *113*, 302.
- (167) Baffour-Awuah, N. Y. A.; Zimmer, M. *Chem. Phys.* **2004**, *303*, 7.
- (168) Dong, J.; Abulwerdi, F.; Baldrige, A.; Kowalik, J.; Solntsev, K. M.; Tolbert, L. M. *J. Am. Chem. Soc.* **2008**, *130*, 14096.
- (169) Kang, J.; Zhao, G.; Xu, J.; Yang, W. *Chem. Commun.* **2010**, *46*, 2868.

- (170) Chuang, W. T.; Hsieh, C. C.; Lai, C. H.; Lai, C. H.; Shih, C. W.; Chen, K. Y.; Hung, W. Y.; Hsu, Y. H.; Chou, P. T. *J. Org. Chem.* **2011**, *76*, 8189.
- (171) Hsieh, C. C.; Chou, P. T.; Shih, C. W.; Chuang, W. T.; Chung, M. W.; Lee, J.; Joo, T. *J. Am. Chem. Soc.* **2011**, *133*, 2932.
- (172) Baranov, M. S.; Lukyanov, K. A.; Borissova, A. O.; Shamir, J.; Kosenkov, D.; Slipchenko, L. V.; Tolbert, L. M.; Yampolsky, I. V.; Solntsev, K. M. *J. Am. Chem. Soc.* **2012**, *134*, 6025.
- (173) Wu, L. X.; Burgess, K. *J. Am. Chem. Soc.* **2008**, *130*, 4089.
- (174) Fang, X.; Wang, Y.; Wang, D.; Zhao, G.; Zhang, W.; Ren, A.; Wang, H.; Xu, J.; Gao, B.-R.; Yang, W. *J. Phys. Chem. Lett.* **2014**, *5*, 92.
- (175) Hsu, Y.-H.; Chen, Y.-A.; Tseng, H.-W.; Zhang, Z.; Shen, J.-Y.; Chuang, W.-T.; Lin, T.-C.; Lee, C.-S.; Hung, W.-Y.; Hong, B.-C.; Liu, S.-H.; Chou, P.-T. *J. Am. Chem. Soc.* **2014**, *136*, 11805.





## Introduction to Associated Manuscripts

Numerous structural analogues of GFP core chromophore have been prepared previously, yet only a few synthetic routes have been utilized. In the associated manuscripts, which are in the process of submission for publication, we report a simple and facile technique to synthesize locked and unlocked GFP analogues via oxazolinone formation. The locked analogues synthesized are brightly fluorescent in the solid state but poorly fluoresce in solution, indicating that rotation of the exocyclic double bond persists in solution. From this observation we planned and synthesized ortho-locked analogues, in which a seven-membered ring is formed via hydrogen bonding between the benzylidene and imidazolinone moieties. This ortho-locked compound not only shows greater fluorescence than *p*-HBDI, it shows a dual emission.

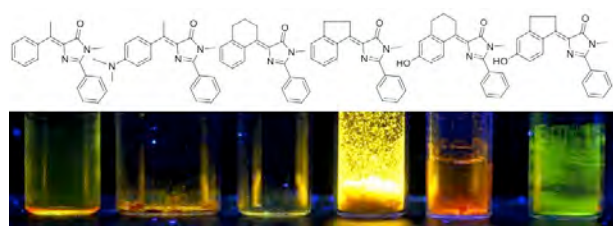


# An Efficient and Concise Method to Synthesize Locked GFP Chromophore Analogues

Soumit Chatterjee and Peter Karuso\*

Department of Chemistry and Biomolecular Sciences, Macquarie University, Sydney, NSW 2109, Australia

*Supporting Information: Synthesis of all the compounds, 1D and 2D NMR spectra and steady state absorption and emission spectra. This material is available free of charge via the Internet at <http://pubs.acs.org>.*



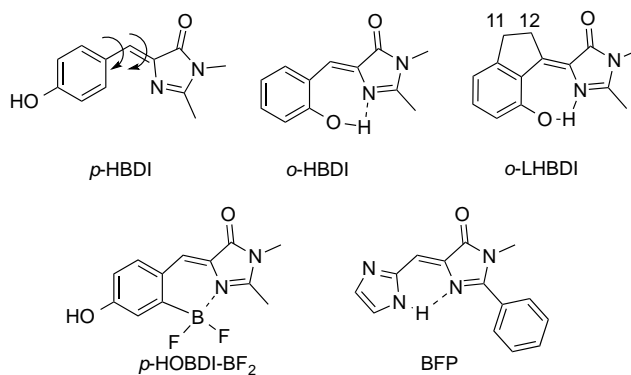
**ABSTRACT:** A series of GFP analogues, which are fluorescent in the solid state at room temperature, have been synthesized via oxazolone formation. The oxazolone formation process involves a condensation reaction in the presence of a Lewis acid following a Knoevenagel condensation. A ring opened intermediate is formed which cyclizes readily upon heating to produce the imidazolone. This method is faster, simpler and has higher yields than alternative methods.

The Green Fluorescent Protein (GFP) family is extensively used in cell biology as a genetically encoded, fluorescent marker.<sup>1-6</sup> The chromophore in wild-type GFP is 5-(4-hydroxybenzylidene)-3,5-dihydro-4H-imidazol-4-one (*p*-HBDI).<sup>7</sup> However, the isolated chromophore is non-fluorescent ( $\phi_f < 10^{-4}$ ) in contrast to the protein ( $\phi_f = 0.8$ ).<sup>8-10</sup> This has been found to be due to non-radiative pathways ( $\phi$  and  $\tau$  rotation in the excited states) for the free fluorophore that are not available to the chromophore inside the constrained GFP  $\beta$ -barrel.<sup>11-14</sup> Miyashita published a failed attempt to produce room temperature fluorophores based on HBDI in this journal that relied on a 1-step synthesis.<sup>15</sup> Chou and coworkers were the first to synthesize a derivative (*o*-HBDI; 4-(2-hydroxybenzylidene)-1,2-dimethyl-1H-imidazol-5(4H)-one) where intramolecular hydrogen bonding hindered  $\phi$  and  $\tau$  rotation, resulting in decreased non-radiative decay (Chart 1) but still relative poor fluorescence.<sup>9</sup>

Tolbert and coworkers as well as Burges and coworkers synthesized Zn<sup>2+</sup> and BF<sub>2</sub> coordinated pyridyl derivatives of GFP chromophore, which were fluorescent due to the restricted rotation about  $\phi$  and  $\tau$ .<sup>16,17</sup> Yang and coworkers synthesized imidazole derivatives of GFP type chromophores (BFP) which are blue fluorescent.<sup>18</sup> More recently, a different approach towards the synthesis of a series of structurally locked GFP core chromophores has been developed by Chou and coworkers.<sup>19</sup> In this approach, a five membered ring eliminates  $\phi$  rotation and *ortho*-hydroxyl hinders  $\tau$  rotation (*o*-LHBDI, Chart 1). Together, these modifications result in

enhanced fluorescence ( $\phi_f = 0.18$  in toluene) at room temperature. We independently developed the same sort of approach but using a superior synthetic methodology which we report here.

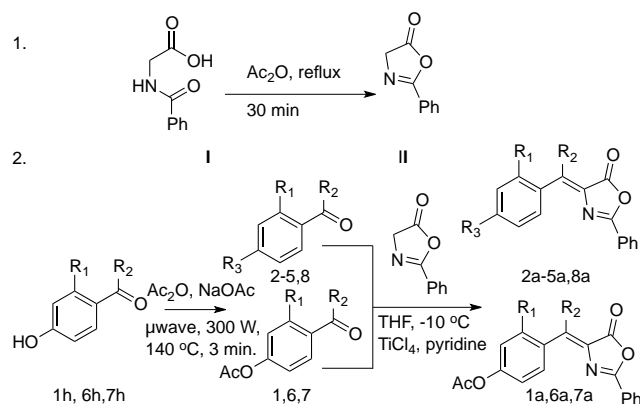
**Chart 1.** Molecular structures of *p*-HBDI, *o*-HBDI, *o*-LHBDI, *p*-HOBDI-BF<sub>2</sub> and BFP



Although numerous structural analogues have been prepared previously, few synthetic routes have been utilized. In general, these routes start with Erlenmeyer azalactone synthesis, in which the reaction of *N*-acylglycines with arylaldehydes and sodium acetate in acetic anhydride results in the formation of 4-arylidene-5-oxazolinones. Direct condensation

of the oxazolinones with primary amines in the presence of a base yielding 4-arylidene-5-imidazolinones became the most common approach.<sup>8,20</sup> However, the Erlenmeyer method was found to be non-effective to produce the oxazolinones using arylketones due to their poor reactivity compared to aldehydes. A number of synthetic methodologies, including catalytic lead acetate, triethylamine and phosphorous oxychloride, failed to form the oxazolinone. An alternate route was constructed following Knoevenagel condensation reaction.<sup>19,21,22</sup> This method had been successfully implemented by Chou and co-workers to synthesize *o*-LHBDI and *p*-LHBDI by condensation of hydroxy-1-indanones and imidazolinones but, the oxazolinone was not formed as an intermediate.<sup>19</sup> This method intrigued us and we focused to retain the conventional path of oxazolinone formation as these can themselves be used as fluorescent analogues as reported earlier.<sup>23</sup> A series of oxazolinones were synthesized by the condensation of the arylketones with previously synthesized phenyl oxazolinone with substantial yield. Moreover, the reactions were complete within a much smaller time scale (4-5 hrs).

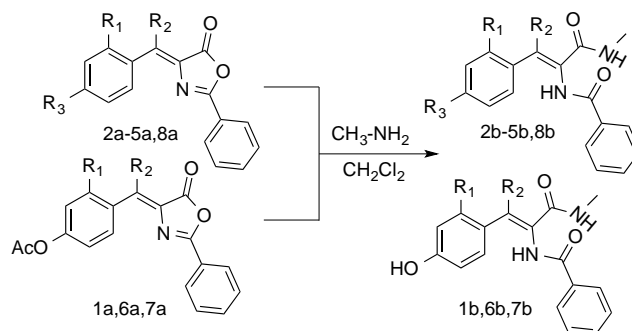
**Scheme 1.** Condensation of arylketones and phenyloxazolinone by Knoevenagel reaction



NMR showed that for a few compounds both *Z*- and *E*- isomers were formed (Supporting information). But, these isomers were not separated keeping in mind that eventually they could lead to yield the isomeric mixture of the final imidazolinone and could be separated there after. To our surprise, imidazolinones from the oxazolinones were not formed following conventional method of refluxing them with primary amine in presence of base and using ethanol as solvent except for 1. Rather, a white precipitate formed which was collected upon filtration and NMR analysis showed it to be the ring opened *N*-alkyl-2-acylamino-3-arylacrylamides (1b-8b). Formation of this type of compounds have been previously reported by Lee *et al.*<sup>20</sup> The oxazolinones were then dissolved in minimum amount of dichloromethane and stirred with acetonitrile saturated with dry methylamine (2 equivalents) at room temperature to yield the ring opened acrylamindes. The idea of using acetonitrile saturated with methylamine was to suppress the nucleophilic attack from water that could form the acids instead of the desired amides. The reactions were fast and were over within 15 min for most cases, but longer period of stirring (1 hr) with addition of 2 more equivalents of methylamine were required for a few arylketones (6,7). The onset of the reaction could be observed by the formation of white precipitates while the progress of the reaction could be monitored by TLC. For the OAc-arylketones (1,6,7), the yellow colour of

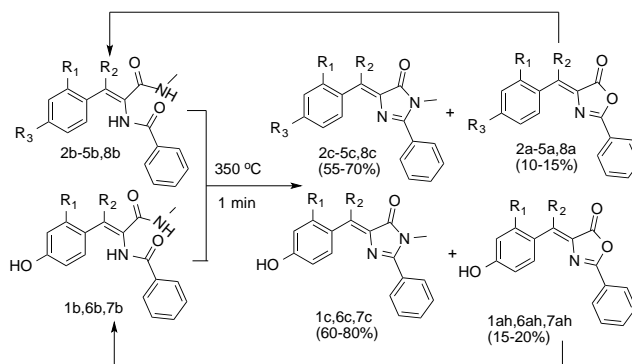
the oxazolinones (1a, 6a, 7a) changed to orange upon addition of methylamine, indicating the depletion of acetoxy group. The yields were found to be ~ 98-100% in general and ~80-90% for the acetoxy-arylketones (1,6,7).

**Scheme 2.** Nucleophilic ring opening of oxazolinones



The final step of the desired imidazolinone formation required dehydrative cyclization of the acrylamides. To get the final imidazolinones, initially 2b was taken as a standard and a gamut of trials were carried out following literature procedures but all them were unsuccessful.

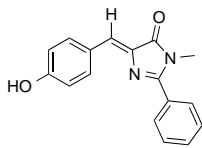
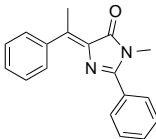
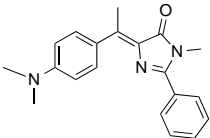
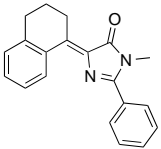
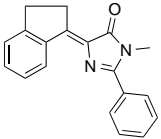
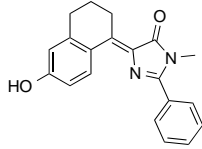
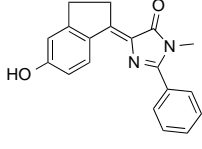
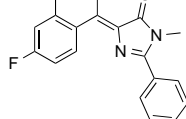
**Scheme 3.** Dehydrative condensation of ring opened acrylamindes



Mitsunobu reaction, commonly used for dehydration-condensation, that is refluxing of acrylamides in pyridine, also failed.<sup>24</sup> Fortuitous heating of a TLC plate to dry pyridine off from it showed formation of a yellow spot in the product column. Upon eluting with solvent (PE/EtOAc), two distinct yellow bands appeared and were visible to the naked eye; one band had the same *R<sub>f</sub>* value as 1a, the respective oxazolinone and a new, relatively polar band. Pyridine was then dried off from the reaction mixture (acrylamide+pyridine) and it was then heated vigorously using a heat gun until the colour of the acrylamide changed. The yellow product was dissolved in DCM and was purified by flash chromatography. NMR analysis of the spots revealed them to be the desired imidazolinone and the oxazolinone respectively. Oxazolinone is probably formed due to the nucleophilic attack of water to the imidazolinone. Following this method, we tried to standardize the parameters to prepare the imidazolinones and found that heating of the solid, white acrylamides (the intermediate) using a furnace at 350 °C just for 1 min can lead to the formation of the desired products. This method is much more efficient and significantly less time consuming than Mitsunobu reaction,

commonly used for dehydration-condensation or other reported method of refluxing in pyridine.<sup>10,24</sup>

**Table 1.** Dehydrative condensation of ring opened acrylamides

Entry	Product	<i>t</i> (min)	Yield (%)
1c		1	80
2c		1	70
3c		1	65
4c		1	65
5c		1	62
6c		1	60
7c		1	60
8c		1	57

The percentage yield of the product varies from 57–80%, but the oxazolinone formed (15–20%) as a side product can again be used and the cumulative yield of the reaction becomes ~90%. For the hydroxy-arylketones (1,6,7), upon the

dehydrative cyclization, hydroxy-oxazolinones (1ah,6ah,7ah) are formed along with the desired imidazolinones (1c,6c,7c). The hydroxy-oxazolinones (1ah,6ah,7ah) can be again acetylated and used to increase the yield. NMR shows that only the *cis* isomer is formed for all imidazolinones.

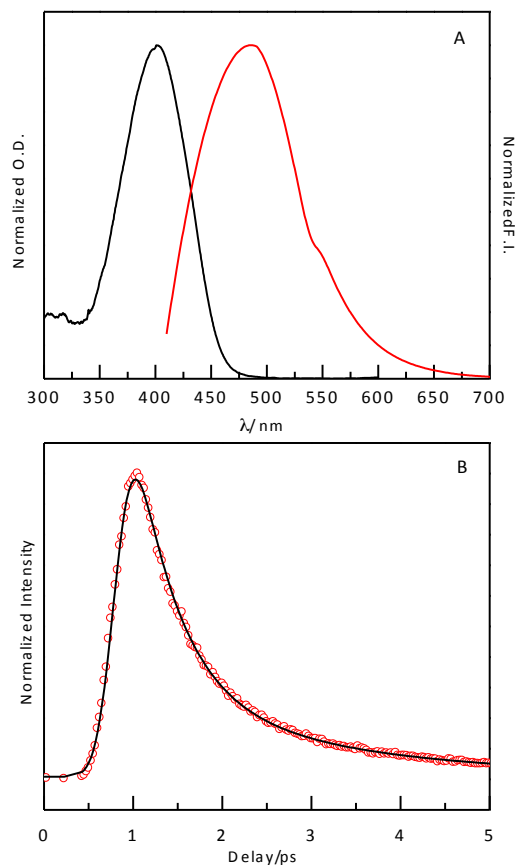


**Figure 1.** A) Normalized absorption and emission spectra and B) femtosecond fluorescence upconversion decay trace of 7c in water.  $\lambda_{\text{exc}} = 400 \text{ nm}$ ;  $\lambda_{\text{em}} = 490 \text{ nm}$

Steady state absorption and emission spectra were recorded for each compound (Figure 1A, supporting information) in solution. It was found that compound 3c was non-fluorescent. 30 times higher quantum yield than that of *p*-HBDI was obtained for 5c, which was the highest amongst all the imidazolinones. Higher quantum yield of 5c over 4c can be rationalized by possession of a six-membered ring in the tetralone derivative, which can undergo facile conformational change (boat  $\leftrightarrow$  chair) and likely to destabilize the excited state. On the otherhand, compound 6c and 7c had comparable quantum yield because of formation of the phenoxide. Femtosecond fluorescent transients were also recorded for the imidazolinones in water and in *tert*-butanol (Figure 1B, supporting information). The decays got over within 5 ps, indicating very fast relaxation process, which was in agreement with the poor quantum yields of these compounds. This indicated that restricting the single bond rotation alone could not alter the molecular dynamics and that the exocyclic double bond rotation was inevitable. The faster component of < 1 ps predominated for all the compounds in the solvents studied. It

was found that presence of *p*-OH did not affect the decays as was found from the respective temporal parameters of 4c-6c and 5c-7c (Table S4). Rather, presence of indanone ring somewhat slowed the dynamics over the tetralone ones as was evident from the respective temporal parameters between 4c-5c and 6c-7c (Table S4). This was accounted well with the slightly higher quantum yields of the indanone compounds than that of the tetralone ones on the basis of facile conformational change (boat  $\leftrightarrow$  chair  $\leftrightarrow$  boat) in the latter.

In conclusion, we have developed a simple and facile technique to synthesize locked and unlocked GFP analogues via oxazolinone formation. The cumulative yields of the end products are found to be much higher than before. The final step of the reaction needs simple heating of the ring-opened acrylamides for a minute or so and has never been reported before to our knowledge. The locked analogues synthesized are found to be brightly fluorescent in solid state but poorly fluoresce in solution, indicating that the rotation of the exocyclic double bond persists in solution phase. From this observation we planned and synthesized an ortho-locked analogue, in which a seven-membered ring is formed between the benzyldene and imidazolinone moieties via hydrogen bonding. This ortho-locked compound not only showed greater fluorescence than any of the imidazolinones reported above, it showed a dual emission. The detailed study will be discussed thoroughly in a separate publication later. For the unlocked and locked GFP analogues discussed above, detailed steady state and time resolved investigation with solvent variation and in microheterogeneous media can help us to design HBDI derivatives with higher quantum yield.

## SUPPORTING INFORMATION

Synthesis of all the compounds, 1D and 2D NMR spectra, steady state absorption and emission spectra and femtosecond fluorescence decay traces. *This material is available free of charge via the Internet at <http://pubs.acs.org>, and can be found in the experimental chapter as well as in the appendices of the thesis.*

## Corresponding Author

\* Fax: (+612-9850-8313). E-mail: peter.karuso@mq.edu.au

## ACKNOWLEDGMENT

This research is supported by the Australian Research Council (DP0877999) to P.K. We gratefully acknowledge the Australian Research Council for the funding support of S.C. We thank Prof. Anindya Datta for permitting us to use absorption spectrophotometer, fluorimeter and fluorescence upconversion instrument in his laboratory.

## REFERENCES

- (1) Chudakov, D. M.; Matz, M. V.; Lukyanov, S.; Lukyanov, K. A. *Physiol. Rev.* **2010**, *90*, 1103.
- (2) Tsien, R. Y. *Annu. Rev. Biochem.* **1998**, *67*, 509.
- (3) Sullivan, K. F.; Kay, S. A. *Green Fluorescent Proteins*, 1999.
- (4) Paige, J. S.; Wu, K. Y.; Jaffrey, S. R. *Science* **2011**, *333*, 642.
- (5) Addison, K.; Heisler, I. A.; Conyard, J.; Dixon, T.; Bulman Page, P. C.; Meech, S. R. *Faraday Discuss.* **2013**, *163*, 277.
- (6) Cheng, C.-W.; Huang, G.-J.; Hsu, H.-Y.; Prabhakar, C.; Lee, Y.-P.; Diao, E. W.-G.; Yang, J.-S. *J. Phys. Chem. B* **2013**, *117*, 2705.
- (7) Cody, C. W.; Prasher, D. C.; Westler, W. M.; Prendergast, F. G.; Ward, W. W. *Biochemistry* **1993**, *32*, 1212.
- (8) Kojima, S.; Ohkawa, H.; Hirano, T.; Maki, S.; Niwa, H.; Ohashi, M.; Inouye, S.; Tsuji, F. I. *Tetrahedron Lett.* **1998**, *39*, 5239.
- (9) Chen, K. Y.; Cheng, Y. M.; Lai, C. H.; Hsu, C. C.; Ho, M. L.; Lee, G. H.; Chou, P. T. *J. Am. Chem. Soc.* **2007**, *129*, 4534.
- (10) Hsieh, C.-C.; Chou, P.-T.; Shih, C.-W.; Chuang, W.-T.; Chung, M.-W.; Lee, J.; Joo, T. *J. Am. Chem. Soc.* **2011**, *133*, 2932.
- (11) Weber, W.; Helms, V.; McCammon, J. A.; Langhoff, P. W. *Proc. Natl. Acad. Sci. U.S.A.* **1999**, *96*, 6177.
- (12) Mandal, D.; Tahara, T.; Webber, N. M.; Meech, S. R. *Chem. Phys. Lett.* **2002**, *358*, 495.
- (13) Litvinenko, K. L.; Webber, N. M.; Meech, S. R. *J. Phys. Chem. A* **2003**, *107*, 2616.
- (14) Mandal, D.; Tahara, T.; Meech, S. R. *J. Phys. Chem. B* **2004**, *108*, 1102.
- (15) Ikejiri, M.; Tsuchino, M.; Chihara, Y.; Yamaguchi, T.; Imanishi, T.; Obika, S.; Miyashita, K. *Org. Lett.* **2012**, *14*, 4406.
- (16) Baranov, M. S.; Lukyanov, K. A.; Borissova, A. O.; Shamir, J.; Kosenkov, D.; Slipchenko, L. V.; Tolbert, L. M.; Yampolsky, I. V.; Solntsev, K. M. *J. Am. Chem. Soc.* **2012**, *134*, 6025.
- (17) Wu, L. X.; Burgess, K. *J. Am. Chem. Soc.* **2008**, *130*, 4089.
- (18) Fang, X.; Wang, Y.; Wang, D.; Zhao, G.; Zhang, W.; Ren, A.; Wang, H.; Xu, J.; Gao, B.-R.; Yang, W. *J. Phys. Chem. Lett.* **2014**, *5*, 92.
- (19) Hsu, Y.-H.; Chen, Y.-A.; Tseng, H.-W.; Zhang, Z.; Shen, J.-Y.; Chuang, W.-T.; Lin, T.-C.; Lee, C.-S.; Hung, W.-Y.; Hong, B.-C.; Liu, S.-H.; Chou, P.-T. *J. Am. Chem. Soc.* **2014**, *136*, 11805.
- (20) Lee, C.-Y.; Chen, Y.-C.; Lin, H.-C.; Jhong, Y.; Chang, C.-W.; Tsai, C.-H.; Kao, C.-L.; Chien, T.-C. *Tetrahedron* **2012**, *68*, 5898.
- (21) Wu, L.; Burgess, K. *J. Am. Chem. Soc.* **2008**, *130*, 4089.
- (22) Baldrige, A.; Solntsev, K. M.; Song, C.; Tanioka, T.; Kowalik, J.; Hardcastle, K.; Tolbert, L. M. *Chem. Commun.* **2010**, *46*, 5686.
- (23) Kang, J.; Zhao, G.; Xu, J.; Yang, W. *Chem. Commun.* **2010**, *46*, 2868.
- (24) Mitsunobu, O. *Synthesis* **1981**, *1*, 1.

**Supporting Information**  
**Of**  
**An Efficient and Concise Method to Synthesize Locked GFP Chromophore**  
**Analogs**

Soumit Chatterjee and Peter Karuso<sup>\*</sup>

Department of Chemistry and Biomolecular Sciences, Macquarie University,  
Sydney, NSW 2109, Australia





## Materials and Experimental Procedure

Unless otherwise stated, all chemicals and reagents were received from Sigma-Aldrich (Castle Hill, Australia) and used without further purification. Chloroform, dichloromethane, diethyl ether, ethanol, ethyl acetate, light petroleum, methanol, tetrahydrofuran were obtained from ChemSupply (Australia). HPLC grade acetonitrile was obtained from BDH/Merck (Germany), and was used without further purification. Spectroscopy grade acetonitrile from Spectrochem was distilled over  $\text{CaH}_2$  and the distillate passed through activated neutral alumina immediately prior to use. Spectroscopy grade *tert*-butanol from Spectrochem, Mumbai, India was used as received.

## Equipment

$^1\text{H}$  NMR and  $^{13}\text{C}$  NMR spectra were recorded in 5 mm Pyrex tubes (Wilmad, USA) on either a Bruker Avance DPX400 400 MHz or AVII600 600 MHz spectrometer. All spectra were obtained at 25 °C, processed using Bruker Topspin 3.2 and referenced to residual solvent ( $\text{CDCl}_3$  7.26/77.16 ppm;  $\text{DMSO-d}_6$  2.49/39.8 ppm). Infrared spectra were taken on a Perkin Elmer paragon 1000PC FTIR spectrometer, or Nicolet iS10 FT-IR Spectrometer (Thermo Scientific, Australia). UV-Vis absorption spectra are recorded on JASCO V-530 double beam absorption spectrophotometer with a slit width of 1.0 nm at room temperature or on Varian Cary-eclipse spectrophotometer.

Low resolution mass spectrometry was performed by electrospray ionisation (ESI) MS in positive or negative polarity mode as required on a Shimadzu LC-20A prominence system coupled to a LCMS-2010 EV mass spectrometer using LCMSsolution 3.21 software. LC-MS experiments were carried out on a Gemini C18 column (Phenomenex, Australia)  $150.0 \times 2.00$  mm,  $110\text{\AA}$ ,  $3\text{ }\mu\text{m}$ .

High resolution mass data were obtained from ESI in positive polarity mode on a Waters Q-TOF Ultima Tandem Quadrupole/Time-of-Flight ESI mass spectrometer, performed by the Mass Spectrometry Unit at the University of Illinois, USA.

HPLC analysis was performed on a Shimadzu 10AD-VP system running Class-VP 7.4 SP1 software or a Waters manual 6000A pump. Analytical, semipreparative and preparative HPLC were performed on Gemini C18 HPLC columns (Phenomenex): Gemini-NX C18 250.0 × 4.6 mm, 110Å, 5 µm; Gemini C18 250.0 × 10.0 mm, 110Å, 10 µm; Gemini-NX C18 150.0 × 21.2 mm, 110Å, 5 µm.

TLC was performed with Merck Kieselgel 60 F254 plates with viewing under ultraviolet light (254 nm and 365 nm). Flash column chromatography was performed on silica gel (60 Å 0.040–0.063 mm, 230-400 mesh ASTM from Grace Chemicals, Melbourne).

After reverse phase HPLC, acetonitrile was evaporated and the residual water removed by lyophilization. The freeze dryer system was from Labconco (USA).

Melting point was measured using DSC 2010 differential scanning calorimeter from TA instruments.

### Steady State Measurements

All experiments were carried out at 25 °C by using double distilled water or freshly distilled solvents. In aqueous solutions, pH was 7.1, measured by pH meter (ISFETCOM, model S2K712, JAPAN). The baseline for absorbance was recorded using air as a reference. Steady state fluorescence spectra were recorded having the source and the detector at right angle. The source was a Xenon lamp pulsed at 80 Hz, with 2 µs FWHM pulse with peak power equivalent to 75 kW and the Hamamatsu R928 photomultiplier tube, respectively. The excitation and emission slits were kept constant at 5 nm and the PMT voltage was 600 volt for all the experiments unless mentioned elsewhere.

All fluorescence spectra were corrected for changes in absorbance using equation 1, where the absorbance is at the wavelength of excitation. This procedure nullifies the changes in intensity that might arise due to concentration<sup>1</sup>

$$F.I.^{Corrected} = \frac{F.I.^{Observed}}{1 - 10^{-Absorbance}} \quad 1$$

For the quantum yield measurements, the experiments were carried out back to back to maintain identical conditions. The relative quantum yield for the fluorophore can be calculated by integrating the fluorescence spectra by using equation 2, which gives the area under the curve

$$\phi_{f_{Rel}}^f = l_{em} = \int_{\lambda_1}^{\lambda_2} \text{Fluorescence spectrum} \quad 2$$

Here,  $l_{em}$  is the area under the curve in fluorescence emission spectra of the fluorophore at a given excitation wavelength; The absolute quantum yield is given by equation 3<sup>2</sup>

$$\phi_f^{abs} = \frac{\phi_f^f}{\phi_s^s} \times \phi_s^{abs} \times \frac{n_f^2}{n_s^2} \quad 3$$

where  $\phi_f^f$  and  $\phi_s^s$  are the relative quantum yields of the fluorophore and the standard,  $\phi_s^{abs}$  is the absolute quantum yield of the standard known from the literature and  $n$  corresponds to the refractive index of the solvent in which the measurements are done. The quantum yields for our experiments were calculated using Quinine sulphate in 0.5 M H<sub>2</sub>SO<sub>4</sub> ( $\phi_f = 0.546$ )<sup>3</sup> as standard.

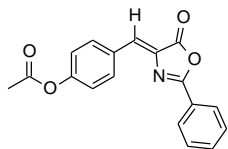
### **Femtosecond Upconversion Experiment**

The output of femtosecond pulsed oscillator from the mode-locked Ti:sapphire laser (Tsunami, Spectra Physics, USA) pumped by 5 W DPSS laser (Millennia, Spectra Physics), centred at 800 nm and with a repetition rate of 80 MHz, was used as the gate pulse for the femtosecond fluorescence upconversion experiments. The second harmonic (400 nm) of this pulse was used as the source of excitation for the sample placed in a rotating cell for the experiments with epicocconone and its analogues. The power of the second harmonic light is restricted to 5 mW at the sample in order to minimize photobleaching. The fluorescence from the sample is upconverted in a nonlinear crystal (0.5 mm BBO,  $\theta = 38^\circ$ ,  $\phi = 90^\circ$ ) by mixing with the gate pulse, which consists of a portion of the fundamental beam. The upconverted light is dispersed in a monochromator and detected using photon counting electronics. A cross-correlation function obtained using the Raman scattering from ethanol has a FWHM of 300 fs. The femtosecond fluorescence decays have been fitted using a Gaussian function of the same FWHM as the excitation pulse. The fluorescence decays were recorded at the magic angle polarization with respect to the excitation pulse on FOG 100 fluorescence optically gated

upconversion spectrometer (CDP Systems Corp., Russia). The resolution was in appropriate multiples of the minimum step size of the instrument, i.e. 0.78 fs/step. The decays were analyzed by iterative reconvolution using a homemade program.<sup>4</sup>

## Synthesis of GFP analogues

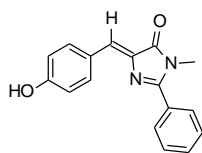
**(Z)-4-((5-oxo-2-phenyloxazol-4(5H)-ylidene)methyl)phenylacetate (1a).** To a solution of 4-



formylphenyl acetate (0.13 mL, 0.82 mmol) in acetic anhydride (5 mL) was added hippuric acid (0.14 g, 0.82 mmol) and sodium acetate (0.067 g, 0.82 mmol) and the reaction mixture was refluxed for two hours, cooled and

then poured into ice water (30 mL) and stirred for 20 min. The precipitate was filtered, washed several times with ice cold ethanol and dried *in vacuo*. The product was recrystallized from DCM/PE and to yield oxazolylidene (**1a**) as a pale yellow solid (1.5 g, 60%) which was used immediately in the next step, m.p. 180.5 °C [lit. m.p. 179 °C]<sup>5</sup>; UV (acetonitrile)  $\lambda_{\text{max}}$  364 nm ( $\epsilon$  = 95000); IR (ATR)  $\nu_{\text{max}}$  1793, 1755, 1653  $\text{cm}^{-1}$ ; <sup>1</sup>H NMR (400 MHz, CDCl<sub>3</sub>)  $\delta$  8.25 (d,  $J$  = 8.6 Hz, 2H), 8.18 (d,  $J$  = 7.5 Hz, 2H), 7.62 (t,  $J$  = 7.32 Hz, 1H), 7.54 (t,  $J$  = 7.32 Hz, 2H), 7.23 (m, 3H), 2.34 (s, 3H); <sup>13</sup>C NMR (125 MHz, CDCl<sub>3</sub>)  $\delta$  170.75, 163.65, 133.08, 132.99, 131.13, 129.23, 128.97, 128.91, 128.64, 127.97, 125.99, 125.95, 55.16.

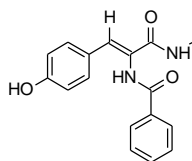
**(Z)-4-(4-hydroxybenzylidene)-1-methyl-2-phenyl-1H-imidazol-5(4H)-one (1c).** To an ethanolic



solution of (Z)-4-((5-oxo-2-phenyloxazol-4(5H)-ylidene)methyl)phenyl acetate (**1a**, 0.1 g, 0.33 mmol) was added aqueous methylamine (40%, 0.1 mL) and potassium carbonate (0.045 g, 0.33 mmol) and the solution was refluxed under N<sub>2</sub> for three hours, cooled extracted with ethyl acetate (20 mL), washed with

water (3 × 50 mL) and concentrated *in vacuo*. The crude product was purified by flash chromatography to provide the imidazolone (**1c**, 0.032 g, 35%) as a bright yellow solid (0.032 g, 35%), m.p. 203 °C; UV (acetonitrile)  $\lambda_{\text{max}}$  297 nm ( $\epsilon$  = 30700); IR (ATR)  $\nu_{\text{max}}$  3169, 1673, 1640  $\text{cm}^{-1}$ ; <sup>1</sup>H NMR (600 MHz, CDCl<sub>3</sub>)  $\delta$  8.15 (d,  $J$  = 8.78 Hz, 2H), 7.84 (dd,  $J$  = 8.00, 1.5 Hz, 2H), 7.55 (m, 3H), 7.24 (s, 1H), 6.88 (d,  $J$  = 6.78 Hz, 2H), 3.36 (s, 3H); <sup>13</sup>C NMR (150 MHz, CDCl<sub>3</sub>)  $\delta$  158.40, 135.04, 131.56, 129.71, 128.99, 128.80, 127.30, 116.13, 29.24; MS (ESI)  $m/z$  279; HRMS (ESI) calcd. for C<sub>17</sub>H<sub>15</sub>N<sub>2</sub>O<sub>2</sub>  $m/z$  279.1133 [M+H<sup>+</sup>], found  $m/z$  279.1134.

Alternatively, (Z)-4-((5-oxo-2-phenyloxazol-4(5H)-ylidene)methyl)phenyl acetate (**1a**, 0.1 g, 0.33



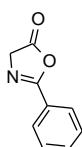
mmol) was dissolved in  $\text{CH}_2\text{Cl}_2$  and acetonitrile saturated with dry methylamine (0.15 mL) was added to it and the mixture was stirred for 1 hour.

A white precipitate was formed, which is soluble in excess acetonitrile. The reaction mixture was concentrated in vacuo and washed with cold  $\text{CH}_2\text{Cl}_2$  and

dried to yield (Z)-N-(1-(4-hydroxyphenyl)-3-(methyamino)-3-oxoprop-1-en-2-yl)benzamide (**1b**, 0.97 g, 100%), m.p. 144 °C; UV (acetonitrile)  $\lambda_{\text{max}}$  389 nm ( $\epsilon = 16600$ ); IR (ATR)  $\nu_{\text{max}}$  3237, 1648  $\text{cm}^{-1}$ ;  $^1\text{H}$  NMR (400 MHz,  $\text{DMSO}-d_6$ )  $\delta$  9.77 (s, 1H), 8.0 (d,  $J = 7.13$  Hz, 2H), 7.91 (quart,  $J = 4.57$  Hz, 1H), 7.47 (m, 3H), 7.37 (d,  $J = 8.6$  Hz, 2H), 7.18 (s, 1H), 6.70 (d,  $J = 8.6$  Hz, 2H), 2.64 (d,  $J = 3.58$  Hz, 3 H);  $^{13}\text{C}$  NMR (125 MHz,  $\text{DMSO}-d_6$ )  $\delta$  166.66, 166.53, 159.00, 134.72, 132.43, 132.03, 130.55, 129.13, 128.77, 127.82, 125.93, 116.23, 27.20; MS (ESI)  $m/z$  297; HRMS (ESI) calcd. for  $\text{C}_{17}\text{H}_{17}\text{N}_2\text{O}_3$   $m/z$  297.1234 [ $\text{M}+\text{H}^+$ ], found  $m/z$  297.1239.

**1b** was heated in furnace at 350 °C for 60 seconds to give an orange solid which was purified by flash chromatography to yield the imidazolone **1c** (0.074 g, 80%).

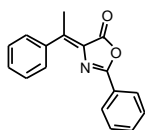
2-phenyloxazol-5(4H)-one (**II**) was prepared following literature procedure.<sup>6</sup> Briefly hippuric



acid (**I**, 2 g, 0.012 mol) was added to acetic anhydride (8 mL) and the solution was heated at 90 °C for 30 min until all the hippuric acid had dissolved and the colour of the solution became dark orange. The solution was then cooled and poured into ice-

diethyl ether mixture (100 mL). The organic layer was repeatedly washed with water then 1%  $\text{NaHCO}_3$  solution to remove the traces of acetic acid. The ether layer was dried over  $\text{MgSO}_4$  and concentrated in vacuo to yield the phenyl oxazolone (**II**) as a yellow solid (1.5 g, 77%), m.p. 85 °C [lit. m.p. 84-86 °C]<sup>6</sup>;  $^1\text{H}$  NMR (400 MHz,  $\text{CDCl}_3$ )  $\delta$  7.99 (d,  $J = 7.13$  Hz, 2 H) 7.58 (t,  $J = 7.4$  Hz, 1 H), 7.49 (t,  $J = 7.6$  Hz, 1 H), 4.42 (s, 2 H);  $^{13}\text{C}$  NMR (125 MHz,  $\text{CDCl}_3$ )  $\delta$  170.8, 163.7, 133.1, 133.0, 129.0, 128.0, 126.0, 55.2.

(Z)-2-phenyl-4-(1-phenylethylidene)oxazol-5(4H)-one (**2a**). THF (10 mL) was chilled under  $\text{N}_2$

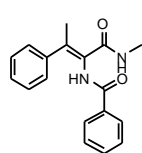


to -10 °C. To it,  $\text{TiCl}_4$  (0.075 mL, 0.685 mmol) in  $\text{CH}_2\text{Cl}_2$  (0.2 mL) was added and stirred for 10 min. To the stirring solution, 4-acetylphenyl acetate (**2**, 0.1028 mL, 0.83 mmol) was added and the mixture was stirred for five min, then 2-

phenyloxazol-5(4H)-one (**II**, 0.267 g, 1.66 mmol) was added and stirred for a further 20 min. To the mixture, pyridine (0.15 mL) was added dropwise. The black mixture was stirred for a further 5 hours and was monitored by TLC until there were no starting materials left. The reaction was

then quenched with saturated ammonium chloride solution (3 mL) and extracted with ethyl acetate (3 × 10 mL). The organic layer was washed thoroughly with water (4 × 10 mL) and brine solution (2 × 10 mL) and concentrated under vacuo. The oxazolone was purified by flash chromatography and recrystallized from DCM/PE to yield a yellow solid (**2a**, 0.077 g, 35%), m.p. 110 °C [lit m.p. 108-110 °C]<sup>7,8</sup>; UV (acetonitrile)  $\lambda_{\text{max}}$  346 nm ( $\epsilon$  = 28500); IR (ATR)  $\nu_{\text{max}}$  1783, 1756  $\text{cm}^{-1}$ ; <sup>1</sup>H NMR (400 MHz, CDCl<sub>3</sub>)  $\delta$  8.08 (m, 1H), 8.06 (m, 1H), 7.89 (m, 1H), 7.87 (m, 1H), 7.55 (m, 1H), 7.49 (m, 1H), 7.47 (m, 2H), 7.46 (m, 2H), 2.8 (s, 3H); <sup>13</sup>C NMR (125 MHz, CDCl<sub>3</sub>)  $\delta$  166.97, 160.57, 149.40, 139.06, 132.80, 131.39, 130.10, 130.07, 128.92, 128.27, 128.08, 125.99, 18.51.

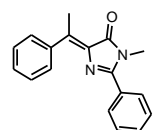
**(Z)-N-(1-(methylamino)-1-oxo-3-phenylbut-2-en-2-yl)benzamide (2b).** (Z)-2-phenyl-4-(1-phenylethylidene)oxazol-5(4H)-one (**2a**, 0.1 g, 0.38 mmol) was dissolved in



CH<sub>2</sub>Cl<sub>2</sub> (2 mL) and acetonitrile saturated with dry methylamine (0.15 mL) was added to it and the mixture was stirred for 15 min. A white precipitate was formed.

The reaction mixture was concentrated in vacuo and washed with cold CH<sub>2</sub>Cl<sub>2</sub> (3 × 3 mL) and dried in vacuo to yield (Z)-N-(1-(methylamino)-1-oxo-3-phenylbut-2-en-2-yl)benzamide (**2b**, 0.098 g, 98%) as a white powder that was used in the next step without further purification, m.p. 245 °C; UV (acetonitrile)  $\lambda_{\text{max}}$  294 nm ( $\epsilon$  = 10300); IR (ATR)  $\nu_{\text{max}}$  3278, 1638  $\text{cm}^{-1}$ ; <sup>1</sup>H NMR (400 MHz, DMSO-*d*<sub>6</sub>)  $\delta$  9.31 (s, 1H), 7.85 (quart, *J* = 4.76 Hz, 1H), 7.65 (d, *J* = 7.7 Hz, 2H), 7.45 (t, *J* = 8.05 Hz, 1H), 7.36 (t, *J* = 7.6 Hz, 2H), 7.25 (m, 4H), 7.19 (dd, *J* = 3.00 Hz, 1H), 2.65 (d, *J* = 4.6 Hz, 3H), 2.24 (s, 3H); <sup>13</sup>C NMR (125 MHz, DMSO-*d*<sub>6</sub>)  $\delta$  167.05, 166.87, 142.09, 138.63, 134.77, 132.15, 128.92, 128.84, 128.50, 128.30, 128.13, 127.76, 26.76, 21.34; MS (ESI) *m/z* 295; HRMS (ESI) calcd. for C<sub>18</sub>H<sub>19</sub>N<sub>2</sub>O<sub>2</sub> *m/z* 295.1441 [M+H<sup>+</sup>], found *m/z* 295.1447.

**(Z)-1-methyl-2-phenyl-4-(1-phenylethylidene)-1H-imidazol-5(4H)-one (2c).** (Z)-N-(1-(methylamino)-1-oxo-3-phenylbut-2-en-2-yl)benzamide (**2b**, 0.1 g, 0.34 mmol)



was kept in furnace at 350 °C for 60 seconds to give an orange-yellow product which was purified by flash chromatography to yield the imidazolone as an orange-yellow oil (**2c**, 0.066 g, 70%) as a mixture of isomers.

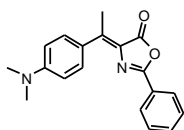
Upon separation by chromatography a 7:1:: major:minor compounds were found which even on HPLC purification was not separated as there was facile isomerization to change one isomer into another. The compounds were tried to be crystallized but could not be done. The mixture of the

compounds were tried to separate and identify by NMR signals, but nothing could be concluded based on NOE signals. Both the isomers showed correlation between the ortho proton of benzyl group and the allylic ethyl proton. The only differences found were a change in chemical shift and higher  $^{15}\text{N}$ - $^1\text{H}$  correlation for the major isomer.

Major isomer: UV (acetonitrile)  $\lambda_{\text{max}}$  356 nm ( $\epsilon = 6600$ ); IR (ATR)  $\nu_{\text{max}}$  1640, 1626  $\text{cm}^{-1}$ ;  $^1\text{H}$  NMR (600 MHz,  $\text{CDCl}_3$ )  $\delta$  7.85 (m, 2H,  $-\text{CH}_{\text{ar}}$ ), 7.74 (m, 2H,  $-\text{CH}_{\text{ar}}$ ), 7.49 (m, 3H,  $-\text{CH}_{\text{ar}}$ ), 7.42 (m, 2H,  $-\text{CH}_{\text{ar}}$ ), 7.36 (m, 1H,  $-\text{CH}_{\text{ar}}$ ), 3.34 (s, 3H,  $-\text{NCH}_3$ ) 2.85 (s, 3H,  $-\text{CH}_3$ );  $^{13}\text{C}$  NMR (125 MHz,  $\text{CDCl}_3$ )  $\delta$  171.02, 158.94, 146.90, 140.02, 136.73, 131.04, 130.30, 129.73, 129.23, 128.92, 128.79, 128.65, 128.24, 128.05, 127.41, 127.05, 28.93, 18.50;  $^{15}\text{N}$  NMR (60.8 MHz,  $\text{CDCl}_3$ )  $\delta$  242, 199; MS (ESI)  $m/z$  277; HRMS (ESI) calcd. for  $\text{C}_{18}\text{H}_{17}\text{N}_2\text{O}$   $m/z$  277.1336  $[\text{M}+\text{H}^+]$ , found  $m/z$  277.1341.

Minor isomer: UV (acetonitrile)  $\lambda_{\text{max}}$  359 nm ( $\epsilon = 6650$ ); IR (ATR)  $\nu_{\text{max}}$  1696, 1627  $\text{cm}^{-1}$ ;  $^1\text{H}$  NMR (600 MHz,  $\text{CDCl}_3$ )  $\delta$  7.78 (m, 2H,  $-\text{CH}_{\text{ar}}$ ), 7.54 (m, 3H,  $-\text{CH}_{\text{ar}}$ ), 7.49 (m, 2H,  $-\text{CH}_{\text{ar}}$ ), 7.42 (m, 3H,  $-\text{CH}_{\text{ar}}$ ), 3.21 (s, 3H,  $-\text{NCH}_3$ ), 2.62 (s, 3H,  $-\text{CH}_3$ );  $^{13}\text{C}$  NMR (125 MHz,  $\text{CDCl}_3$ )  $\delta$  168.10, 159.71, 149.53, 138.69, 137.39, 131.25, 131.11, 130.34, 129.76, 129.65, 129.29, 129.14, 128.99, 128.85, 128.70, 128.55, 128.43, 128.27, 128.13, 28.81, 22.78;  $^{15}\text{N}$  NMR (60.8 MHz,  $\text{CDCl}_3$ )  $\delta$  200; MS (ESI)  $m/z$  277; HRMS (ESI) calcd. for  $\text{C}_{18}\text{H}_{17}\text{N}_2\text{O}$   $m/z$  277.1336  $[\text{M}+\text{H}^+]$ , found  $m/z$  277.1341.

**(Z)-4-(1-(4-(dimethylamino)phenyl)ethylidene)-2-phenyloxazol-5(4H)-one (3a).** THF (10 mL)

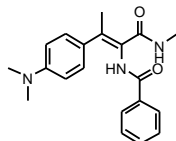


was chilled under  $\text{N}_2$  to  $-10^\circ\text{C}$ . To it,  $\text{TiCl}_4$  (0.075 mL, 0.685 mmol) in  $\text{CH}_2\text{Cl}_2$  (0.2 mL) was added and stirred for 10 min. To the stirring solution, 1-(4-(dimethylamino)phenyl)ethanone (0.1 g, 0.61 mmol) was added and the mixture was stirred for five min, then 2-phenyloxazol-5(4H)-one (**II**, 0.196 g, 1.22 mmol) was added and stirred for a further 20 min. To the mixture, pyridine (0.15 mL) was added dropwise. The black mixture was stirred for a further 5 hours and was monitored by TLC until there were no starting materials left. The reaction was then quenched with saturated ammonium chloride solution (3 mL) and extracted with ethyl acetate ( $3 \times 10$  mL). The organic layer was washed thoroughly with water ( $4 \times 10$  mL) and brine solution ( $2 \times 10$  mL) and concentrated under vacuo. The oxazolone was purified by flash chromatography and recrystallized from DCM/PE to yield a bright orange solid (0.075 g, 40%), m.p.  $165^\circ\text{C}$ ; UV

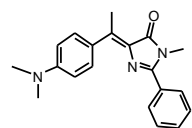


(acetonitrile)  $\lambda_{\max}$  445 nm ( $\epsilon = 24500$ ); IR (ATR)  $\nu_{\max}$  2918, 1735, 1627  $\text{cm}^{-1}$ ;  $^1\text{H}$  NMR (400 MHz,  $\text{CDCl}_3$ )  $\delta$  8.09 (m, 4H), 7.49 (m, 3H), 6.83 (m, 2H), 3.09 (s, 6H), 2.78 (s, 3H);  $^{13}\text{C}$  NMR (125 MHz,  $\text{CDCl}_3$ )  $\delta$  167.61, 160.04, 159.64, 158.71, 151.26, 149.31, 132.66, 132.16, 131.05, 128.85, 128.25, 127.73, 127.02, 126.50, 112.25, 111.94, 40.63, 17.45; MS (ESI)  $m/z$  307; HRMS (ESI) calcd. for  $\text{C}_{19}\text{H}_{19}\text{N}_2\text{O}_2$   $m/z$  307.1442  $[\text{M}+\text{H}^+]$ , found  $m/z$  307.1447.

**(Z)-N-(3-(4-(dimethylamino)phenyl)-1-(methylamino)-1-oxobut-2-en-2-yl)benzamide (3b).** (Z)-



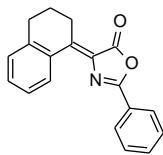
4-(1-(4-(dimethylamino)phenyl)ethylidene)-2-phenyloxazol-5(4H)-one (**3a**, 0.1 g, 0.33 mmol) was dissolved in  $\text{CH}_2\text{Cl}_2$  (2 mL) and acetonitrile saturated with dry methylamine (0.15 mL) was added to it and the mixture was stirred for 15 min. A white precipitate was formed. The reaction mixture was concentrated in vacuo and washed with cold  $\text{CH}_2\text{Cl}_2$  (3  $\times$  3 mL) and dried in vacuo to give (Z)-N-(3-(4-(dimethylamino)phenyl)-1-(methylamino)-1-oxobut-2-en-2-yl)benzamide (**3b**, 0.11 g, 100%) as a white powder that was used in the next step without further purification, m.p. 137  $^\circ\text{C}$ ; UV (acetonitrile)  $\lambda_{\max}$  314 nm ( $\epsilon = 12100$ ); IR (ATR)  $\nu_{\max}$  3340, 3208, 1640  $\text{cm}^{-1}$ ;  $^1\text{H}$  NMR (400 MHz,  $\text{DMSO}-d_6$ )  $\delta$  9.26 (s, 1H), 7.74 (m, 3H), 7.47 (t,  $J = 7.5$  Hz, 1H), 7.38 (t,  $J = 7.5$  Hz, 2H), 7.13 (d,  $J = 8.6$  Hz, 2H), 6.59 (d,  $J = 8.9$  Hz, 2H), 2.82 (s, 6H), 2.63 (d,  $J = 4.6$  Hz, 3H), 2.18 (s, 1H);  $^{13}\text{C}$  NMR (125 MHz,  $\text{DMSO}-d_6$ )  $\delta$  167.58, 166.80, 150.45, 137.59, 134.81, 132.15, 129.36, 128.96, 128.58, 126.40, 112.41, 26.77, 21.08; MS (ESI)  $m/z$  338; HRMS (ESI) calcd. for  $\text{C}_{20}\text{H}_{24}\text{N}_3\text{O}_2$   $m/z$  338.1871  $[\text{M}+\text{H}^+]$ , found  $m/z$  338.1869.



**(Z)-4-(1-(4-(dimethylamino)phenyl)ethylidene)-1-methyl-2-phenyl-1H-imidazol-5(4H)-one (3c).** (Z)-N-(3-(4-(dimethylamino)phenyl)-1-

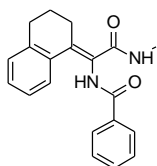
(methylamino)-1-oxobut-2-en-2-yl)benzamide (**3b**, 0.1 g, 0.3 mmol) was kept in furnace at 350  $^\circ\text{C}$  for 60 seconds to give an orange-yellow product which was purified by flash chromatography to yield the imidazolone as a yellow solid (0.071 g, 65%), m.p. 178.5  $^\circ\text{C}$ ; UV (acetonitrile)  $\lambda_{\max}$  430 nm ( $\epsilon = 31400$ ); IR (ATR)  $\nu_{\max}$  3314, 1679  $\text{cm}^{-1}$ ;  $^1\text{H}$  NMR (600 MHz,  $\text{CDCl}_3$ )  $\delta$  8.06 (m, 2H,  $-\text{CH}_{\text{ar}}$ ), 7.77 (m, 2H,  $-\text{CH}_{\text{ar}}$ ), 7.49 (m, 3H,  $-\text{CH}_{\text{ar}}$ ), 6.73 (m, 2H,  $-\text{CH}_{\text{ar}}$ ), 3.35 (s, 3H,  $-\text{NCH}_3$ ), 3.03 (m, 6H,  $-\text{N}(\text{CH}_3)_2$ ), 2.85 (s, 3H,  $-\text{CH}_3$ );  $^{13}\text{C}$  NMR (150 MHz,  $\text{CDCl}_3$ )  $\delta$  171.08, 156.55, 151.31, 147.29, 134.36, 132.67, 130.59, 130.28, 128.74, 128.63, 127.10, 111.35, 40.25, 28.94, 17.52;  $^{15}\text{N}$  NMR (60.8 MHz,  $\text{CDCl}_3$ )  $\delta$  100, 200; MS (ESI)  $m/z$  320; HRMS (ESI) calcd. for  $\text{C}_{20}\text{H}_{22}\text{N}_3\text{O}$   $m/z$  320.1764  $[\text{M}+\text{H}^+]$ , found  $m/z$  320.1763.

**(Z)-4-(3,4-dihydronaphthalen-1(2H)-ylidene)-2-phenyloxazol-5(4H)-one (4a).** THF (10 mL)



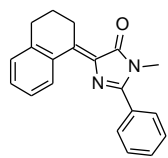
was chilled under N<sub>2</sub> to -10°C. To it, TiCl<sub>4</sub> (0.075 mL, 0.685 mmol) in CH<sub>2</sub>Cl<sub>2</sub> (0.2 mL) was added and stirred for 10 min. To the stirring solution, tetralone (0.0912 mL, 0.685 mmol) was added and the mixture was stirred for five min, then 2-phenyloxazol-5(4H)-one (**II**, 0.165 g, 1.03 mmol) was added and stirred for a further 20 min. To the mixture, pyridine (0.15 mL) was added dropwise. The black mixture was stirred for a further 5 hours and was monitored by TLC until there were no starting materials left. The reaction was then quenched with saturated ammonium chloride solution (3 mL) and extracted with ethyl acetate (3 × 10 mL). The organic layer was washed thoroughly with water (4 × 10 mL) and brine solution (2 × 10 mL) and concentrated under vacuo. The oxazolone was purified by flash chromatography and recrystallized from DCM/PE to yield a yellow solid (0.07 g, 35%), m.p. 140 °C. [lit. m.p 140 °C]; UV (acetonitrile) λ<sub>max</sub> = 365 nm (ε = 31000); IR (ATR) ν<sub>max</sub> 1789, 1756, 1636 cm<sup>-1</sup>; <sup>1</sup>H NMR (400 MHz, CDCl<sub>3</sub>) δ 8.91 (m, 1H), 8.12 (m, 2H), 7.57 (m, 1H), 7.50 (m, 2H) 7.36 (m, 2H), 7.22 (m, 1H), 3.35 (t, *J* = 6.2 Hz, 2H), 2.87 (t, *J* = 6.2 Hz, 2H), 1.96 (quin, *J* = 6.2 Hz, 2H); <sup>13</sup>C NMR (125 MHz, CDCl<sub>3</sub>) δ 167.11, 160.39, 148.86, 142.77, 133.17, 132.92, 132.70, 130.94, 128.97, 128.01, 126.29, 30.64, 28.27, 22.58; MS (ESI) *m/z* 290; HRMS (ESI) calcd. for C<sub>19</sub>H<sub>16</sub>NO<sub>2</sub> *m/z* 290.1184 [M+H<sup>+</sup>], found *m/z* 290.1181.

**(Z)-N-(1-(3,4-dihydronaphthalen-1(2H)-ylidene)-2-(methylamino)-2-oxoethyl)benzamide (4b).**



(Z)-4-(3,4-dihydronaphthalen-1(2H)-ylidene)-2-phenyloxazol-5(4H)-one (**4a**, 0.1 g, 0.35 mmol) was dissolved in CH<sub>2</sub>Cl<sub>2</sub> (2 mL) and acetonitrile saturated with dry methylamine (0.15 mL) was added to it and the mixture was stirred for 15 min. A white precipitate was formed. The reaction mixture was concentrated in vacuo and washed with cold CH<sub>2</sub>Cl<sub>2</sub> (3 × 3 mL) and dried in vacuo to yield (Z)-N-(1-(3,4-dihydronaphthalen-1(2H)-ylidene)-2-(methylamino)-2-oxoethyl)benzamide (**4b**, 0.11 g, 100%) as a white powder that was used in the next step without further purification, m.p. 230 °C; UV (acetonitrile) λ<sub>max</sub> 300 nm (ε = 50000); IR (ATR) ν<sub>max</sub> 3251, 1640 cm<sup>-1</sup>; <sup>1</sup>H NMR (400 MHz, DMSO-*d*<sub>6</sub>) δ 9.71 (br, s, 1H), 7.91 (d, *J* = 4.21 Hz, 1H), 7.85 (m, 2H), 7.52 (m, 1H), 7.43 (m, 3 H), 7.15 (m, 2H), 7.01 (m, 1 H), 2.74 (t, *J* = 6.6 Hz, 2H), 2.66 (m, 5H), 1.79 (quin, *J* = 6.5 Hz, 2H); <sup>13</sup>C NMR (125 MHz, DMSO-*d*<sub>6</sub>) δ 167.33, 166.65, 139.97, 135.67, 135.48, 132.28, 129.34, 129.04, 128.66, 128.45, 126.86, 125.94, 29.61, 28.71, 26.80, 25.15; MS (ESI) *m/z* 321; HRMS (ESI) calcd. for C<sub>20</sub>H<sub>21</sub>N<sub>2</sub>O<sub>2</sub> *m/z* 321.1605 [M+H<sup>+</sup>], found *m/z* 321.1603.

**(Z)-4-(3,4-dihydronaphthalen-1(2H)-ylidene)-1-methyl-2-phenyl-1H-imidazol-5(4H)-one (4c).**

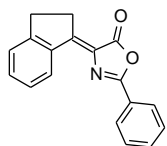


**(Z)-N-(1-(3,4-dihydronaphthalen-1(2H)-ylidene)-2-(methylamino)-2-**

**oxoethyl)benzamide (4b**, 0.1 g, 0.31 mmol) was kept in furnace at 350 °C for 60 seconds to give an orange-yellow product which was purified by flash chromatography to yield the imidazolone as a yellow solid (0.062 g, 65%), m.p.

133 °C; UV (acetonitrile)  $\lambda_{\text{max}}$  = 376 nm ( $\epsilon$  = 12000); IR (ATR)  $\nu_{\text{max}}$  1680  $\text{cm}^{-1}$ ;  $^1\text{H}$  NMR (600 MHz,  $\text{CDCl}_3$ )  $\delta$  8.93 (m, 1H,  $-\text{CH}_{\text{ar}}$ ), 7.82 (d,  $J$ =8.02 Hz, 2H,  $-\text{CH}_{\text{ar}}$ ), 7.51 (m, 3H,  $-\text{CH}_{\text{ar}}$ ), 7.29 (m, 2H,  $-\text{CH}_{\text{ar}}$ ), 7.17 (m, 1H,  $-\text{CH}_{\text{ar}}$ ), 3.44 (t,  $J$  = 6.46 Hz, 2H,  $-\text{CH}_2$ ), 3.36 (s, 3H,  $-\text{NCH}_3$ ), 2.84 (t,  $J$  = 6.25 Hz, 2 H,  $-\text{CH}_2$ ), 1.95 (quin,  $J$  = 6.35 Hz, 2 H,  $-\text{CH}_2$ );  $^{13}\text{C}$  NMR (150 MHz,  $\text{CDCl}_3$ )  $\delta$  171.14, 158.59, 146.31, 142.65, 134.78, 133.71, 133.66, 131.04, 130.06, 129.98, 128.87, 128.70, 128.66, 126.12, 30.69, 29.02, 28.13, 22.74;  $^{15}\text{N}$  NMR (60.8 MHz,  $\text{CDCl}_3$ )  $\delta$  200; MS (ESI)  $m/z$  303; HRMS (ESI) calcd. for  $\text{C}_{20}\text{H}_{19}\text{N}_2\text{O}$   $m/z$  303.1502 [ $\text{M}+\text{H}^+$ ], found  $m/z$  303.1497.

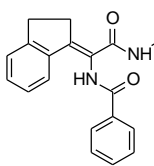
**(Z)-4-(2,3-dihydro-1H-inden-1-ylidene)-2-phenyloxazol-5(4H)-one (5a).** THF (10 mL) was



chilled under  $\text{N}_2$  to -10 °C. To it,  $\text{TiCl}_4$  (0.083 mL, 0.76 mmol) in  $\text{CH}_2\text{Cl}_2$  (0.2 mL) was added and stirred for 10 min. To the stirring solution, indanone (0.1 g, 0.76 mmol) was added and the mixture was stirred for five min, then 2-phenyloxazol-5(4H)-one (**II**, 0.183 g, 1.14 mmol) was added and stirred for a

further 20 min. To the mixture, pyridine (0.2 mL) was added dropwise. The black mixture was stirred for a further 5 hours and was monitored by TLC until there were no starting materials left. The reaction was then quenched with saturated ammonium chloride solution (3 mL) and extracted with ethyl acetate ( $3 \times 10$  mL). The organic layer was washed thoroughly with water ( $4 \times 10$  mL) and brine solution ( $2 \times 10$  mL) and concentrated under vacuo. The oxazolone was purified by flash chromatography and recrystallized from DCM/PE to yield a yellow solid (0.088 g, 42%), m.p. 155 °C; UV (acetonitrile)  $\lambda_{\text{max}}$  375 nm ( $\epsilon$  = 61000); IR (ATR)  $\nu_{\text{max}}$  1775, 1747  $\text{cm}^{-1}$ ;  $^1\text{H}$  NMR (400 MHz,  $\text{CDCl}_3$ )  $\delta$  8.76 (m, 1H), 8.17 (m, 2H), 7.53 (m, 3H), 7.40 (m, 3H), 3.37 (t,  $J$  = 5.6 Hz, 2H), 3.17 (t,  $J$  = 5.6 Hz, 2H);  $^{13}\text{C}$  NMR (125 MHz,  $\text{CDCl}_3$ )  $\delta$  167.10, 160.16, 155.45, 152.35, 139.26, 132.44, 132.12, 129.34, 128.91, 127.81, 127.50, 126.90, 126.41, 125.35, 30.87, 30.68; MS (ESI)  $m/z$  276; HRMS (ESI) calcd. for  $\text{C}_{18}\text{H}_{14}\text{NO}_2$   $m/z$  276.1019 [ $\text{M}+\text{H}^+$ ], found  $m/z$  276.1025.

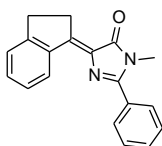
**(Z)-N-(1-(2,3-dihydro-1H-inden-1-ylidene)-2-(methylamino)-2-oxoethyl)benzamide (5b).** (Z)-



4-(2,3-dihydro-1H-inden-1-ylidene)-2-phenyloxazol-5(4H)-one (**5a**, 0.1 g, 0.36 mmol) was dissolved in CH<sub>2</sub>Cl<sub>2</sub> (2 mL) and acetonitrile saturated with dry methylamine (0.15 mL) was added to it and the mixture was stirred for 15 min.

A white precipitate was formed. The reaction mixture was concentrated in vacuo and washed with cold CH<sub>2</sub>Cl<sub>2</sub> (3 × 3 mL) and dried in vacuo to yield (Z)-N-(1-(2,3-dihydro-1H-inden-1-ylidene)-2-(methylamino)-2-oxoethyl)benzamide (**5b**, 0.11 g, 100%) as a white powder that was used in the next step without further purification, m.p. 248 °C; UV (acetonitrile) λ<sub>max</sub> = 305 nm (ε = 4200); IR (ATR) ν<sub>max</sub> 3322, 3236, 1637 cm<sup>-1</sup>; <sup>1</sup>H NMR (400 MHz, DMSO-*d*<sub>6</sub>) δ 9.88 (br, s, 1H), 8.07 (d, *J* = 7.14 Hz, 2H), 7.79 (quart, *J* = 4.39 Hz 1H), 7.60 (m, 2H), 7.49-7.56 (m, 2H), 7.36 (d, *J* = 7.5 Hz, 1H), 7.25 (t, *J* = 7.5 Hz, 1H), 7.11 (t, *J* = 7.14 Hz, 1H), 3.18 (t, *J* = 6.77 Hz, 2H), 2.96 (t, *J* = 6.77 Hz, 2H), 2.66 (d, *J* = 4.8 Hz, 3H); <sup>13</sup>C NMR (125 MHz, DMSO-*d*<sub>6</sub>) δ 167.12, 166.48, 149.53, 146.61, 140.08, 134.55, 132.48, 130.09, 129.22, 128.75, 127.26, 126.26, 126.15, 123.19, 32.15, 31.03, 26.90; MS (ESI) *m/z* 307; HRMS (ESI) calcd. for C<sub>19</sub>H<sub>19</sub>N<sub>2</sub>O<sub>2</sub> *m/z* 307.1441 [M+H<sup>+</sup>], found *m/z* 307.1447.

**(Z)-4-(2,3-dihydro-1H-inden-1-ylidene)-1-methyl-2-phenyl-1H-imidazol-5(4H)-one (5c).** (Z)-

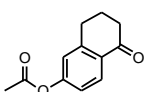


N-(1-(2,3-dihydro-1H-inden-1-ylidene)-2-(methylamino)-2-oxoethyl)benzamide

(**5b**, 0.1 g, 0.33 mmol) was kept in furnace at 350 °C for 60 seconds to give an orange-yellow product which was purified by flash chromatography to yield the

imidazolone as a yellow solid (0.058 g, 62%), m.p. 128 °C; UV (acetonitrile) λ<sub>max</sub> 380 nm (ε = 4600); IR (ATR) ν<sub>max</sub> 1727, 1689 cm<sup>-1</sup>; <sup>1</sup>H NMR (600 MHz, CDCl<sub>3</sub>) δ 8.83 (d, *J* = 7.69 Hz, 1H, -CH<sub>ar</sub>), 7.86 (m, 2H, -CH<sub>ar</sub>), 7.54 (m, 3H, -CH<sub>ar</sub>), 7.36 (m, 3H, -CH<sub>ar</sub>), 3.47 (t, *J* = 5.6 Hz, 2H, -CH<sub>2</sub>), 3.37 (s, 3H, -NCH<sub>3</sub>), 3.20 (t, *J* = 5.6 Hz, 2H, -CH<sub>2</sub>); <sup>13</sup>C NMR (150 MHz, CDCl<sub>3</sub>) δ 170.80, 158.19, 152.75, 152.00, 140.03, 133.11, 131.33, 130.98, 130.11, 129.70, 128.90, 128.69, 127.34, 125.21, 31.04, 30.76, 28.96; <sup>15</sup>N NMR (60.8 MHz, CDCl<sub>3</sub>) δ 200; MS (ESI) *m/z* 289; HRMS (ESI) calcd. for C<sub>19</sub>H<sub>17</sub>N<sub>2</sub>O *m/z* 289.1333 [M+H<sup>+</sup>], found *m/z* 289.1341.

**5-oxo-5,6,7,8-tetrahydronaphthalen-2-yl acetate (6).** 5-oxo-5,6,7,8-tetrahydronaphthalen-2-yl

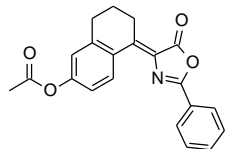


acetate (**6h**, 0.5 g, 3.1 mmol) was added to acetic anhydride (5 mL) and 2 equivalent of sodium acetate (0.51 g, 6.2 mmol). The reaction mixture was

irradiated in a microwave reactor (SEM) for 3 min (300 W, 140 °C). The mixture was then poured in ice cold water and extracted with ethylacetate. The organic layer was washed

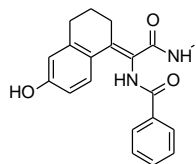
thoroughly with water (4 × 25 mL) and concentrated in vacuo. Purification by flash chromatography gave the pure product (0.61 g, 97%), m.p. 62 °C [lit. m.p. 62.5 °C].<sup>9</sup>

**(Z)-5-(5-oxo-2-phenyloxazol-4(5H)-ylidene)-5,6,7,8-tetrahydronaphthalen-2-yl acetate (6a).**



THF (10 mL) was chilled under N<sub>2</sub> to -10 °C. To it, TiCl<sub>4</sub> (0.052 mL, 0.49 mmol) in CH<sub>2</sub>Cl<sub>2</sub> (0.2 mL) was added and stirred for 10 min. To the stirring solution, 5-oxo-5,6,7,8-tetrahydronaphthalen-2-yl acetate (**6h**, 0.1 g, 0.49 mmol) was added and the mixture was stirred for five min, then 2-phenyloxazol-5(4H)-one (**II**, 0.12 g, 0.74 mmol) was added and stirred for a further 20 min. To the mixture, pyridine (0.2 mL) was added dropwise. The black mixture was stirred for a further 5 hours and was monitored by TLC until there were no starting materials left. The reaction was then quenched with saturated ammonium chloride solution (3 mL) and extracted with ethyl acetate (3 × 10 mL). The organic layer was washed thoroughly with water (4 × 10 mL) and brine solution (2 × 10 mL) and concentrated under vacuo. The oxazolone was purified by flash chromatography and recrystallized from methanol/water to yield a yellow-orange solid (0.068 g, 40%), m.p. 158 °C; UV (acetonitrile) λ<sub>max</sub> 368 nm (ε = 16000); IR (ATR) ν<sub>max</sub> 1789, 1750, 1680 cm<sup>-1</sup>; <sup>1</sup>H NMR (400 MHz, CDCl<sub>3</sub>) δ 9.02 (d, *J* = 8.8 Hz, 1H), 8.11 (d, *J* = 7.14 Hz, 2H), 7.57 (t, *J* = 7.23 Hz, 3H), 7.50 (d, *J* = 7.14 Hz, 1H), 7.09 (dd, *J* = 8, 2.26 Hz, 1H), 6.98 (s, 1H), 3.34 (t, *J* = 6.50 Hz, 2 H), 2.87 (t, *J* = 6.22 Hz, 2 H), 2.33 (s, 3 H), 1.96 (quin, *J* = 6.36 Hz, 2 H); <sup>13</sup>C NMR (125 MHz, CDCl<sub>3</sub>) δ 169.28, 167.05, 160.46, 152.31, 147.63, 144.52, 134.82, 132.76, 130.63, 128.99, 128.01, 127.87, 126.14, 121.63, 119.63, 30.75, 28.05, 22.38, 21.37; MS (ESI) *m/z* 348; HRMS (ESI) calcd. for C<sub>21</sub>H<sub>18</sub>NO<sub>4</sub> *m/z* 348.1235 [M+H<sup>+</sup>], found *m/z* 348.1236.

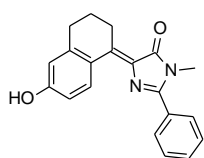
**(Z)-N-(1-(6-hydroxy-3,4-dihydronaphthalen-1(2H)-ylidene)-2-(methylamino)-2-**



**oxoethyl)benzamide (6b).** (Z)-5-(5-oxo-2-phenyloxazol-4(5H)-ylidene)-5,6,7,8-tetrahydronaphthalen-2-yl acetate (**6a**, 0.1 g, 0.29 mmol) was dissolved in CH<sub>2</sub>Cl<sub>2</sub> (2 mL) and acetonitrile saturated with dry methylamine (0.15 mL) was added to it and the mixture was stirred for 15 min. A white precipitate was formed. The reaction mixture was concentrated in vacuo and washed with cold CH<sub>2</sub>Cl<sub>2</sub> (3 × 3 mL) and dried in vacuo to give (Z)-N-(1-(2,3-dihydro-1H-inden-1-ylidene)-2-(methylamino)-2-oxoethyl)benzamide (**6b**, 0.77 g, 80%) as a white powder that was used in the next step without

further purification, m.p. 125 °C; UV (acetonitrile)  $\lambda_{\max}$  303 nm ( $\epsilon$  = 15100); IR (ATR)  $\nu_{\max}$  3364, 3273, 1644  $\text{cm}^{-1}$ ;  $^1\text{H}$  NMR (400 MHz,  $\text{DMSO-}d_6$ )  $\delta$  9.61 (s, 1H), 7.85 (d,  $J$  = 7.5 Hz, 2H), 7.8 (quart,  $J$  = 4.57 Hz, 1H), 7.53 (t,  $J$  = 7.32 Hz, 1H), 7.45 (t,  $J$  = 7.4 Hz, 2H), 7.3 (d,  $J$  = 8.6 Hz, 1H), 6.54 (d,  $J$  = 2.2 Hz, 1H), 6.42 (dd,  $J$  = 8, 2.38 Hz, 1H), 2.58-2.72 (m, 7H), 1.75 (quin,  $J$  = 6.40 Hz, 2H);  $^{13}\text{C}$  NMR (125 MHz,  $\text{DMSO-}d_6$ )  $\delta$  167.64, 166.58, 157.94, 141.57, 135.83, 134.77, 132.20, 130.02, 129.03, 128.64, 126.24, 124.86, 115.43, 113.54, 29.97, 29.19, 26.80, 23.91; MS (ESI)  $m/z$  337; HRMS (ESI) calcd. for  $\text{C}_{20}\text{H}_{21}\text{N}_2\text{O}_3$   $m/z$  337.1552 [ $\text{M}+\text{H}^+$ ], found  $m/z$  337.1552.

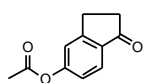
**(Z)-4-(6-hydroxy-3,4-dihydronaphthalen-1(2H)-ylidene)-1-methyl-2-phenyl-1H-imidazol-**



**5(4H)-one (6c).** (Z)-N-(1-(6-hydroxy-3,4-dihydronaphthalen-1(2H)-ylidene)-2-(methylamino)-2-oxoethyl)benzamide (**6b**, 0.1 g, 0.30 mmol) was kept in furnace at 350 °C for 60 seconds to give an orange-yellow product which was purified by flash chromatography to yield the imidazolone as a yellow

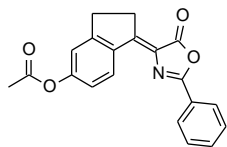
solid (0.057 g, 60%), m.p. 236 °C; UV (acetonitrile)  $\lambda_{\max}$  389 nm ( $\epsilon$  = 250000); IR (ATR)  $\nu_{\max}$  3364, 3271, 1643  $\text{cm}^{-1}$ ;  $^1\text{H}$  NMR (600 MHz,  $\text{CDCl}_3$ )  $\delta$  8.91 (d,  $J$  = 8.75 Hz, 1H,  $-\text{CH}_{\text{ar}}$ ), 7.79 (m, 2H,  $-\text{CH}_{\text{ar}}$ ), 7.53 (m, 3H,  $-\text{CH}_{\text{ar}}$ ), 6.73 (dd,  $J$  = 8.88, 2.77 Hz, 1H,  $-\text{CH}_{\text{ar}}$ ), 6.59 (d,  $J$  = 2.81 Hz, 1H,  $-\text{CH}_{\text{ar}}$ ), 3.42 (t,  $J$  = 6.44 Hz, 2H,  $-\text{CH}_2$ ), 3.35 (s, 3H,  $-\text{NCH}_3$ ), 2.77 (t,  $J$  = 6.28 Hz, 2H,  $-\text{CH}_2$ ), 1.91 (quin,  $J$  = 6.34 Hz, 2H,  $-\text{CH}_2$ );  $^{13}\text{C}$  NMR (150 MHz,  $\text{CDCl}_3$ )  $\delta$  171.02, 157.64, 157.38, 146.59, 145.38, 136.07, 133.35, 130.90, 130.09, 128.98, 128.87, 128.68, 126.69, 115.02, 113.89, 30.97, 28.99, 28.30, 22.65;  $^{15}\text{N}$  NMR (60.8 MHz,  $\text{CDCl}_3$ )  $\delta$ ; MS (ESI)  $m/z$  319; HRMS (ESI) calcd. for  $\text{C}_{20}\text{H}_{19}\text{N}_2\text{O}_2$   $m/z$  319.1441 [ $\text{M}+\text{H}^+$ ], found  $m/z$  319.1447.

**1-oxo-2,3-dihydro-1H-inden-5-yl acetate (7).** 5-hydroxy-2,3-dihydro-1H-inden-1-one (**7h**, 0.5 g,



3.37 mmol) was added to acetic anhydride (5 mL) and 2 equivalent of sodium acetate (0.55 g, 7.74 mmol). The reaction mixture was irradiated in a microwave reactor (SEM) for 3 min (300 W, 140 °C). The mixture was then poured in ice cold water and extracted with ethylacetate. The organic layer was washed thoroughly with water (4  $\times$  25 mL) and concentrated in vacuo. Purification by flash chromatography gave the pure product (0.62 g, 97%), m.p. 93 °C [lit. m.p. 93-94 °C].<sup>10</sup>

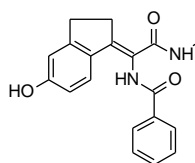
**(Z)-1-(5-oxo-2-phenyloxazol-4(5H)-ylidene)-2,3-dihydro-1H-inden-5-yl acetate (7a).** THF (10



mL) was chilled under N<sub>2</sub> to -10 °C. To it, TiCl<sub>4</sub> (0.058 mL, 0.53 mmol) in CH<sub>2</sub>Cl<sub>2</sub> (0.2 mL) was added and stirred for 10 min. To the stirring solution, 1-oxo-2,3-dihydro-1H-inden-5-yl acetate (**7h**, 0.1 g, 0.53 mmol) was added and the mixture was stirred for five min, then 2-phenyloxazol-5(4H)-one

(**II**, 0.13 g, 0.85 mmol) was added and stirred for a further 20 min. To the mixture, pyridine (0.2 mL) was added dropwise. The black mixture was stirred for a further 5 hours and was monitored by TLC until there were no starting materials left. The reaction was then quenched with saturated ammonium chloride solution (3 mL) and extracted with ethyl acetate (3 × 10 mL). The organic layer was washed thoroughly with water (4 × 10 mL) and brine solution (2 × 10 mL) and concentrated under vacuo. The oxazolone was purified by flash chromatography and recrystallized from methanol/water to yield a bright green-yellow solid (0.071 g, 40%), m.p. 198 °C; UV (acetonitrile) λ<sub>max</sub> 377 nm (ε = 52500); IR (ATR) ν<sub>max</sub> 1751, 1651 cm<sup>-1</sup>; <sup>1</sup>H NMR (400 MHz, CDCl<sub>3</sub>) δ 8.79 (d, *J* = 8.6 Hz, 1H), 8.15 (m, 2H), 7.54 (m, 3H), 7.18 (m, 1H), 7.13 (dd, *J* = 8.51, 2.29 Hz, 1H), 3.44 (t, *J* = 5.85 Hz, 2 H), 3.22 (t, *J* = 5.85 Hz, 2H), 2.34 (s, 3H); <sup>13</sup>C NMR (125 MHz, CDCl<sub>3</sub>) δ 169.28, 167.15, 160.41, 154.10, 154.04, 153.81, 137.08, 132.58, 132.48, 130.45, 130.20, 128.99, 127.90, 127.74, 126.90, 126.40, 121.35, 121.02, 118.53, 31.05, 30.97, 21.36; MS (ESI) *m/z* 334; HRMS (ESI) calcd. for C<sub>20</sub>H<sub>16</sub>NO<sub>4</sub> *m/z* 334.1071 [M+H<sup>+</sup>], found *m/z* 334.1079.

**(Z)-N-(1-(5-hydroxy-2,3-dihydro-1H-inden-1-ylidene)-2-(methylamino)-2-oxoethyl)benzamide (7b).**

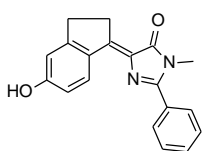


(**7b**). (Z)-1-(5-oxo-2-phenyloxazol-4(5H)-ylidene)-2,3-dihydro-1H-inden-5-yl acetate (**7a**, 0.1 g, 0.3 mmol) was dissolved in CH<sub>2</sub>Cl<sub>2</sub> (2 mL) and acetonitrile saturated with dry methylamine (0.15 mL) was added to it and the mixture was stirred for 15 min. A white precipitate was formed. The reaction mixture was

concentrated in vacuo and washed with cold CH<sub>2</sub>Cl<sub>2</sub> (3 × 3 mL) and dried in vacuo to yield (Z)-N-(1-(5-hydroxy-2,3-dihydro-1H-inden-1-ylidene)-2-(methylamino)-2-oxoethyl)benzamide (**7b**, 0.082 g, 85%) as a white powder that was used in the next step without further purification, m.p. 256 °C; UV (acetonitrile) λ<sub>max</sub> 306 nm (ε = 18700); IR (ATR) ν<sub>max</sub> 3251, 1652 cm<sup>-1</sup>; <sup>1</sup>H NMR (400 MHz, DMSO-*d*<sub>6</sub>) δ 9.68 (s, 1H), 8.04 (d, *J* = 7.32 Hz, 2H), 7.58 (m, 2H), 7.50 (t, *J* = 7.2 Hz, 2H), 7.37 (d, *J* = 8.6 Hz, 1H), 6.70 (s, 1H), 6.46 (dd, *J* = 8.0, 2.01 Hz, 1H), 3.16 (t, *J* = 6.6 Hz, 2H), 2.85 (t, *J* = 6.6 Hz, 2H), 2.61 (d, *J* = 4.57 Hz, 3H); <sup>13</sup>C NMR (125 MHz, DMSO-*d*<sub>6</sub>) δ

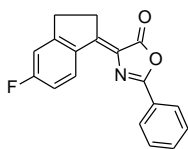
167.38, 166.48, 159.76, 152.10, 147.06, 134.74, 132.337, 131.20, 129.18, 128.73, 127.50, 119.80, 115.07, 112.23, 32.48, 30.91, 26.91; MS (ESI)  $m/z$  323; HRMS (ESI) calcd. for  $C_{19}H_{19}N_2O_3$   $m/z$  323.1394  $[M+H^+]$ , found  $m/z$  323.1396.

**(Z)-4-(5-hydroxy-2,3-dihydro-1H-inden-1-ylidene)-1-methyl-2-phenyl-1H-imidazol-5(4H)-one**



**(7c).** (Z)-N-(1-(5-hydroxy-2,3-dihydro-1H-inden-1-ylidene)-2-(methyldamino)-2-oxoethyl)benzamide (**7b**, 0.1 g, 0.31 mmol) was kept in furnace at 350 °C for 60 seconds to give an orange-yellow product which was purified by flash chromatography to yield the imidazolone (0.057 g, 60%), m.p. 247 °C; UV (acetonitrile)  $\lambda_{max}$  394 nm ( $\epsilon = 260000$ ); IR (ATR)  $\nu_{max}$  3384, 1675  $cm^{-1}$ ;  $^1H$  NMR (600 MHz,  $CDCl_3$ )  $\delta$  8.66 (d,  $J = 8.41$  Hz, 1H,  $-CH_{ar}$ ), 7.81 (m, 2H,  $-CH_{ar}$ ), 7.49 (m, 3H,  $-CH_{ar}$ ), 6.83 (m, 2H,  $-CH_{ar}$ ), 4.67 (b, s, 1H,  $-OH$ ), 3.42 (t,  $J = 5.54$  Hz, 2H,  $-CH_2$ ), 3.34 (s, 3H,  $-NCH_3$ ), 3.09 (t,  $J = 5.64$  Hz, 2H,  $-CH_2$ );  $^{13}C$  NMR (150 MHz,  $CDCl_3$ )  $\delta$  170.54, 161.14, 156.39, 155.19, 153.73, 131.84, 131.23, 130.65, 130.55, 130.34, 128.76, 128.52, 116.02 111.58, 31.32, 30.86, 28.83;  $^{15}N$  NMR (60.8 MHz,  $CDCl_3$ )  $\delta$  200; MS (ESI)  $m/z$  305; HRMS calcd. for  $C_{19}H_{17}N_2O_2$   $m/z$  305.1287  $[M+H^+]$ , found  $m/z$  305.1290.

**((Z)-4-(5-fluoro-2,3-dihydro-1H-inden-1-ylidene)-2-phenyloxazol-5(4H)-one (8a).**

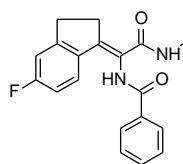


mL) was chilled under  $N_2$  to -10 °C. To it,  $TiCl_4$  (0.072 mL, 0.66 mmol) in  $CH_2Cl_2$  (0.2 mL) was added and stirred for 10 min. To the stirring solution, 5-fluoro-2,3-dihydro-1H-inden-1-one (**8**, 0.1 g, 0.66 mmol) was added and the mixture was stirred for five min, then 2-phenyloxazol-5(4H)-one (**II**, 0.16 g, 1.0 mmol) was added and stirred for a further 20 min. To the mixture, pyridine (0.2 mL) was added dropwise. The black mixture was stirred for a further 5 hours and was monitored by TLC until there were no starting materials left. The reaction was then quenched with saturated ammonium chloride solution (3 mL) and extracted with ethyl acetate ( $3 \times 10$  mL). The organic layer was washed thoroughly with water ( $4 \times 10$  mL) and brine solution ( $2 \times 10$  mL) and concentrated under vacuo. The oxazolone was purified by flash chromatography and recrystallized from methanol/water to yield a yellow solid (0.071 g, 37%), m.p. 182 °C; UV (acetonitrile)  $\lambda_{max} = 374$  nm ( $\epsilon = 2656$ ); IR (ATR)  $\nu_{max}$  1767, 1657  $cm^{-1}$ ;  $^1H$  NMR (400 MHz,  $CDCl_3$ )  $\delta$  8.79 (dd,  $J = 8.0, 5.5$  Hz, 1H), 8.15 (d,  $J = 7.14$  Hz, 2H), 7.54 (m, 3 H), 7.1 (t,  $J = 8.4$  Hz, 2H), 3.45 (t,  $J = 5.75$



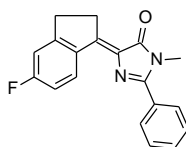
Hz, 2H), 3.22 (t,  $J = 5.48$  Hz, 2H);  $^{13}\text{C}$  NMR (125 MHz,  $\text{CDCl}_3$ )  $\delta$  167.08, 166.78, 164.24, 160.34, 155.15, 155.06, 153.87, 135.62, 132.57, 131.30, 131.20, 128.98, 127.85, 126.36, 115.66, 115.43, 112.42, 112.20, 31.12, 31.00; MS (ESI)  $m/z$  294; HRMS (ESI) calcd. for  $\text{C}_{18}\text{H}_{13}\text{NOF}$   $m/z$  294.0929  $[\text{M}+\text{H}^+]$ , found  $m/z$  294.0930.

**(Z)-N-(1-(5-fluoro-2,3-dihydro-1H-inden-1-ylidene)-2-(methylamino)-2-oxoethyl)benzamide**



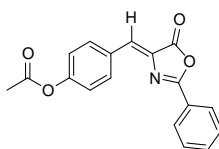
**(8b).** (Z)-4-(5-fluoro-2,3-dihydro-1H-inden-1-ylidene)-2-phenyloxazol-5(4H)-one (**8a**, 0.1 g, 0.34 mmol) was dissolved in  $\text{CH}_2\text{Cl}_2$  (2 mL) and acetonitrile saturated with dry methylamine (0.15 mL) was added to it and the mixture was stirred for 15 min. A white precipitate was formed. The reaction mixture was concentrated in vacuo and washed with cold  $\text{CH}_2\text{Cl}_2$  ( $3 \times 3$  mL) and dried in vacuo to give (Z)-N-(1-(5-fluoro-2,3-dihydro-1H-inden-1-ylidene)-2-(methylamino)-2-oxoethyl)benzamide (**8b**, 0.105 g, 95%) as a white powder that was used in the next step without further purification, m.p. 259 °C; UV (acetonitrile)  $\lambda_{\text{max}}$  303 nm ( $\epsilon = 31400$ ); IR (ATR)  $\nu_{\text{max}}$  3318, 3224, 1637  $\text{cm}^{-1}$ ;  $^1\text{H}$  NMR (400 MHz,  $\text{DMSO}-d_6$ )  $\delta$  9.87 (br. s., 1H), 8.07 (d,  $J = 7.14$  Hz, 2H), 7.80 (quart,  $J = 4.0$  Hz, 1H), 7.56 (m, 4H), 7.20 (dd,  $J = 8.0, 2.01$  Hz, 1H), 6.9 (dt,  $J = 8.0, 2.20$  Hz, 1H), 3.22 (t,  $J = 6.86$  Hz, 2H), 2.97 (t,  $J = 6.86$  Hz, 2H), 2.66 (d,  $J = 6.86$  Hz, 3H);  $^{13}\text{C}$  NMR (125 MHz,  $\text{DMSO}-d_6$ )  $\delta$  167.04, 166.49, 162.28, 152.55, 152.46, 144.45, 136.51, 134.47, 132.53, 129.23, 128.78, 127.89, 127.81, 122.83, 114.78, 114.56, 112.98, 112.77, 32.47, 31.04, 26.90; MS (ESI)  $m/z$  325; HRMS (ESI) calcd. for  $\text{C}_{19}\text{H}_{18}\text{N}_2\text{O}_2\text{F}$   $m/z$  325.1352  $[\text{M}+\text{H}^+]$ , found  $m/z$  325.1352.

**(Z)-4-(5-fluoro-2,3-dihydro-1H-inden-1-ylidene)-1-methyl-2-phenyl-1H-imidazol-5(4H)-one**

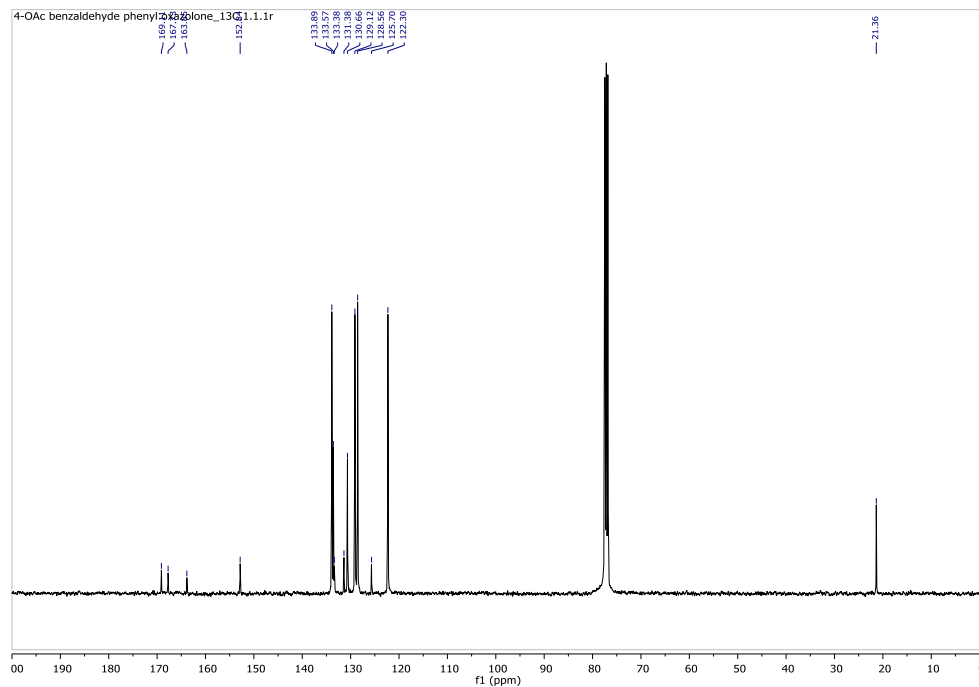
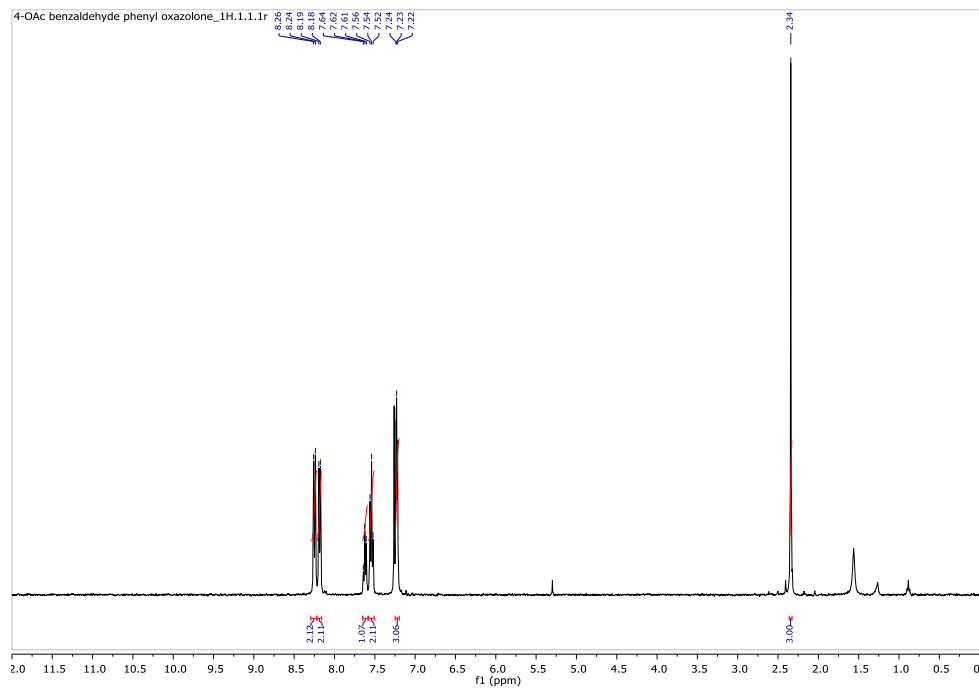


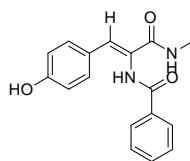
**(8c).** (Z)-N-(1-(5-fluoro-2,3-dihydro-1H-inden-1-ylidene)-2-(methylamino)-2-oxoethyl)benzamide (**8b**, 0.1 g, 0.31 mmol) was kept in furnace at 350 °C for 60 seconds to give an yellow product which was purified by flash chromatography to yield the imidazolone (0.094 g, 57%), m.p. 154 °C; UV (acetonitrile)  $\lambda_{\text{max}}$  376 nm ( $\epsilon = 20816$ ); IR (ATR)  $\nu_{\text{max}}$  3045, 2919, 1691  $\text{cm}^{-1}$ ;  $^1\text{H}$  NMR (600 MHz,  $\text{CDCl}_3$ )  $\delta$  8.82 (t,  $J = 4.8$  Hz, 1H,  $-\text{CH}_{\text{ar}}$ ), 7.83 (d,  $J = 4.8$  Hz, 2H,  $-\text{CH}_{\text{ar}}$ ), 7.56 (m, 3H,  $-\text{CH}_{\text{ar}}$ ), 7.05 (m, 2H,  $-\text{CH}_{\text{ar}}$ ), 3.49 (t,  $J = 5.93$  Hz, 2H,  $-\text{CH}_2$ ), 3.37 (s, 3H,  $-\text{NCH}_3$ ), 3.20 (t,  $J = 5.93$  Hz, 2H,  $-\text{CH}_2$ );  $^{13}\text{C}$  NMR (150 MHz,  $\text{CDCl}_3$ )  $\delta$  170.71, 165.89, 164.21, 158.30, 154.66, 154.60, 151.21, 136.28, 131.50, 131.44, 131.05, 130.02, 129.05, 128.94, 128.74, 128.67, 115.28, 115.13, 112.19, 112.15, 112.04, 112.00, 31.16, 31.12, 28.97;  $^{15}\text{N}$  NMR (60.8 MHz,  $\text{CDCl}_3$ )  $\delta$  200; MS (ESI)  $m/z$  307; HRMS (ESI) calcd. for  $\text{C}_{19}\text{H}_{16}\text{N}_2\text{OF}$   $m/z$  307.1247  $[\text{M}+\text{H}^+]$ , found  $m/z$  307.1247.

## 1D and 2D NMR spectra of GFP analogues

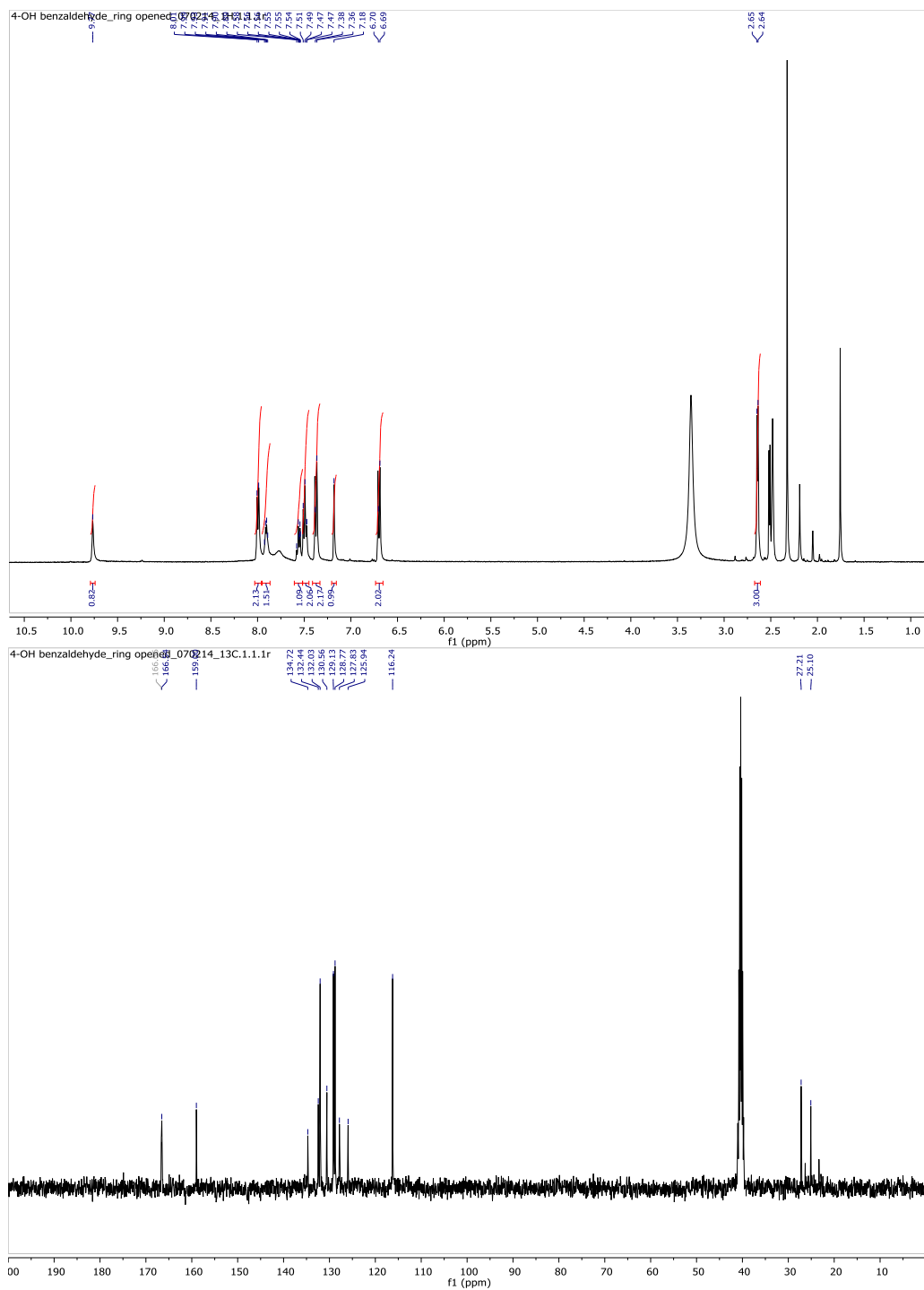


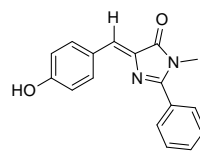
(1a)



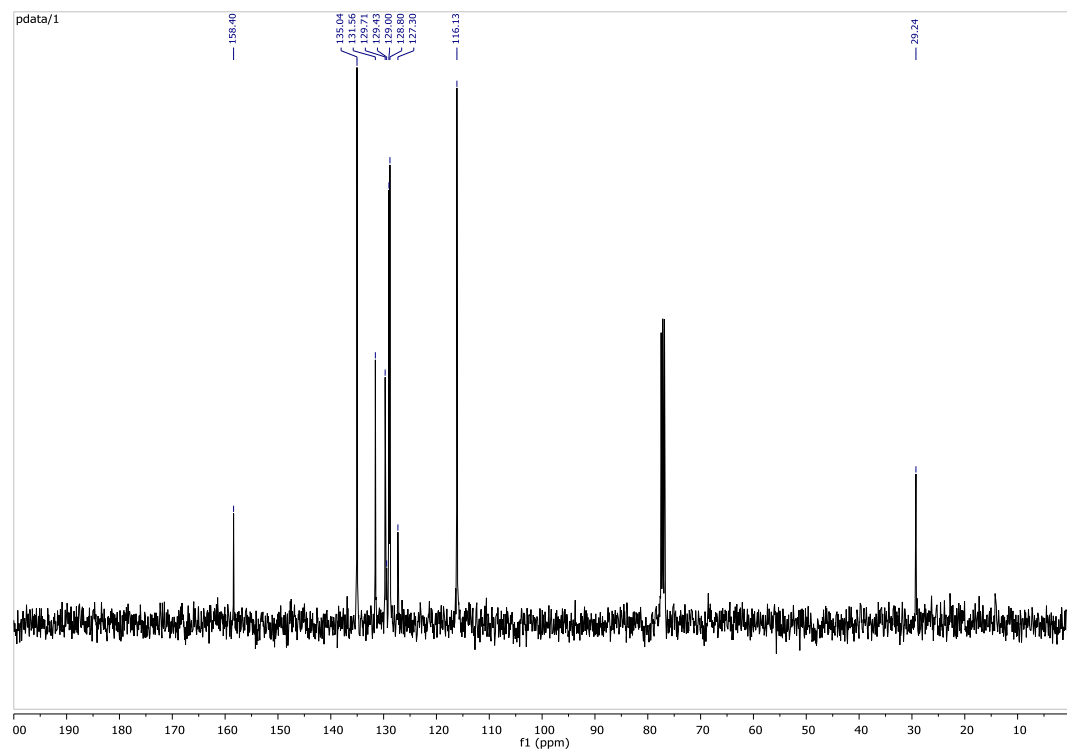
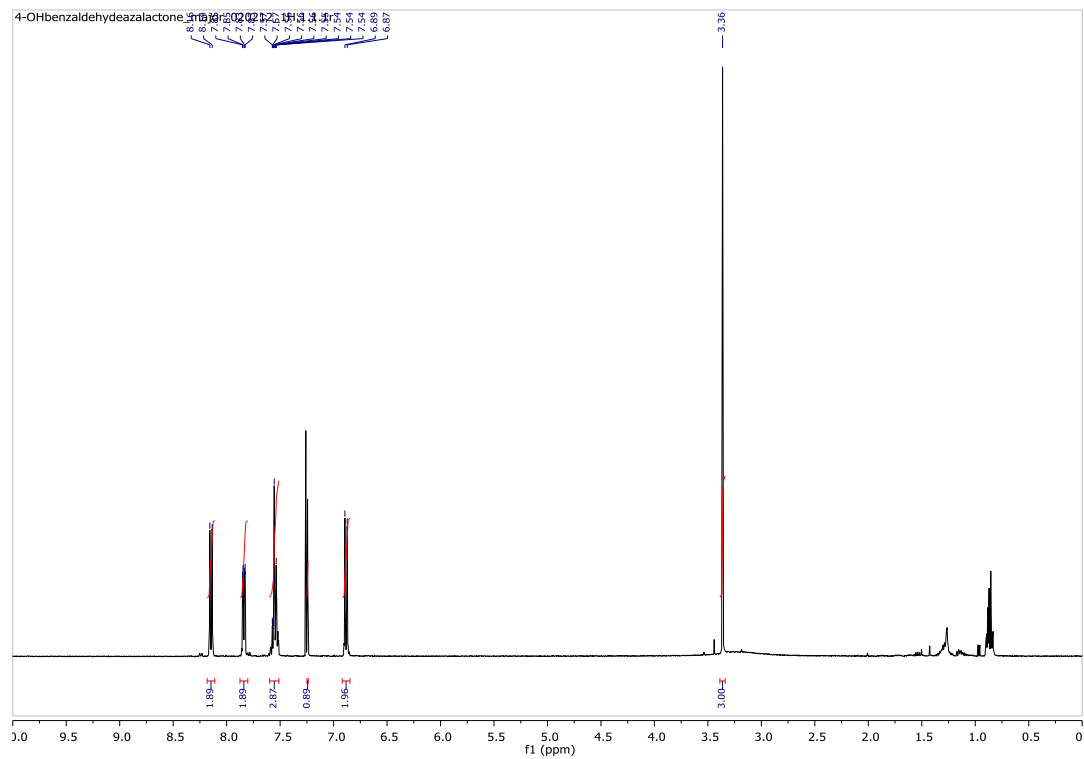


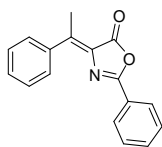
(1b)



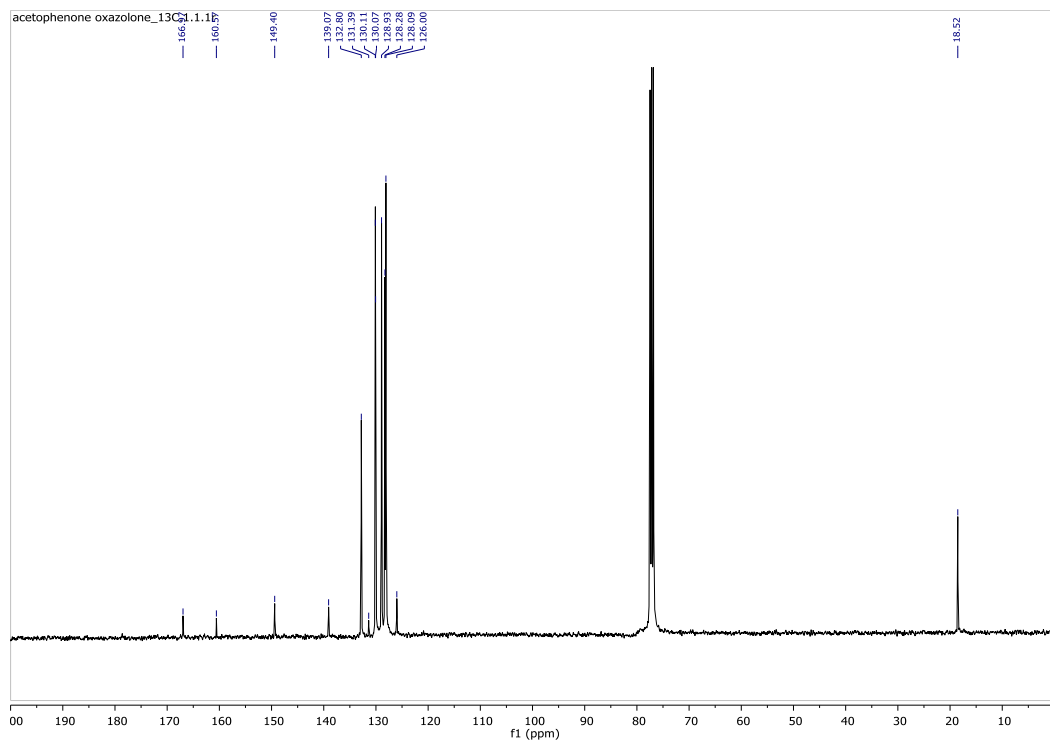
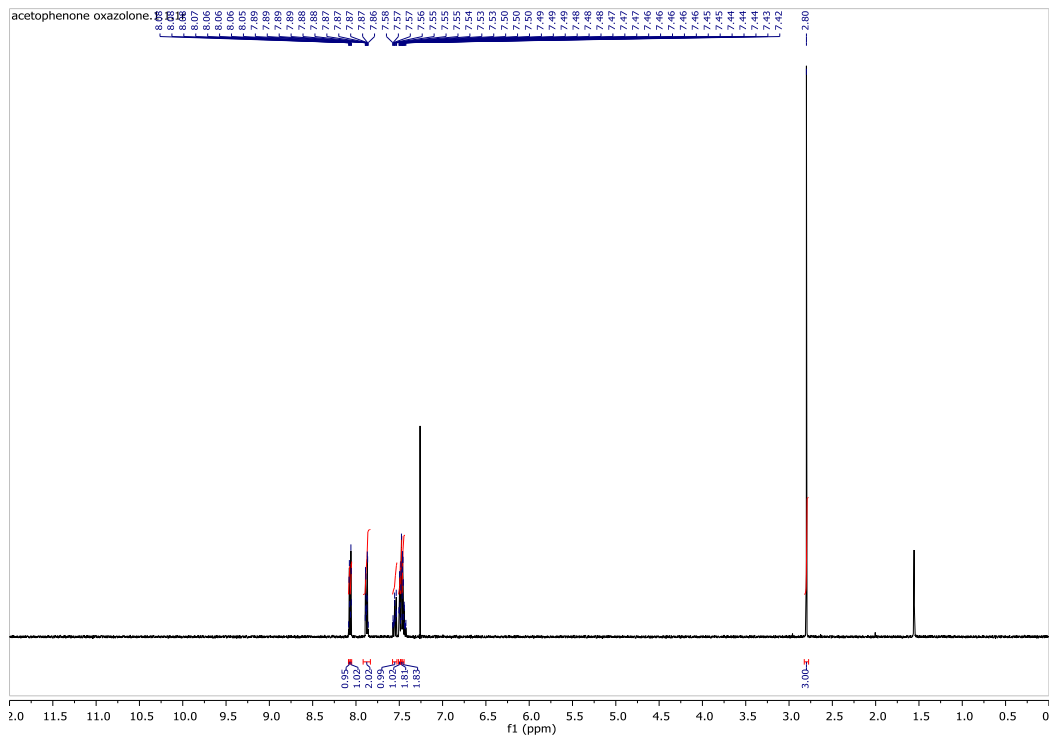


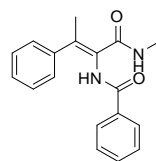
(1c)



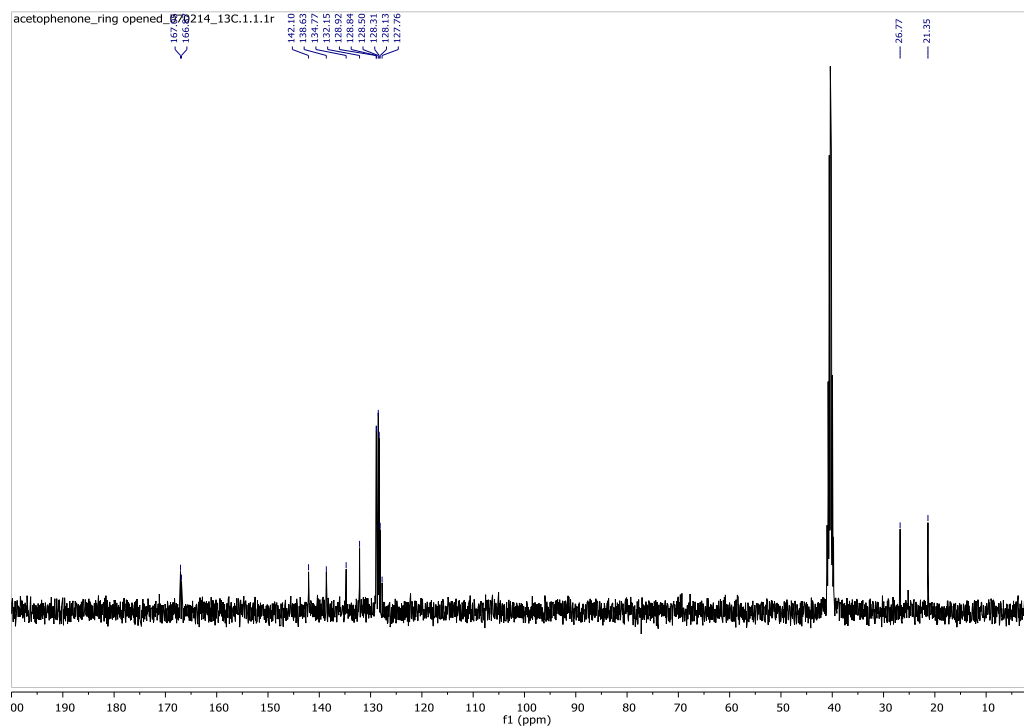
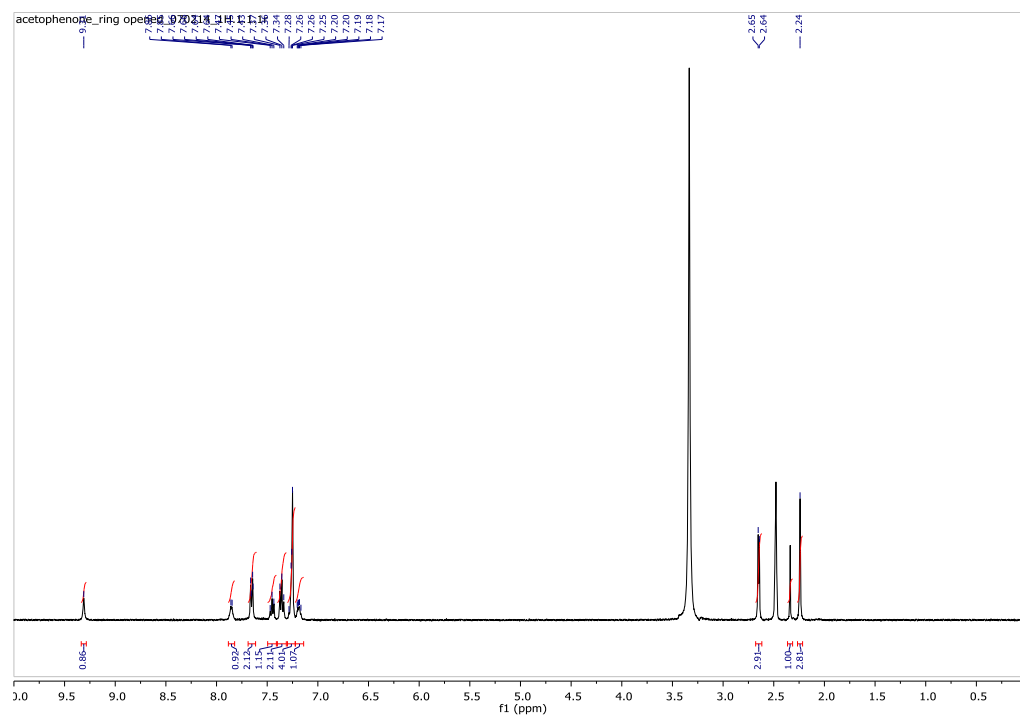


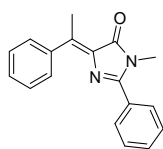
(2a)



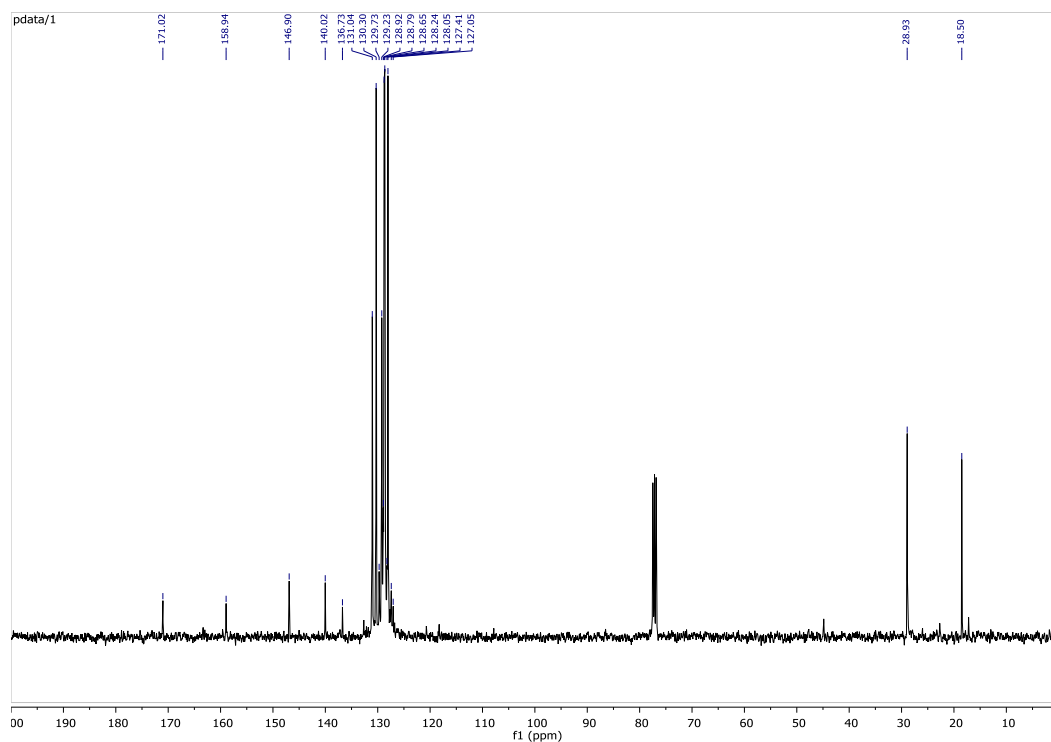
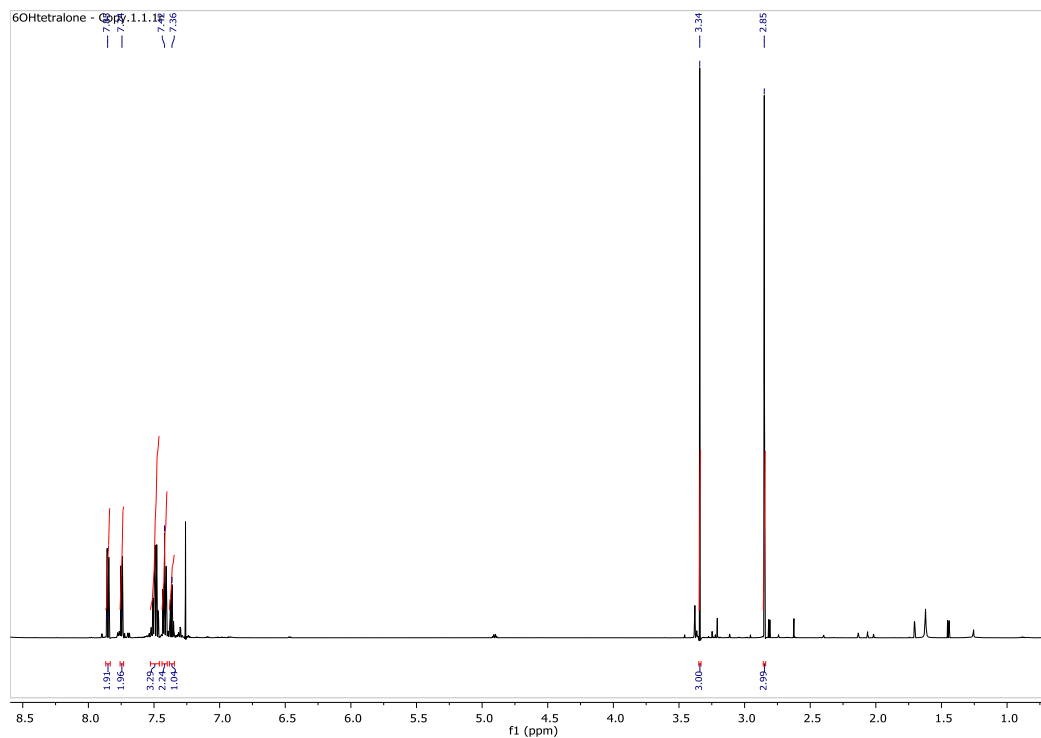


(2b)

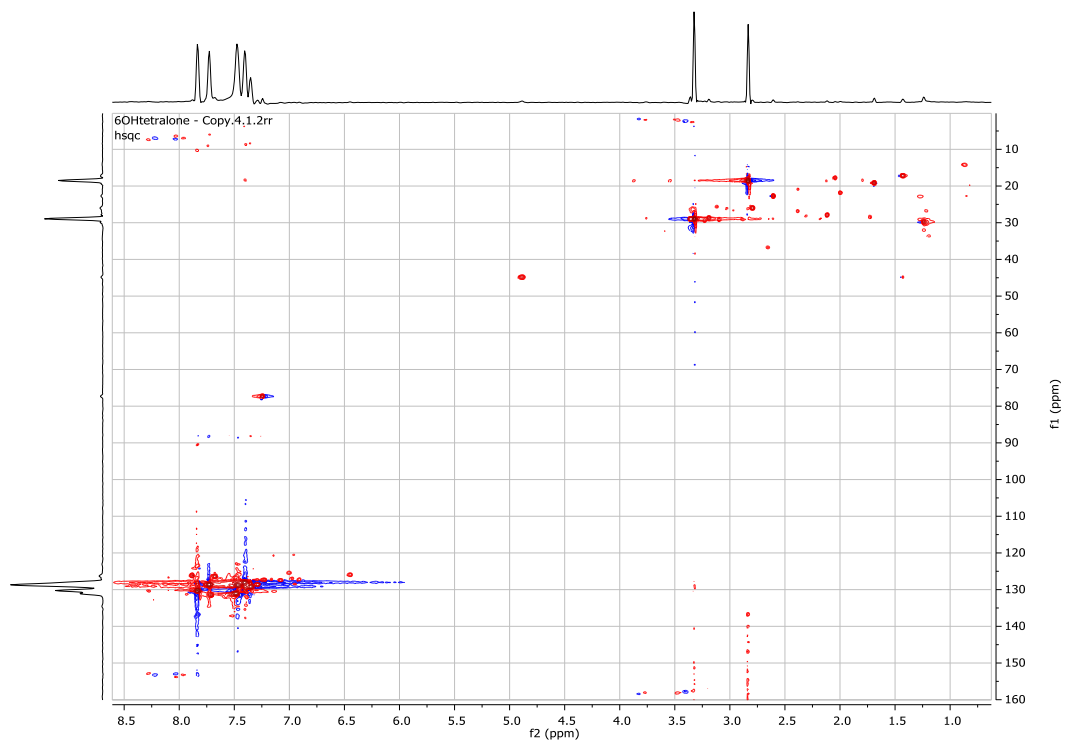




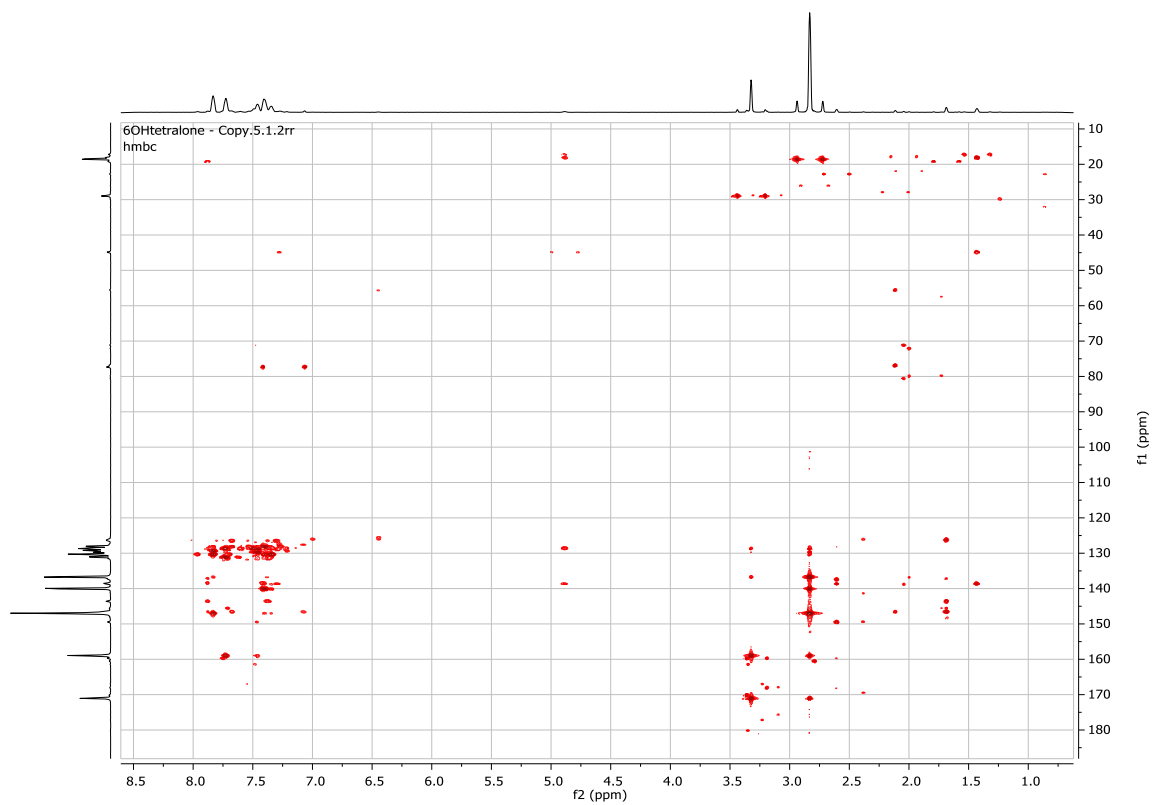
(2c major)



### HSQC of 2c (major)

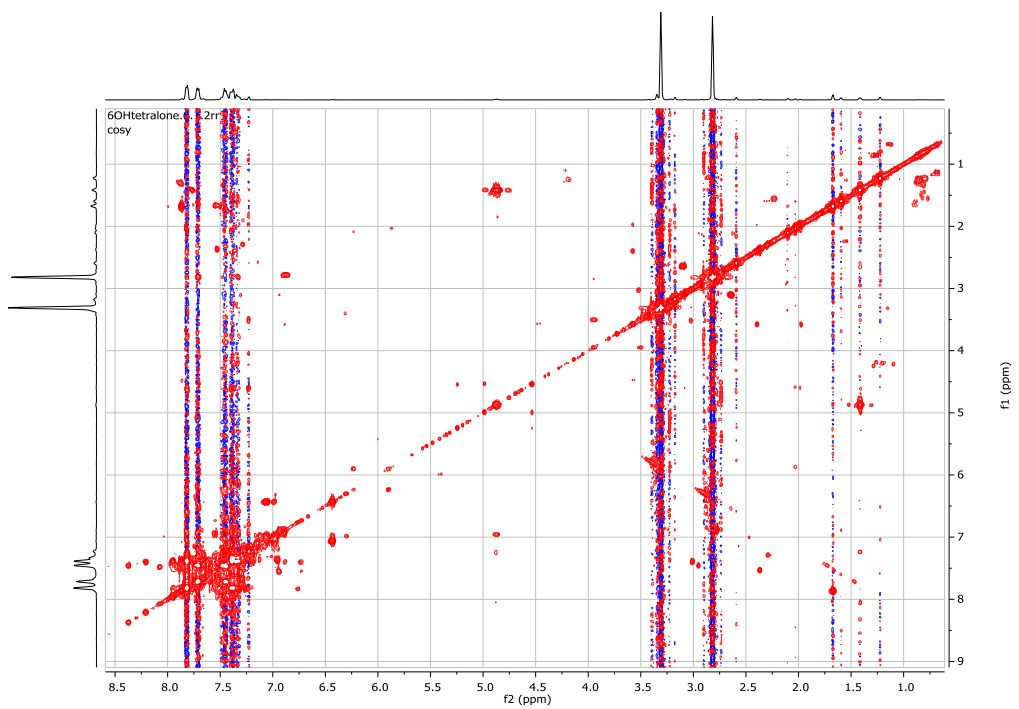


### HMBC of 2c (major)

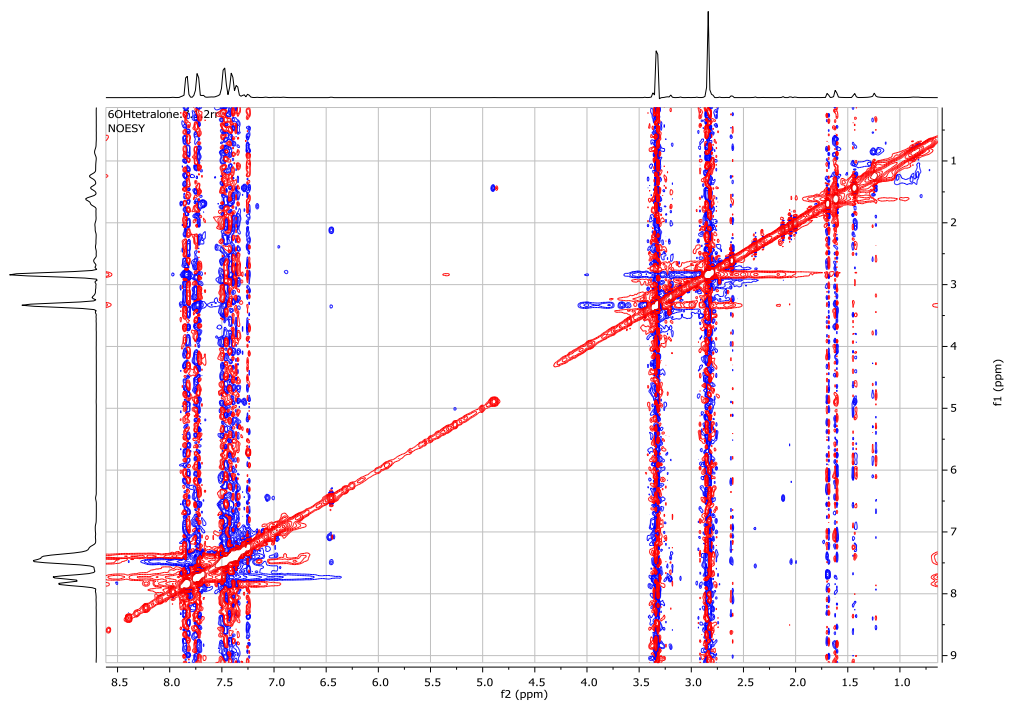




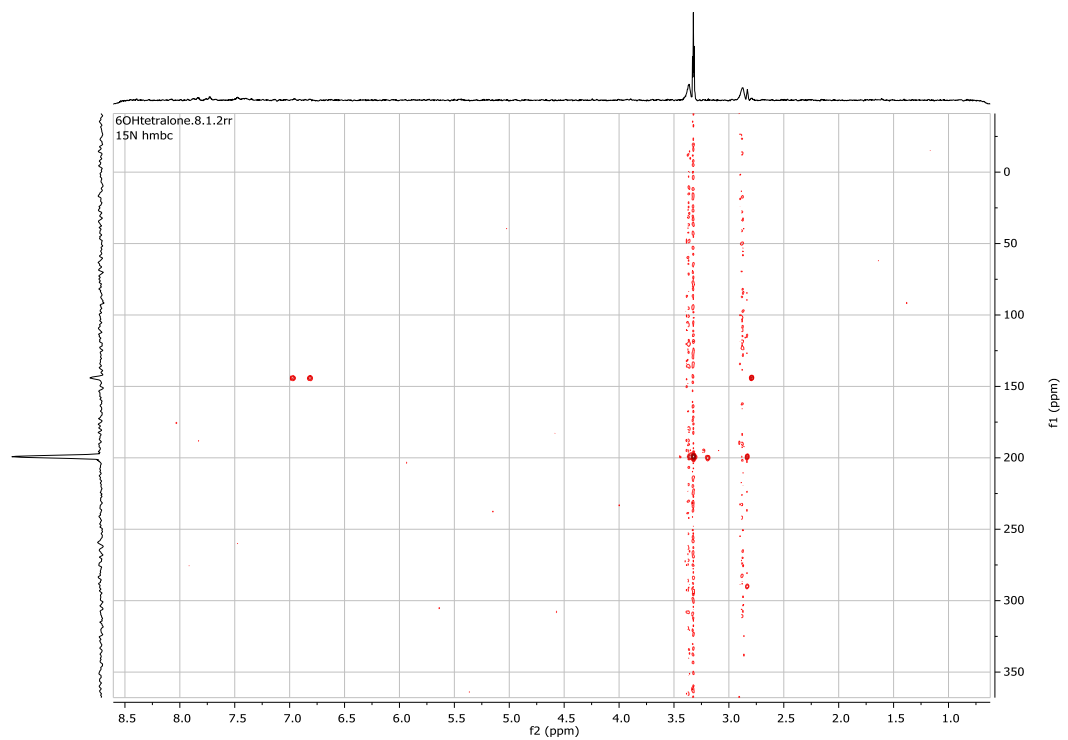
COSY of 2c (major)

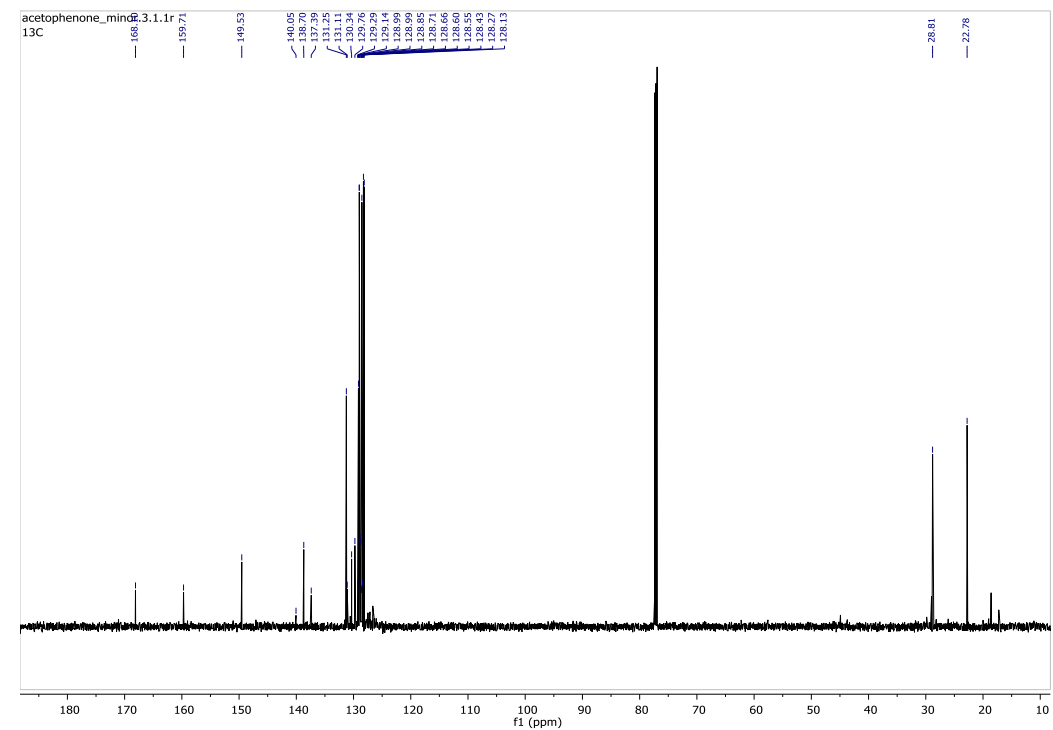
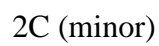


NOESY of 2c (major)

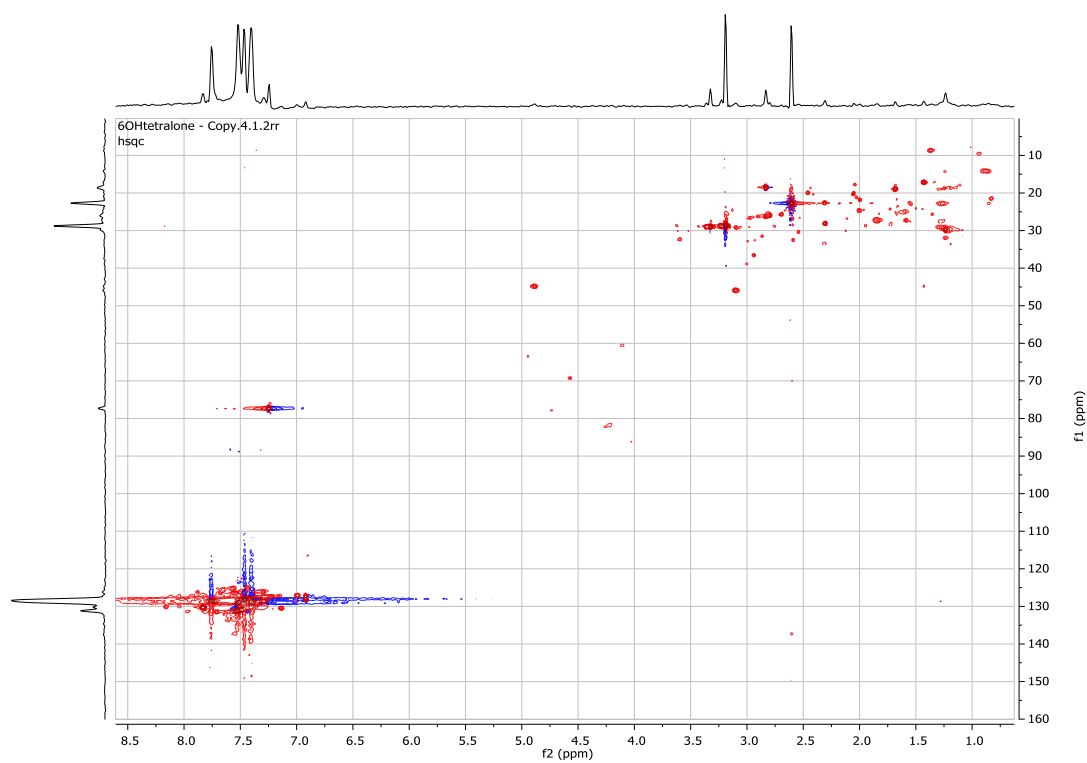


15N HMBC of 2c (major)

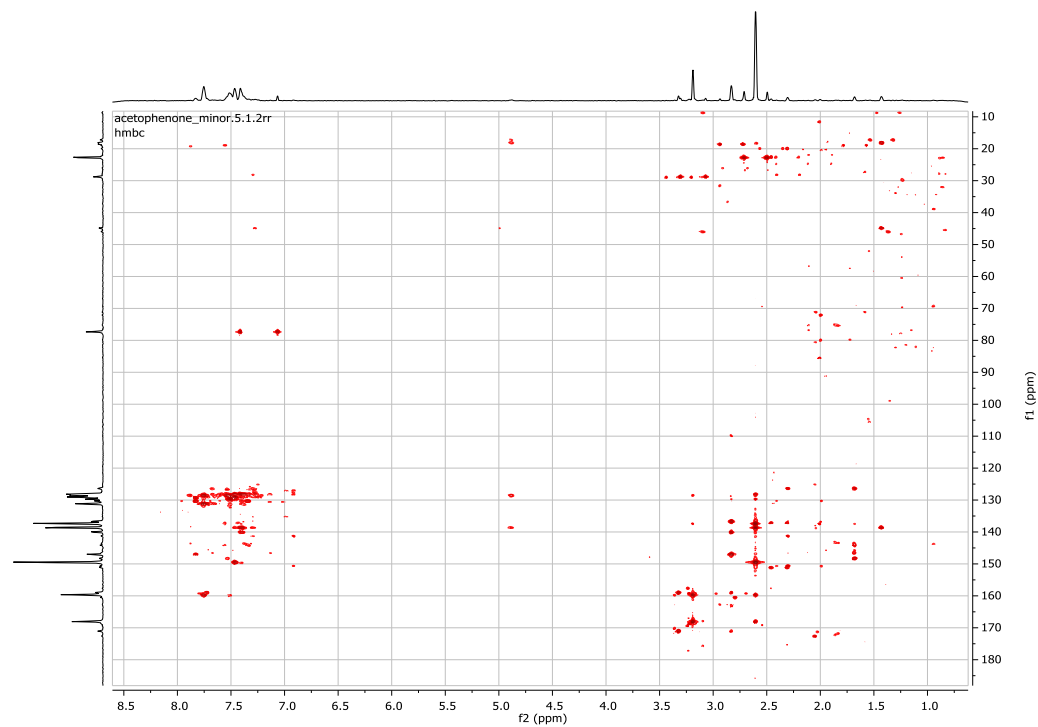




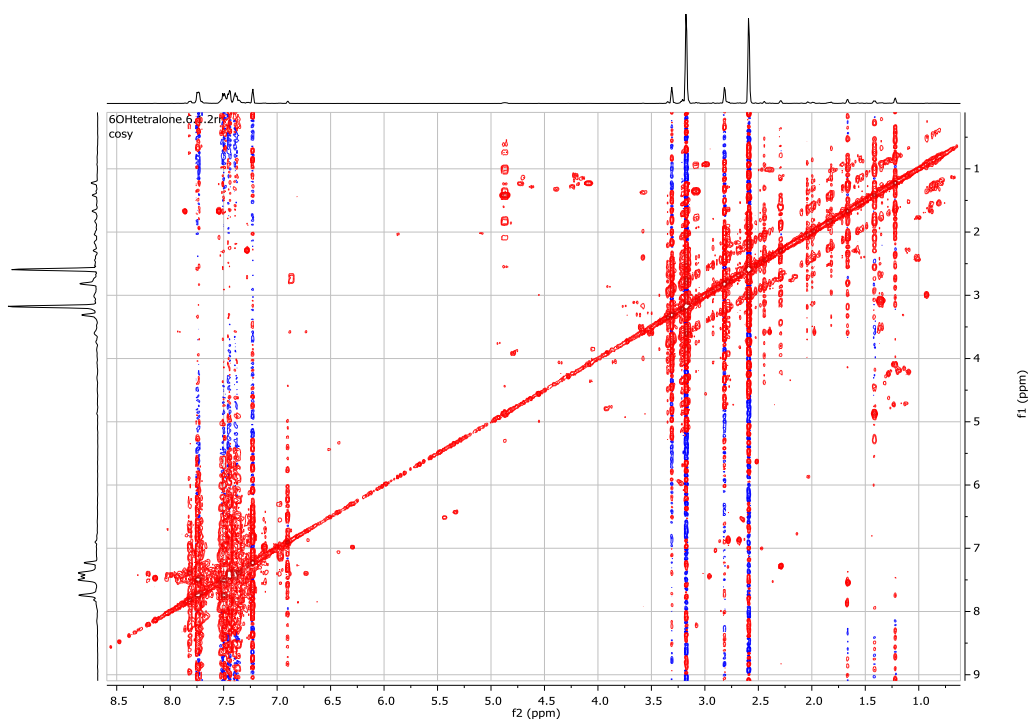
### HSQC of 2c (minor)



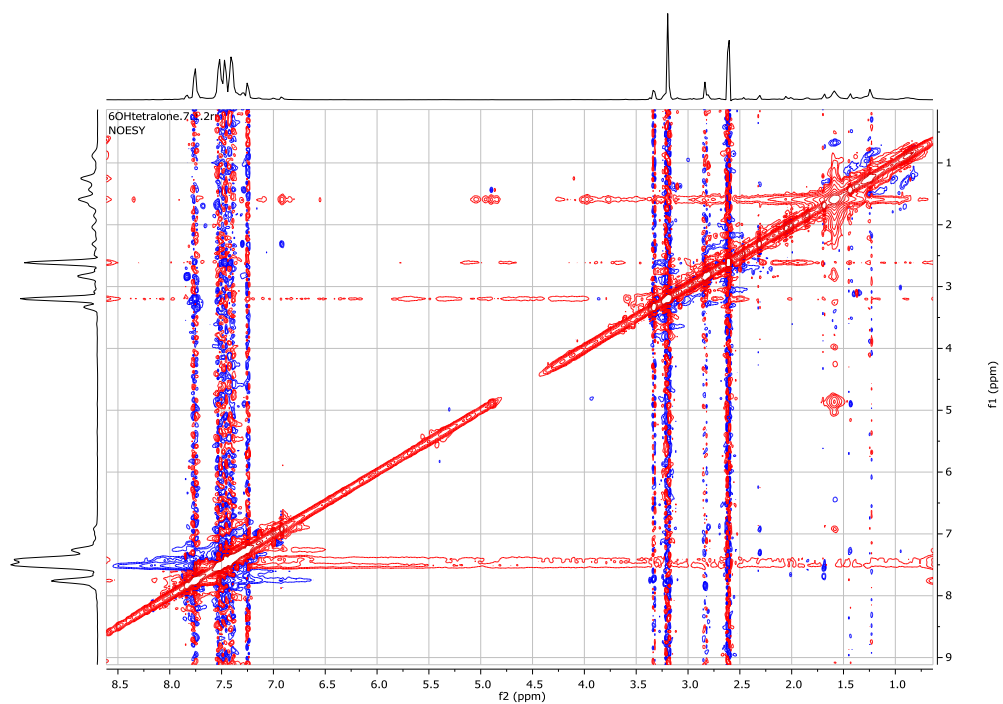
### HMBC of 2c (minor)



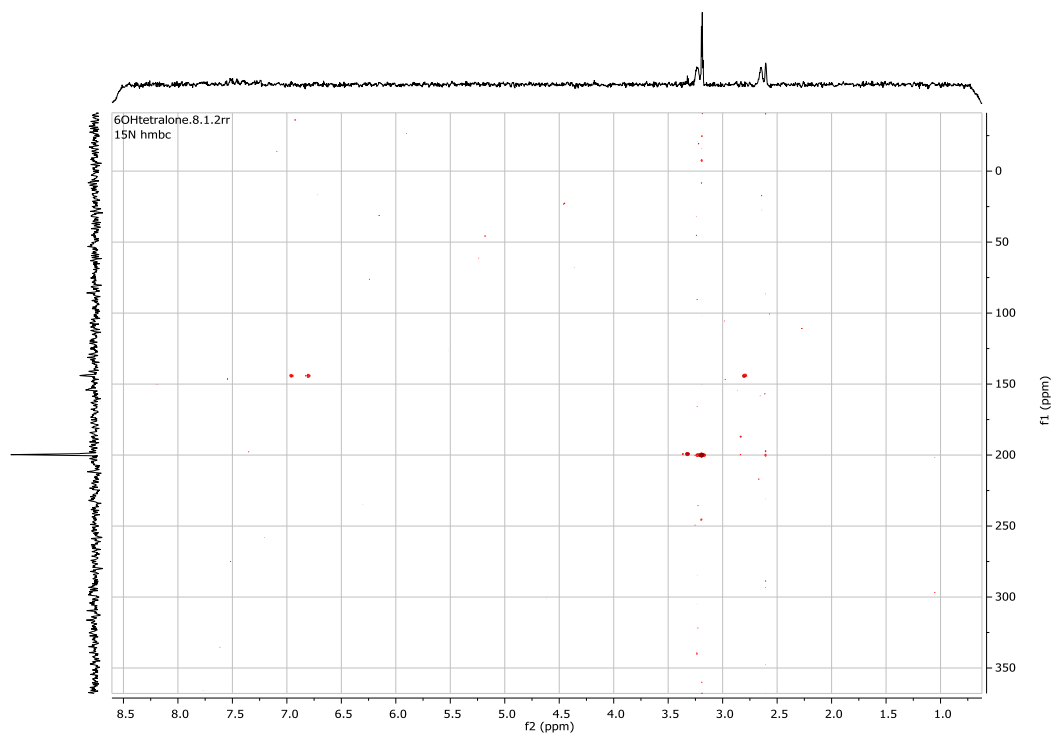
COSY of 2c (minor)

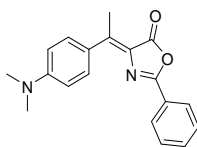


NOESY of 2c (minor)

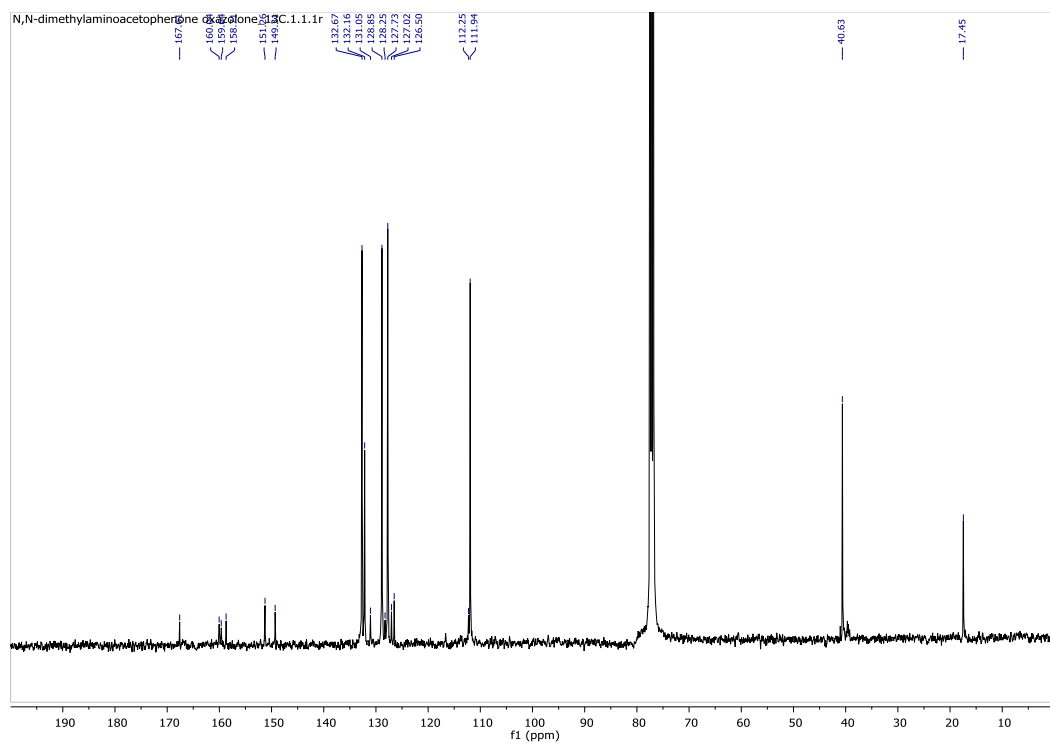
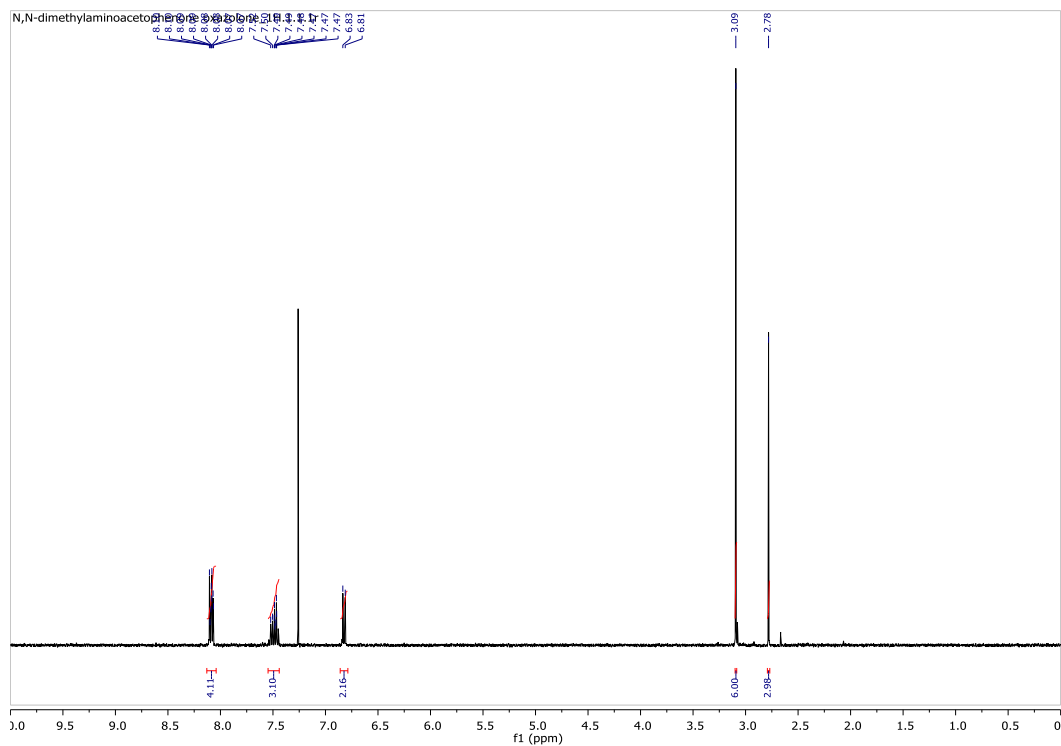


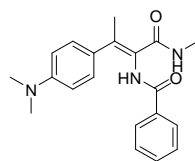
# 15N HMBC of 2c (minor)



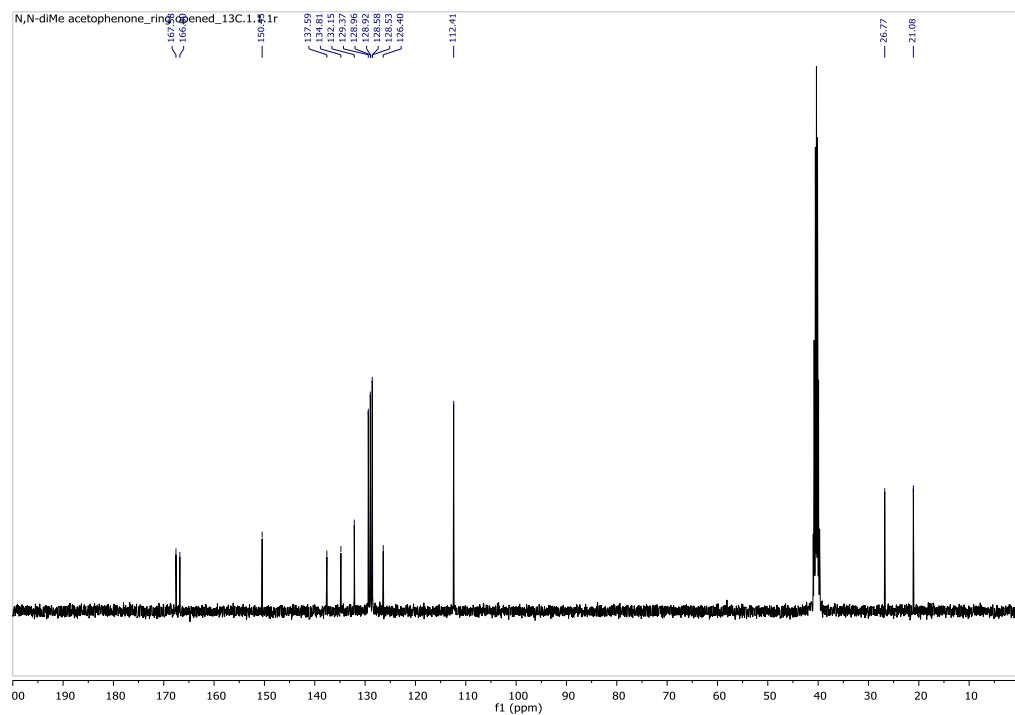
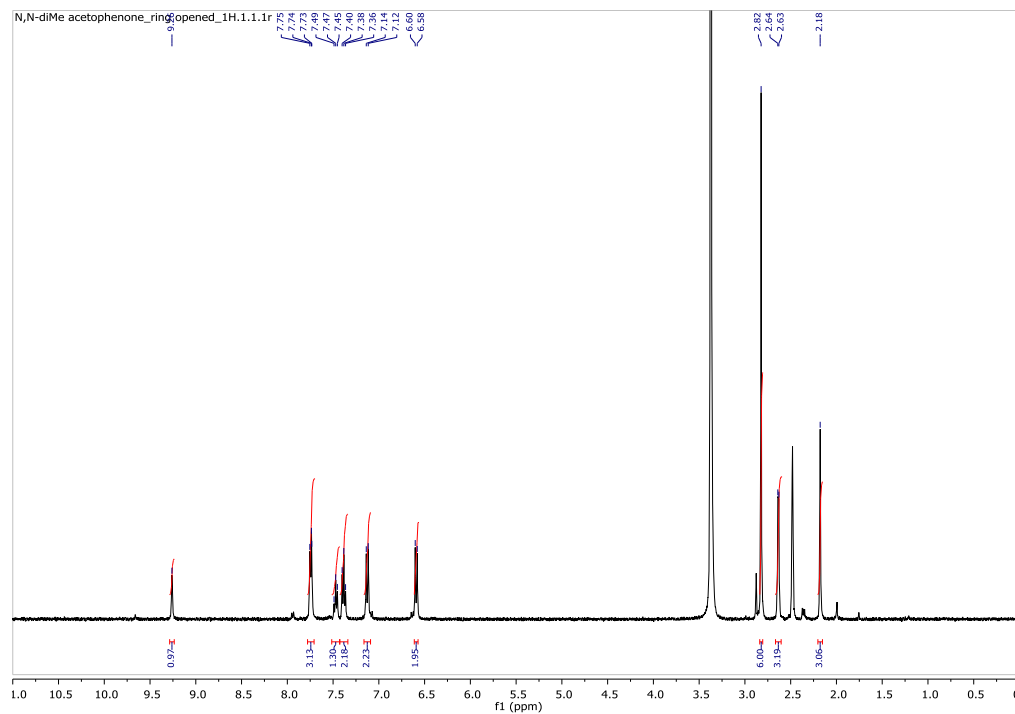


(3a)

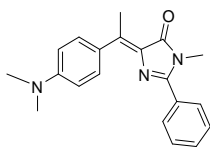




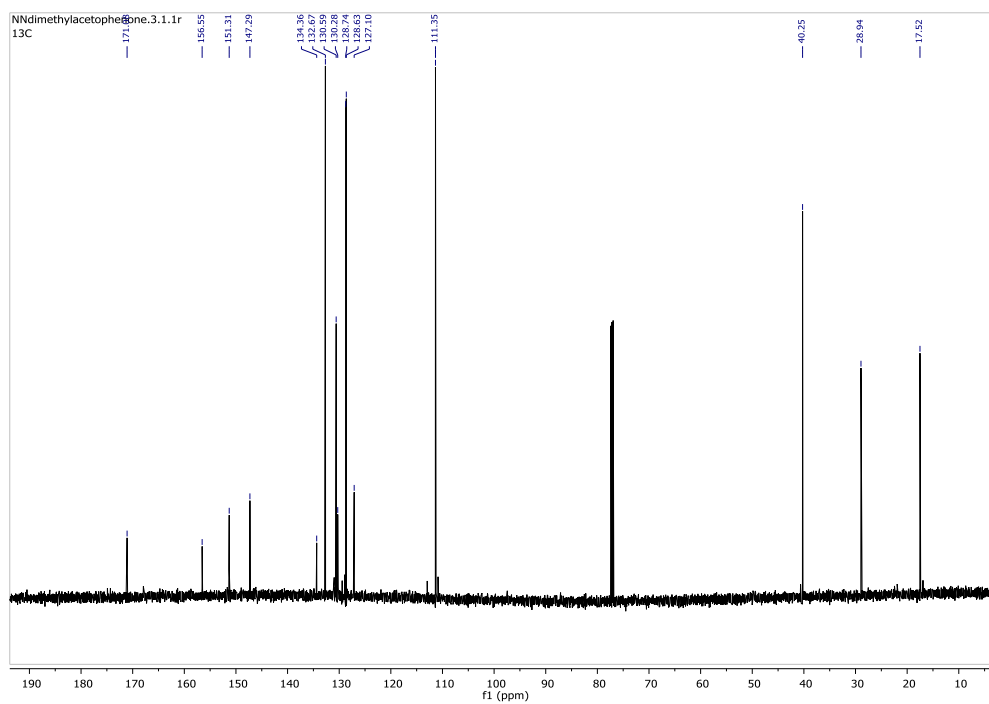
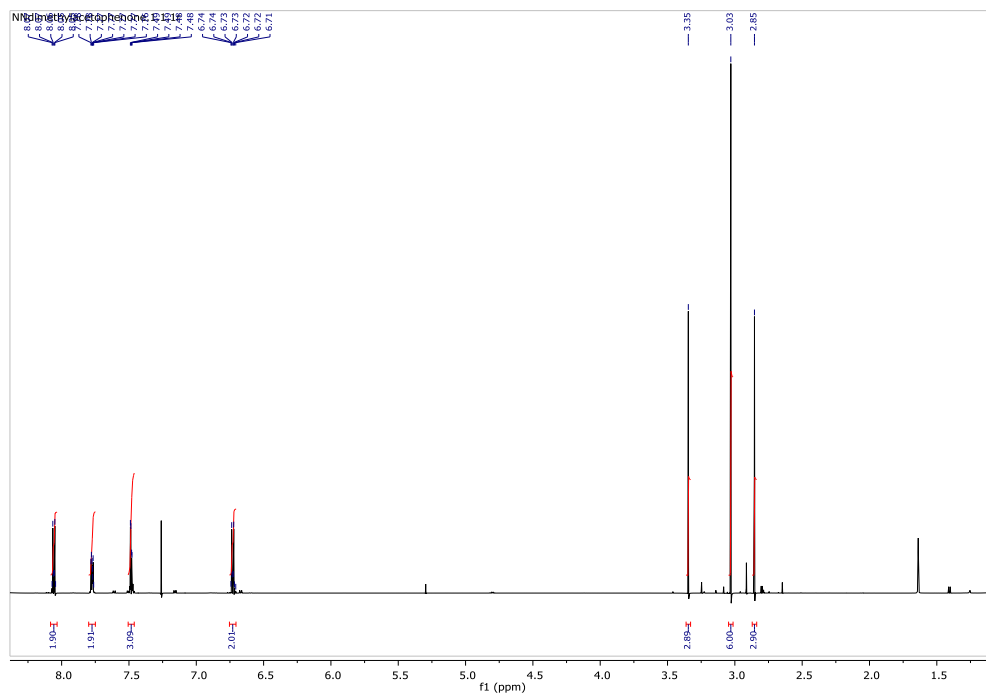
(3b)



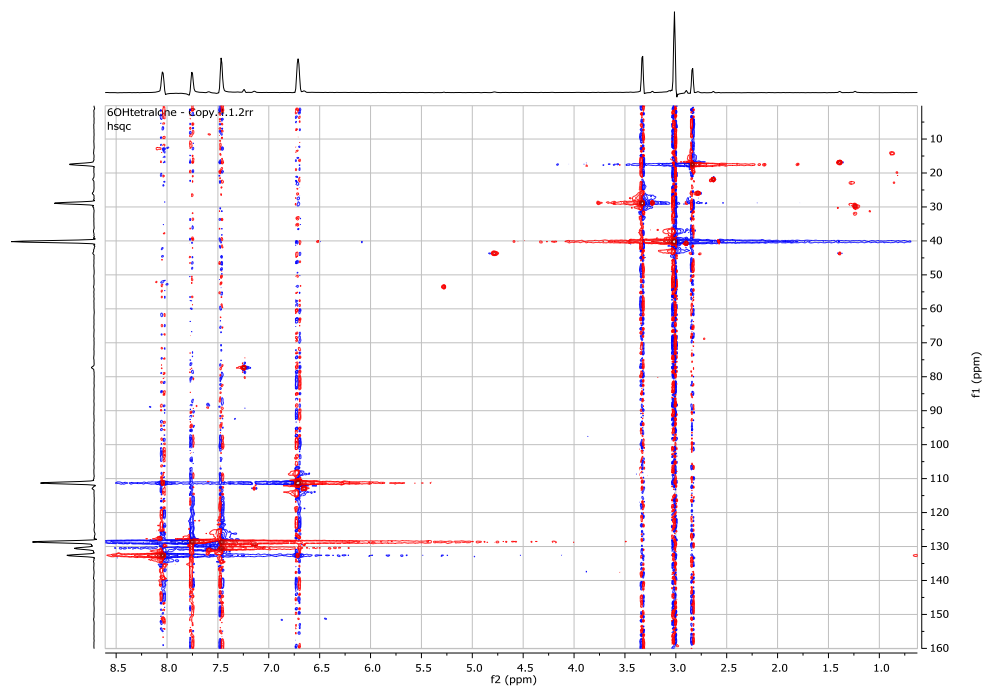




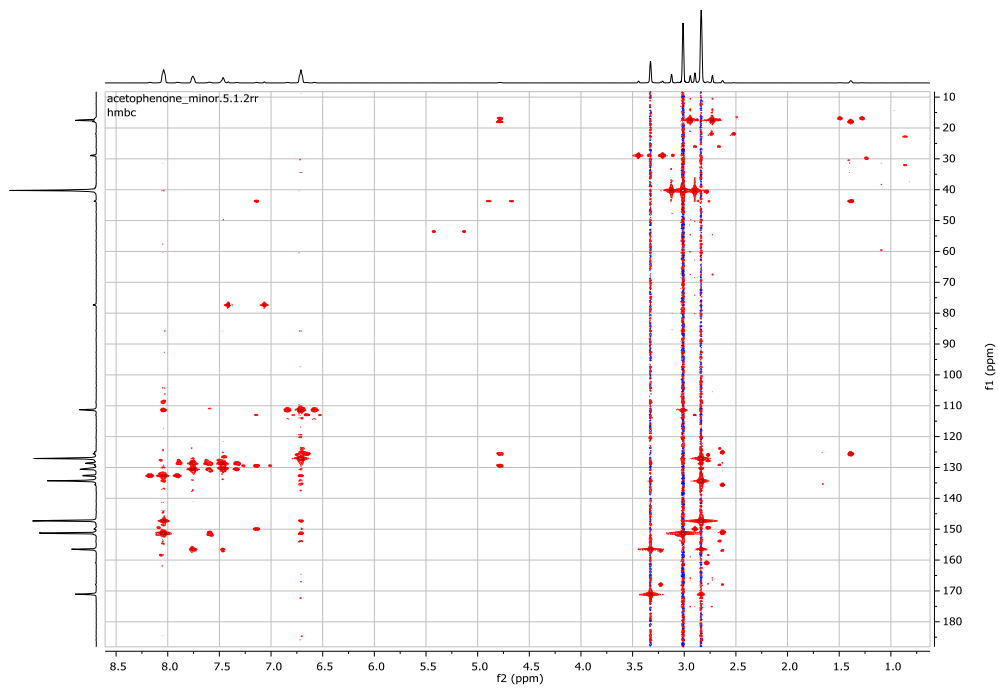
(3c)



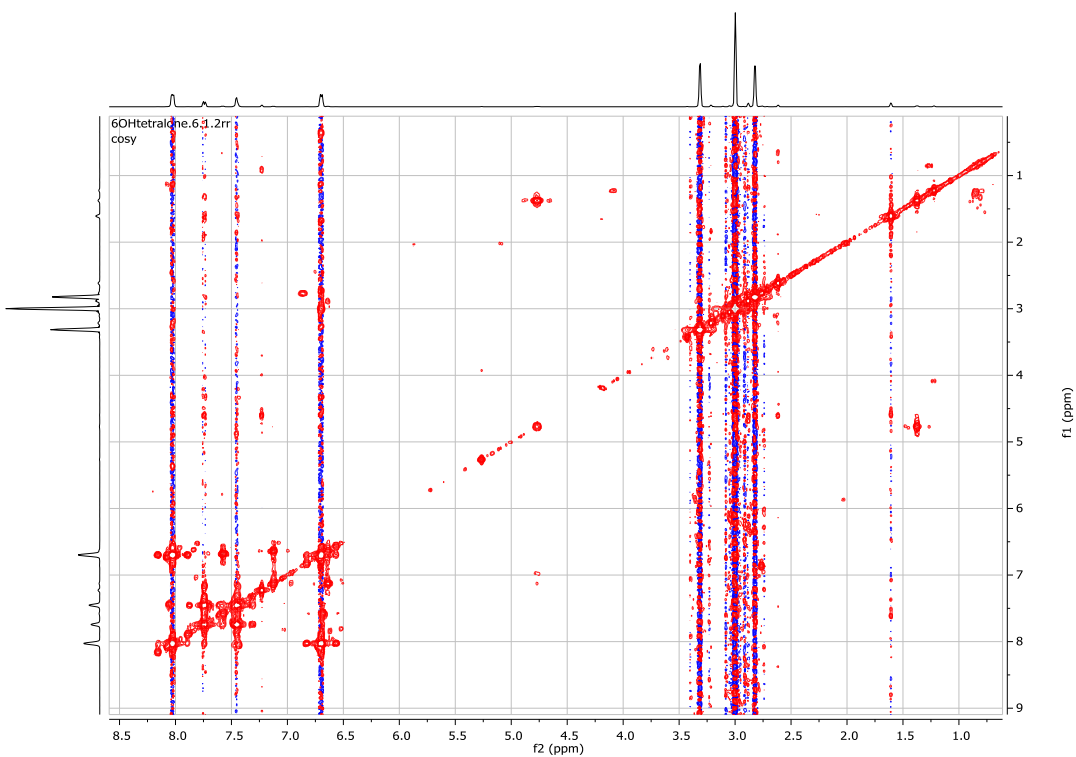
### HSQC of 3c



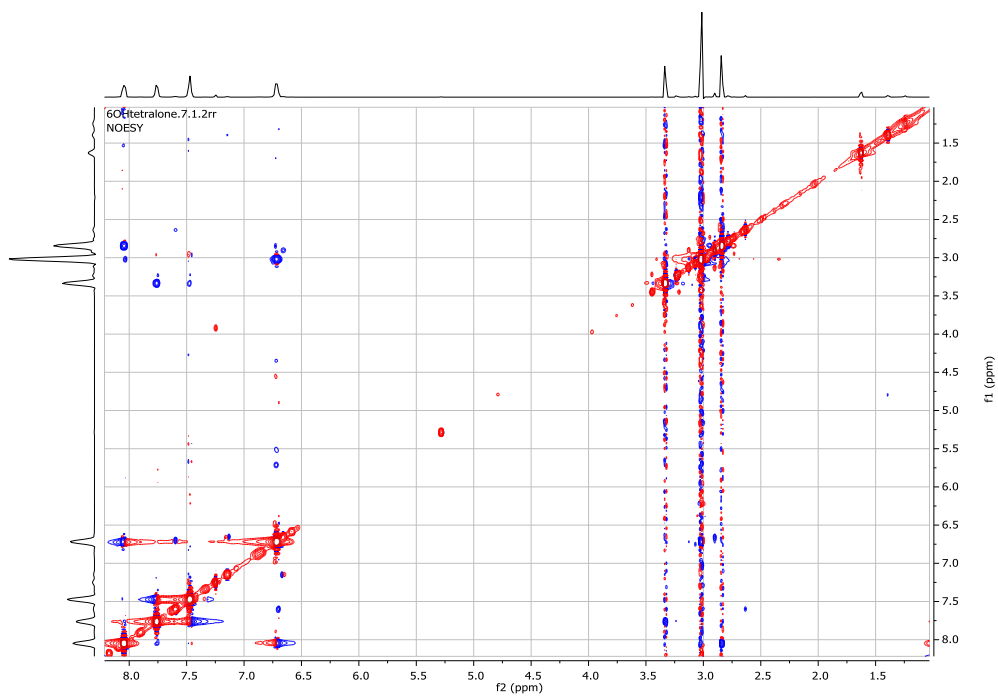
### HMBC of 3c



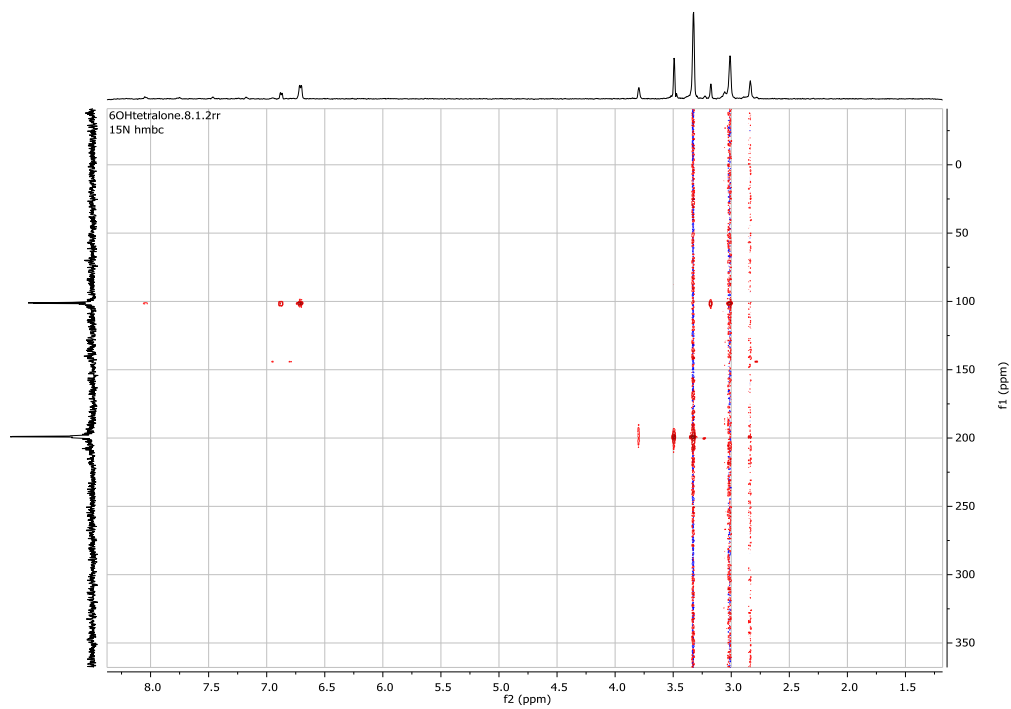
COSY of 3c

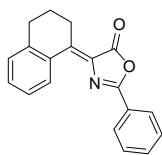


NOESY of 3c

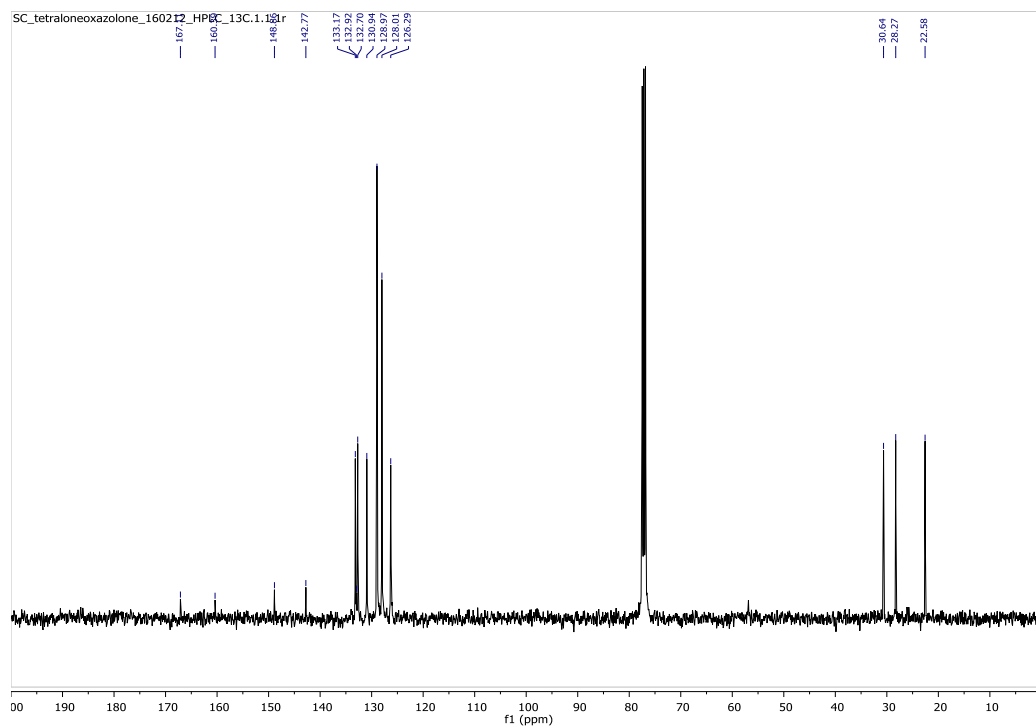
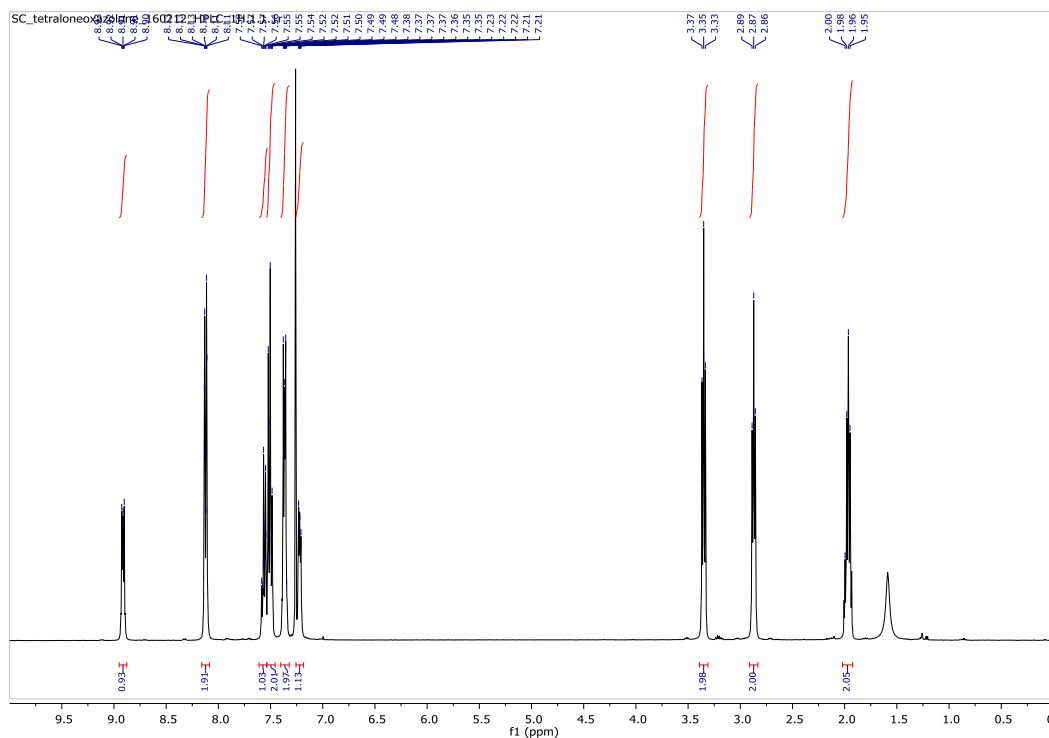


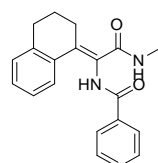
# 15N HMBC of 3c



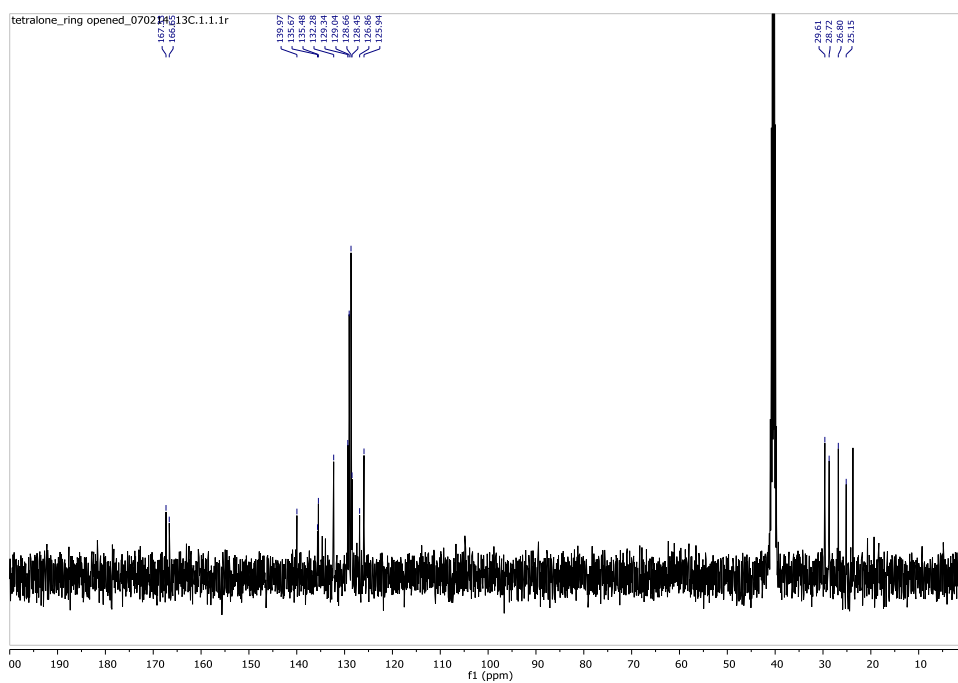
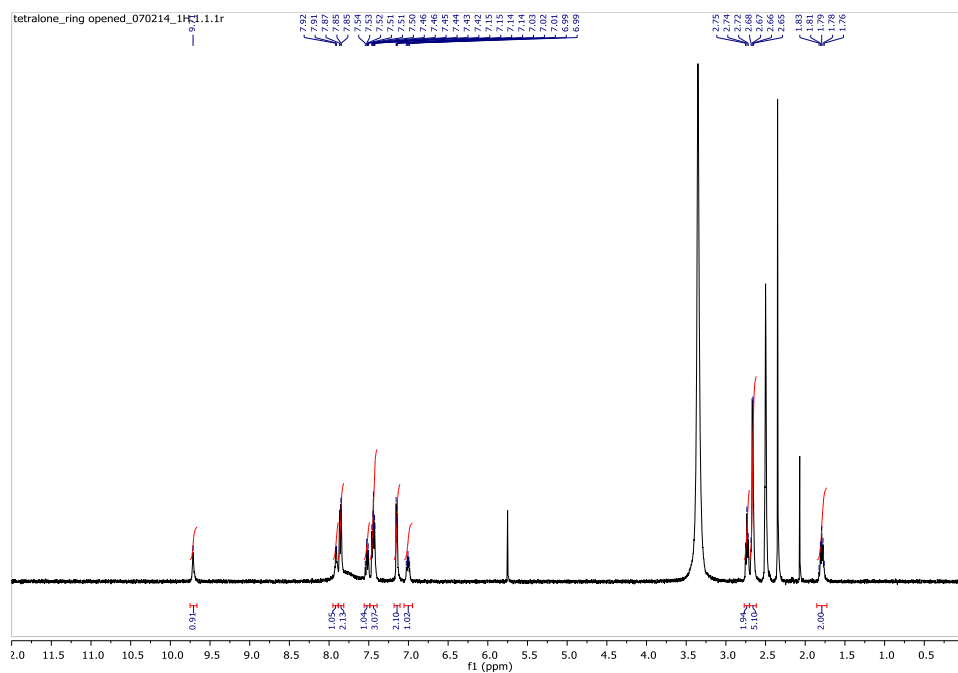


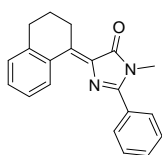
(4a)



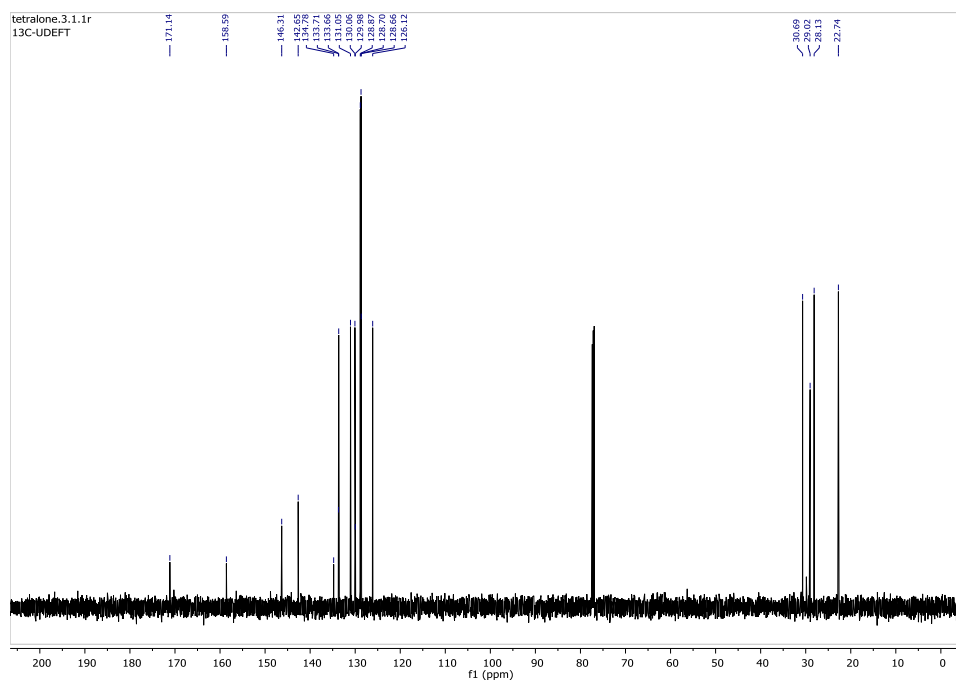
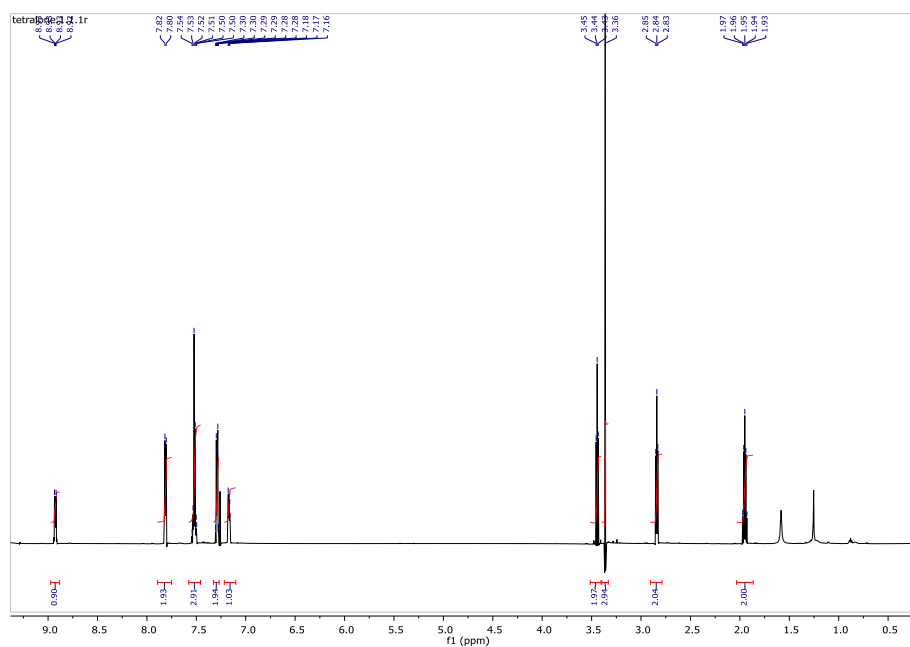


(4b)

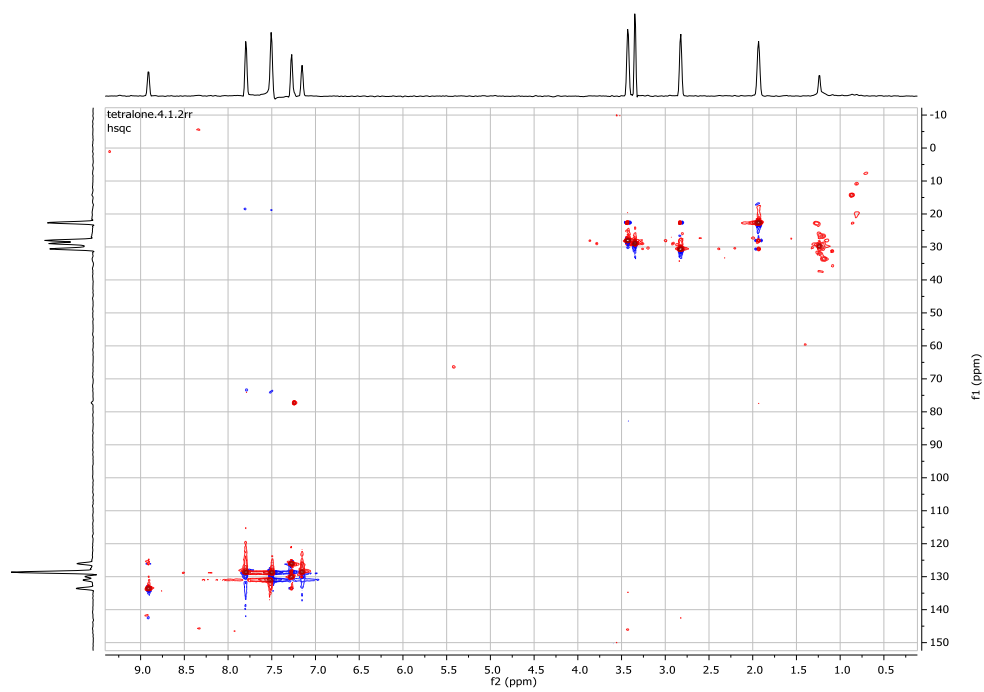




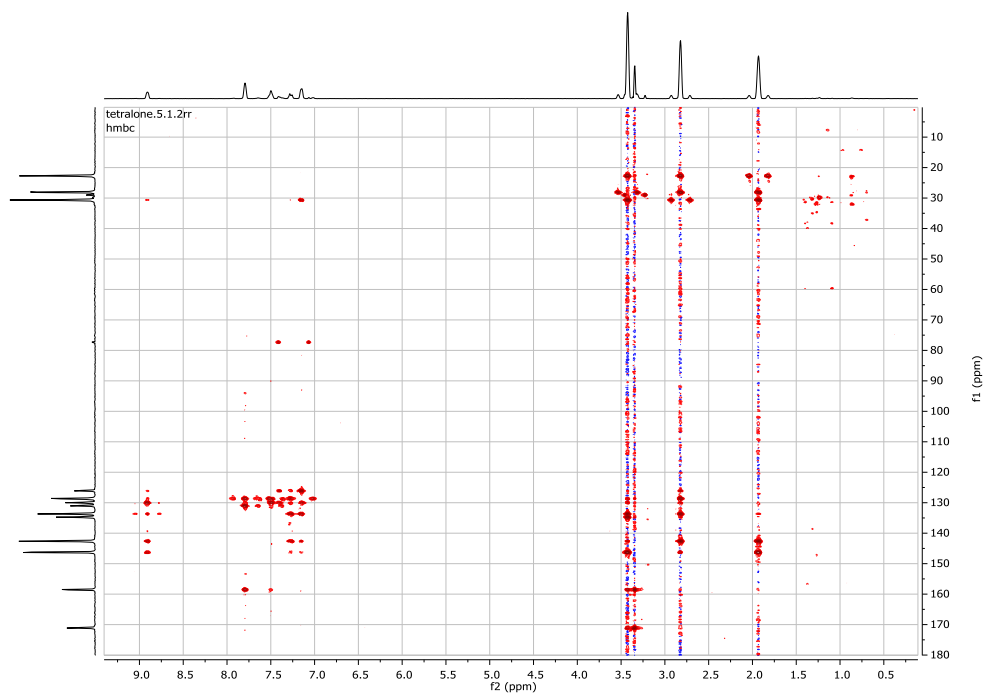
(4c)



### HSQC of 4c



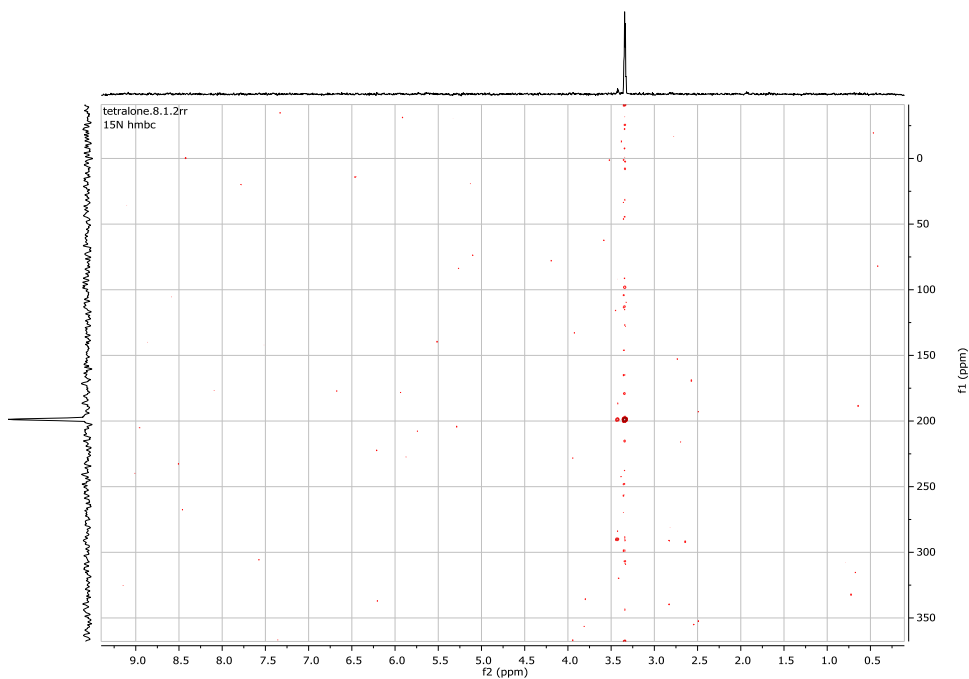
### HMBC of 4c

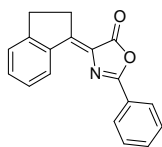




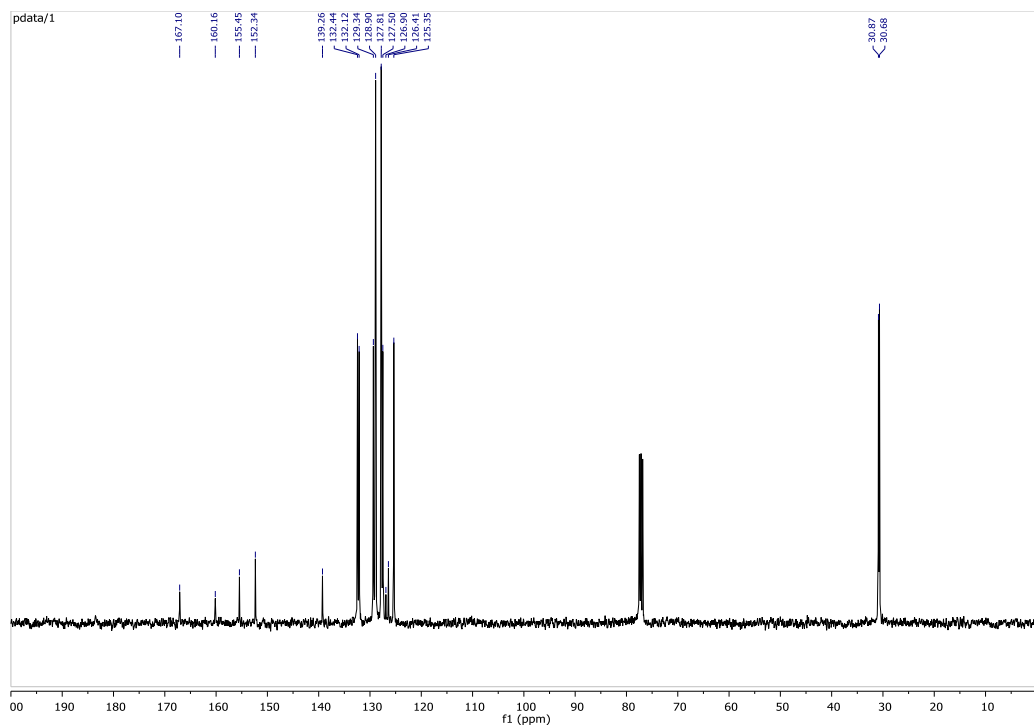
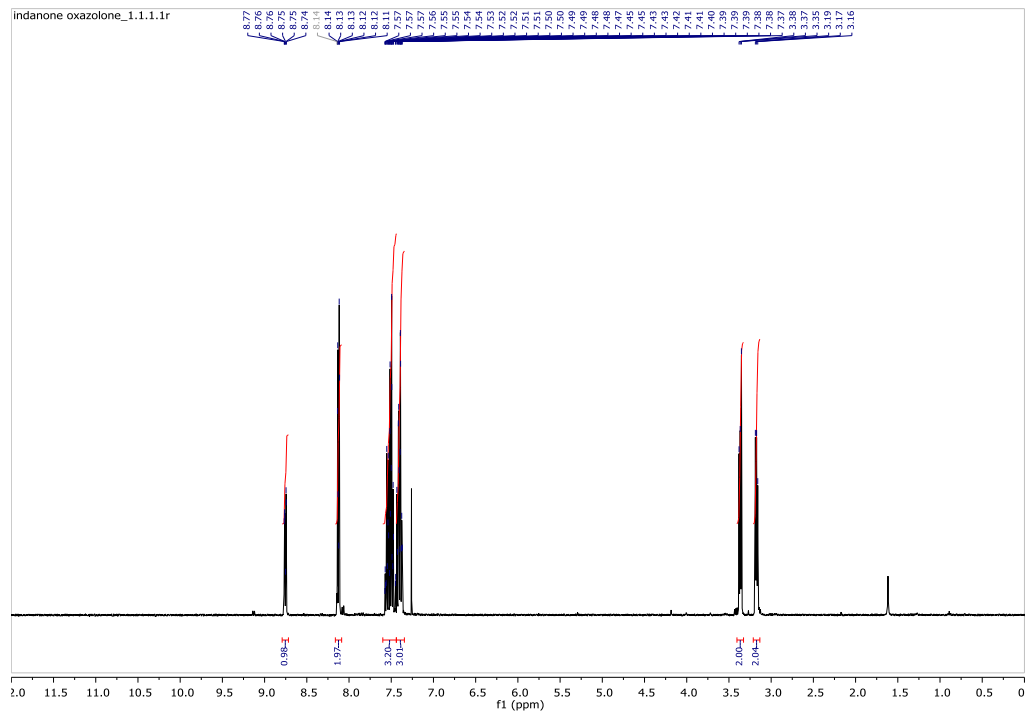


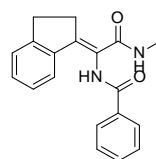
# 15N HMBC of 4c



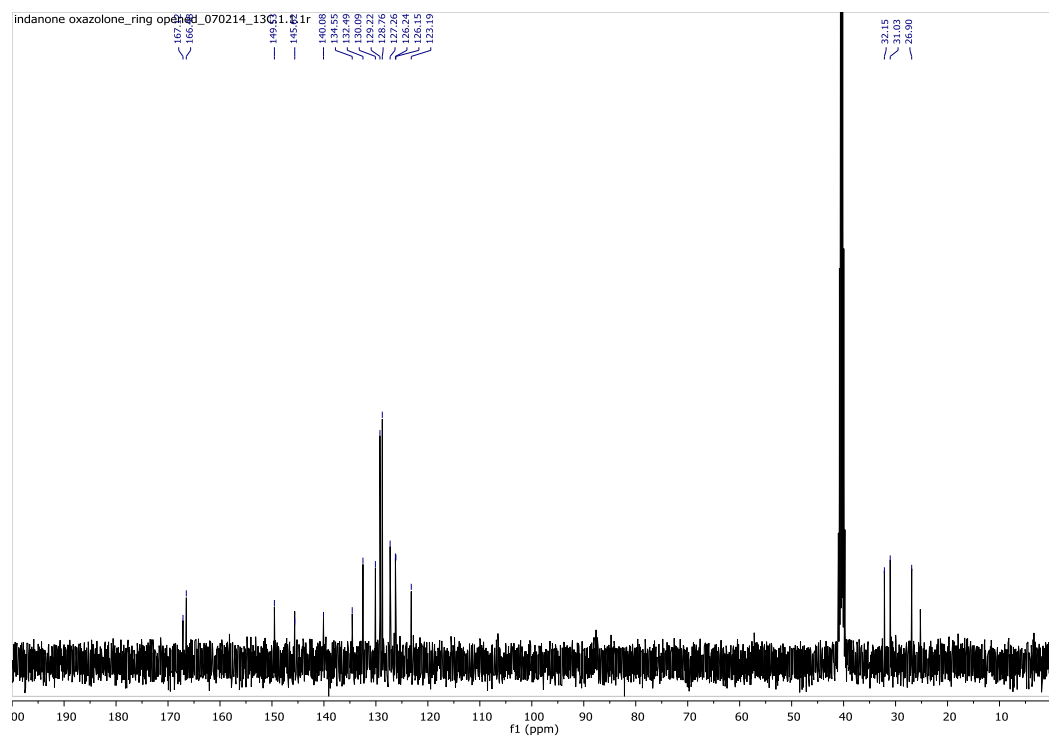
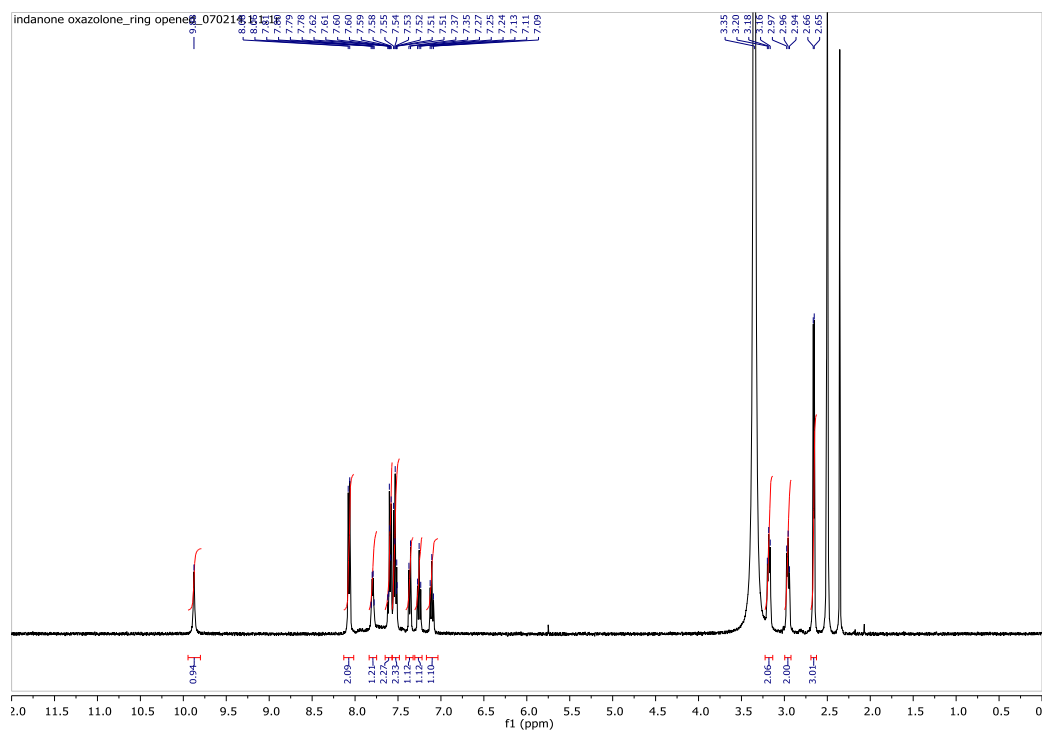


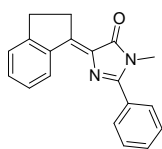
(5a)



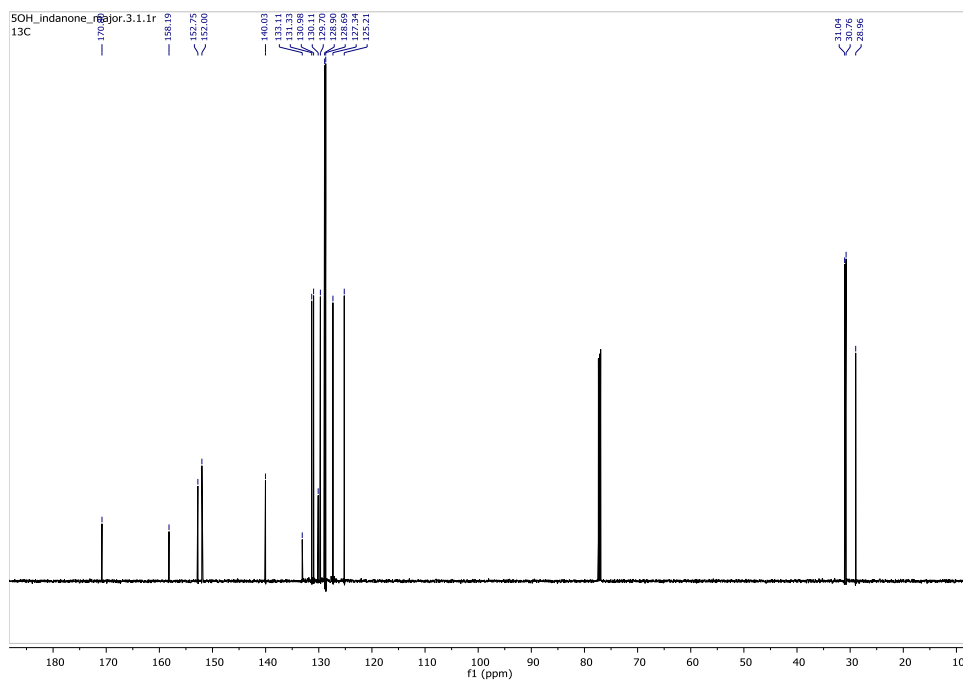
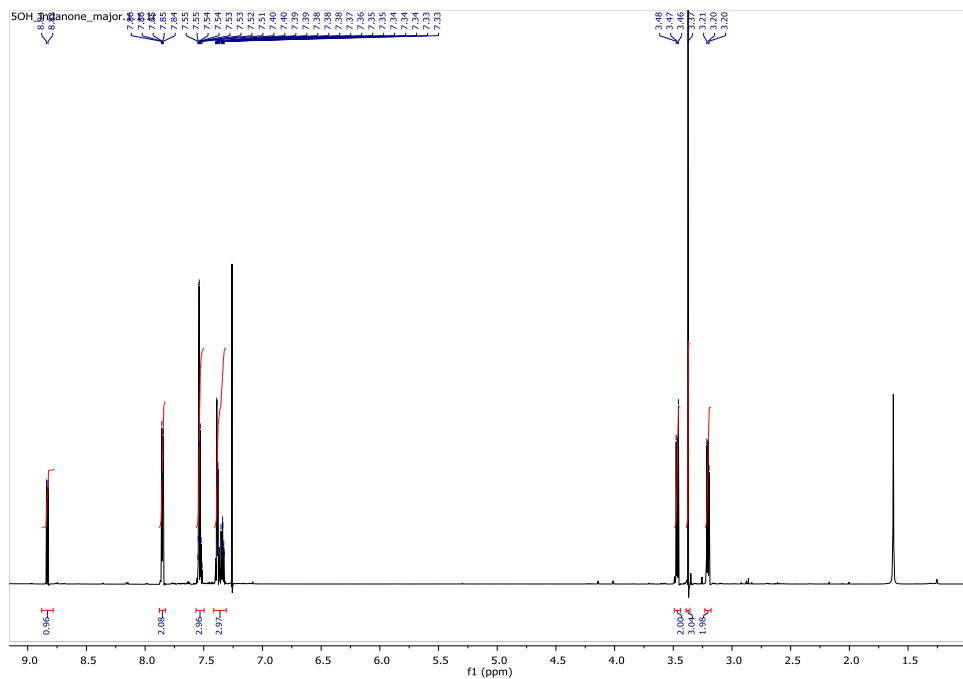


(5b)

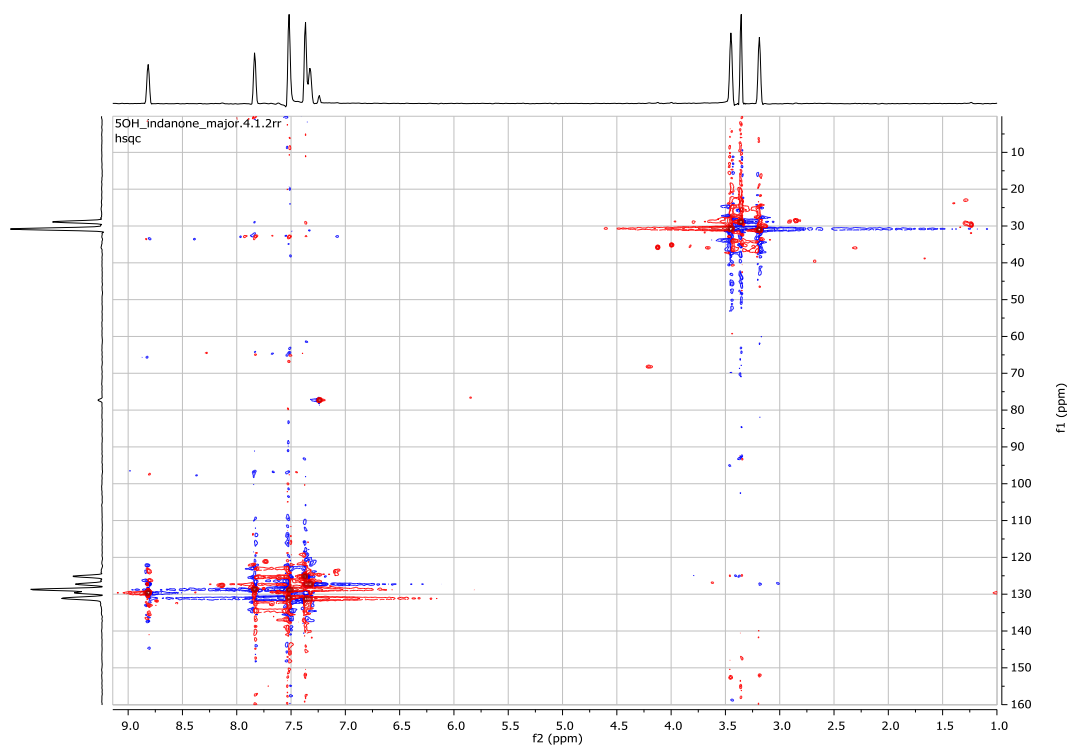




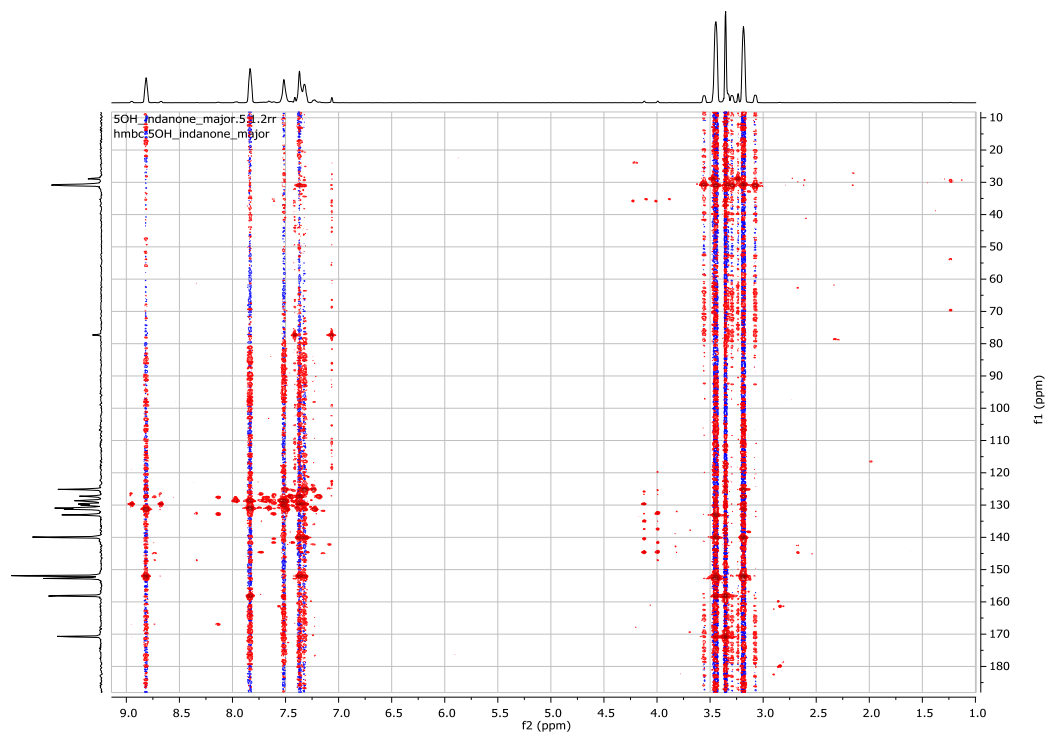
(5c)



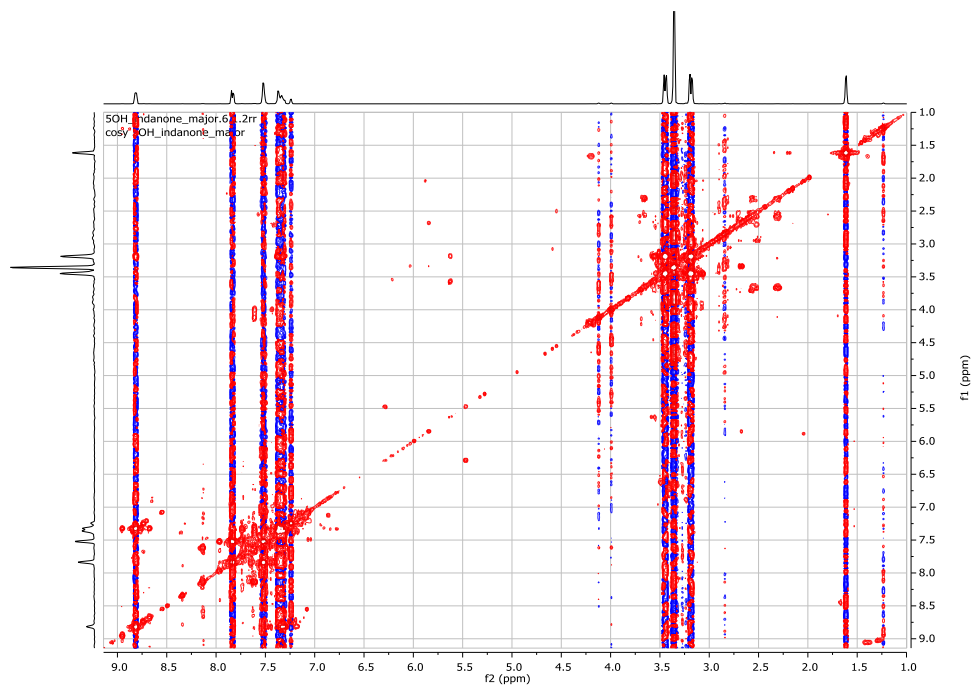
# HSQC of 5c



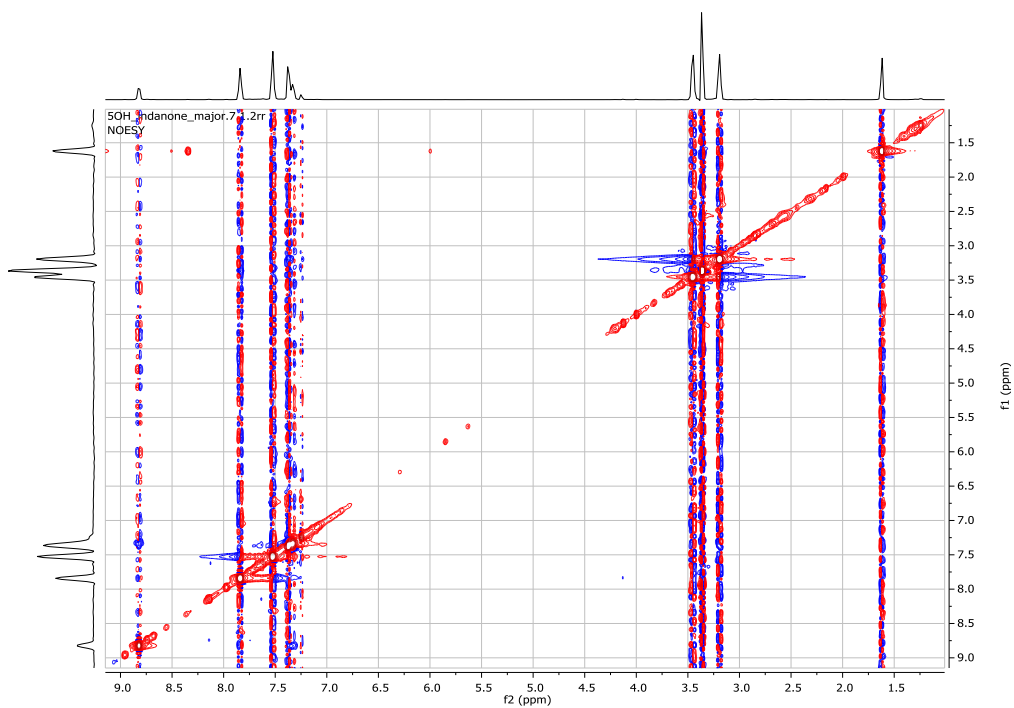
# HMBC of 5c



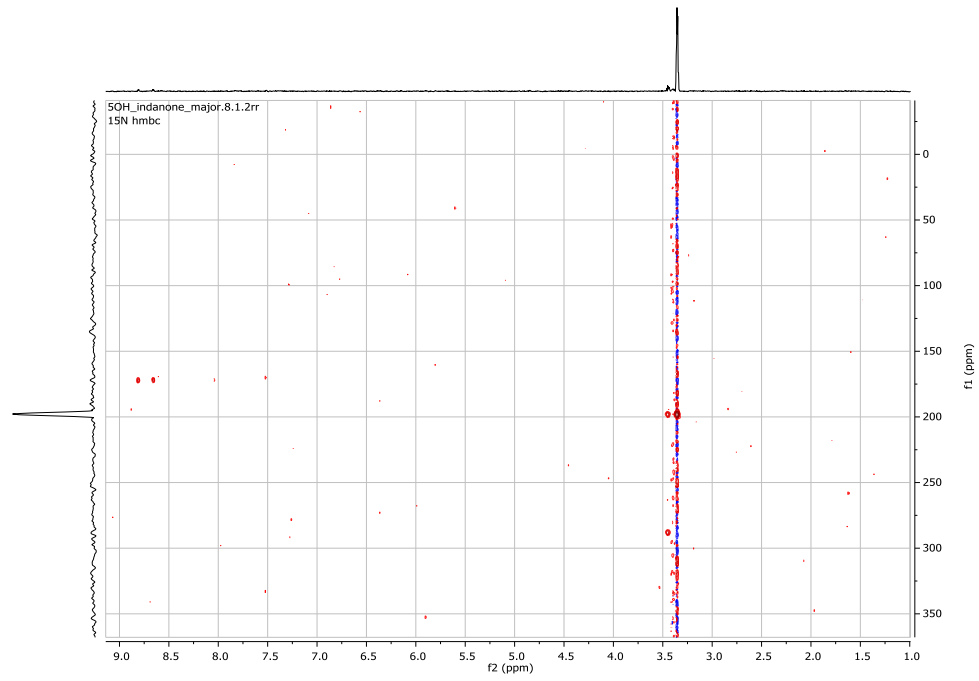
COSY of 5c



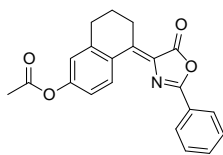
NOESY of 5c



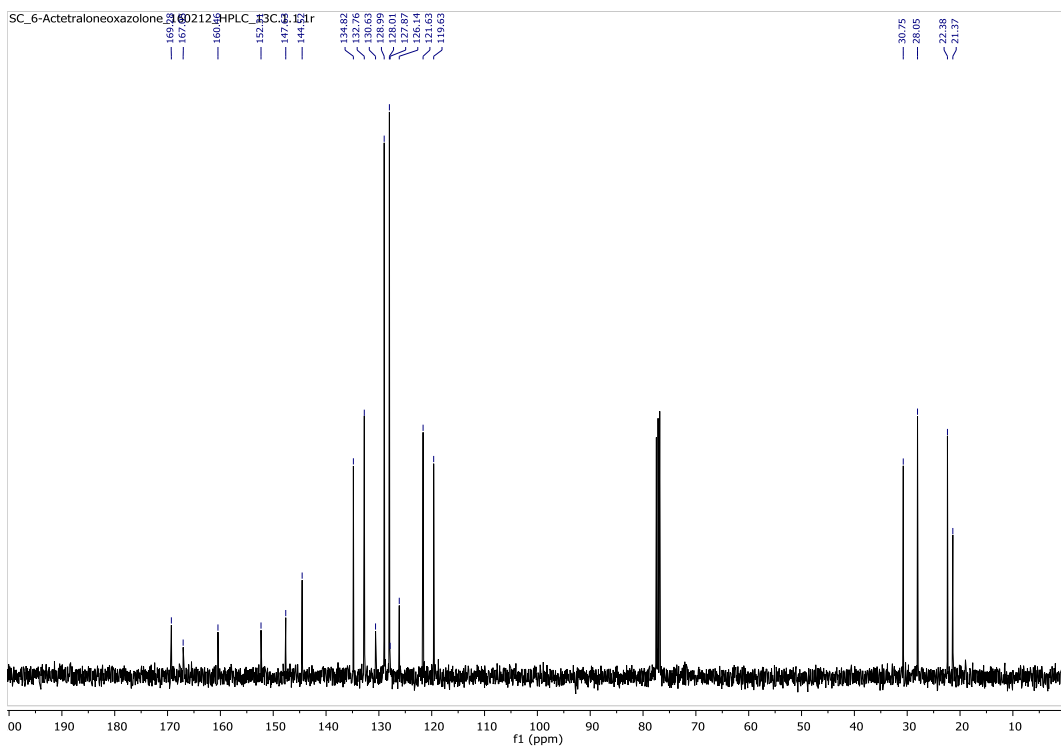
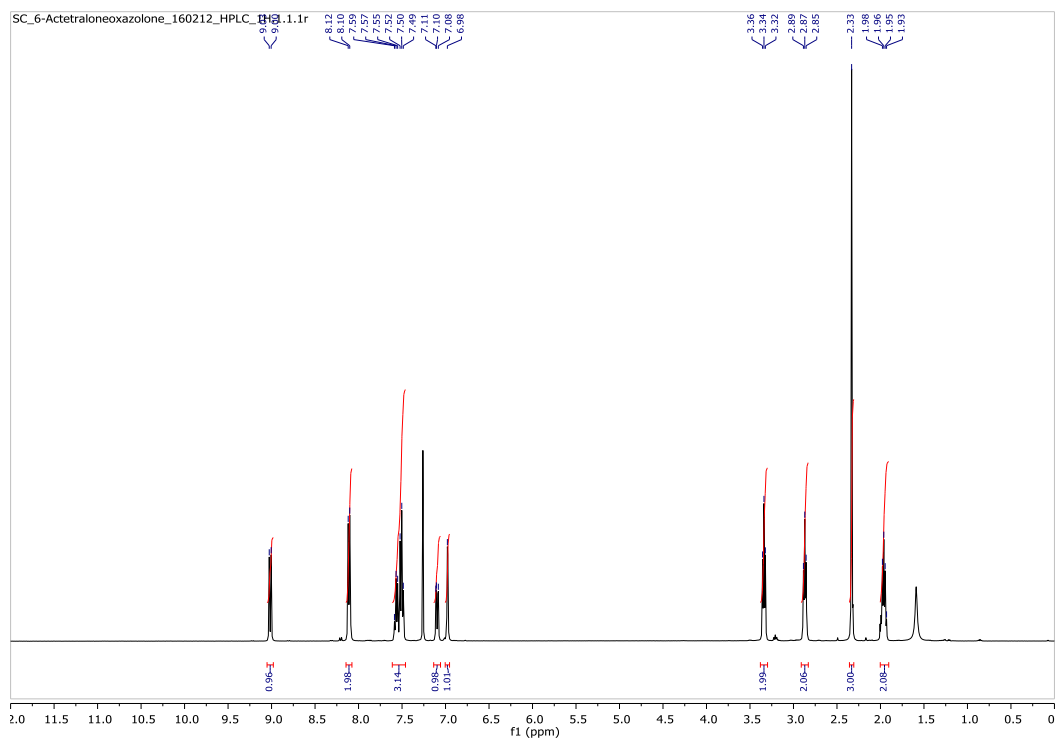
# 15N HMBC of 5c

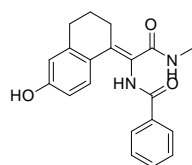




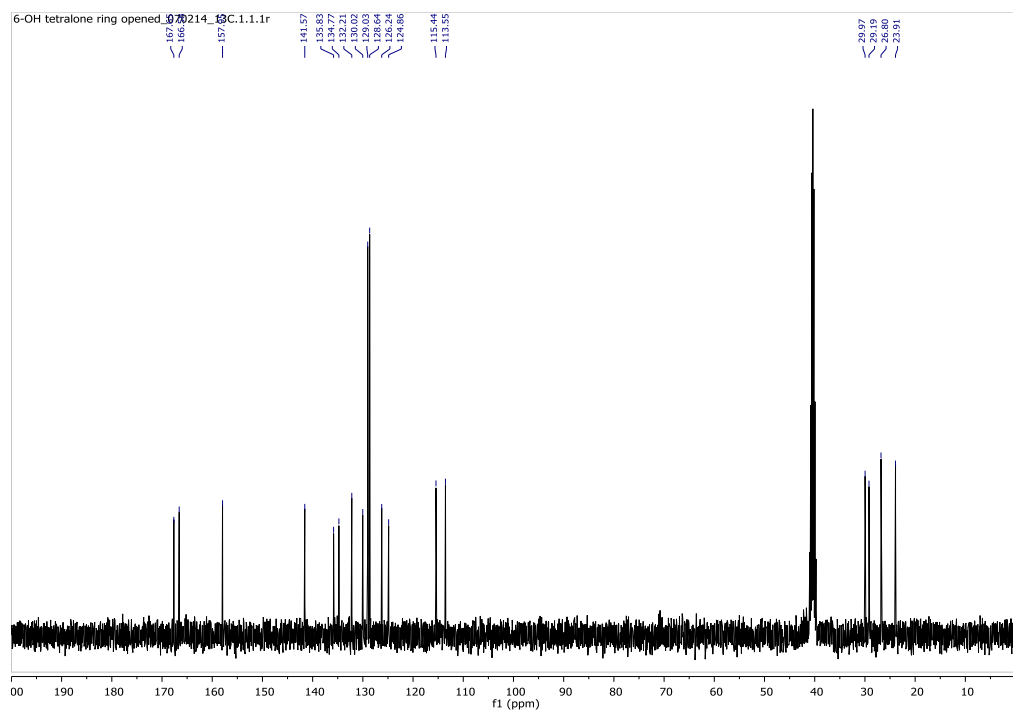
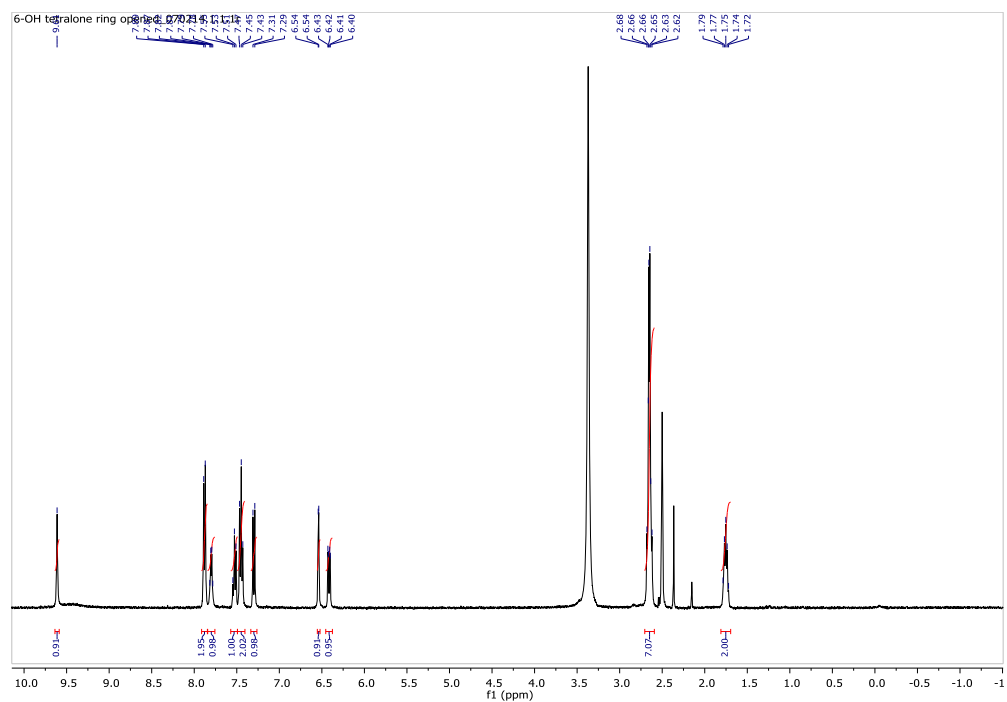


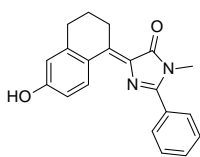
(6a)



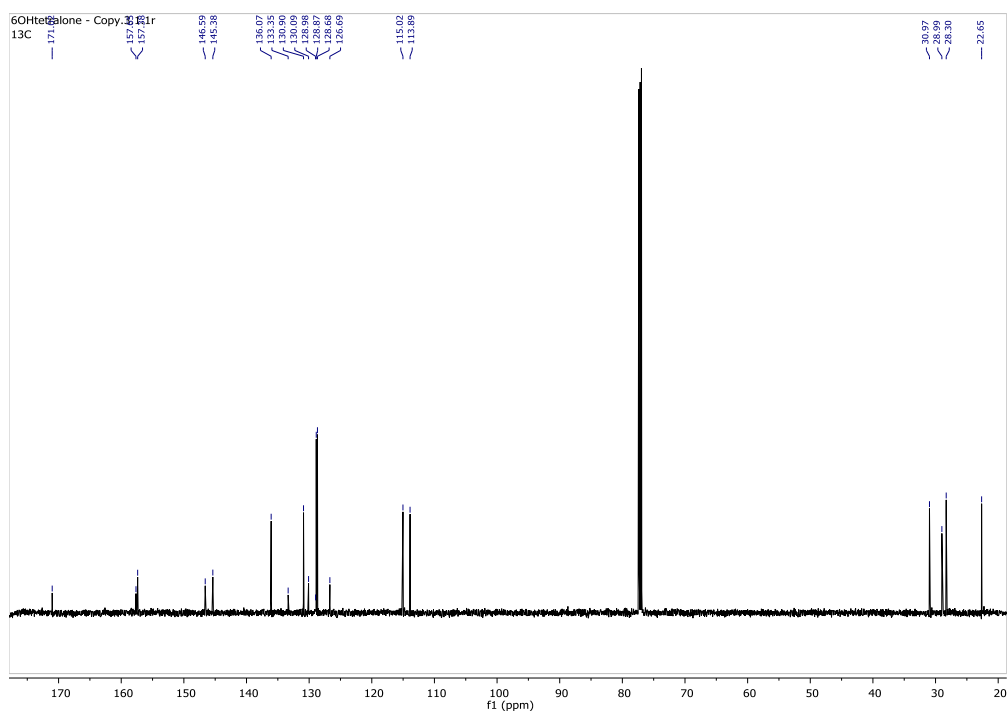
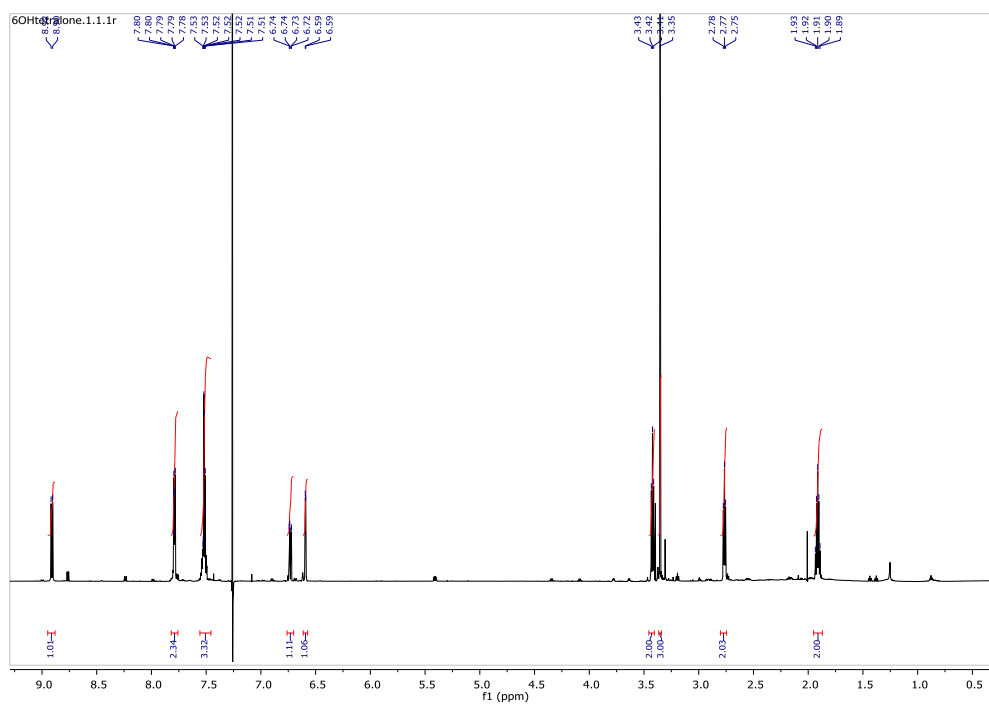


(6b)

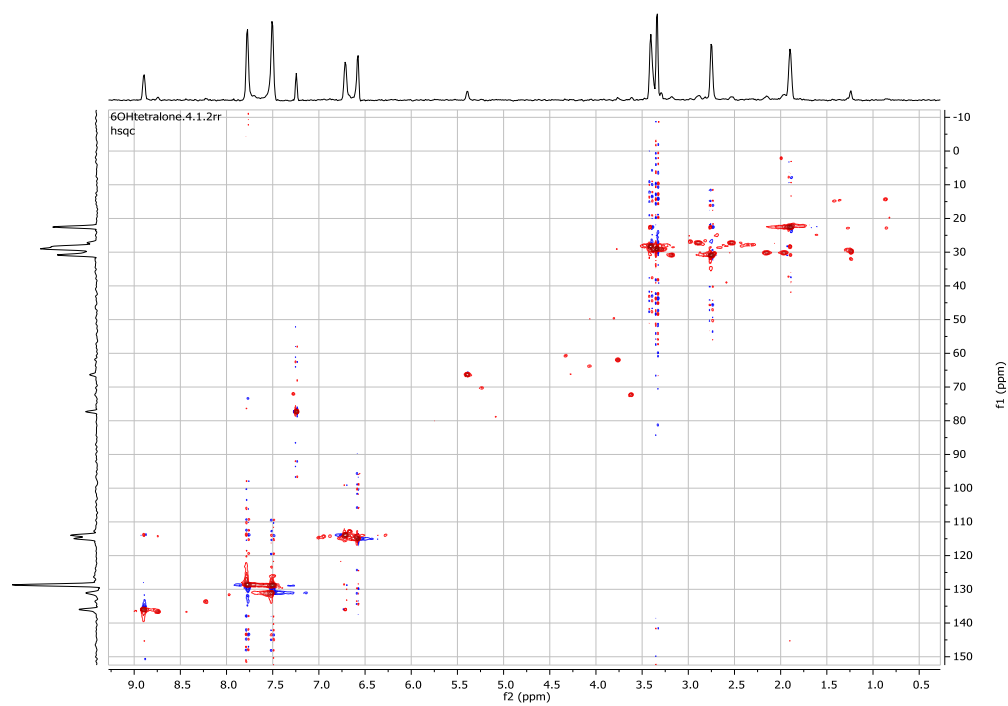




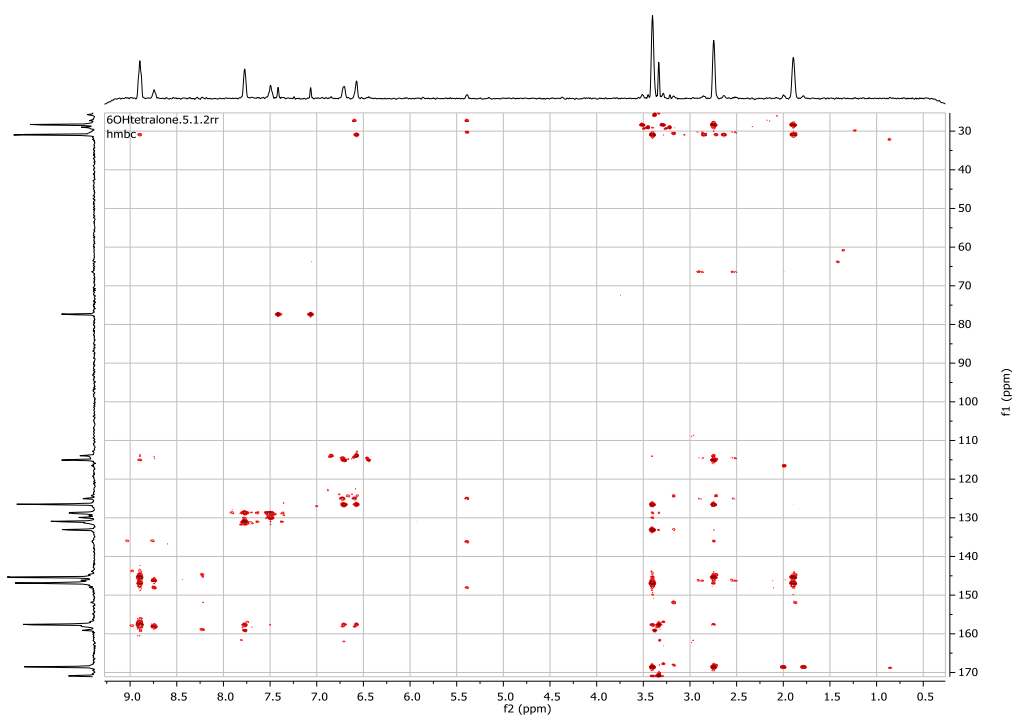
(6c)



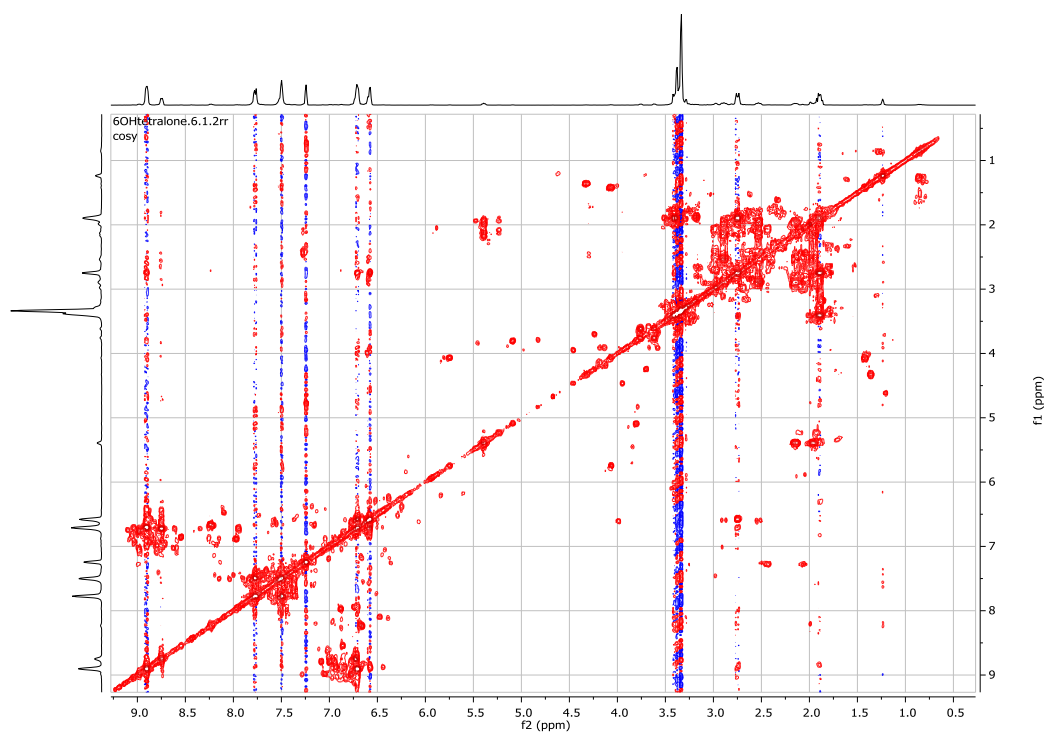
# HSQC of 6c



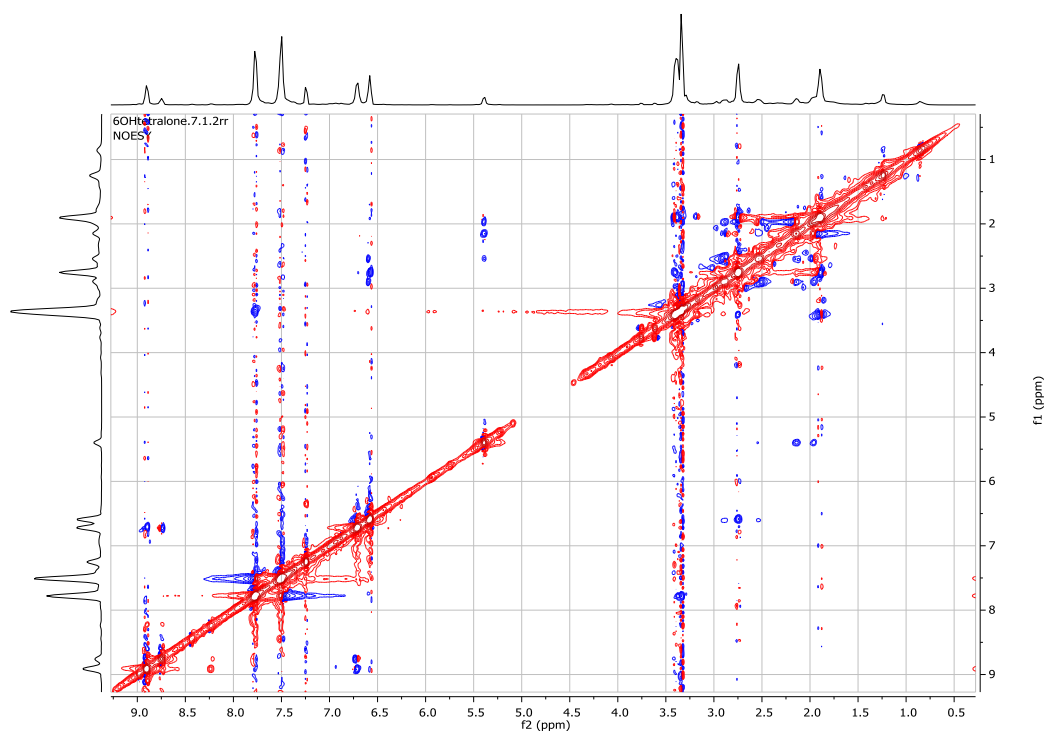
# HMBC of 6c



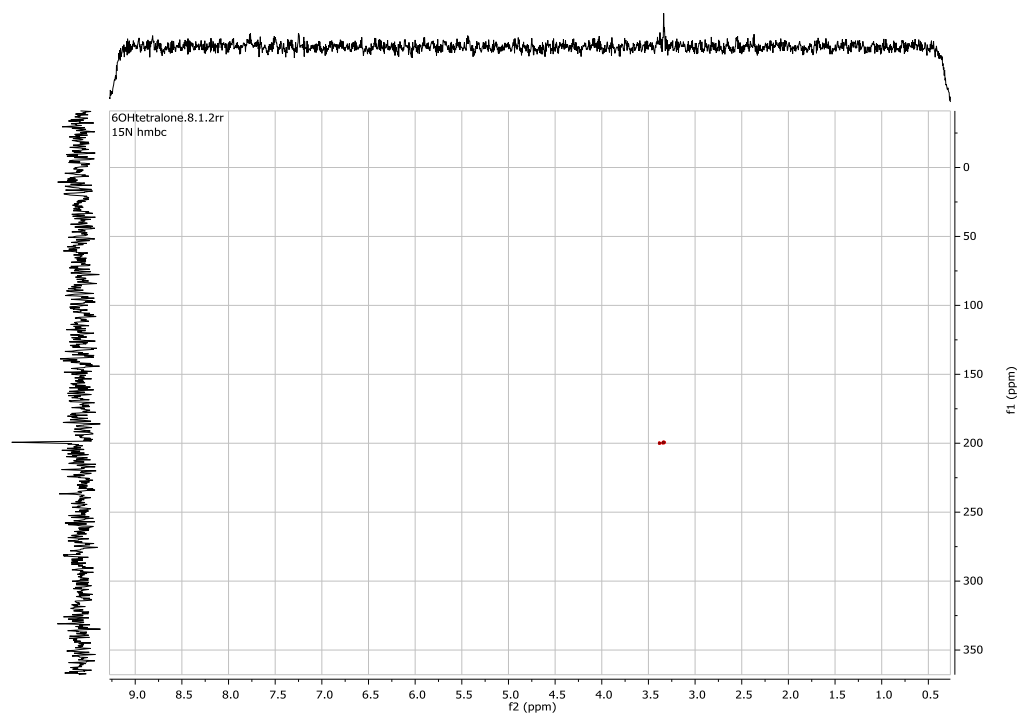
COSY of 6c

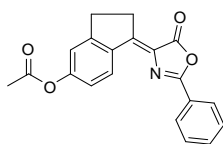


NOESY of 6c

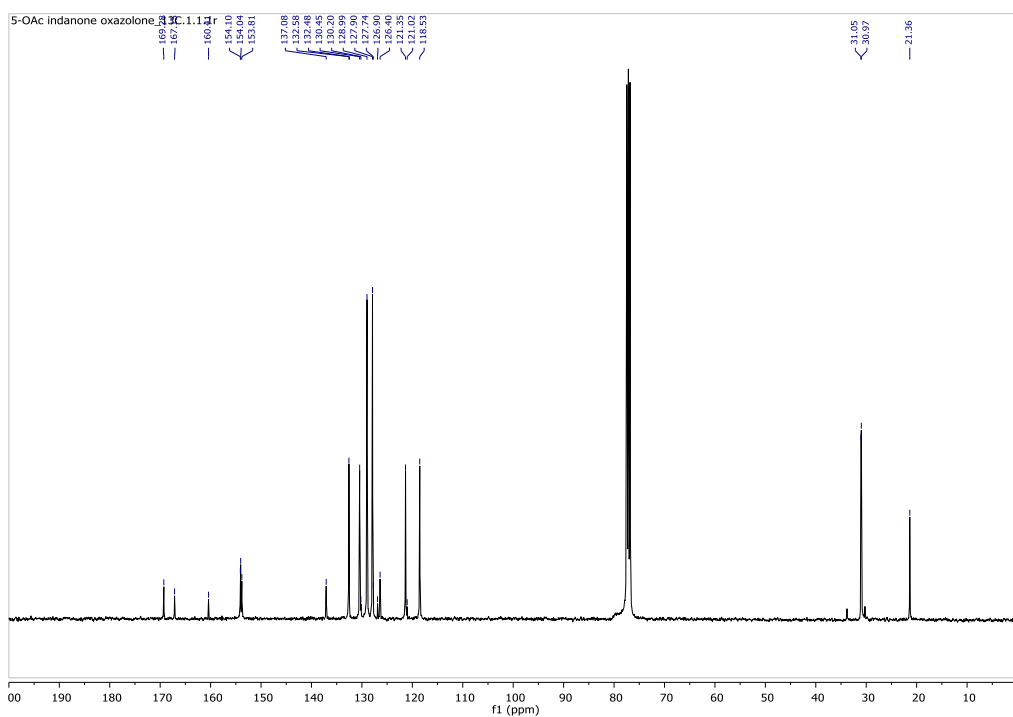
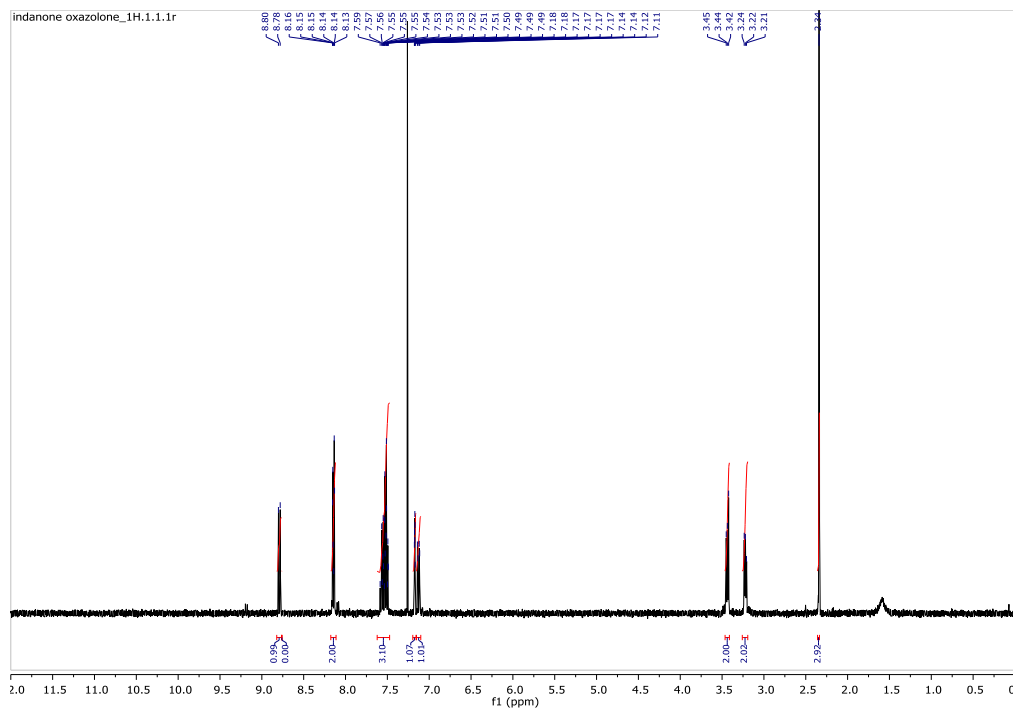


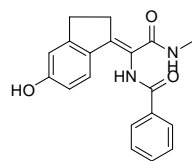
# 15N HMBC of 6c



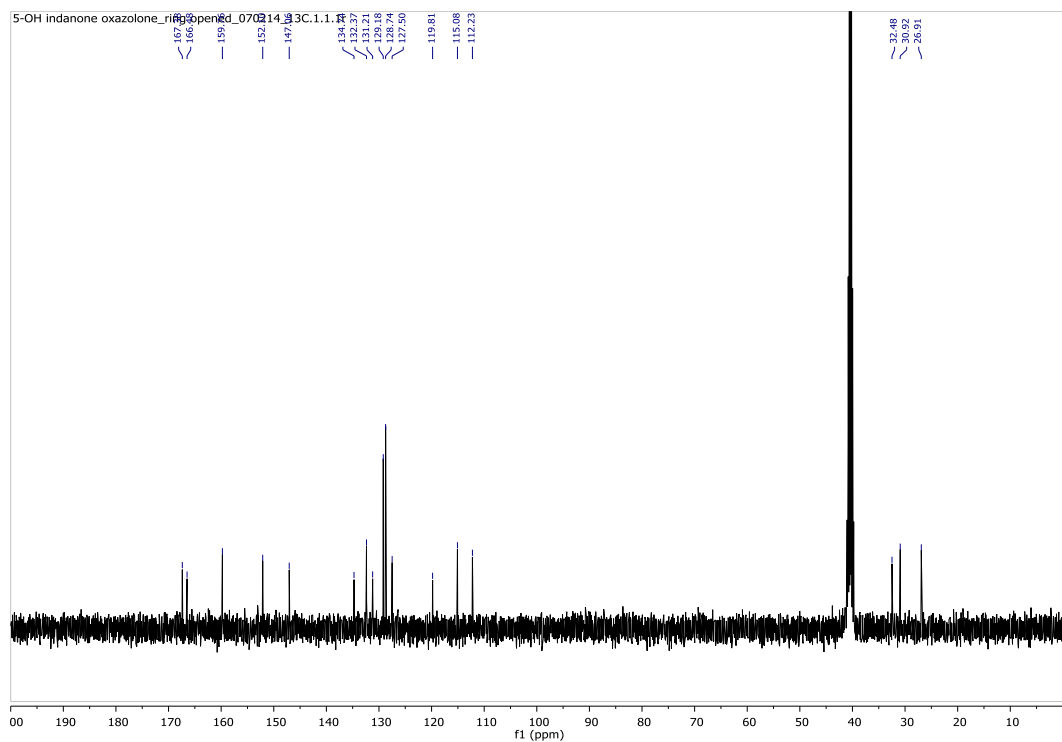
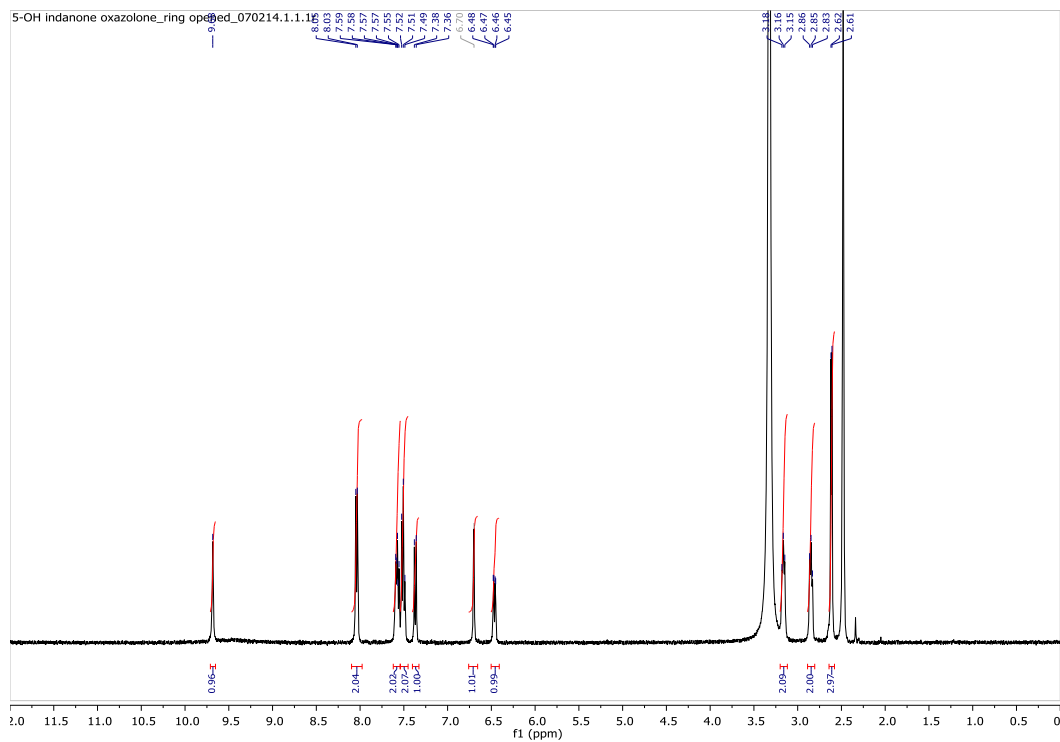


(7a)

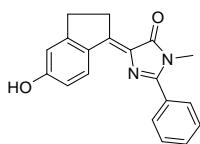




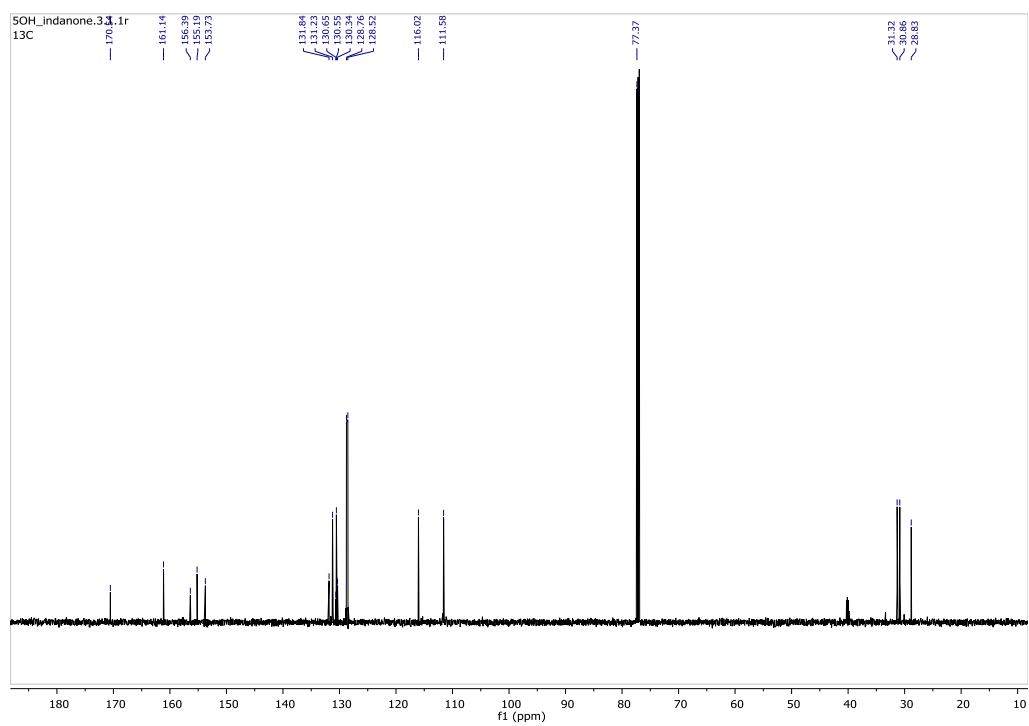
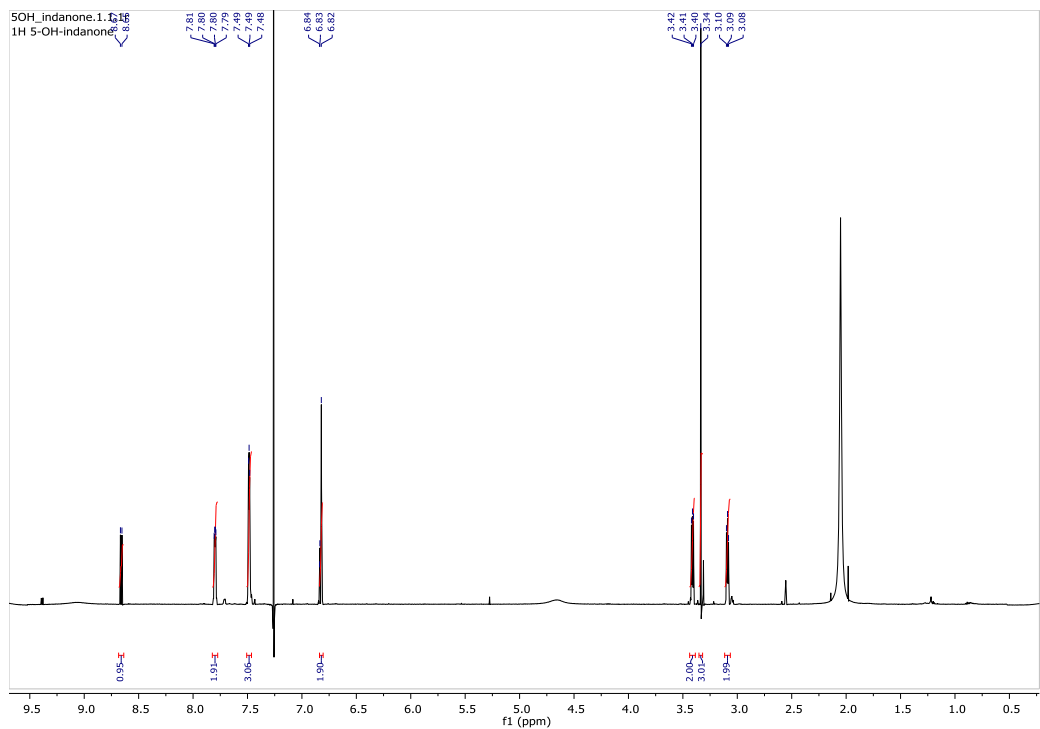
(7b)



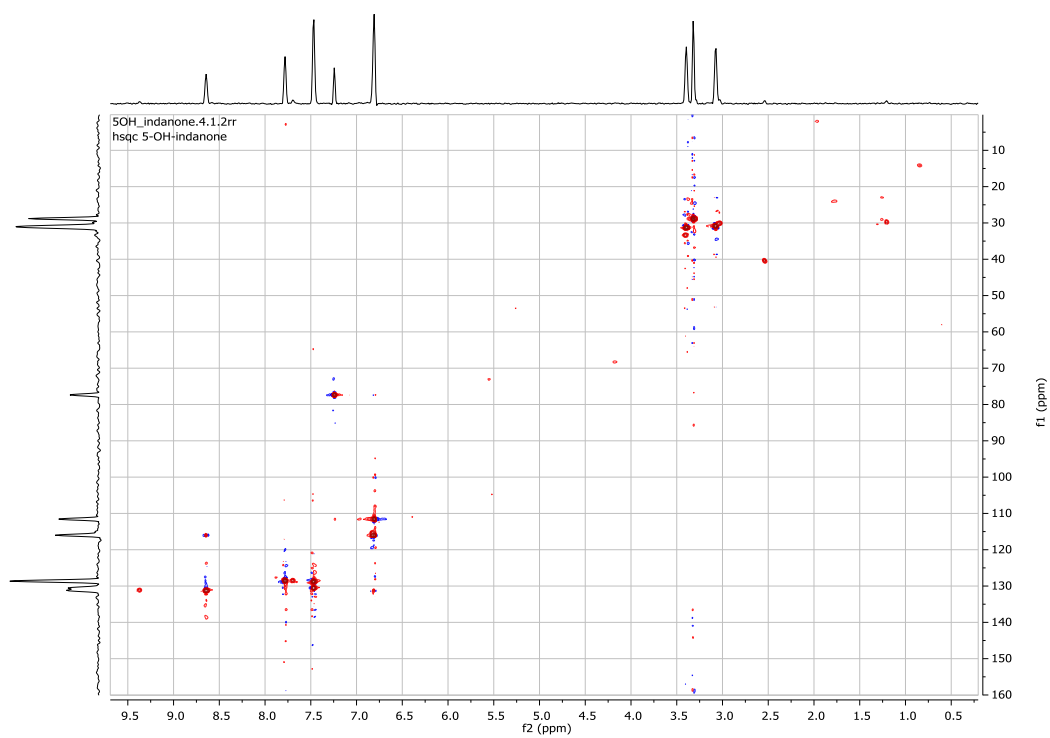




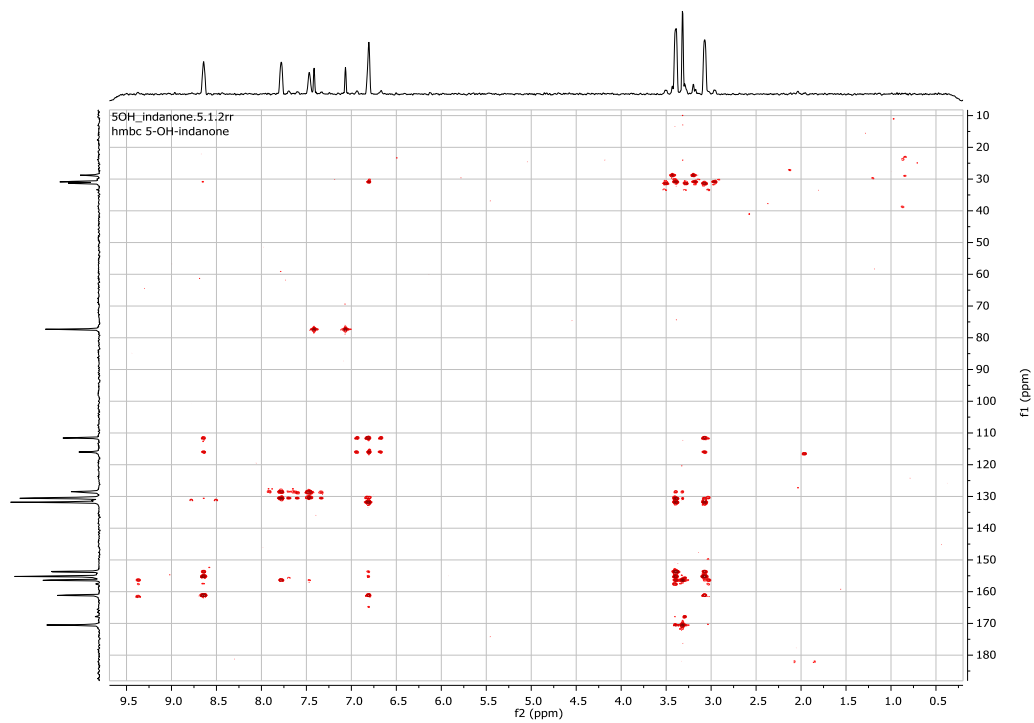
(7c)



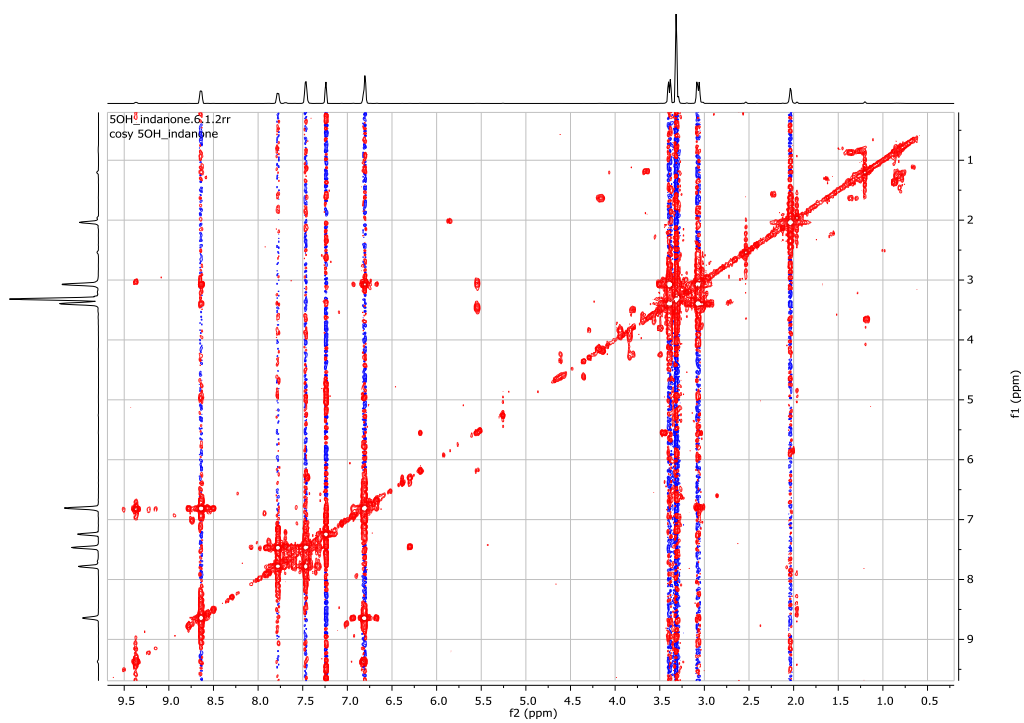
# HSQC of 7c



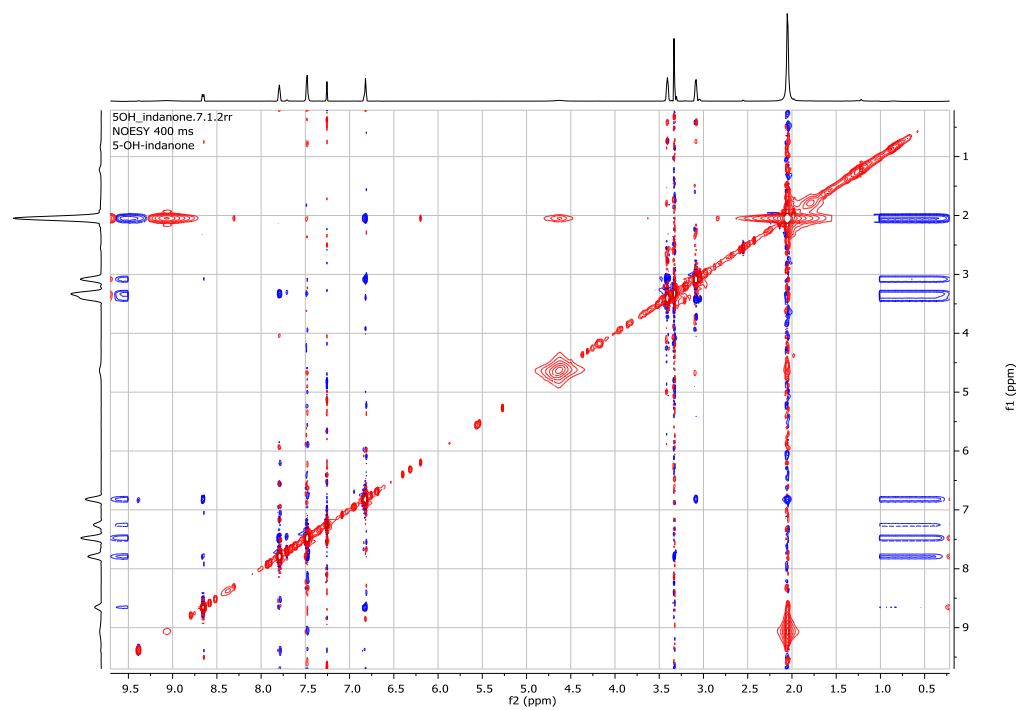
# HMBC of 7c



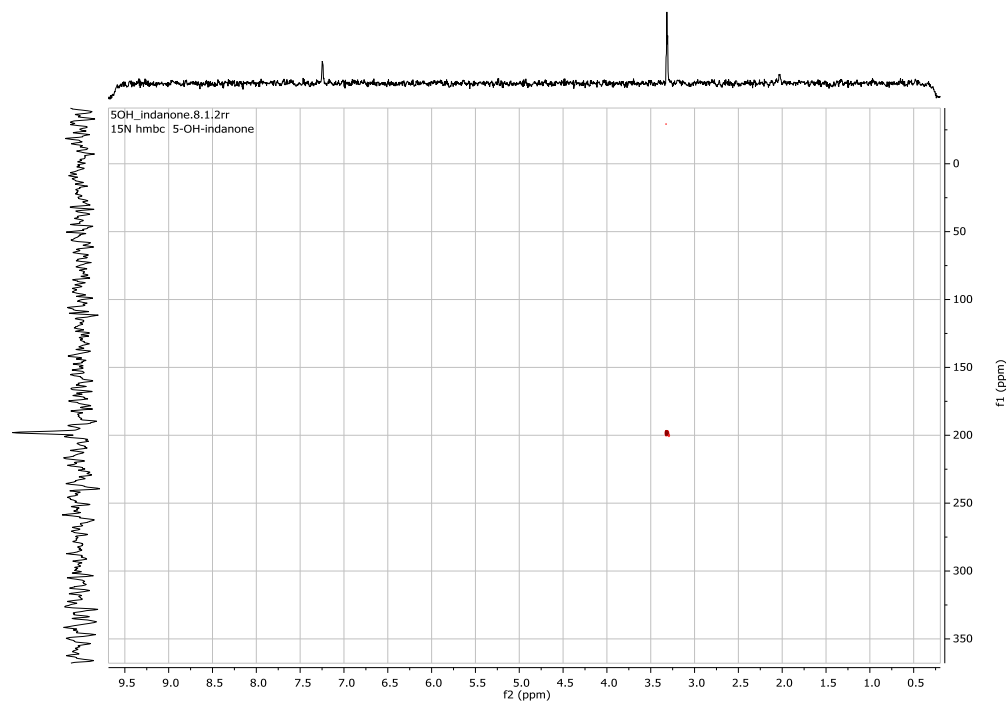
COSY of 7c

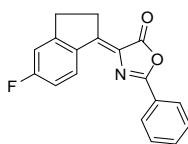


NOESY of 7c

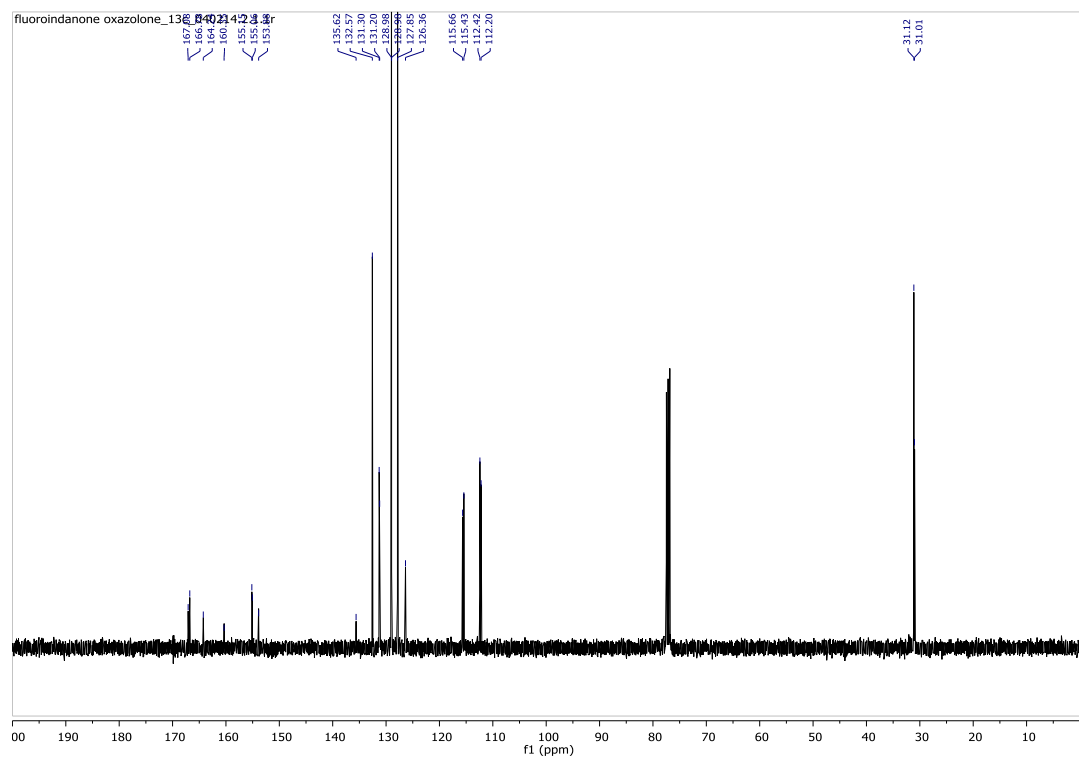
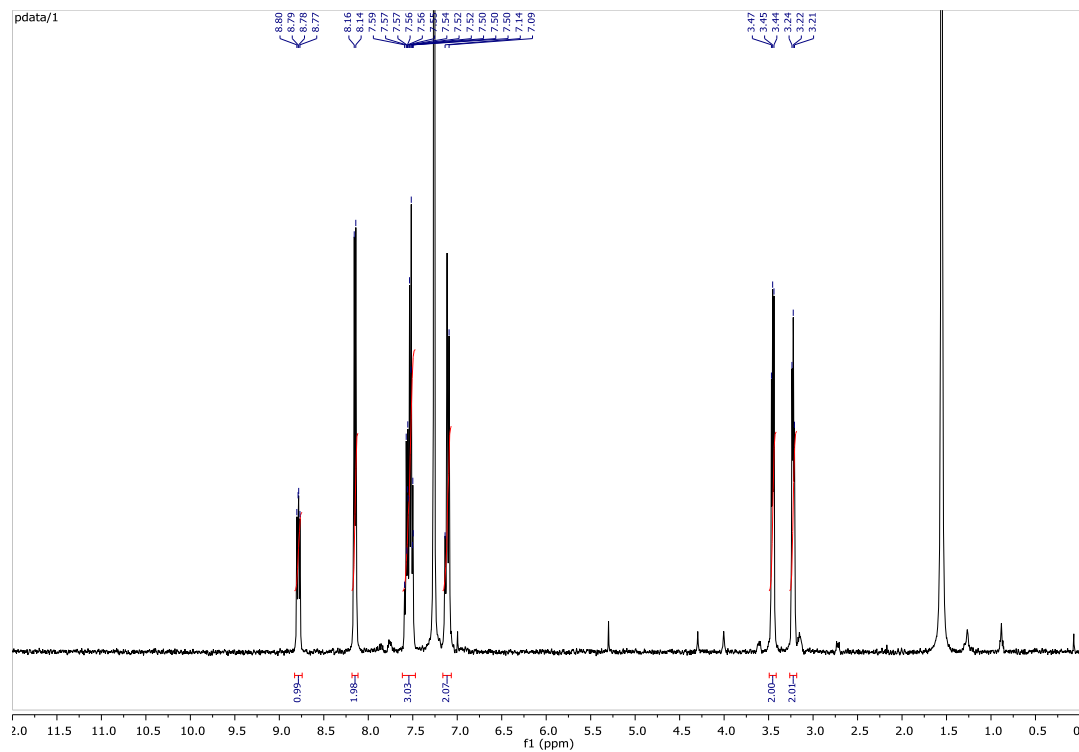


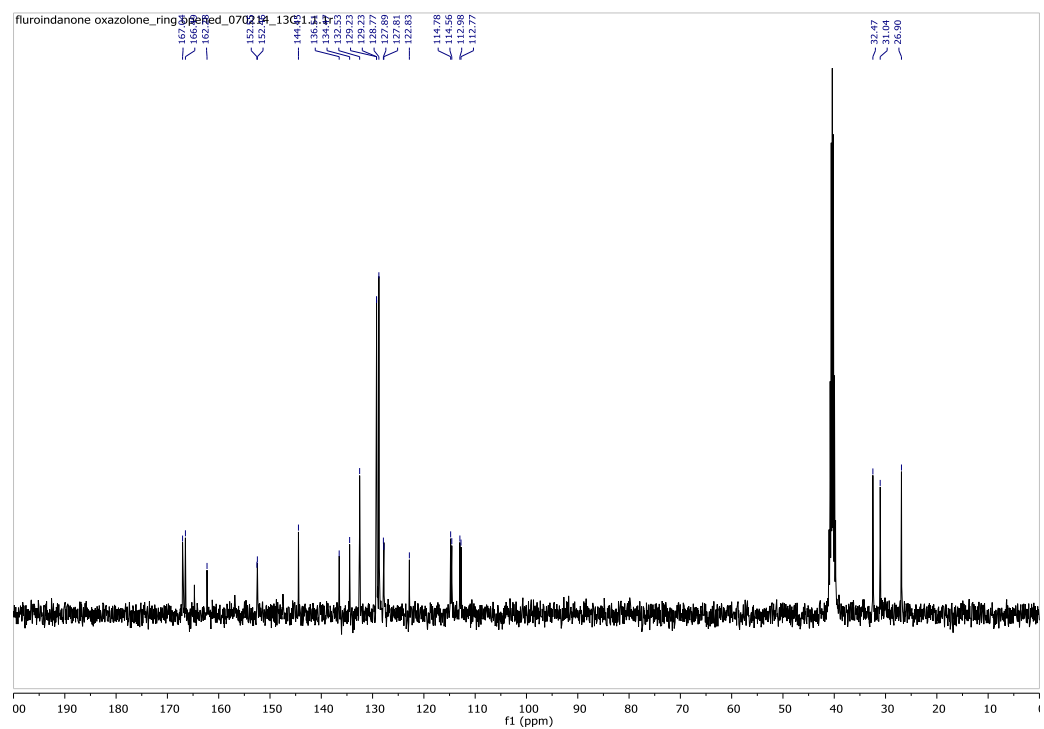
# 15N HMBC of 7c

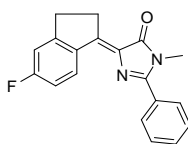




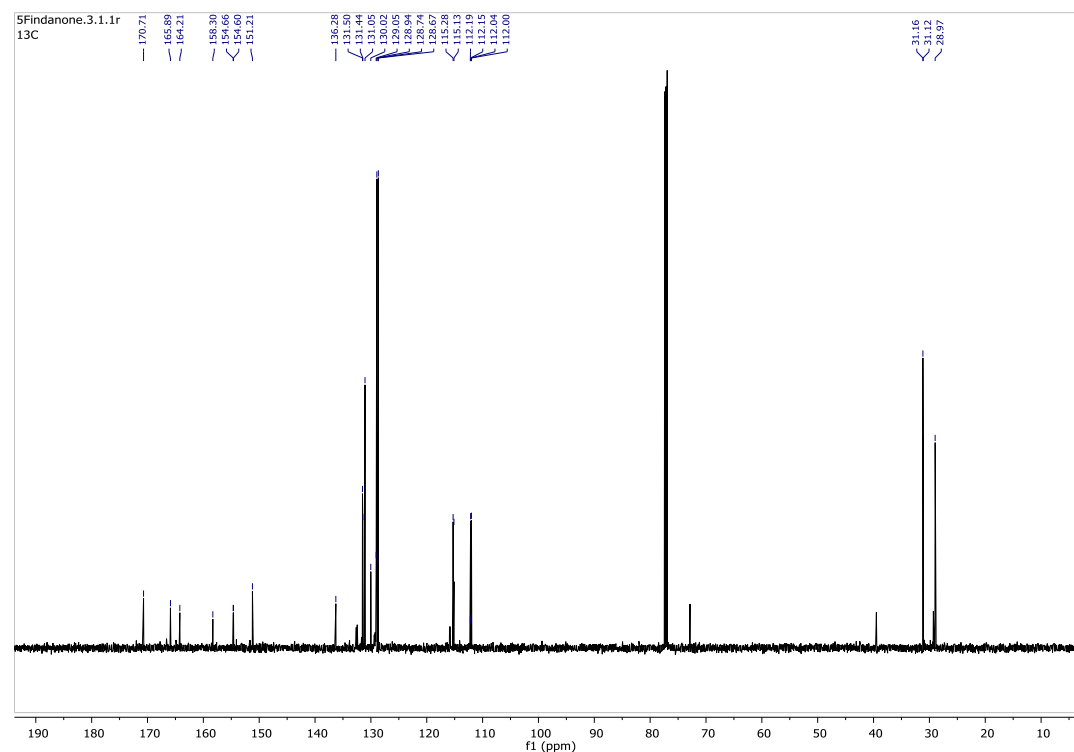
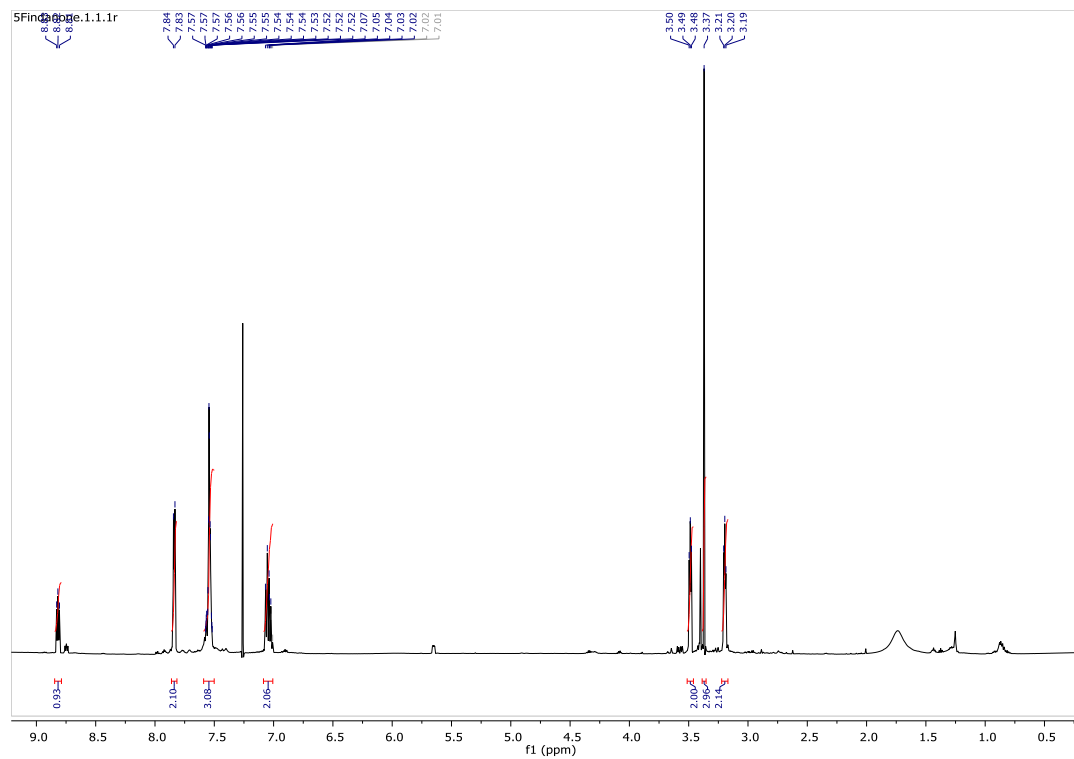
(8a)



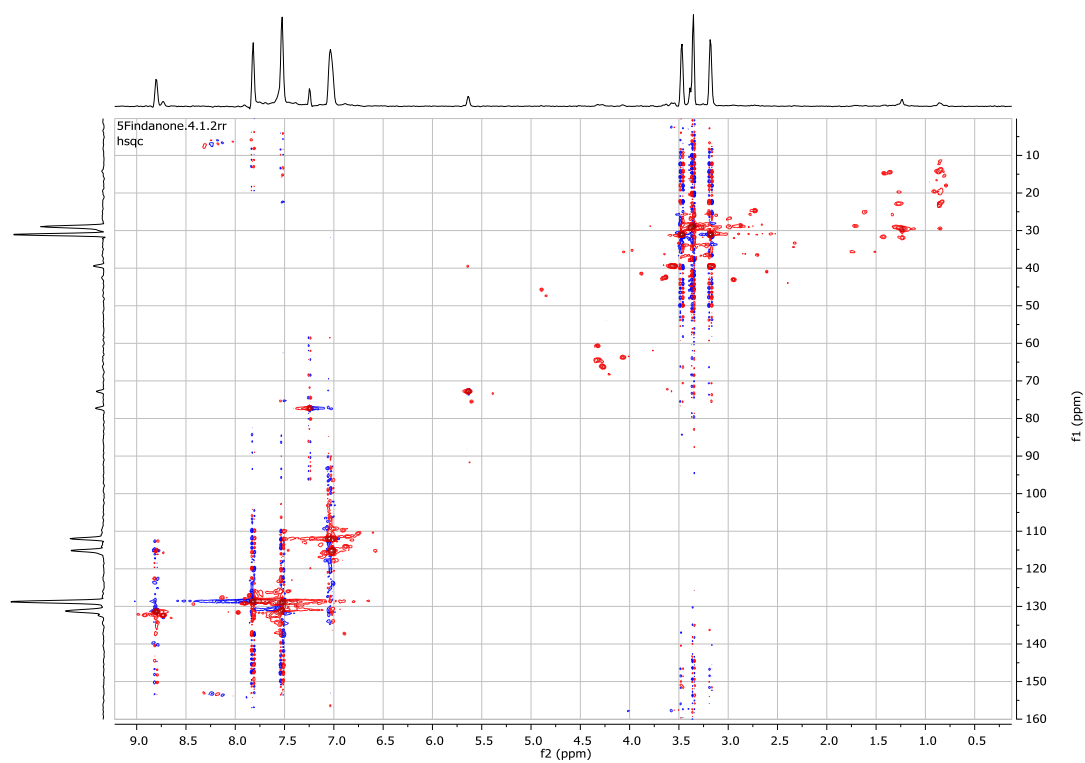




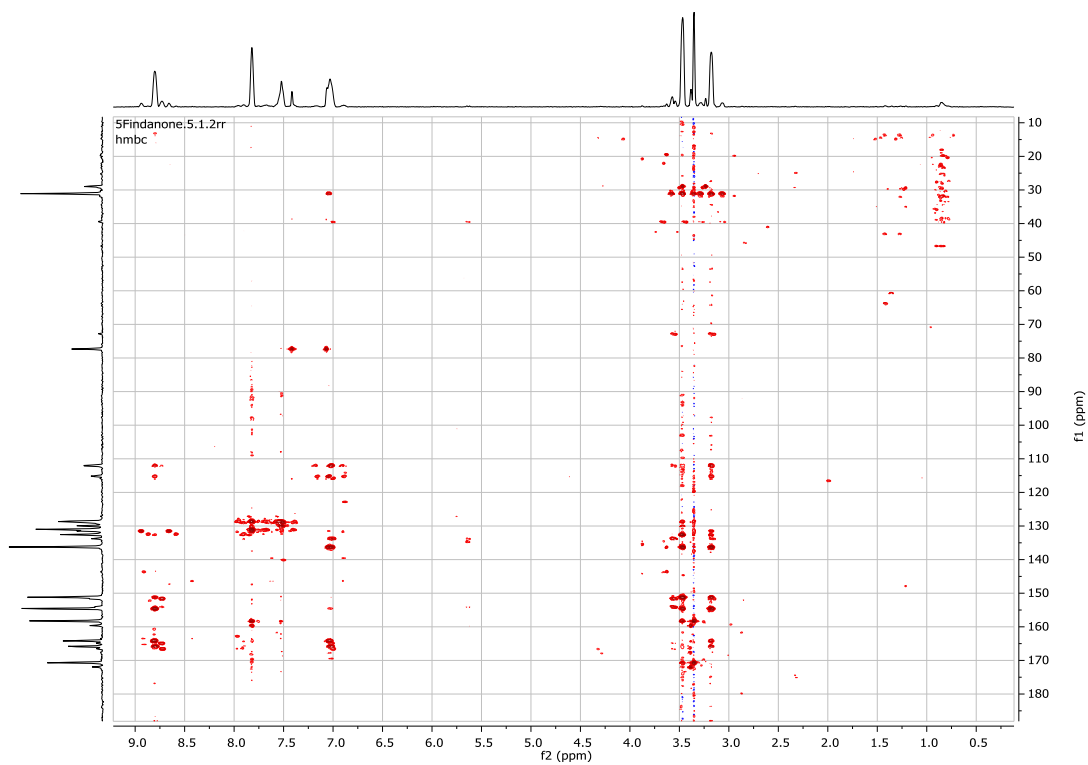
(8c)



# HSQC of 8c

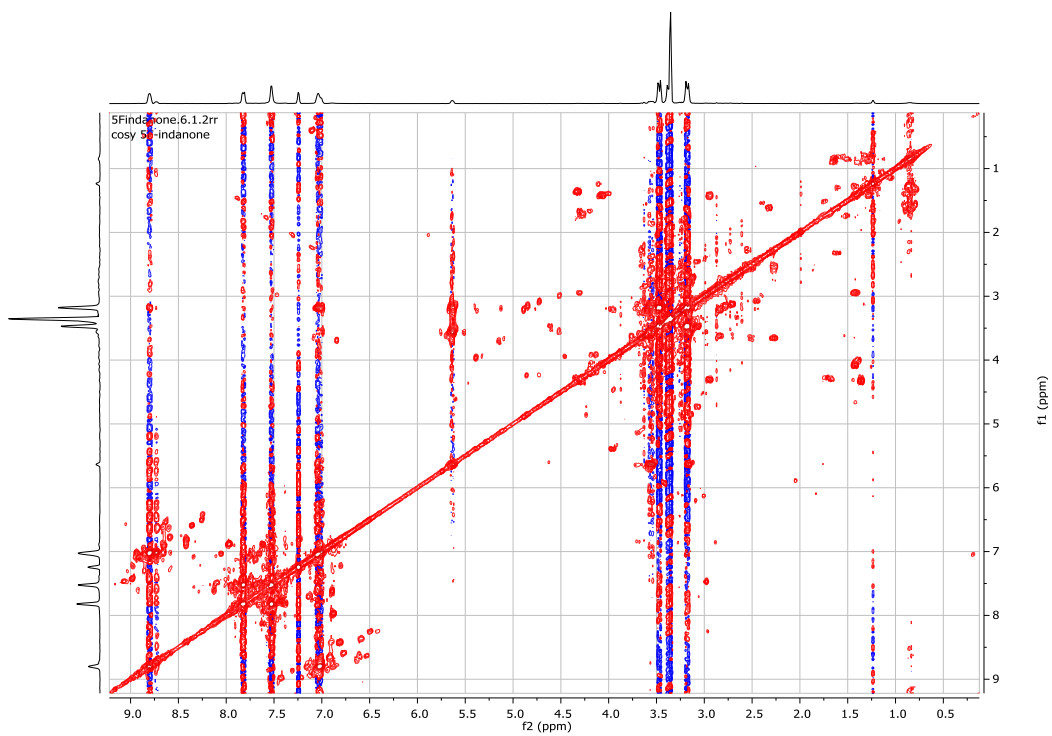


# HMBC of 8c

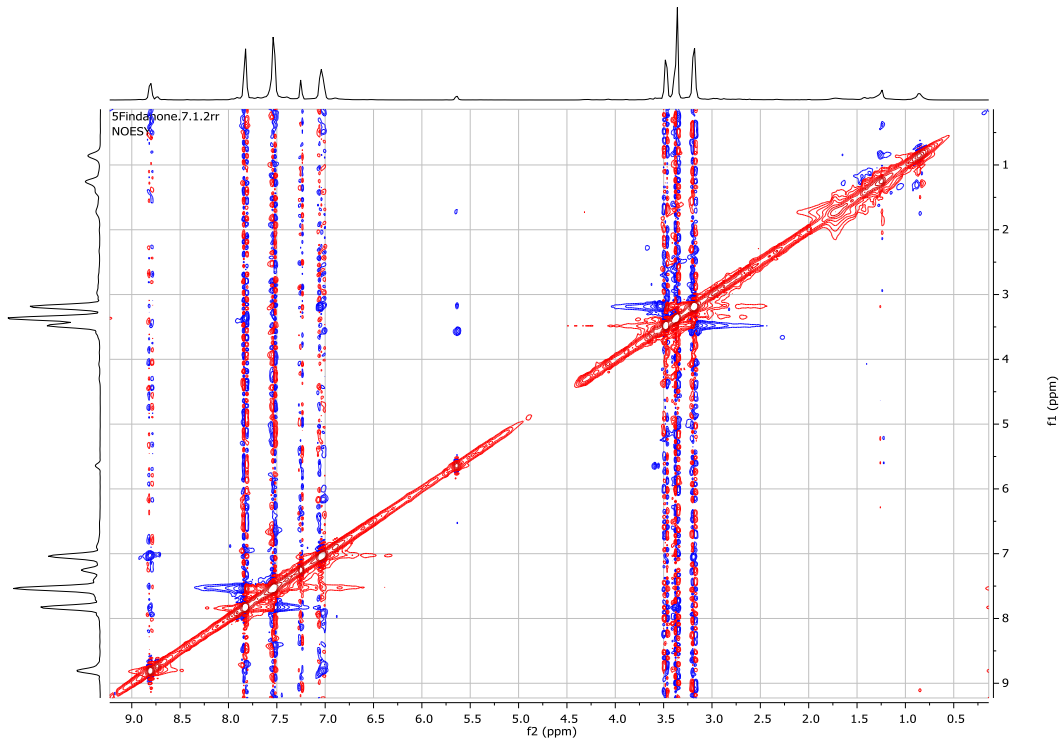




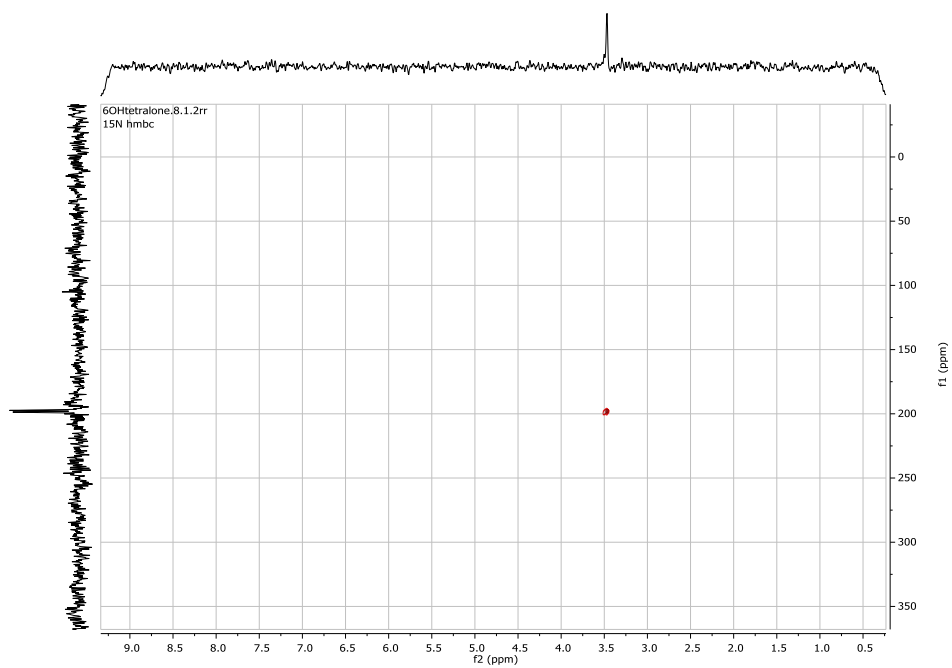
COSY of 8c



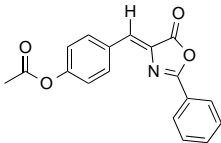
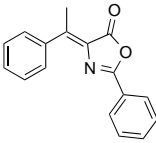
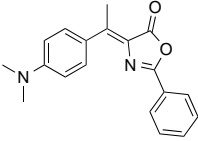
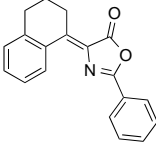
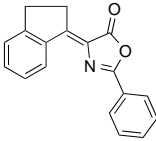
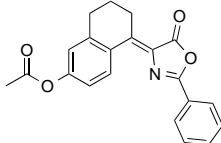
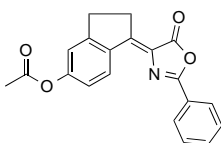
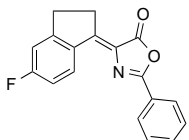
NOESY of 8c



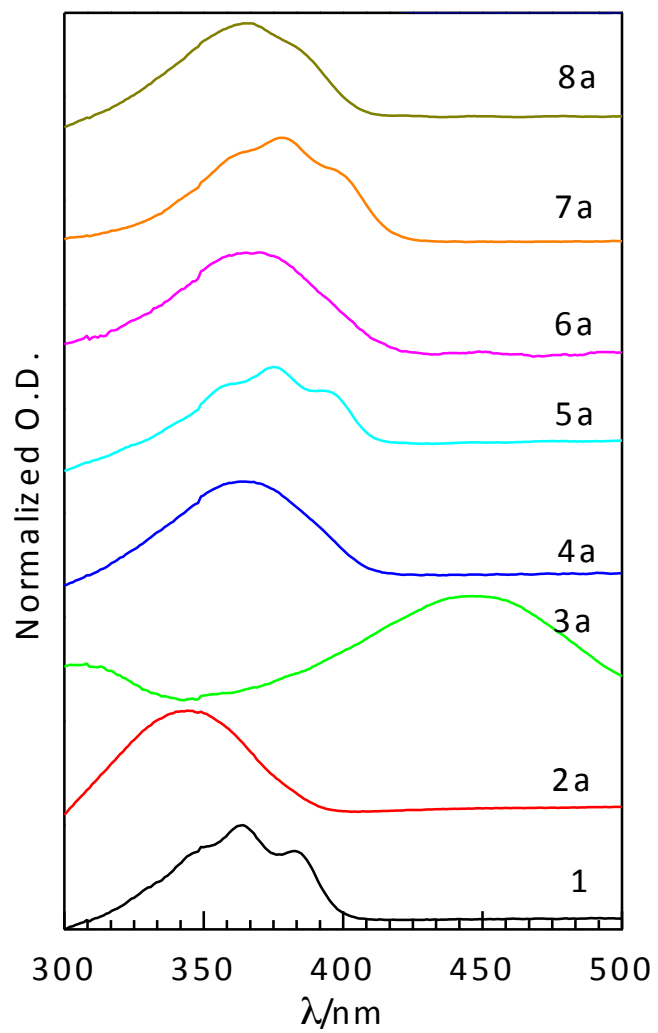
# 15N HMBC of 8c



**Table S1.** Condensation of arylketones with phenyloxazolone

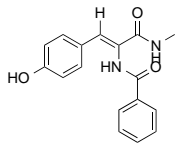
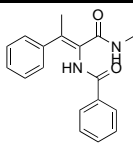
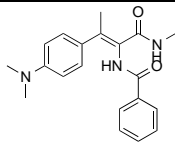
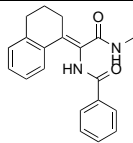
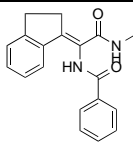
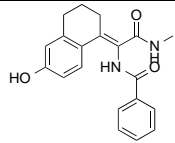
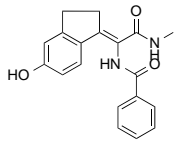
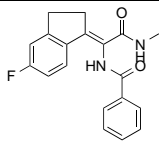
Entry	Product	<i>t</i> (hr)	Yield (%)
1a*			
2a		5	35
3a		5	40
4a		5	35
5a		5	42
6a		5	40
7a		5	40
8a		5	37

\* Prepared via Erlenmeyer azlactone process



**Figure S1.** Normalized absorption spectra of oxazolones in acetonitrile.

**Table S2.** Nucleophilic ring opening of oxazolinones

Entry	Product	<i>t</i> (min)	Yield (%)
1b		60	100
2b		15	98
3b		15	100
4b		15	100
5b		15	100
6b		15	80
7b		15	80
8b		15	95

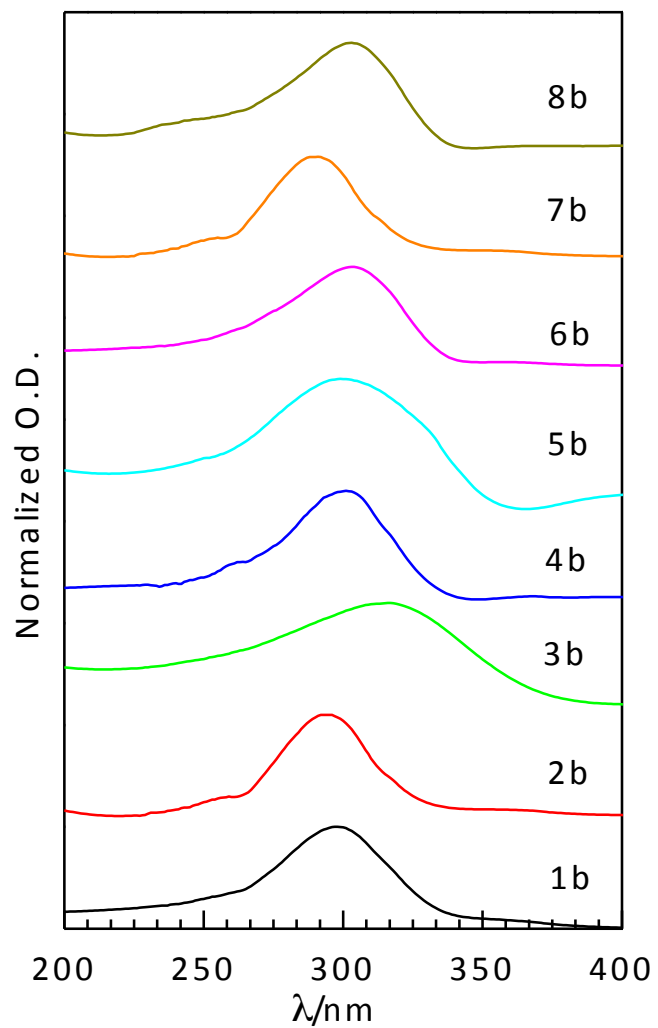


**Figure S2.** Normalized absorption spectra of ring-opened acrylamides in acetonitrile.

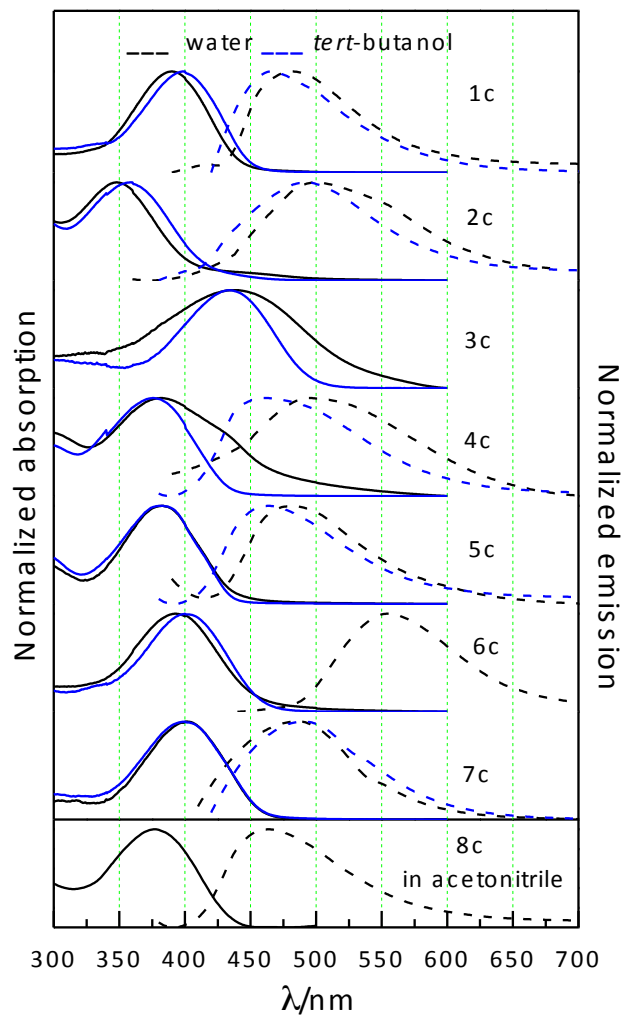


**Figure S3.** Steady state absorption and emission spectra of imidozolinone (1c-5c,7c) in water and *tert*-butanol, 6c in water and 8c in acetonitrile. 3c is non-fluorescent.

**Table S3.** Steady state absorption and emission data for imidazolinones

Entry	Solvent	$\lambda_{\text{abs}}^{\text{max}}$ (nm)	$\lambda_{\text{em}}^{\text{max}}$ (nm)	$\phi_{\text{f}}$ $\times 10^{-4}$
1c	water	390	480	1.9
	<i>tert</i> -butanol	398	470	4.2
2c (major)	water	347	496	2.2
	<i>tert</i> -butanol	357	492	1.6
3c*	water	436	-	-
	<i>tert</i> -butanol	436	-	-
4c	water	379	497	14
	<i>tert</i> -butanol	379	460	19
5c	water	381	481	30
	<i>tert</i> -butanol	381	461	25
6d	water	391	552	8.7
	<i>tert</i> -butanol	403	-	-
7d	water	400	488	6.6
	<i>tert</i> -butanol	400	489	4.4
8c	acetonitrile	377	463	-

\*Non-fluorescent



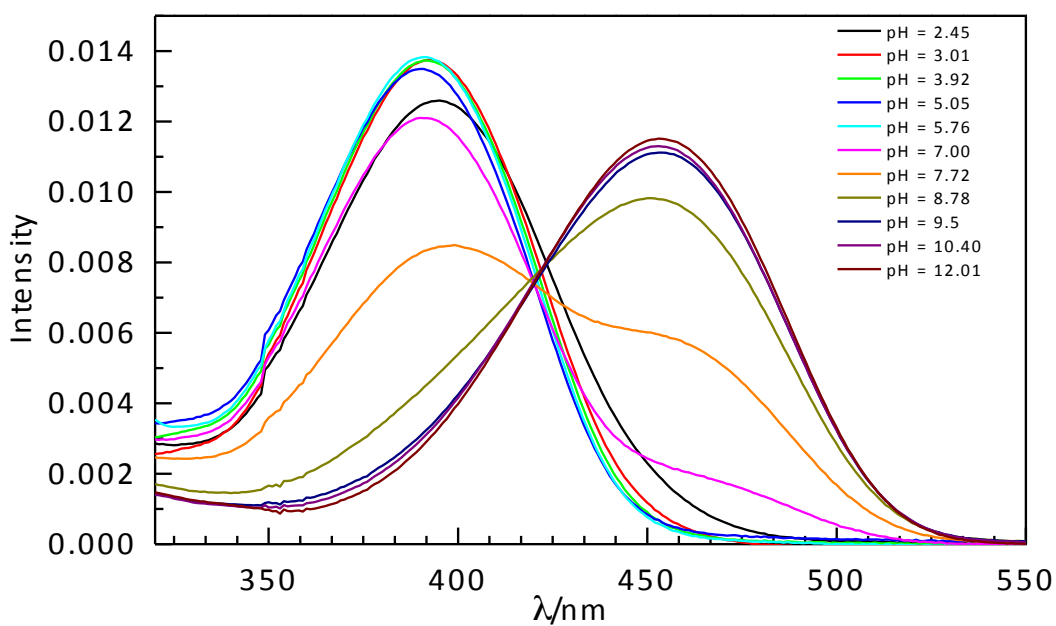


**Figure S4.** Area normalized absorption spectra of 2c with varying pH.

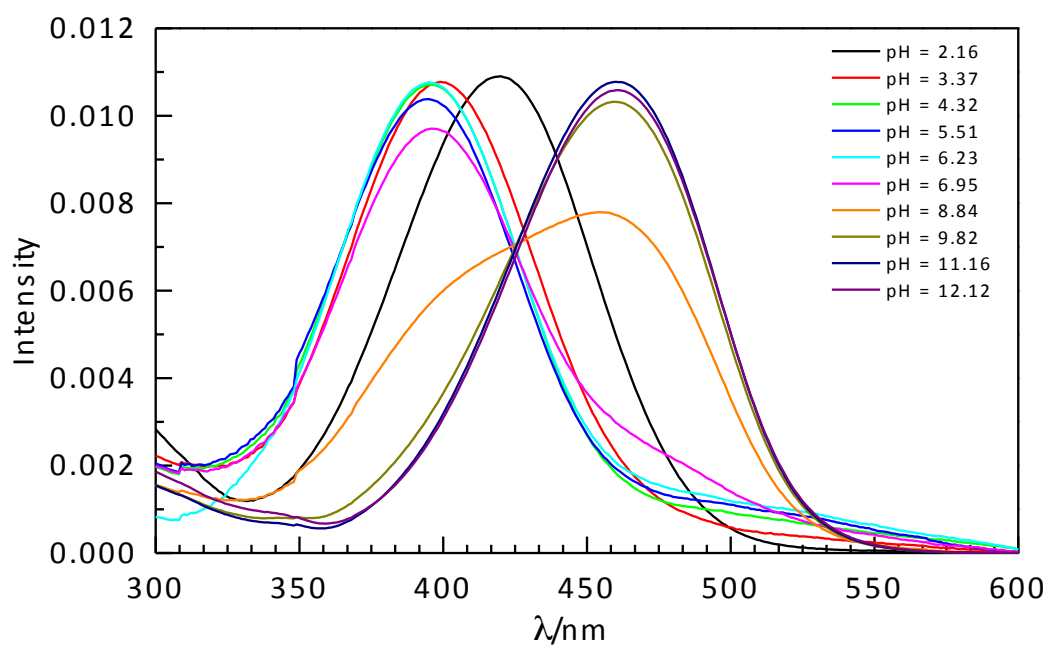


**Figure S5.** Area normalized absorption spectra of 6c with varying pH.

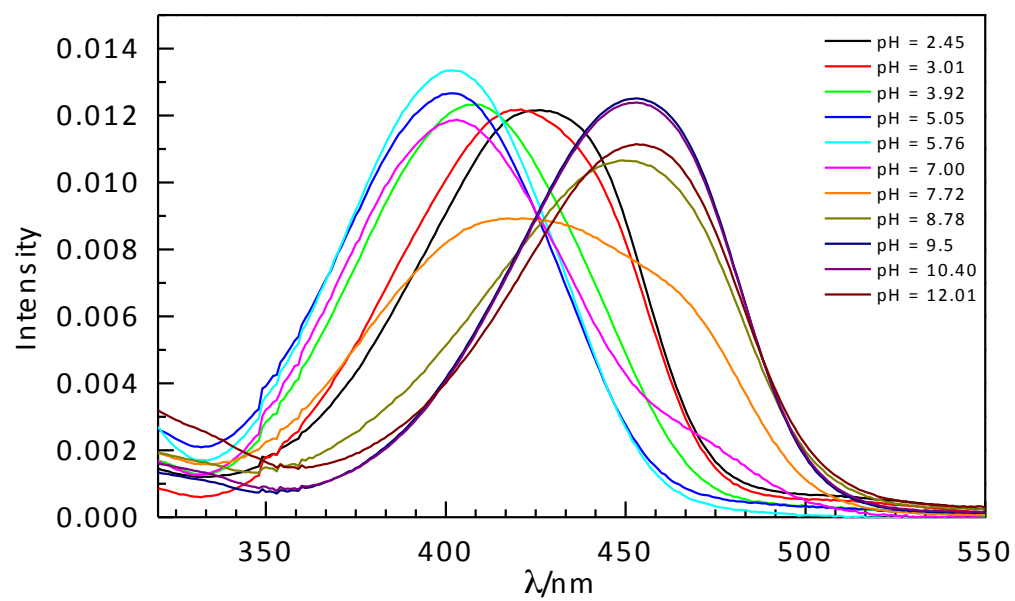


**Figure S6.** Area normalized absorption spectra of 7c with varying pH.

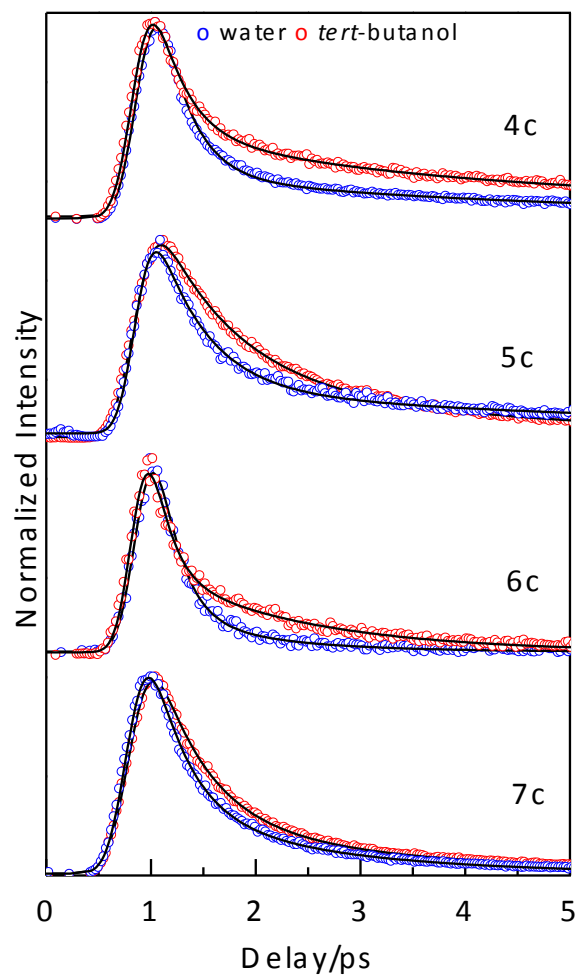


**Figure S7.** Femtosecond upconversion decay traces of locked imidazolinones (4c, 5c, 6c, 7c).

**Table S4.** Temporal parameters from upconversion decay traces of imidazolinones

Compound	Solvent	$\tau_1$	$a_1$	$\tau_2$	$a_2$	$\tau_3$	$a_3$
4c	H <sub>2</sub> O	0.30	0.90	3.60	0.10		
	<sup>t</sup> BuOH	0.30	0.70	2.30	0.20	15	0.10
5c	H <sub>2</sub> O	0.50	0.85	5.00	0.15		
	<sup>t</sup> BuOH	0.70	0.75	3.00	0.25		
6c	H <sub>2</sub> O	0.20	0.90	1.00	0.10		
	<sup>t</sup> BuOH	0.20	0.75	1.5	0.25		
7c	H <sub>2</sub> O	0.35	0.80	1.60	0.20		
	<sup>t</sup> BuOH	0.50	0.80	2.10	0.20		

## References

- (1) Adhikary, R.; Barnes, C. A.; Trampel, R. L.; Wallace, S. J.; Kee, T. W.; Petrich, J. W. *J. Phys. Chem. B* **2011**, *115*, 10707.
- (2) Lakowicz, J. R. *Principles of Fluorescence Spectroscopy*; 3rd ed.; Springer, USA, 2006.
- (3) Eaton, D. F. *Pure Appl. Chem.* **1988**, *60*.
- (4) Burai, T. N.; Mukherjee, T. K.; Lahiri, P.; Panda, D.; Datta, A. *J. Chem. Phys.* **2009**, *131*, 034504.
- (5) Cook, A. H.; Harris, G.; Sir Heilbron, I. *J. Chem. Soc.* **1948**, 1060.
- (6) Conway, P. A.; Devine, K.; Paradisi, F. *Tetrahedron* **2009**, *65*, 2935.
- (7) Alías, M.; López, M. P.; Cativiela, C. *Tetrahedron* **2004**, *60*, 885.
- (8) Cativiela, C.; Diaz De Villegas, M. D.; Meléndez, E. *J. Heterocycl. Chem.* **1985**, *22*, 1655.
- (9) Knowles, A. M.; Lawson, A.; Boyd, G. V.; Newberry, R. A. *J. Chem. Soc. C: Organic* **1971**, 598.
- (10) Rioz-Martínez, A.; de Gonzalo, G.; Vicente, G. *Synthesis* **2010**, *1*, 110.

# Room Temperature Dual Fluorescence of a Locked GFP Chromophore

Soumit Chatterjee,<sup>†</sup> Anindya Datta<sup>\*,‡</sup> and Peter Karuso<sup>\*,†</sup>

<sup>†</sup> Department of Chemistry and Biomolecular Sciences, Macquarie University, Sydney, NSW 2109, Australia

<sup>‡</sup> Department of Chemistry, Indian Institute of Technology Bombay, Powai, Mumbai 400076, India

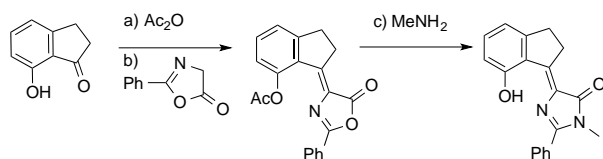
## Supporting Information Placeholder

**ABSTRACT:** A structurally a locked GFP analogue with a phenyl group at C(1) of the imidazolone has been synthesized. Rotation around the exocyclic bonds is hindered in this molecule, resulting in room temperature fluorescence. Unlike the methyl-substituted analogue, this compound exhibits dual emission at room temperature at 455 and 610 nm in water. The quantum yield (6% in water) is 500 times greater than that of the unlocked analogues, but less than that of the methyl derivatives reported recently (18% in toluene). This reveals, for the first time, the electronic effect of the phenyl at C(1) and proves that ESIPT is disrupted by the presence of a phenyl group. The lower quantum yield can be rationalized by the formation of a new emission band, which arises from cis-trans isomerization of the excited state. Interestingly, the fluorescence quantum yield is maximum in aqueous solutions and less in toluene, which is exactly opposite of the trends observed in the methylated analogue. This observation is rationalized by the involvement of hydrogen bonded water bridges for the present compound, in the ESIPT process.

Green fluorescence protein (GFP) is widely used in molecular biology and biotechnology as a genetically encoded fluorescent tag.<sup>1-7</sup> Its strong green fluorescence ( $\phi_f = 0.8$ ) is ascribed to its chromophore 4-(4-hydroxybenzylidene)-1,2-dimethyl-1*H*-imidazol-5(4*H*)-one (*p*-HBDI, Scheme S1), which is anchored by covalent and hydrogen bonds inside the  $\beta$ -barrel structure of the protein.<sup>8</sup> The photophysics of this chromophore involves the excited state proton transfer (ESPT) to the E222 residue, through the proton relay of water molecules. The resulting anionic excited state of *p*-HBDI is believed to be responsible for the intense green fluorescence.<sup>9-11</sup> Surprisingly, the isolated chromophore is es-

entially non-fluorescent at room temperature.<sup>12,13</sup> This has been attributed to the photoisomerization at the exocyclic C=C bond (Scheme S1), resulting an internal conversion to the ground state within 1 ps and no fluorescence.<sup>14-24</sup> The field of photophysics of the GFP chromophore, in spite of being well traversed, continues to be an area of intense research and conflicting theories, with the aim of producing small molecule fluorophores based on the GFP chromophore. This is important as the GFP chromophore is small and with the correct design elements will find application in protein labeling and super high resolution microscopy. Very recently, a different approach towards synthesizing a series of structurally locked GFP core chromophores has been developed by Chou and coworkers.<sup>25</sup> In this approach, a five membered ring stops the rotation of the C(4)-C(5) bond (Scheme S1). Additionally, a seven membered hydrogen bonded ring allows ESIPT. Together, these modifications result in a dramatic enhancement of fluorescence of *o*-LHBDI (ortho locked HBDI, Scheme S1) at room temperature ( $\phi_f = 0.18$  in toluene), opening up tremendous prospects in biotechnology and in the field of devices like OLED (organic light emitting diodes), due to an amplified spontaneous emission. The emission peak was observed at  $\sim 600$  nm and was ascribed to be originating from the tautomer formed via ESIPT.<sup>25</sup>

In this manuscript, we report the photophysics of an analog of *o*-LHBDI (Scheme 1 and scheme S1) where the methyl group at C(1) is replaced by a phenyl group (*o*-LHBPI; *o*-Locked HydroxyBenzylidene-*p*-PhenylImidazolinone). *o*-LHBPI showed remarkably different steady state absorption and emission behavior compared to *o*-LHBDI. These differences could be exploited for super high resolution microscopy (e.g. STORM) if the dual emission observed can be switched.

**Scheme 1.** Synthesis of *o*-LHBPI<sup>a</sup>

<sup>a</sup> Reagents and conditions: (a)  $\text{Ac}_2\text{O}$ ,  $\text{NaOAc}$  (2.0 equiv.),  $\mu\text{wave}$  300W, 140 °C, 3 min; (b) azalactone 1 (1.2 equiv.), pyridine (1 equiv.),  $\text{TiCl}_4$  (1.5 equiv.)/THF, -10 °C, 2 h, 45% over two steps. (c) 40% aqueous  $\text{MeNH}_2$ ,  $\text{K}_2\text{CO}_3$  (2 equiv.), reflux, 3 hr, 40% yield. (See supporting information)

The absorption spectra of *o*-LHBPI exhibit two peaks, approximately at 370 nm and 410 nm in all the solvents studied (Figure 1, S9). The solvent effect on the spectral features is small. For  $\lambda_{\text{ex}} = 370$  nm, dual emission is observed. It is tempting to ascribe the higher energy band to normal emission and the lower energy band to tautomer emission (Figure 1). The bands are red shifted in toluene, *tert*-butanol and methanol solutions compared to those in aqueous and ethanolic solutions (Table S1) The ratio of integrated intensities of the normal and tautomer bands is excitation wavelength dependent and varies from solvent to solvent (Figure S10). The normal emission is predominant in acetonitrile and methanol, while the bands are almost equally strong in toluene. In ethanol, water and *tert*-butanol, the tautomer band is predominant. Dual emission is observed for  $\lambda_{\text{ex}} = 410$  nm as well, with the tautomer band being the prominent one. In acetonitrile, the normal band is hardly visible. Very recently, similar features have been reported in the absorption spectra of another *ortho*-locked GFP chromophore analogue (*o*-LHBDI). However the normal emission band is not observed in *o*-LHBDI.<sup>25</sup> The only structural difference between *o*-LHBDI and *o*-LHBPI is that the methyl group at C(1) of the imidazolone group is replaced by a phenyl group in the second. This substitution seems to be responsible for the rather non-trivial effect on the spectra discussed above. This indicates that the ESPT process in this molecule is hindered to some extent, which could be related to ground state and/or excited state phenomena, as has been discussed later. Secondly, it is surprising that the fluorescence quantum yield is greatest in water and lower in aprotic solvents, even though ESPT is usually hindered by the formation of “blocked” structures in protic solvents.<sup>26,27</sup> This seems to indicate the involvement of one or more water molecules as a proton relay, which has previously been reported to facilitate ESPT in some cases.<sup>28-30</sup>

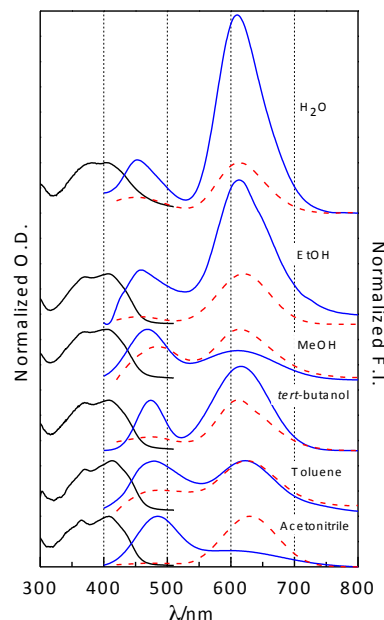


**Figure 1.** Steady state absorption and emission spectra of *o*-LHBPI in different solvents; The black solid lines denote normalized absorption spectra; (A) blue solid lines (—) denote normalized emission spectra at  $\lambda_{\text{ex}} = 370$  nm, (B) red dashed lines (---) denote emission spectra at  $\lambda_{\text{ex}} = 410$  nm.

At this point, it is worthwhile to compare the absorption and excitation spectra, in order to understand if the ground state is homogeneous or not. The fluorescence excitation spectrum monitored at  $\lambda_{\text{em}} = 475$  nm peaks at 360 nm, which is the position of the higher energy absorption maximum (Figure 2). The one spectrum monitored at  $\lambda_{\text{em}} = 610$  nm, however, peaks at  $\sim 370$  and 620 nm respectively and is a good match with the absorption spectra in all the solvents (Figure 2A), but the corresponding peak intensities are reversed. To resolve this, the absorption and fluorescence excitation spectra (monitored at  $\lambda_{\text{em}} = 610$  nm) are fitted to a sum of three Gaussian functions, one of which is held at a maximum at 267 nm corresponding to the benzenoid band, the onset of which can be seen in the absorption as well as in the excitation spectra.

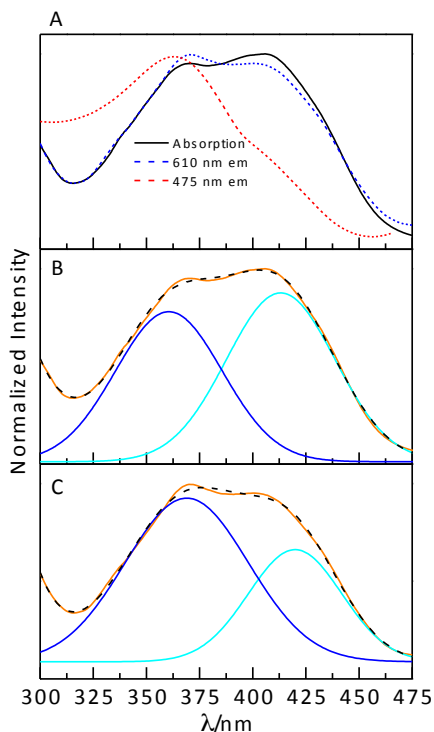


**Figure 2.** (A) Normalized absorption and excitation spectra in methanol.  $\lambda_{em} = 475$  nm and  $\lambda_{em} = 610$  nm respectively. (B) Absorption spectrum as a sum of three-Gaussian functions. (C) Excitation spectrum ( $\lambda_{em} = 610$  nm) as a sum of three-Gaussian functions.

The absorption spectra are not affected significantly by pH, except for the appearance of a 20 nm red shifted band at pH = 12, marking the formation of the anionic ground state of the molecule. The tautomer emission band is suppressed above pH = 10, possibly because the anion, which does not have a phenolic hydrogen atom, cannot undergo ESPT. (Figure S11, S12, S13). The fluorescence spectra at different pH do not exhibit an isoemissive point, but upon area normalization, a pseudo-isoemissive point occurs at 557 nm (Figure 12A), indicating a two-state process. The ratio of the areas under the two Gaussian components is pH-independent in acidic media, but appears to approach a point of inflexion at very high pH (Figure S13). Upon 410 nm excitation, a similar trend is observed (Figure S12B).

Fluorescence transients at 475 nm are the identical for excitation wavelengths of 370 nm and 410 nm and are complete within 2 ps. Transients at 610 nm could not be recorded for excitation wavelength of 370 nm, due to an instrumental limitation. For an excitation at 410 nm, the transients at 610 nm are found to be significantly slower than those at 475 nm. No perceivable risetime was observed (Figure S15). The decays, except those in aqueous solution, are biexponential, with components in picosecond and tens of picosecond regime. An additional subpicosecond component is required in the aqueous solution (Table S2).

The occurrence of ESPT gains support from the PES shown in Figure 3. The ultrafast nature of the “normal” emission indicates very facile ESPT, which is in line with the methyl-substituted analogue. The question that remains to be answered is why the “normal” emission is observed at all, unlike in the methyl-substituted analogue. An explanation may be attempted by combining the understanding developed from the steady state spectra and the PES in Scheme S2. The trans isomer is higher in energy than the cis isomer of the normal form by 8.5 kcal mol<sup>-1</sup>.

It is possible that both the isomers coexist and have different absorption spectra, the trans form having a higher energy absorption than the cis form. Upon exciting the cis form at 410 nm, ESPT takes place immediately. However, upon exciting the trans isomer at 375 nm, photoisomerization has to take place before ESPT can occur. This additional step hinders to ESPT to an extent that the “normal” band is perceivable (Figure 3).

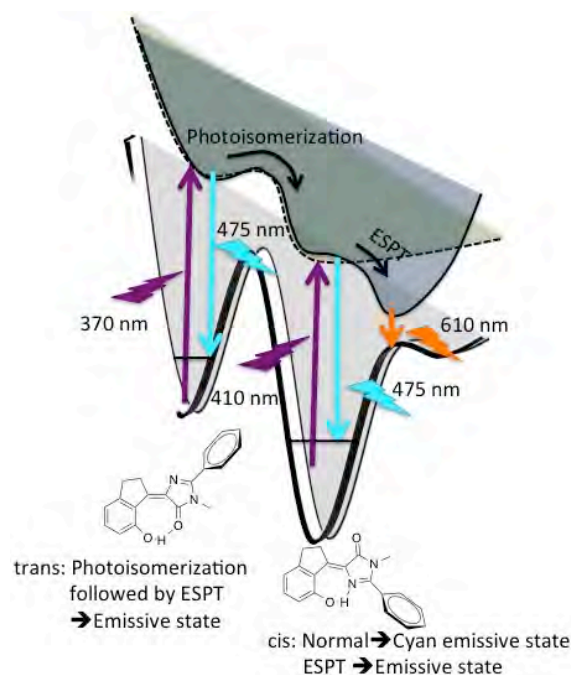


**Figure 3.** Schematic of possible excited state dynamics associated with o-LHBPI.

The ultrafast component in aqueous solution may be assigned to the intramolecular hydrogen bonding leading to ESIPT, while the 6 ps component is due to the intermolecular hydrogen bonded network via monohydrate formation and leading to proton transfer. As has been proposed for *o*-HBDI, the possibility of vibronic relaxation of the tautomer reaching thermal equilibrium can also hold good for *o*-LHBPI considering the sub picosecond component.<sup>13</sup> Faster components of 1.4 ps and 1.5 ps in *tert*-butanol and methanol can be rationalized by our postulated polyhydrate type formation, which makes it more difficult for the intramolecular hydrogen bonding to form. The relatively slower component can



be assigned to the population decay time of the tautomer and is found to be solvent dependent. But, unlike *o*-HBDI, no direct relation with solvent viscosity is found in this case; rather it is found that the stability of the excited state depends on the interplay of solvent polarity and viscosity. In water, the tri-exponential fit is comprised of a sub-picosecond component of  $\sim 300$  fs, while a slower component of 6 ps is also found. The decay time is 75 ps for water.

The effect of phenyl substitution in the *o*-locked GFP chromophore analogue is found to be non-trivial. The fluorescence quantum yield is lower than the methyl-substituted analogue, possibly because of the rotation of the phenyl ring, which provides an additional nonradiative channel of deactivation. Unlike the methyl-substituted analogue reported very recently by Chou and co-workers, dual emission is observed at room temperature, indicating a hindrance to the ESIPT process that leads to the formation of the emissive phototautomer. The observation is rationalized by the occurrence of trans and cis isomers in the ground state. While the cis isomer undergoes ultrafast ESIPT, the trans isomer has to undergo photoisomerization before ESIPT can occur, leading to the emission from the “normal” form. Another significant difference with the methyl substituted analogue is the greater fluorescence quantum yield in water, compared to that in aprotic solvents. This indicates the involvement of a hydrogen bonded water bridge in the ESIPT process.

## ASSOCIATED CONTENT

### Supporting Information.

Synthetic procedure, yield and characterization of the compounds, NMR spectra and additional steady state spectra are provided. This material is available free of charge via the Internet at <http://pubs.acs.org>.

## AUTHOR INFORMATION

### Corresponding Author

\*Fax: +612-9850-8313; email: [peter.karuso@mq.edu.au](mailto:peter.karuso@mq.edu.au) Phone: +612 9850 8290

\*Fax: +9122-2570-7152; email: [anindya@chem.iitb.ac.in](mailto:anindya@chem.iitb.ac.in) Phone: +9122 2576 7149

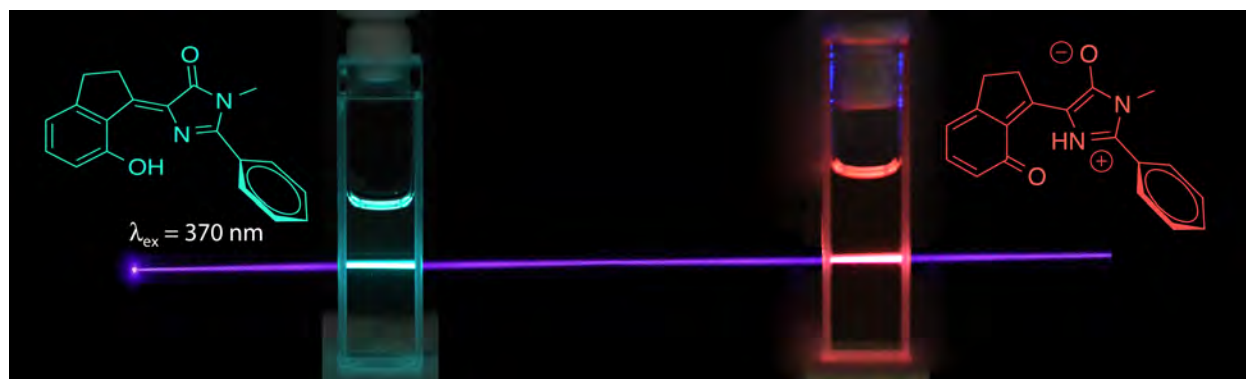
## ACKNOWLEDGMENT

This research is supported by the Australian Research Council (DP0877999) to PK and AD and a SERC DST grant to AD. Support from a FIST grant to the Department of Chemistry, IIT Bombay, is gratefully acknowledged. S.C. acknowledges the Australian Research Council for financial support.

## REFERENCES

- (1) Chalfie, M.; Tu, Y.; Euskirchen, G.; Ward, W. W.; Prasher, D. C. *Science* **1994**, 263, 802.
- (2) Haseloff, J.; Siemering, K. R.; Prasher, D. C.; Hodge, S. *Proc. Natl. Acad. Sci. U.S.A.* **1997**, 94, 2122.
- (3) Tsien, R. Y. *Annu. Rev. Biochem.* **1998**, 67, 509.
- (4) Sullivan, K. F.; Kay, S. A. *Green Fluorescent Proteins*, 1999.
- (5) Zimmer, M. *Chem. Rev.* **2002**, 102, 759.
- (6) Chudakov, D. M.; Matz, M. V.; Lukyanov, S.; Lukyanov, K. A. *Physiol. Rev.* **2010**, 90, 1103.
- (7) Paige, J. S.; Wu, K. Y.; Jaffrey, S. R. *Science* **2011**, 333, 642.
- (8) Branchini, B. R.; Lusins, J. O.; Zimmer, M. *J. Biomol. Struct. Dyn.* **1997**, 14, 441.
- (9) Stoner-Ma, D.; Melief, E. H.; Nappa, J.; Ronayne, K. L.; Tonge, P. J.; Meech, S. R. *J. Phys. Chem. B* **2006**, 110, 22009.
- (10) Stoner-Ma, D.; Jaye, A. A.; Ronayne, K. L.; Nappa, J.; Meech, S. R.; Tonge, P. J. *J. Am. Chem. Soc.* **2008**, 130, 1227.
- (11) Fang, C.; Frontiera, R. R.; Tran, R.; Mathies, R. A. *Nature* **2009**, 462, 200.
- (12) Chen, K. Y.; Cheng, Y. M.; Lai, C. H.; Hsu, C. C.; Ho, M. L.; Lee, G. H.; Chou, P. T. *J. Am. Chem. Soc.* **2007**, 129, 4534.
- (13) Hsieh, C.-C.; Chou, P.-T.; Shih, C.-W.; Chuang, W.-T.; Chung, M.-W.; Lee, J.; Joo, T. *J. Am. Chem. Soc.* **2011**, 133, 2932.
- (14) Saltiel, J.; Waller, A. S.; Sears, D. F. *J. Am. Chem. Soc.* **1993**, 115, 2453.
- (15) Todd, D. C.; Fleming, G. R. *J. Chem. Phys.* **1993**, 98, 269.
- (16) Weber, W.; Helms, V.; McCammon, J. A.; Langhoff, P. W. *Proc. Natl. Acad. Sci. U.S.A.* **1999**, 96, 6177.
- (17) Mandal, D.; Tahara, T.; Webber, N. M.; Meech, S. R. *Chem. Phys. Lett.* **2002**, 358, 495.
- (18) Litvinenko, K. L.; Webber, N. M.; Meech, S. R. *J. Phys. Chem. A* **2003**, 107, 2616.
- (19) Ishii, K.; Takeuchi, S.; Tahara, T. *Chem. Phys. Lett.* **2004**, 398, 400.
- (20) Mandal, D.; Tahara, T.; Meech, S. R. *J. Phys. Chem. B* **2004**, 108, 1102.
- (21) Usman, A.; Mohammed, O. F.; Nibbering, E. T. J.; Dong, J.; Solntsev, K. M.; Tolbert, L. M. *J. Am. Chem. Soc.* **2005**, 127, 11214.
- (22) Gepshtein, R.; Huppert, D.; Agmon, N. *J. Phys. Chem. B* **2006**, 110, 4434.
- (23) Stavrov, S. S.; Solntsev, K. M.; Tolbert, L. M.; Huppert, D. *J. Am. Chem. Soc.* **2006**, 128, 1540.
- (24) Rafiq, S.; Rajbongshi, B. K.; Nair, N. N.; Sen, P.; Ramanathan, G. *J. Phys. Chem. A* **2011**, 115, 13733.
- (25) Hsu, Y.-H.; Chen, Y.-A.; Tseng, H.-W.; Zhang, Z.; Shen, J.-Y.; Chuang, W.-T.; Lin, T.-C.; Lee, C.-S.; Hung, W.-Y.; Hong, B.-C.; Liu, S.-H.; Chou, P.-T. *J. Am. Chem. Soc.* **2014**, 136, 11805.
- (26) Dzugas, T. P.; Schmidt, J.; Aartsma, T. J. *Chem. Phys. Lett.* **1986**, 127, 336.
- (27) Das, K.; Sarkar, N.; Majumdar, D.; Bhattacharyya, K. *Chem. Phys. Lett.* **1992**, 198, 443.
- (28) Abou-Zied, O. K. *J. Phys. Chem. B* **2007**, 111, 9879.
- (29) Abou-Zied, O. K.; Al-Hinai, A. T. *J. Phys. Chem. A* **2006**, 110, 7835.
- (30) Abou-Zied, O. K. *J. Phys. Chem. B* **2010**, 114, 1069.





Supporting Information

For

Room Temperature Dual Fluorescence of a Locked  
GFP Chromophore

*Soumit Chatterjee,<sup>†</sup> Anindya Datta,<sup>‡</sup> Peter Karuso,<sup>†</sup>*

Department of Chemistry and Biomolecular Sciences

Macquarie University, Sydney, NSW 2109, Australia

and

Department of Chemistry

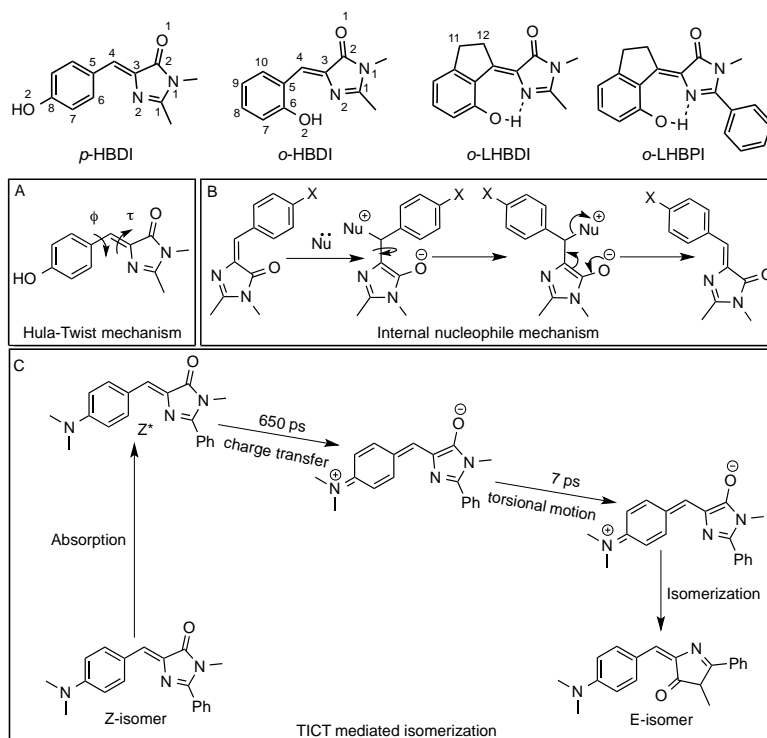
Indian Institute of Technology Bombay, Powai, Mumbai 400076, India

---

<sup>†</sup>Department of Chemistry and Biomolecular Sciences, Macquarie University.

<sup>‡</sup> Department of Chemistry, Indian Institute of Technology Bombay.

To whom correspondence should be addressed. Email: [peter.karuso@mq.edu.au](mailto:peter.karuso@mq.edu.au) Phone: +612 9850 8290, Fax: +612 9850 8313 and [anindya@chem.iitb.ac.in](mailto:anindya@chem.iitb.ac.in) Phone: +9122 2576 7149, Fax: +9122 2576 3480



**Scheme S1.** Molecular structures of *p*-HBDI, *o*-HBDI, *o*-LHBDI and *o*-LHBPI and schematic representation of different mechanisms A) Hula-Twist,<sup>1-3</sup> B) Internal nucleophilic attack<sup>4</sup> and C) TICT (twisted intramolecular charge transfer) mediated isomerization,<sup>5</sup> proposed so far for the ultrafast nonradiative relaxation of HBDI and analogues

**Design and Synthesis.** We reasoned that the hula-twist non-radiative pathway for *p*-HBDI could be inhibited by introducing a 5- or 6-membered ring between C(10) and C(4). We successfully synthesized these compounds (Supporting Information) but were disappointed to find that they were only very weakly fluorescent in solution. However, they were very fluorescent in the solid phase indicating the isomerization about the C(3)-C(4) double bond ( $\tau$ ) was occurring in solution. We reasoned that this could be further inhibited by using an ortho-phenol instead of para-phenol.

The primary challenge of the synthesis was the relatively poor reactivity of the ketones compared to aldehydes. For aldehydes, simply refluxing with phenyl oxazolone in acetic anhydride/acetic acid for 5 hours resulted in the *p*-HBDI analogue in excellent yields. This method was not successful when using a ketone. Several methods were tried, including catalytic lead acetate, triethylamine and phosphorus oxychloride. However, TiCl<sub>4</sub> in THF and a stoichiometric amount

of pyridine yielded (Z)-3-(5-oxo-2-phenyloxazol-4(5H)-ylidene)-2,3-dihydro-1H-inden-4-yl acetate (*o*-AcBPA) in a moderate yield (Scheme 2).<sup>6-8</sup> *o*-LHBPI was obtained by deacylation with aqueous methylamine and potassium carbonate.

The structure of the final product was conformed by NMR spectroscopy and HRMS. In particular, we determined that in organic solvent (CDCl<sub>3</sub>) that *o*-LHBPI exists solely in the “cis” (Z) form. This is based on NOE measurements and molecular mechanics that show that the only H-H distance that is appreciably difference in the cis- and trans-isomers is the distance between the phenol proton and the ortho-protons on the aromatic ring. In the trans the distance is 6.05 Å and in the cis-isomer it is 3.55 Å. The NOE measurements indicated a distance of 3.26 Å, which could only be the cis-isomer.

**Synthesis and Characterization.** Unless otherwise stated, all chemicals and reagents were received from Sigma-Aldrich (Castle Hill, Australia) and used without further purification. Dichloromethane, diethyl ether, ethanol, ethyl acetate, light petroleum, methanol, tetrahydrofuran and toluene were obtained from ChemSupply (Australia). HPLC grade acetonitrile was obtained from BDH/Merck (Germany), and was used without further purification. Spectroscopy grade acetonitrile from Spectrochem was distilled over CaH<sub>2</sub> and the distillate passed through activated neutral alumina immediately prior to use. Spectroscopy grade *tert*-butanol from Spectrochem, Mumbai, India was used as received. <sup>1</sup>H NMR and <sup>13</sup>C NMR spectra were recorded in 5 mm Pyrex tubes (Wilma, USA) on either a Bruker Avance DPX-400 400 MHz or AVII-600 600 MHz spectrometer. All spectra were obtained at 25 °C, processed using Bruker Topspin 3.2 and referenced to residual solvent (CDCl<sub>3</sub> 7.26/77.16 ppm; DMSO-d<sub>6</sub> 2.49/39.8 ppm). Infrared spectra were taken on a Perkin Elmer paragon 1000PC FTIR spectrometer, or Nicolet iS90 FT-IR Spectrometer (Thermo Scientific, Australia). Low resolution mass spectrometry was performed by electrospray ionization (ESI) MS in positive or negative polarity mode as required on a Shimadzu LC-20A prominence system coupled to a LCMS-2010 EV mass spectrometer using LCMSsolution 3.21 software. LC-MS experiments were carried out on a Gemini C18 column (Phenomenex, Australia) 150.0 × 2.00 mm, 110Å, 3 µm. High resolution mass data were obtained from ESI in positive polarity mode on a Waters Q-TOF Ultima Tandem Quadrupole/Time-of-Flight ESI mass spectrometer, performed by the Mass Spectrometry Unit at the University of Illinois, USA. Melting point was measured using DSC

2010 differential scanning calorimeter from TA instruments. pH was measured using (ISFETCOM, model S2K712, JAPAN) pH meter.

**3-oxo-2,3-dihydro-1H-inden-4-yl acetate (7-OAc indanone).** 7-Hydroxy-2,3-dihydro-1H-inden-1-one (0.5 g, 3.37 mmol) was added to acetic anhydride (5 mL) and 2 equivalent of sodium acetate (0.55 g, 7.74 mmol). The reaction mixture was irradiated in a microwave reactor (SEM) for 3 min (300 W, 140 °C). The mixture was then poured in ice cold water and extracted with ethylacetate. The organic layer was washed thoroughly with water (4 × 25 mL) and concentrated in vacuo. Purification by flash chromatography gave the pure acetoxindanone (0.62 g, 97%), as white crystals. m.p. 76 °C [lit m.p. 75-77 °C].<sup>9</sup> <sup>1</sup>H NMR (400 MHz, CDCl<sub>3</sub>) δ 7.58 (t, *J* = 7.80 Hz, 1H), 7.33 (d, *J* = 8.00 Hz, 1H), 6.97 (d, *J* = 7.70 Hz, 1H), 3.13 (t, *J* = 5.90 Hz, 2H), 2.66 (t, *J* = 5.90 Hz, 2H), 2.39 (s, 3H).

**2-phenyloxazol-5(4H)-one (phenyl oxazolone).** Hippuric acid (2 g, 0.012 mol) was added to acetic anhydride (8 mL) and the solution was heated at 90 °C for 30 min until all the hippuric acid had dissolved and the colour of the solution became dark orange. The solution was then cooled and poured into ice-diethyl ether mixture (100 mL). The organic layer was repeatedly washed with water then 1% NaHCO<sub>3</sub> solution to remove the traces of acetic acid. The ether layer was dried over MgSO<sub>4</sub> and concentrated *in vacuo* to yield the phenyl oxazolone as a yellow solid (1.5 g, 77%), m.p. 85 °C [lit. m.p. 84-86 °C];<sup>10</sup> <sup>1</sup>H NMR (400 MHz, CDCl<sub>3</sub>) δ 7.99 (d, *J* = 7.13 Hz, 2 H) 7.58 (t, *J* = 7.4 Hz, 1 H), 7.49 (t, *J* = 7.6 Hz, 1 H), 4.42 (s, 2 H); <sup>13</sup>C NMR (125 MHz, CDCl<sub>3</sub>) δ 170.8, 163.7, 133.1, 133.0, 129.0, 128.0, 126.0, 55.2.

**(Z)-3-(5-oxo-2-phenyloxazol-4(5H)-ylidene)-2,3-dihydro-1H-inden-4-yl acetate (o-AcBPA ).** THF (10 mL) was chilled under N<sub>2</sub> to -10 °C. To it, TiCl<sub>4</sub> (0.058 mL, 0.53 mmol) in CH<sub>2</sub>Cl<sub>2</sub> (0.2 mL) was added and stirred for 10 min. To the stirring solution, 3-oxo-2,3-dihydro-1H-inden-4-yl acetate (7-OAc indanone; 0.1 g, 0.53 mmol) was added and the mixture was stirred for 5 min, then 2-phenyloxazol-5(4H)-one (phenyl oxazolone, 0.13 g, 0.85 mmol) was added and stirred for a further 20 min. To the mixture, pyridine (0.2 mL) was added dropwise. The black mixture was stirred for a further 5 hours and was monitored by TLC until the starting material had disappeared. The reaction was then quenched with saturated ammonium chloride solution (3 mL) and extracted with ethyl acetate (3 × 10 mL). The combined organic layer was washed thoroughly with water (4 × 10 mL) then brine solution (2 × 10 mL) and concentrated under

vacuum. The oxazolone was purified by flash chromatography and recrystallized from methanol/water to yield a yellow solid (0.071 g, 40%), m.p. 192 °C; UV (acetonitrile)  $\lambda_{\text{max}}$  365 nm ( $\epsilon = 36800$ ); IR (ATR)  $\nu_{\text{max}}$  1790, 1780, 1751, 1640  $\text{cm}^{-1}$ ;  $^1\text{H}$  NMR (400 MHz,  $\text{CDCl}_3$ )  $\delta$  7.07 (m, 2H), 7.53 (m, 4H), 7.30 (d,  $J = 7.50$  Hz, 1H), 7.06 (d,  $J = 7.87$  Hz, 1H), 3.49 (t,  $J = 5.90$  Hz, 2H), 3.18 (t,  $J = 5.90$  Hz, 2H), 2.24 (s, 3H);  $^{13}\text{C}$  NMR (125 MHz,  $\text{CDCl}_3$ )  $\delta$  169.33, 166.99, 153.59, 153.47, 148.19, 133.46, 132.80, 131.56, 129.06, 128.07, 126.15, 123.06, 122.11, 32.68, 31.43, 22.12; MS (ESI)  $m/z$  334; HRMS (ESI) calcd. for  $\text{C}_{20}\text{H}_{16}\text{NO}_4$   $m/z$  334.1073  $[\text{M}+\text{H}^+]$ , found  $m/z$  334.1079.

**(Z)-4-(7-hydroxy-2,3-dihydro-1H-inden-1-ylidene)-1-methyl-2-phenyl-1H-imidazol-5(4H)-one (o-LHBPI).** (Z)-3-(5-oxo-2-phenyloxazol-4(5H)-ylidene)-2,3-dihydro-1H-inden-4-yl acetate (*o*-AcBPA; 0.1 g, 0.30 mmol) was added to aqueous methylamine (40%; 0.1 mL) and potassium carbonate (0.04 g, 0.3 mmol) and the solution was refluxed under  $\text{N}_2$  for three hours, cooled, extracted with ethyl acetate ( $2 \times 10$  mL), washed with water ( $3 \times 50$  mL) and concentrated *in vacuo*. The crude product was purified by flash chromatography to provide the imidazolone **8c** (0.04 g, 45%) as a green-yellow solid, m.p. 192.5 °C; UV (acetonitrile)  $\lambda_{\text{max}}$  370 nm ( $\epsilon = 18600$ ), 410 nm ( $\epsilon = 21200$ ) nm; IR (ATR)  $\nu_{\text{max}}$  1686  $\text{cm}^{-1}$ ;  $^1\text{H}$  NMR (600 MHz,  $\text{CDCl}_3$ )  $\delta$  14.87 (s, 1H, -OH), 7.78 (d,  $J = 7.25$  Hz, 1H,  $-\text{CH}_{\text{ar}}$ ), 7.56 (m, 3H,  $-\text{CH}_{\text{ar}}$ ), 7.35 (t,  $J = 7.73$  Hz, 1H,  $-\text{CH}_{\text{ar}}$ ), 6.87 (d,  $J = 7.38$  Hz, 1H,  $-\text{CH}_{\text{ar}}$ ), 6.80 (d,  $J = 8.20$  Hz, 1H,  $-\text{CH}_{\text{ar}}$ ), 3.49 (t,  $J = 5.81$  Hz, 2H,  $-\text{CH}_2$ ), 3.45 (s, 3H,  $-\text{NCH}_3$ ), 3.18 (t,  $J = 7.73$  Hz, 2H,  $-\text{CH}_2$ );  $^{13}\text{C}$  NMR (150 MHz,  $\text{CDCl}_3$ )  $\delta$  167.92, 157.45, 156.87, 154.26, 153.42, 135.53, 131.62, 129.27, 128.40, 128.31, 127.55, 125.57, 116.06, 115.76, 31.31, 30.89, 29.14; MS (ESI)  $m/z$  305; HRMS (ESI) calcd. for  $\text{C}_{19}\text{H}_{17}\text{N}_2\text{O}_2$   $m/z$  305.1295  $[\text{M}+\text{H}^+]$ , found  $m/z$  305.1290.

**Steady state and time resolved fluorescence.** UV-Vis absorption spectra are recorded on JASCO V-530 double beam absorption spectrophotometer with a slit width of 1.0 nm at room temperature or on Varian Cary-eclipse spectrophotometer. Emission spectra are recorded on HORIBA FLUROMAX photon counting fluorimeter with slit width of 5.0 nm for both excitation and emission monochromators. All experiments were carried out at 25 °C by using double distilled water and solvents. The absorbencies of the solutions were kept at  $\sim 1.0$  for the upconversion experiments.

For femtosecond upconversion (FOG 100, CDP), the samples were excited at 370 or 410 nm using the second harmonic of a mode-locked Ti-sapphire laser (Tsunami, Spectra Physics) pumped by a 5W Millennia (Spectra Physics) laser. The fundamental beam (740/820 nm) was frequency doubled in a nonlinear crystal (1 mm BBO,  $\theta = 25^\circ$ ,  $\phi = 90^\circ$ ). The fluorescence emitted from the sample was upconverted in a nonlinear crystal (0.5 mm BBO,  $\theta = 38^\circ$ ,  $\phi = 90^\circ$ ) using the fundamental beam as a gate pulse. The upconverted light is dispersed in a monochromator and detected using photon counting electronics. A cross-correlation function obtained using the Raman scattering from ethanol displayed a full width at half-maximum (fwhm) of  $\sim 300$  fs. The femtosecond fluorescence decays were fitted using a Gaussian function of the same FWHM as the excitation pulse. The fluorescence decays were recorded at the magic angle polarization ( $54.7^\circ$ ) with respect to the excitation pulse on a FOG 100 fluorescence optically gated upconversion spectrometer. The resolution was in appropriate multiples of the minimum step size of the instrument, i.e. 0.78 fs/step. The decays were analyzed by iterative reconvolution using a homemade program.





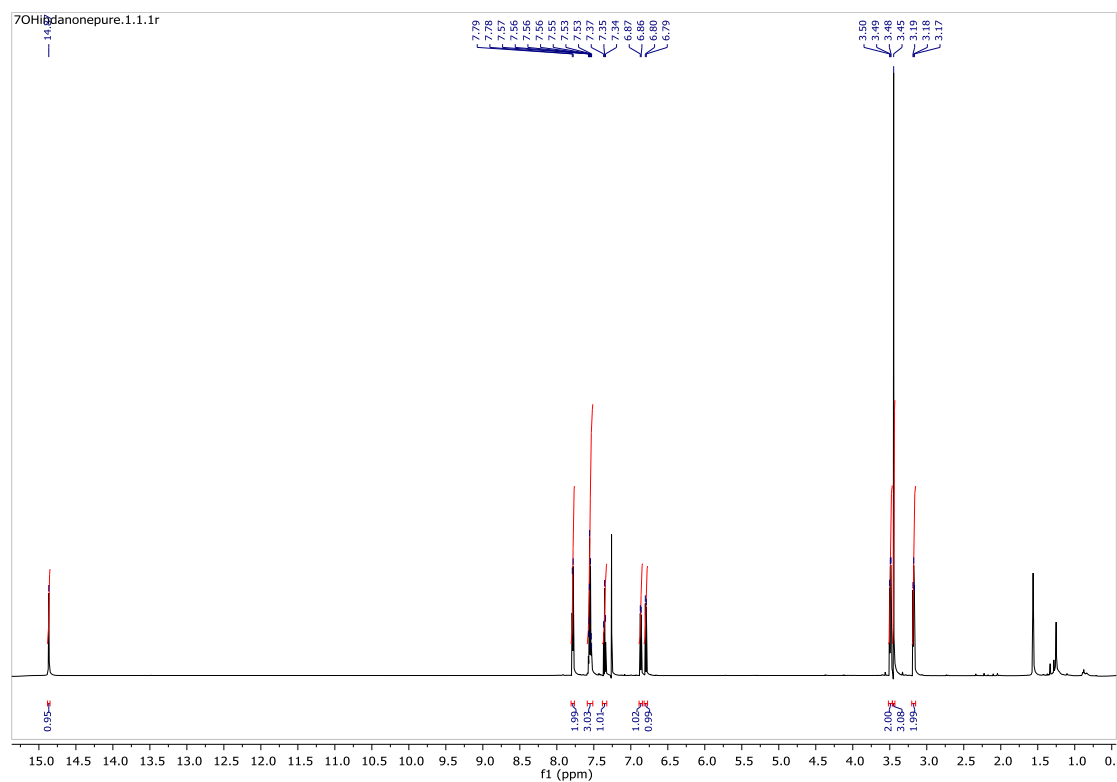


**Figure S3.**  $^1\text{H}$  NMR spectrum of *o*-LHBPI

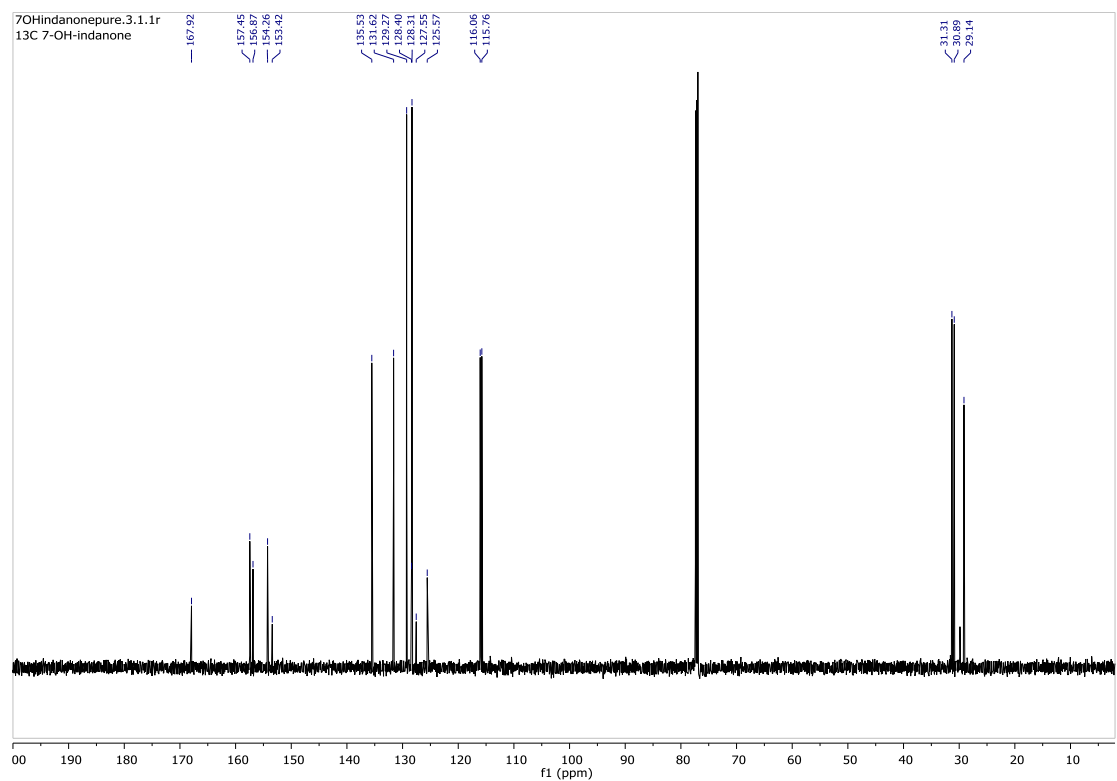


**Figure S4.**  $^{13}\text{C}$  NMR spectrum of *o*-LHBPI

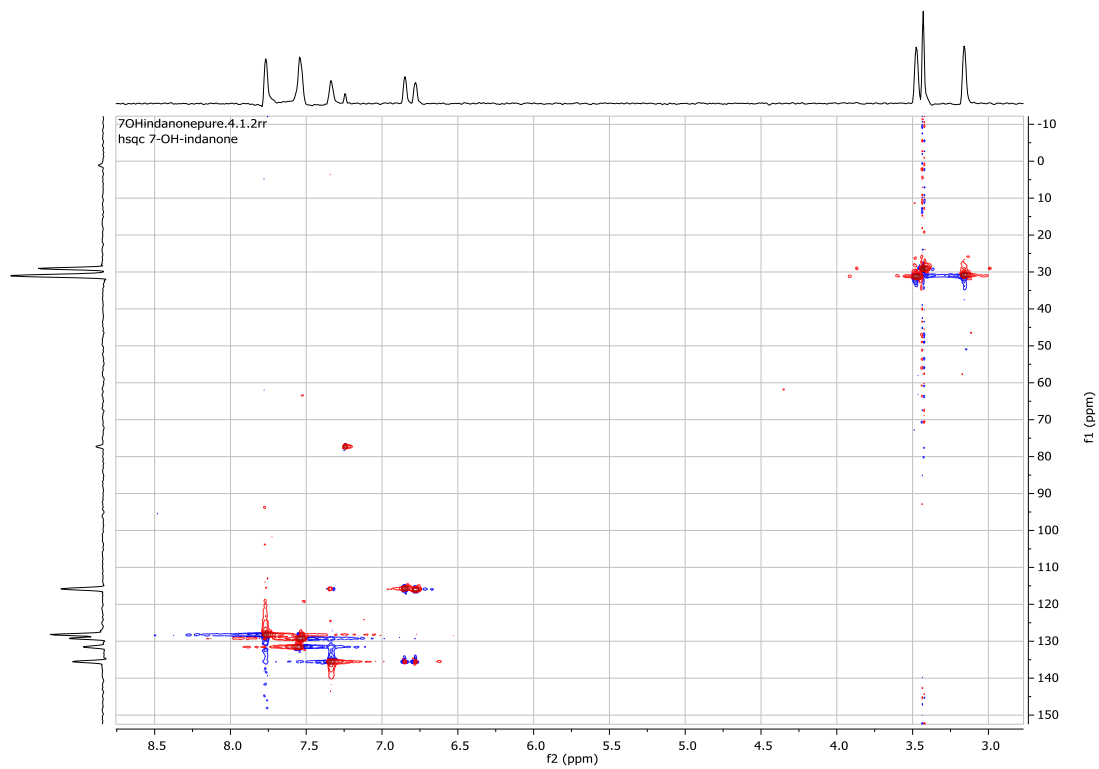


**Figure S5.** HSQC of *o*-LHBPI

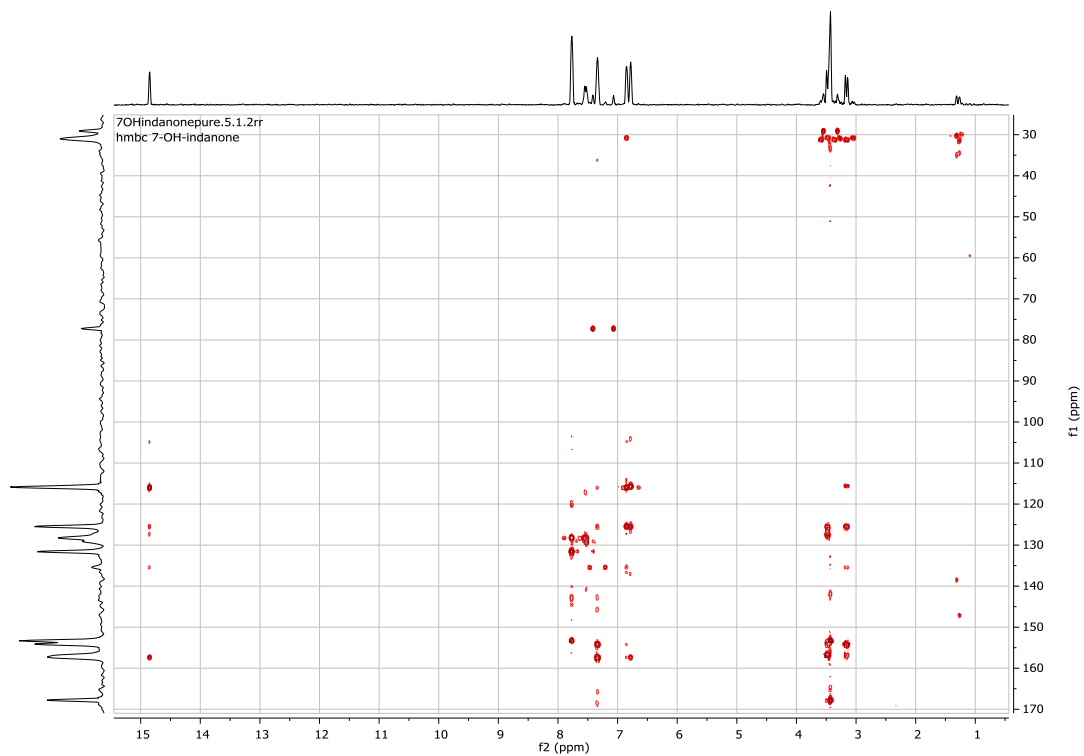


**Figure S6.** HMBC of *o*-LHBPI

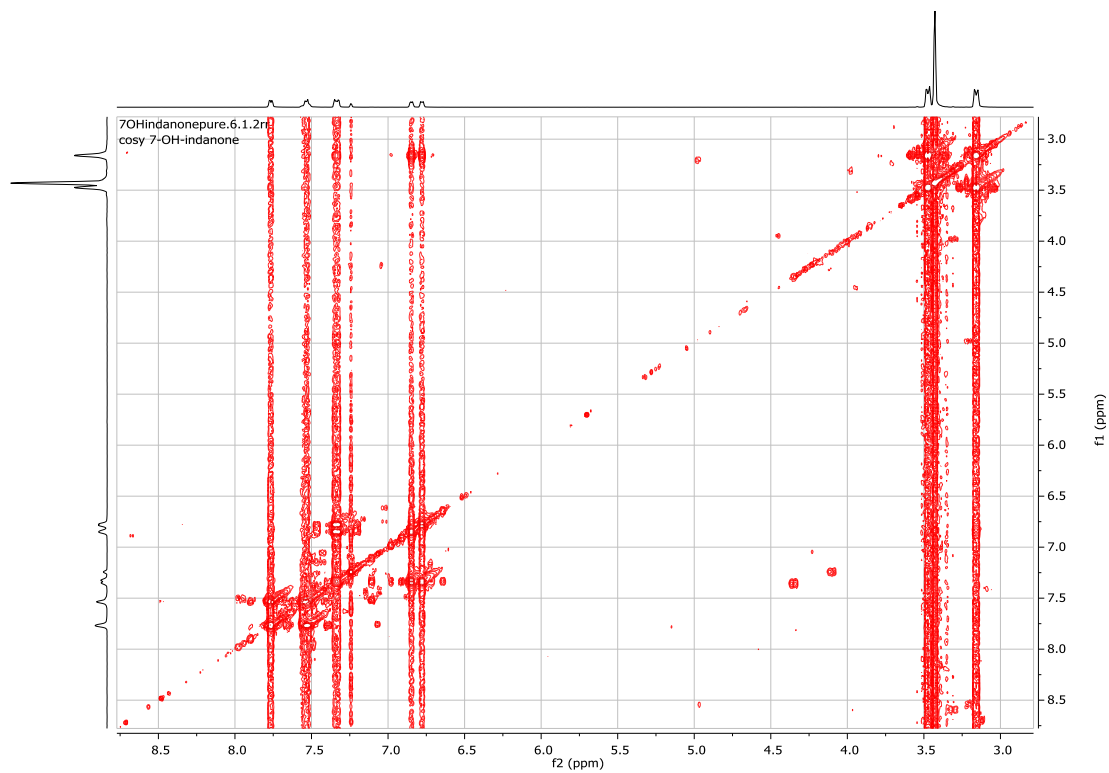


**Figure S7.** COSY of *o*-LHBPI

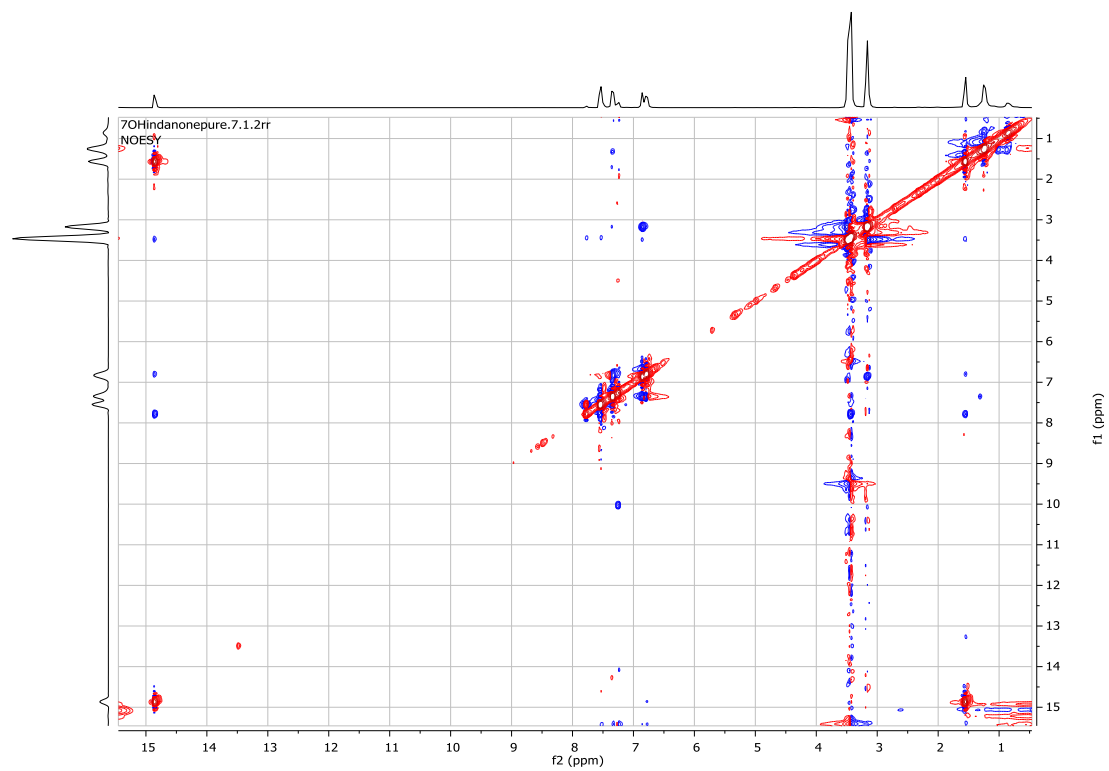


**Figure S8.** NOESY of *o*-LHBPI

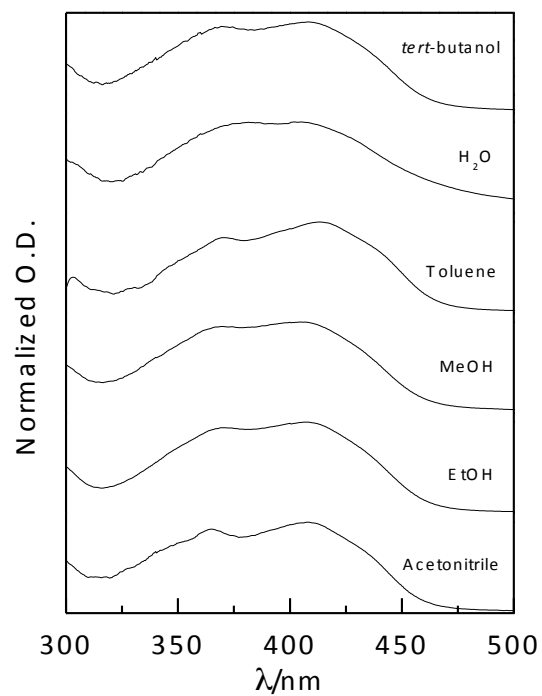


**Figure S9.** Normalized absorption spectra of o-LHBPI in different solvents

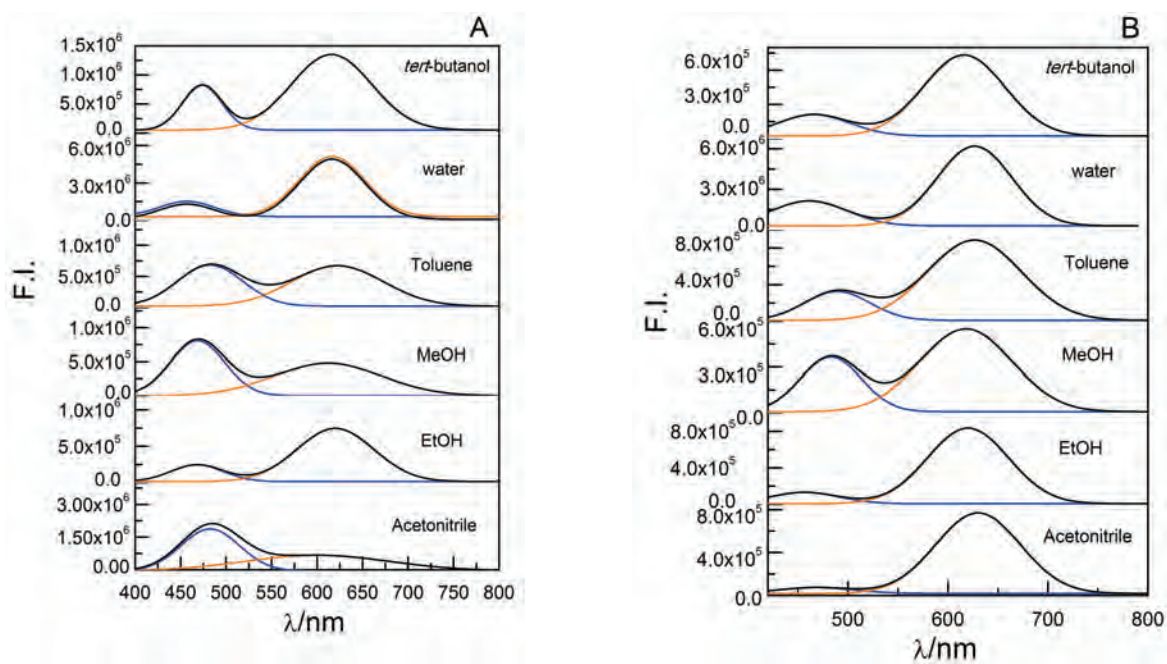


**Figure S10.** Two Gaussian fittings of o-LHBPI emissions in different solvents. (A)  $\lambda_{\text{ex}} = 370$  nm, (B)  $\lambda_{\text{ex}} = 410$  nm.

**Table S1.** Steady state absorption and fluorescence data of *o*-LHBPI

Solvent	$\lambda_{\text{abs}}$ (nm)	$\lambda_{\text{em}}$ (nm) at $\lambda_{\text{ex}} = 370$ nm	$\phi_f \times 10^{-3}$	$\Phi_T \times 10^{-3}$	$\lambda_{\text{em}}$ (nm) at $\lambda_{\text{ex}} = 410$ nm	$\phi_f \times 10^{-3}$	$\Phi_T \times 10^{-3}$
toluene	365	477	3.0	7.0	480	2.3	10.8
	412	620	4.0		624	8.5	
<i>tert</i> -butanol	370	475	2.5	9.0	475	0.9	3.9
	410	616	6.5		610	3.0	
ethanol	370	458	0.8	3.8	457	0.4	3.4
	410	613	3.0		618	3.0	
methanol	370	468	2.0	4.5	485	1.0	3.2
	409	613	2.5		613	2.2	
acetonitrile	365	483	4.8	9.2	475	0.4	3.3
	410	600	4.4		630	2.9	
water	375	455	9.0	43.6	455	17.0	59.5
	410	610	34.6		614	42.5	

$\Phi_T$  = Total quantum yield

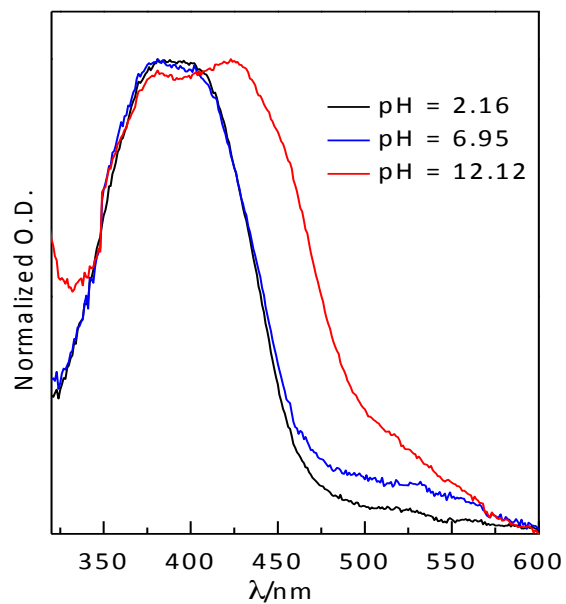


**Figure S11.** Absorption spectra of *o*-LHBPI at pH = 2.16, 6.95 and 12.12.

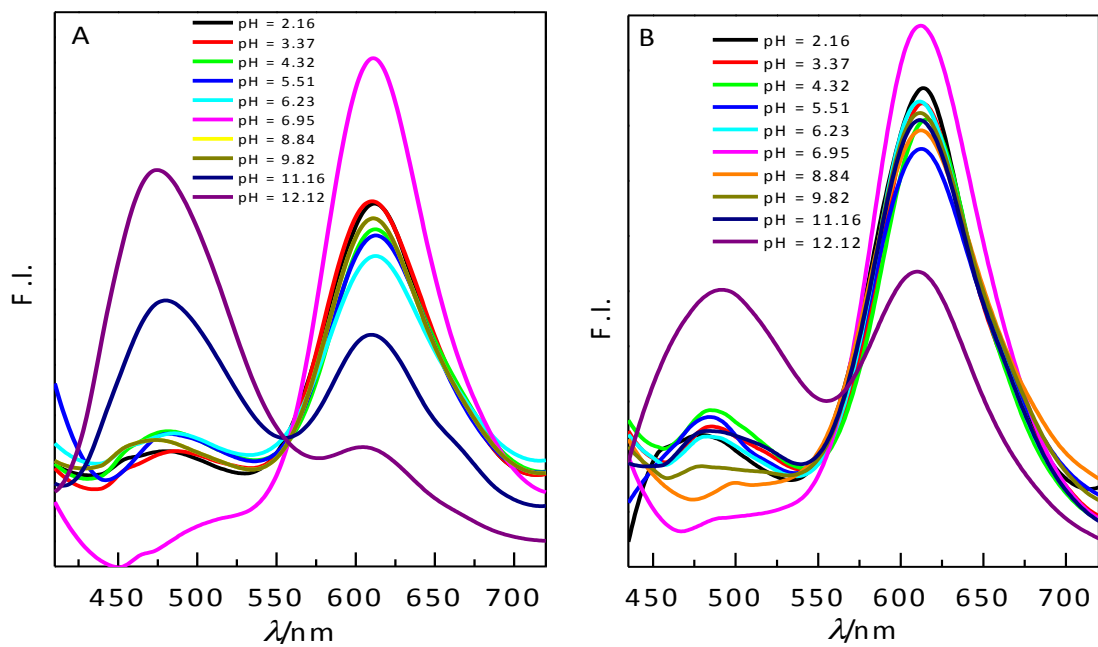


**Figure S12.** Area normalized emission spectra of *o*-LHBPI. (A)  $\lambda_{\text{ex}} = 370$  nm, (B)  $\lambda_{\text{ex}} = 410$  nm

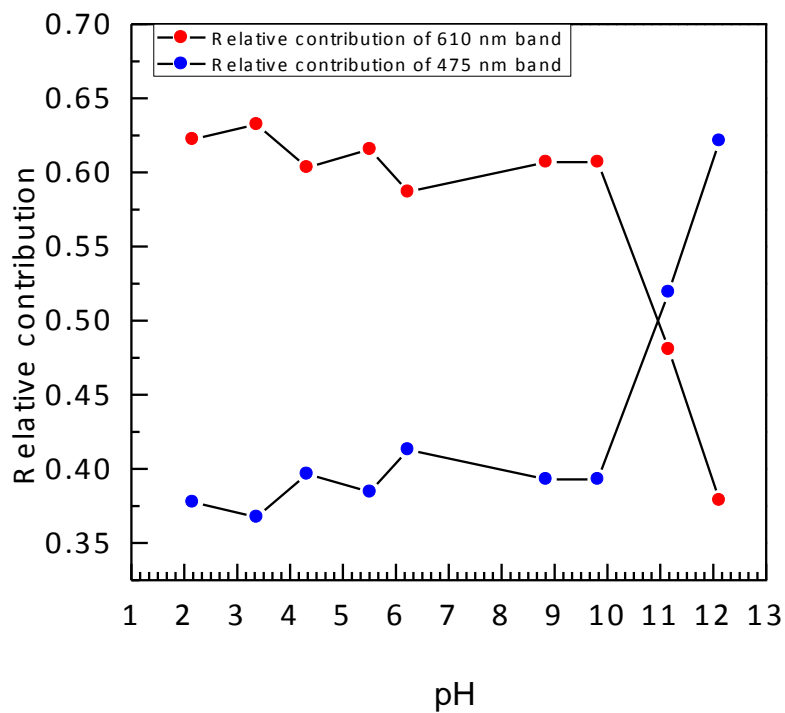


**Figure S13.** Plot of relative area under 475 nm and 610 nm band (after fitting the emission spectra as a sum of two-Gaussian functions) vs. pH at  $\lambda_{\text{ex}} = 370$  nm

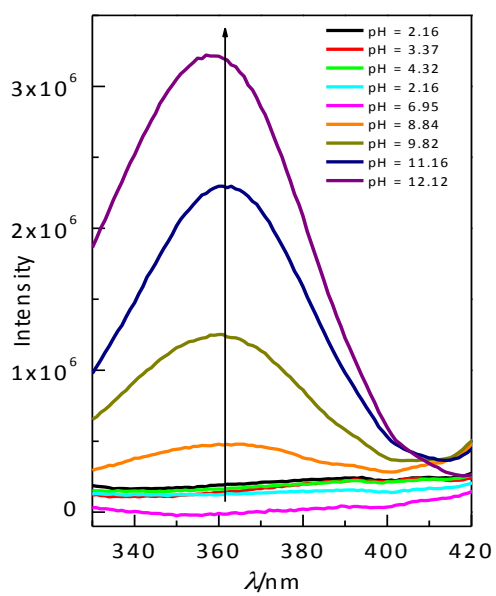


**Figure S14.** Excitation spectra at  $\lambda_{\text{em}} = 475$  nm for different pH.

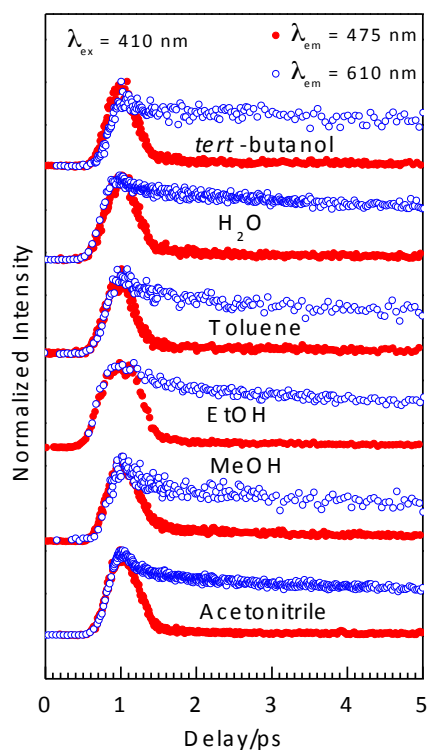
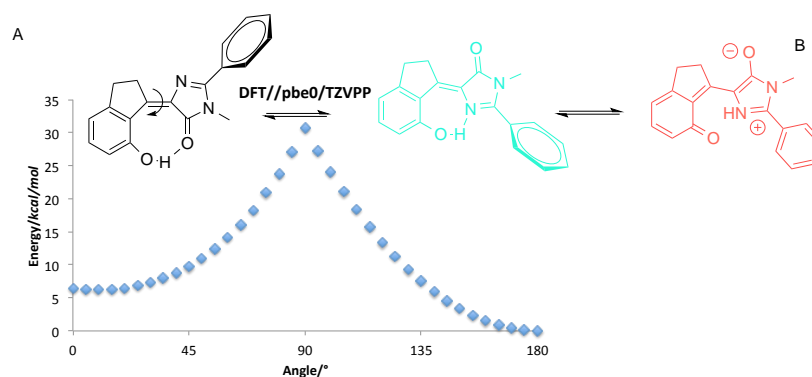


**Figure S15.** Femtosecond fluorescent transients of *o*-LHBPI in different solvents from upconversion experiments.  $\lambda_{\text{ex}} = 410$  nm;  $\lambda_{\text{em}} = 475$  nm and 610 nm

**Table S2.** Temporal parameters of *o*-LHBPI in various solvents from upconversion experiments.  $\lambda_{\text{ex}} = 410$  nm.  $\lambda_{\text{em}} = 610$  nm

Solvent	$\tau_1(\text{ps})$	$a_1$	$\tau_2(\text{ps})$	$a_2$	$\tau_3(\text{ps})$	$a_3$
toluene			0.90	0.45	50	0.55
<i>tert</i> -butanol			1.50	0.25	70	0.75
ethanol			0.90	0.40	40	0.60
methanol			1.40	0.35	40	0.60
acetonitrile			0.40	0.45	25	0.55
water	0.30	0.30	6.00	0.25	75	0.45





**Scheme S2.** (A) Ground state cis-trans isomerization of *o*-LHBPI. (B) Red emissive ESIPT state of *o*-LHBPI

## References

- (1) Weber, W.; Helms, V.; McCammon, J. A.; Langhoff, P. W. *Proc. Natl. Acad. Sci. U.S.A.* **1999**, *96*, 6177.
- (2) Mandal, D.; Tahara, T.; Webber, N. M.; Meech, S. R. *Chem. Phys. Lett.* **2002**, *358*, 495.
- (3) Mandal, D.; Tahara, T.; Meech, S. R. *J. Phys. Chem. B* **2004**, *108*, 1102.
- (4) Dong, J.; Solntsev, K. M.; Tolbert, L. M. *J. Am. Chem. Soc.* **2009**, *131*, 662.
- (5) Rafiq, S.; Rajbongshi, B. K.; Nair, N. N.; Sen, P.; Ramanathan, G. *J. Phys. Chem. A* **2011**, *115*, 13733.
- (6) Sharma, V.; Lansdell, T. A.; Jin, G. Y.; Tepe, J. J. *J. Med. Chem.* **2004**, *47*, 3700.
- (7) Sharma, V.; Tepe, J. J. *Bioorg. Med. Chem. Lett.* **2004**, *14*, 4319.
- (8) Papeo, G.; Poster, H.; Borghi, D.; Varasi, M. *Org. Lett.* **2005**, *7*, 5641.
- (9) Narine, A. A.; Wilson, P. D. *Can. J. Chem.* **2005**, *83*, 413.
- (10) Conway, P. A.; Devine, K.; Paradisi, F. *Tetrahedron* **2009**, *65*, 2935.

## Conclusion

A novel and efficient synthetic route for the preparation of locked and unlocked GFP chromophores has been proposed. The compounds are highly fluorescent in the solid state, while only the *o*-locked analogue shows dual fluorescence in solution. Based on the steady state and time resolved studies, it is been found that the effect of phenyl substitution in the *o*-locked GFP chromophore analogue is non-trivial. The fluorescence quantum yield is lower than the methyl-substituted analogue, possibly because of the rotation of the phenyl ring, which provides an additional nonradiative channel of deactivation. Observance of a dual emission at room temperature indicates a hindrance to the ESIPT process that leads to the formation of the emissive phototautomer. The observation is rationalized by the occurrence of trans and cis isomers in the ground state. While the cis isomer undergoes ultrafast ESIPT, the trans isomer has to undergo photoisomerization before ESIPT can occur, leading to the emission from the “normal” form. Another significant difference with the methyl substituted analogue is the greater fluorescence quantum yield in water, compared to that in aprotic solvents. This indicates the involvement of a hydrogen bonded water bridge in the ESIPT process. Further studies, including computation to unravel the mystery behind the high  $pK_a$  and ultrafast decay of the normal emission, synchronous fluorescence excitation/ emission spectra study as well as femtosecond transient absorption spectroscopy studies should be carried out in future in elucidating the excited-state dynamics of the "locked" chromophore.



## **Chapter 4: Materials and methods**



## 4.1. Materials and Experimental Procedure

Unless otherwise stated, all chemicals and reagents were received from Sigma-Aldrich (Castle Hill, Australia) and used without further purification. Chloroform, dichloromethane, diethyl ether, ethanol, ethyl acetate, light petroleum, methanol, tetrahydrofuran and toluene were obtained from ChemSupply (Australia). HPLC grade acetonitrile was obtained from BDH/Merck (Germany), and was used without further purification. Spectroscopy grade acetonitrile from Spectrochem was distilled over  $\text{CaH}_2$  and the distillate passed through activated neutral alumina immediately prior to use. Butylamine from Qualigens, Mumbai, India, was used as received. Spectroscopy grade *tert*-butanol and DMSO from Spectrochem, Mumbai, India was used as received. Sodium dodecyl sulphate (SDS) from Sigma-Aldrich was recrystallized from methanol–water, prior to use.

### 4.1.1 Equipment

$^1\text{H}$  NMR and  $^{13}\text{C}$  NMR spectra were recorded in 5 mm Pyrex tubes (Wilmad, USA) on either a Bruker Avance DPX400 400 MHz or AVII600 600 MHz spectrometer. All spectra were obtained at 25 °C, processed using Bruker Topspin 3.2 and referenced to residual solvent ( $\text{CDCl}_3$  7.26/77.16 ppm;  $\text{DMSO-d}_6$  2.49/39.8 ppm). Infrared spectra were taken on a Perkin Elmer paragon 1000PC FTIR spectrometer, or Nicolet iS10 FT-IR Spectrometer (Thermo Scientific, Australia). UV-Vis absorption spectra are recorded on JASCO V-530 double beam absorption spectrophotometer with a slit width of 1.0 nm at room temperature or on Varian Cary-eclipse spectrophotometer.

Low resolution mass spectrometry was performed by electrospray ionisation (ESI) MS in positive or negative polarity mode as required on a Shimadzu LC-20A prominence system coupled to a LCMS-2010 EV mass spectrometer using LCMSsolution 3.21 software. LC-MS

experiments were carried out on a Gemini C18 column (Phenomenex, Australia)  $150.0 \times 2.00$  mm,  $110\text{\AA}$ ,  $3\text{ }\mu\text{m}$ .

High resolution mass data were obtained from ESI in positive polarity mode on a Waters Q-TOF Ultima Tandem Quadrupole/Time-of-Flight ESI mass spectrometer, performed by the Mass Spectrometry Unit at the University of Illinois, USA.

HPLC analysis was performed on a Shimadzu 10AD-VP system running Class-VP 7.4 SP1 software or a Waters manual 6000A pump. Analytical, semipreparative and preparative HPLC were performed on Gemini C18 HPLC columns (Phenomenex): Gemini-NX C18  $250.0 \times 4.6$  mm,  $110\text{\AA}$ ,  $5\text{ }\mu\text{m}$ ; Gemini C18  $250.0 \times 10.0$  mm,  $110\text{\AA}$ ,  $10\text{ }\mu\text{m}$ ; Gemini-NX C18  $150.0 \times 21.2$  mm,  $110\text{\AA}$ ,  $5\text{ }\mu\text{m}$ .

TLC was performed with Merck Kieselgel 60 F254 plates with viewing under ultraviolet light (254 nm and 365 nm). Flash column chromatography was performed on silica gel ( $60\text{ }\text{\AA}$  0.040–0.063 mm, 230–400 mesh ASTM from Grace Chemicals, Melbourne).

After reverse phase HPLC, acetonitrile was evaporated and the residual water was removed by lyophilization. The freeze dryer system was from Labconco (USA).

Melting point was measured using DSC 2010 differential scanning calorimeter from TA instruments.

## **4.2. Steady State Measurements**

All experiments were carried out at  $25\text{ }^{\circ}\text{C}$  by using double distilled water or freshly distilled solvents. In aqueous solutions, pH was 7.1, measured by pH meter (ISFETCOM, model S2K712, JAPAN).

#### 4.2.1. Absorption Spectroscopy

The baseline was recorded using air as a reference. The absorbance derived from Lambert-Beer law is given by equation 4.1

$$A = \log \frac{I_0}{I} = \varepsilon \times c \times l \quad 4.1$$

Where,  $I_0$  and  $I$  are the intensities of the incident and transmitted light,  $\varepsilon$  is the molar extinction coefficient for a fixed wavelength at particular temperature,  $c$  is the molar concentration of sample which absorbed the light and  $l$  is the path length of the sample cuvette which is 1 cm. The schematic of the spectrophotometer is shown in Figure 4.1. In spectroscopic titration experiment equal amounts of the surfactants, cyclodextrins were added in the reference cuvette to obtain the absorption of the probe in the given microenvironment. The absorbances of the solutions were kept below 0.1 at the absorption maxima to prevent inner filter effects for steady state measurements and for picosecond-nanosecond time-resolved experiments. The absorbances of the solutions were kept at  $\sim 1.0$  for the upconversion experiments. The absorption and emission spectra were recorded before and after the femtosecond fluorescence decays in order to verify that the samples do not photodegrade.



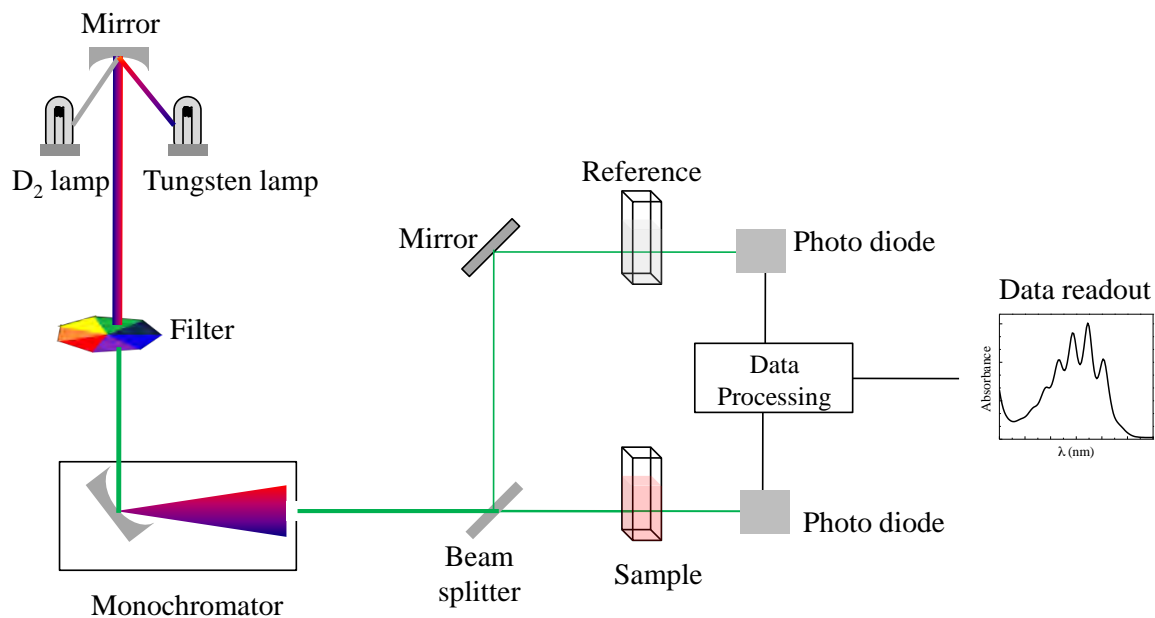


**Figure 4.1.** Schematics of spectrophotometer instrument

#### 4.2.2. Fluorescence Spectroscopy

Steady state fluorescence spectra were recorded on Varian Cary Eclipse fluorimeter. The source and the detector were at right angles to each other. The light source was a Xenon lamp pulsed at 80 Hz, with 2  $\mu$ s FWHM pulse with peak power equivalent to 75 kW and the Hamamatsu R928 photomultiplier tube, respectively. The excitation and emission slits were kept constant at 5 nm and the PMT voltage was 600 volt for all the experiments unless indicated otherwise.

All fluorescence spectra were corrected for changes in absorbance using equation 4.2, where the absorbance is at the wavelength of excitation. This procedure corrects for changes in intensity that might arise due to concentration.<sup>176</sup>

$$F.I. Corrected = \frac{F.I. Observed}{1 - 10^{-Absorbance}} \quad 4.2$$

For the quantum yield measurements, experiments were carried out back to back to maintain identical conditions. The relative quantum yield for the fluorophore can be calculated by integrating the fluorescence spectra by using equation 4.3, which gives the area under the curve.

$$\phi_{f_{Rel}}^f = l_{em} = \int_{\lambda_1}^{\lambda_2} Fluorescence\ spectrum \quad 4.3$$

Here,  $l_{em}$  is the area under the curve in fluorescence emission spectra of the fluorophore at a given excitation wavelength; The absolute quantum yield is given by equation 4.4<sup>6</sup>

$$\phi_f^{abs} = \frac{\phi_f^f}{\phi_f^s} \times \phi_s^{abs} \times \frac{n_f^2}{n_s^2} \quad 4.4$$

where  $\phi_f^f$  and  $\phi_f^s$  are the relative quantum yields of the fluorophore and the standard,  $\phi_s^{abs}$  is the absolute quantum yield of the standard known from the literature and  $n_f$  and  $n_s$  correspond to the refractive indexes of the solvent in which the measurements are done for the fluorophore and the standard respectively. The quantum yields for our experiments were calculated using quinine sulphate in 0.5 M H<sub>2</sub>SO<sub>4</sub> ( $\phi_f = 0.546$ ),<sup>177</sup> Lucifer Yellow CH ( $\phi_f = 0.21$ )<sup>178</sup> and rhodamine 6G ( $\phi_f = 0.94$ )<sup>179</sup> as standards.

### 4.3. Time Resolved Fluorescence Measurements

Time-domain method involves the lifetime measurement in the electronically excited state following the excitation by a  $\delta$ -pulse of light and the fluorescence intensity is measured as a function of time, which provides the important information concerning the excited state processes by the virtue of lifetime ( $\tau$ ). The width of the pulse is short and relatively much shorter than the decay time of the sample.<sup>6</sup>

### 4.3.1. Lifetime

Consider a sample containing a fluorophore, excited with a sharp pulse of light called the  $\delta$ -pulse.<sup>6</sup> A  $\delta$ -pulse is a function that is zero at all points except one point. This results in an initial population ( $n_0$ ) of fluorophores in the excited state. The excited-state population decays according to equation 4.5

$$\frac{dn(t)}{dt} = -(\Gamma + k_{nr}) n(t) \quad 4.5$$

where  $n(t)$  is the number of excited molecules at time  $t$  following excitation,  $\Gamma$  is the emissive rate, and  $k_{nr}$  is the non-radiative decay rate. Emission is a random event, and each excited fluorophore has the same probability of emitting in a given period of time. This results in an exponential decay of the excited state population as equation 4.6.

$$n(t) = n_0 e^{-t/\tau} \quad 4.6$$

The fluorescence intensity is proportional to  $n(t)$ . Hence, equation 4.6 can be written in terms of the time-dependent intensity  $I(t)$  and upon integration with the intensity substituted for the number of molecules yields equation 4.7

$$I(t) = I_0 e^{-t/\tau} \quad 4.7$$

where  $I_0$  is the intensity at time 0. The lifetime  $\tau$  is the inverse of the total decay rate,  $\tau = (\Gamma + k_{nr})^{-1}$ . The fluorescence lifetime can be determined from the slope of a plot of  $\log I(t)$  versus  $t$ , but more commonly by fitting the data to assumed decay models.

Lifetime is the average time  $\langle t \rangle$ , for which a fluorophore remains in the excited state:

$$\langle t \rangle = \frac{\int_0^\infty t I(t) dt}{\int_0^\infty I(t) dt} = \frac{\int_0^\infty t e^{-t/\tau} dt}{\int_0^\infty e^{-t/\tau} dt} = \frac{\tau^2}{\tau} = \tau \quad 4.8$$

For multi- or non-exponential decays, an average lifetime can be calculated using eq. 4.8.

However, this average lifetime can be a complex function of the parameters describing the actual intensity decay.

#### **4.3.2. Time Resolved Fluorescence Measurement in Nanosecond-Picosecond Time Regime**

All the time resolved fluorescence experiments were performed using the time domain method. In the picosecond-nanosecond time regime, the experiments were performed by using time correlated single photon counting (TCSPC) technique.<sup>180</sup> The number of counts at the peak of the time resolved fluorescence was fixed to 5000.

##### ***4.3.2.1. Time Correlated Single Photon Counting Technique***

Experiments were performed on either an IBH Horiba-Yvon fluorocube or on a homemade setup. The data were analyzed using DAS 2.0 or Fluofit software. In these experiments, the samples were excited at 406 nm using a picosecond laser (IBH-N406) and the emission was collected at the magic angle polarization. For the experiments on the Fluorocube, IBH TBX-04-C photomultiplier was used to detect the signal. In the homemade setup, a Hamamatsu MCP photomultiplier (with C10373-02 thermoelectric cooler) was used, after dispersing the signal through a monochromators and PicoHarp 300 electronics as the multichannel analyser (MCA) was used to record the decays. The typical FWHM of the system response was about 140 ps.

A brief description of TCSPC (Figure 4.2) is as follows: the sample is excited by a pulse of light from a laser or a light emitting diode. The excitation beam passes through a polarizer before reaching the sample. The detector is at right angle to the excitation source and fluorescence is collected at the magic angle ( $54.7^\circ$ ) polarization with respect to the excitation to remove any anisotropy components. The detection limit is restricted to 1% to excitation events, *i.e.* the count rate was kept at 1% of the excitation frequency. The time difference between the

excitation and emission photon is stored in a histogram. The abscissa is the time difference between arrival of the excitation photon and the first emitted photon.

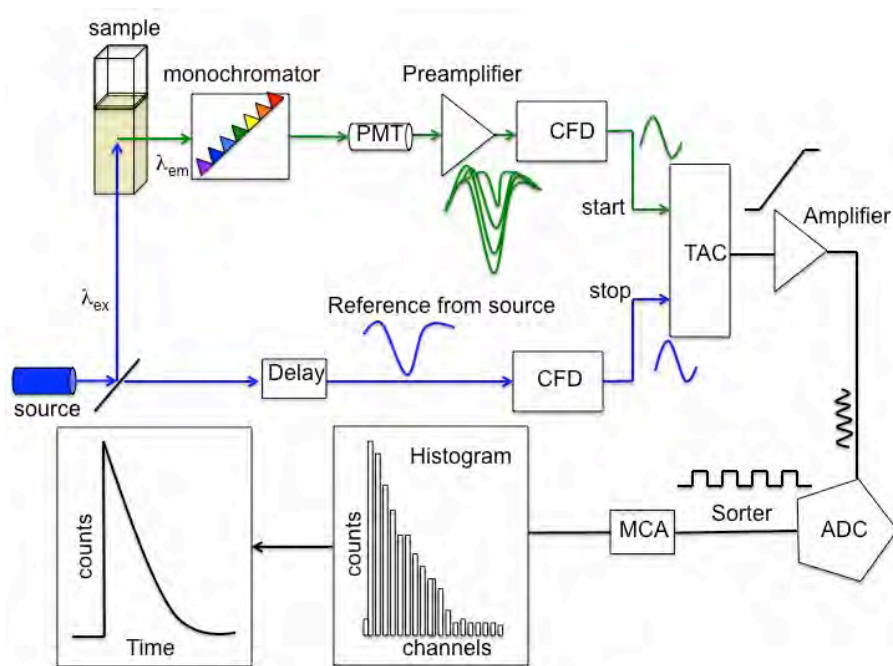


**Figure 4.2.** Schematics of time correlated single photon counting (TCSPC) instrument

A reference signal is generated from a synchronous output of a laser power supply which starts the charging of a capacitor (START signal). A voltage ramp is generated, which increases linearly with time. The first photon from fluorescence, detected by the PMT, produces a STOP signal to the TAC to stop the voltage ramp. This process is considered the “forward” mode of operation. In reality, fluorescence decay is recorded on the TCSPC in a “reverse” mode to avoid overloading the start signal from the laser source with 1 MHz repetition rate and to minimize the dead time which is the time consumed by the TAC to reset during the charging-discharging cycle. In this mode the fluorescence photon act as a START signals while the excitation source is the STOP signal. The TAC now contains a voltage proportional to the time delay ( $\Delta t$ ) between the STOP signal. The TAC now contains a voltage proportional to the time delay ( $\Delta t$ ) between the excitation and emission signals and this is stored as histogram in the MCA.

#### 4.3.2.1.1. Constant Fraction Discriminator (CFD)

If the time of arrival of a photon is measured by setting a threshold on the leading edge of the signal, then there is a spread  $\Delta t$ , called as timing jitter (Figure 4.3), because all pulses do not have the same height. A CFD is a device, which converts pulses of various intensities to reproducible, fast pulses for accurate timing, which is done in the TAC. The TAC splits the signal into two parts. One is delayed by half the pulse width and other half is inverted. These two pulses are recombined and the zero crossing point is taken as the time of arrival of the photon (Figure 4.3). The advantage is that the zero crossing point is independent of the height of the signal and the timing jitter is eliminated.

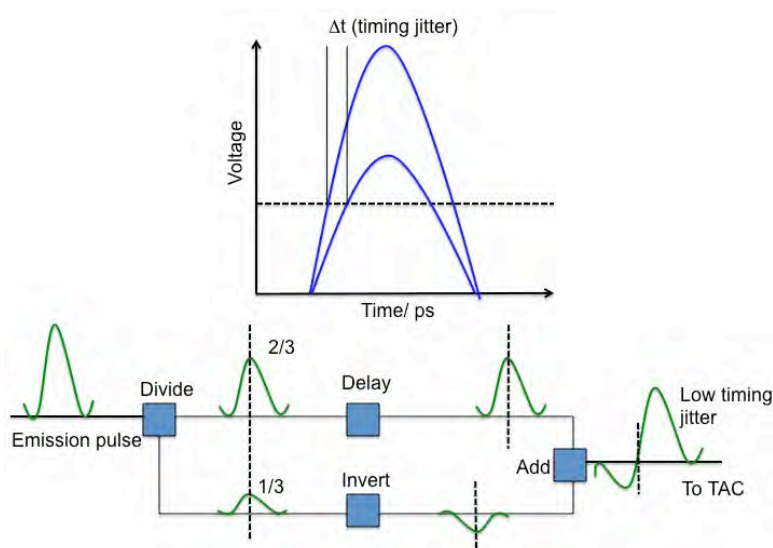


**Figure 4.3.** Schematics of timing jitter and application of Constant Fraction Discriminator (CFG) to eliminate the timing jitter

#### 4.3.2.1.2. Time to Amplitude Converter (TAC)

The TAC measures the time difference between the excitation and emission pulses. The first signal starts charging of a capacitor in the TAC while the second signal stops it. This is followed by a discharge across a resistance, thereby generating a voltage that is proportional to

the difference in the time of arrival between the two signals. For a light source with high repetition rate such as 1 MHz, TCSPC is run in “reverse” mode, where the emission signal acts as the start pulse while the excitation signal acts as stop pulse. If the stop signal does not arrive within a defined time, called the TAC range, the TAC stops charging and the cycle begins again. The time taken by the TAC to reset itself for a charging-discharging cycle is called dead time, which is minimized by operation in the reverse mode.

#### ***4.3.2.1.3. Multi Channel Analyzer (MCA)***

An MCA measures the voltage from the TAC and sorts the photons arriving at a particular time difference. A histogram is plotted after this sorting. The MCA has 8192 channels where the data are stored.

#### ***4.3.2.1.4. Delay Lines***

Delay lines are needed due to significant time delays in all components of the instrument. A photoelectron pulse may take many nanoseconds to exit a detector. Electrical signals in a cable travel about 30 cm in 1 ns. It would be difficult to match all these delays within a couple of nanoseconds in the start and stop detector channels without a way to adjust the delays. The need for matching delays through the components is avoided by the use of calibrated delay lines. Calibrated delay lines are also useful for calibration of the time axis of the MCA. This is accomplished by providing the same input signal to the start and stop channels of the TAC. The electrical signal from ‘start’ is split and both signals are sent to the TAC. The two pulses would arrive with constant time difference. The delay is adjusted and thus the TAC and MCA are calibrated.

### 4.3.3. Analysis of Fluorescence Decay

The time resolved fluorescence intensity,  $I(t)$ , at a particular time is fitted as the sum of exponential functions using equation 4.9, where  $I(t)$  and  $I(0)$  are intensities at time  $t$  and 0, after excitation pulse of light.  $a_i$  and  $\tau_i$  are the amplitude and lifetime of the  $i^{th}$  component respectively.

$$I(t) = I(0) \sum_{i=1}^n a_i e^{-t/\tau_i} \quad 4.9$$

The excitation pulse has a finite width and is not a true  $\delta$ -pulse. This leads to a major issue associated with data analysis, especially at shorter times, as the observed time resolved fluorescence  $N(t)$  is not a true fluorescence signal but a convolution of the instrument response function (IRF) and intensity at time  $t$  after excitation  $I(t)$ , and is expressed by equation 4.10

$$N(t) = \int_0^t R(t' + \delta) I(t - t') dt' \quad 4.10$$

This issue is addressed by employing the technique of iterative reconvolution. The IRF is considered to be made up of many  $\delta$ -functions, each producing its own fluorescence decay. The observed fluorescence intensity at any point of time then becomes the sum of responses to these  $\delta$ -functions. The user provides a gamut of guess values for amplitudes and lifetimes manually. Alternatively, a Monte Carlo simulation using the IBH DAS-v6.2 program, self generates these guess values. A decay profile is generated and convoluted numerically with IRF. This generated curve is compared with the experimental curve using nonlinear regression analysis. The guess values are adjusted till convergence is achieved. The goodness of the fits is judged by the closeness of the value of the reduced  $\chi^2$ , defined by equation 4.11<sup>6</sup>

$$\chi^2 = \frac{1}{n-1} \sum_{k=1}^n \frac{[N(t_k) - N_c(t_k)]^2}{\sigma_k^2} \simeq 1 \quad 4.11$$



where  $N(t_k)$  and  $N_c(t_k)$  are the experimental and calculated values of the time resolved fluorescence intensity at time  $t_k$ ,  $k$  being the data point in question.  $\sigma_k$  is the standard deviation associated with the  $k^{th}$  data point and is defined by equation 4.12

$$\sigma_k = \sqrt{N(t_k)} \quad 4.12$$

The statistics considered for the above approximation is based on a Poisson distribution. The goodness of fit is also judged by the randomness of the weighed residuals of the experimental data with that of the calculated data. The weighed residual  $r(t_k)$  of the data is defined as equation 4.13

$$r(t_k) = \frac{N(t_k) - N_c(t_k)}{\sigma_k} \quad 4.13$$

#### **4.3.4. Time Resolved Fluorescence Measurement in Picosecond-Femtosecond Time Regime**

Femtosecond upconversion fluorescence technique involves measuring the lifetimes of molecules in the femtosecond-picosecond regime. The need of this method arises from the occurrence of an ultrafast processes that cannot be resolved in the TCSPC.

##### **4.3.4.1. Femtosecond Optically Gated (FOG) system**

The Femtosecond Optically Gated (FOG) system uses the nonlinear sum frequency generation (upconversion) technique to get very fine time resolution (Figure 4.4 and Figure 4.5). Laser induced fluorescence (LIF), generated by a femtosecond laser pulse and directed to a nonlinear element, produces sum frequency radiation (SFR) provided that the LIF and a delayed gate pulse (fundamental pulse) overlap spatially as well as temporally at the nonlinear element. The delay time is controlled in such a way so that the best temporal overlap is achieved. SFR photons are counted by PMT and are proportional to the fluorescence signal. For the Ti:Sapphire

laser, operating  $\sim 100$  MHz pulse repetition rate, the maximum photon counting signal is  $2 \times 10^6$  counts  $s^{-1}$ .

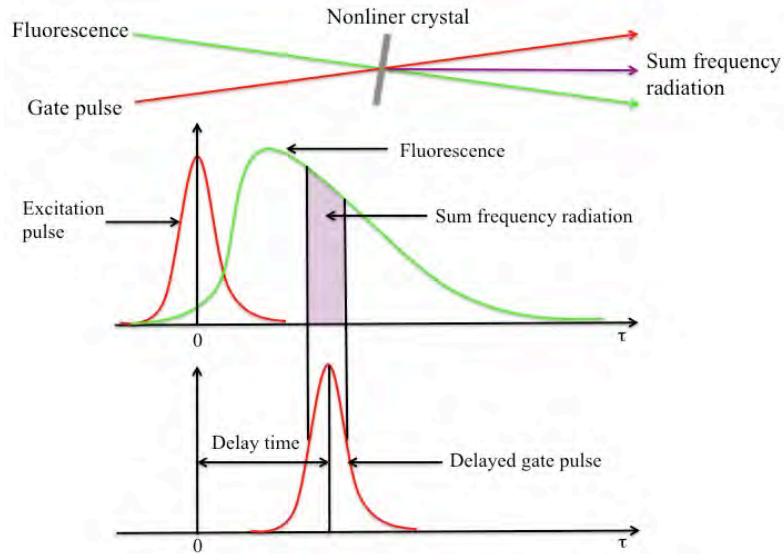


**Figure 4.4.** Schematic representation of fluorescence upconversion. Sum frequency radiation is generated in a nonlinear crystal only during the time that a delayed laser pulse is present.

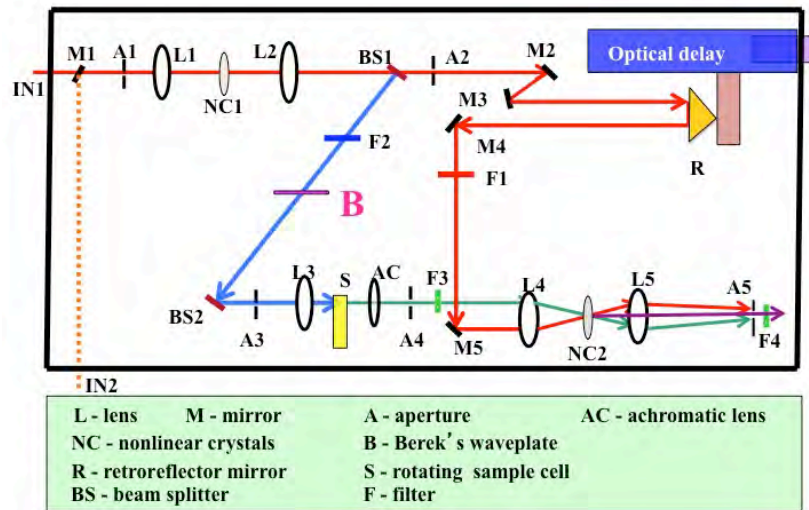


**Figure 4.5.** Schematic representation of FOG system

#### 4.3.4.2.1. The Pump for the Femtosecond Laser: Millennia Pro s-Series

The Millennia Pro is a diode pump, continuous wave solid state laser system, where a diode excites a  $\text{Nd:YVO}_4$  crystal. The diode provides a monochromatic wavelength and is advantageous over using xenon arc lamp. The diode, for our set up, excites  $\text{Nd}^{3+}$  at *ca.* 815 nm.

The excited electrons drop to the  $^4F_{3/2}$  level, which is the upper level of the lasing transition and remain there for almost 60  $\mu\text{s}$ . The most probable lasing occurs due to the  $^4F_{3/2} \rightarrow ^4I_{1/2}$  transition emitting a photon at 1064 nm which is frequency doubled using an LBO (lithium triborate) nonlinear crystal to 532 nm and used as the excitation pulse for the Ti:Sapphire crystal.

#### 4.3.4.2.2. *Tsunami: Mode-locked Ti:Sapphire Laser*

$\text{Ti}^{3+}$  ions are responsible for the lasing action of Ti:Sapphire where  $\text{Ti}_2\text{O}_3$  is doped inside an  $\text{Al}_2\text{O}_3$  matrix. The electronic ground state of the  $\text{Ti}^{3+}$  ion is split into vibrationally broadened levels as shown in figure 4.6

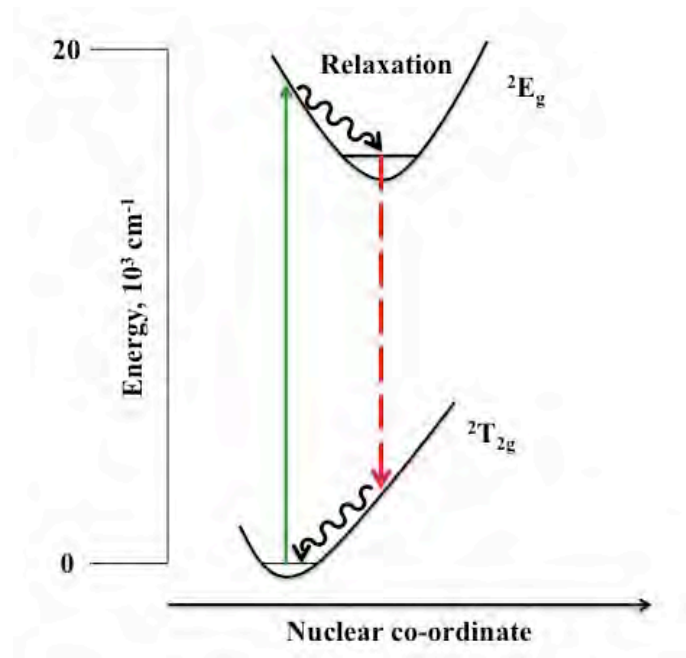


**Figure 4.6.** Schematics of electronic states of  $\text{Ti}^{3+}$

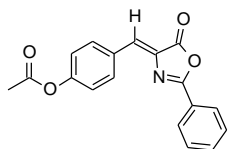
$\text{Ti}^{3+}$  ions have a broad absorption band, ranging from 400 nm to 600 nm. Upon excited by the 532 nm laser (Millennia Pro), fluorescence transition in  $\text{Ti}^{3+}$  occurs from the lower vibrational levels of the excited state to the upper vibrational levels of the ground state and shows a broad emission band from 600 nm to above 1000 nm. The lasing action is only possible above 670 nm as below that the fluorescence overlaps with tail end of absorption.

#### 4.3.4.3. *Experimental Details*

The output of femtosecond pulsed oscillator from the mode-locked Ti:sapphire laser (Tsunami, Spectra Physics, USA) pumped by 5 W DPSS laser (Millennia, Spectra Physics), centred at 800 nm and with a repetition rate of 80 MHz, was used as the gate pulse for the femtosecond fluorescence upconversion experiments. The second harmonic (400 nm) of this pulse was used as the source of excitation for the sample placed in a rotating cell with 1 mm pathlength for the experiments with epicocconone and its analogues. The power of the second harmonic light is restricted to 5 mW at the sample in order to minimize photobleaching. The fluorescence from the sample is upconverted in a nonlinear crystal (0.5 mm BBO,  $\theta = 38^\circ$ ,  $\phi = 90^\circ$ ) by mixing with the gate pulse, which consists of a portion of the fundamental beam. The upconverted light is dispersed in a monochromator and detected using photon counting electronics. A cross-correlation function obtained using the Raman scattering from ethanol has a FWHM of 300 fs. The intensity dependence was checked after each experiment. The femtosecond fluorescence decays have been fitted using a Gaussian function of the same FWHM as the excitation pulse. The fluorescence decays were recorded at the magic angle polarization with respect to the excitation pulse on FOG 100 fluorescence optically gated upconversion spectrometer (CDP Systems Corp., Russia). The resolution was in appropriate multiples of the minimum step size of the instrument, *i.e.* 0.78 fs/step. The decays were analyzed by iterative reconvolution using a homemade program.<sup>181</sup>

## 4.4. Synthesis of GFP Analogues

**(Z)-4-((5-oxo-2-phenyloxazol-4(5H)-ylidene)methyl)phenylacetate (1a).** To a solution of 4-



formylphenyl acetate (0.13 mL, 0.82 mmol) in acetic anhydride (5 mL) was

added hippuric acid (0.14 g, 0.82 mmol) and sodium acetate (0.067 g, 0.82

mmol) and the reaction mixture was refluxed for two hours, cooled and then poured into ice

water (30 mL) and stirred for 20 min. The precipitate was filtered, washed several times with ice

cold ethanol and dried *in vacuo*. The product was recrystallized from DCM/PE and to yield

oxazolylidene (**1a**) as a pale yellow solid (1.5 g, 60%) which was used immediately in the next

step, m.p. 180.5 °C [lit. m.p. 179 °C]<sup>182</sup>; UV (acetonitrile)  $\lambda_{\text{max}}$  364 nm ( $\epsilon$  = 95000); IR (ATR)

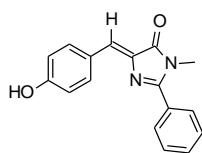
$\nu_{\text{max}}$  1793, 1755, 1653  $\text{cm}^{-1}$ ;  $^1\text{H}$  NMR (400 MHz,  $\text{CDCl}_3$ )  $\delta$  8.25 (d,  $J$  = 8.6 Hz, 2H), 8.18 (d,  $J$  =

7.5 Hz, 2H), 7.62 (t,  $J$  = 7.32 Hz, 1H), 7.54 (t,  $J$  = 7.32 Hz, 2H), 7.23 (m, 3H), 2.34 (s, 3H);  $^{13}\text{C}$

NMR (125 MHz,  $\text{CDCl}_3$ )  $\delta$  170.75, 163.65, 133.08, 132.99, 131.13, 129.23, 128.97, 128.91,

128.64, 127.97, 125.99, 125.95, 55.16.

**(Z)-4-(4-hydroxybenzylidene)-1-methyl-2-phenyl-1H-imidazol-5(4H)-one (1c).** To an ethanolic



solution of (Z)-4-((5-oxo-2-phenyloxazol-4(5H)-ylidene)methyl)phenyl acetate

(**1a**, 0.1 g, 0.33 mmol) was added aqueous methylamine (40%, 0.1 mL) and

potassium carbonate (0.045 g, 0.33 mmol) and the solution was refluxed under

$\text{N}_2$  for three hours, cooled extracted with ethyl acetate (20 mL), washed with water (3  $\times$  50 mL)

and concentrated *in vacuo*. The crude product was purified by flash chromatography to provide

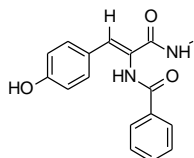
the imidazolone (**1c**, 0.032 g, 35%) as a bright yellow solid (0.032 g, 35%), m.p. 203 °C; UV

(acetonitrile)  $\lambda_{\text{max}}$  297 nm ( $\epsilon$  = 30700); IR (ATR)  $\nu_{\text{max}}$  3169, 1673, 1640  $\text{cm}^{-1}$ ;  $^1\text{H}$  NMR (600

MHz,  $\text{CDCl}_3$ )  $\delta$  8.15 (d,  $J$  = 8.78 Hz, 2H), 7.84 (dd,  $J$  = 8.00, 1.5 Hz, 2H), 7.55 (m, 3H), 7.24 (s,

1H), 6.88 (d,  $J$  = 6.78 Hz, 2H), 3.36(s, 3H);  $^{13}\text{C}$  NMR (150 MHz,  $\text{CDCl}_3$ )  $\delta$  158.40, 135.04,

131.56, 129.71, 128.99, 128.80, 127.30, 116.13, 29.24; MS (ESI)  $m/z$  279; HRMS (ESI) calcd. for  $C_{17}H_{15}N_2O_2$   $m/z$  279.1133  $[M+H]^+$ , found  $m/z$  279.1134.

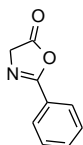


Alternatively, (Z)-4-((5-oxo-2-phenyloxazol-4(5H)-ylidene)methyl)phenyl acetate (**1a**, 0.1 g, 0.33 mmol) was dissolved in  $CH_2Cl_2$  and acetonitrile saturated with dry methylamine (0.15 mL) was added to it and the mixture was stirred for 1 hour. A white precipitate was formed, which is soluble in excess

acetonitrile. The reaction mixture was concentrated in vacuo and washed with cold  $CH_2Cl_2$  and dried to yield (Z)-N-(1-(4-hydroxyphenyl)-3-(methylamino)-3-oxoprop-1-en-2-yl)benzamide (**1b**, 0.97 g, 100%), m.p. 144 °C; UV (acetonitrile)  $\lambda_{max}$  389 nm ( $\epsilon = 16600$ ); IR (ATR)  $\nu_{max}$  3237, 1648  $cm^{-1}$ ;  $^1H$  NMR (400 MHz,  $DMSO-d_6$ )  $\delta$  9.77 (s, 1H), 8.0 (d,  $J = 7.13$  Hz, 2H), 7.91 (quart,  $J = 4.57$  Hz, 1H), 7.47 (m, 3H), 7.37 (d,  $J = 8.6$  Hz, 2H), 7.18 (s, 1H), 6.70 (d,  $J = 8.6$  Hz, 2H), 2.64 (d,  $J = 3.58$  Hz, 3 H);  $^{13}C$  NMR (125 MHz,  $DMSO-d_6$ )  $\delta$  166.66, 166.53, 159.00, 134.72, 132.43, 132.03, 130.55, 129.13, 128.77, 127.82, 125.93, 116.23, 27.20; MS (ESI)  $m/z$  297; HRMS (ESI) calcd. for  $C_{17}H_{17}N_2O_3$   $m/z$  297.1234  $[M+H]^+$ , found  $m/z$  297.1239.

**1b** was heated in furnace at 350 °C for 60 seconds to give an orange solid which was purified by flash chromatography to yield the imidazolone **1c** (0.074 g, 80%).

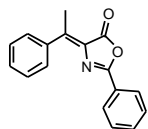
2-phenyloxazol-5(4H)-one (**II**) was prepared following literature procedure.<sup>183</sup>



Briefly hippuric acid (**I**, 2 g, 0.012 mol) was added to acetic anhydride (8 mL) and the solution was heated at 90 °C for 30 min until all the hippuric acid had dissolved and the colour of the solution became dark orange. The solution was then cooled and poured into ice-diethyl ether mixture (100 mL). The organic layer was repeatedly washed with water then 1%  $NaHCO_3$  solution to remove the traces of acetic acid. The ether layer was dried over  $MgSO_4$  and concentrated in vacuo to yield the phenyl oxazolone (**II**) as a yellow solid (1.5 g, 77%), m.p. 85 °C [lit. m.p. 84–86 °C]<sup>183</sup>;  $^1H$  NMR (400 MHz,  $CDCl_3$ )  $\delta$  7.99 (d,  $J = 7.13$  Hz, 2 H) 7.58 (t,  $J =$

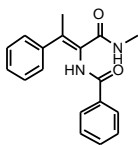
7.4 Hz, 1 H), 7.49 (t,  $J$  = 7.6 Hz, 1 H), 4.42 (s, 2 H);  $^{13}\text{C}$  NMR (125 MHz,  $\text{CDCl}_3$ )  $\delta$  170.8, 163.7, 133.1, 133.0, 129.0, 128.0, 126.0, 55.2.

**(Z)-2-phenyl-4-(1-phenylethylidene)oxazol-5(4H)-one (2a).** THF (10 mL) was chilled under  $\text{N}_2$



to  $-10\text{ }^\circ\text{C}$ . To it,  $\text{TiCl}_4$  (0.075 mL, 0.685 mmol) in  $\text{CH}_2\text{Cl}_2$  (0.2 mL) was added and stirred for 10 min. To the stirring solution, 4-acetylphenyl acetate (**2**, 0.1028 mL, 0.83 mmol) was added and the mixture was stirred for five min, then 2-phenyloxazol-5(4H)-one (**II**, 0.267 g, 1.66 mmol) was added and stirred for a further 20 min. To the mixture, pyridine (0.15 mL) was added dropwise. The black mixture was stirred for a further 5 hours and was monitored by TLC until there were no starting materials left. The reaction was then quenched with saturated ammonium chloride solution (3 mL) and extracted with ethyl acetate ( $3 \times 10\text{ mL}$ ). The organic layer was washed thoroughly with water ( $4 \times 10\text{ mL}$ ) and brine solution ( $2 \times 10\text{ mL}$ ) and concentrated under vacuo. The oxazolone was purified by flash chromatography and recrystallized from DCM/PE to yield a yellow solid (**2a**, 0.077 g, 35%), m.p.  $110\text{ }^\circ\text{C}$  [lit m.p.  $108\text{--}110\text{ }^\circ\text{C}$ ]<sup>184,185</sup>; UV (acetonitrile)  $\lambda_{\text{max}}$  346 nm ( $\epsilon$  = 28500); IR (ATR)  $\nu_{\text{max}}$  1783, 1756  $\text{cm}^{-1}$ ;  $^1\text{H}$  NMR (400 MHz,  $\text{CDCl}_3$ )  $\delta$  8.08 (m, 1H), 8.06 (m, 1H), 7.89 (m, 1H), 7.87 (m, 1H), 7.55 (m, 1H), 7.49 (m, 1H), 7.47 (m, 2H), 7.46 (m, 2H), 2.8 (s, 3H);  $^{13}\text{C}$  NMR (125 MHz,  $\text{CDCl}_3$ )  $\delta$  166.97, 160.57, 149.40, 139.06, 132.80, 131.39, 130.10, 130.07, 128.92, 128.27, 128.08, 125.99, 18.51.

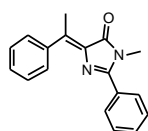
**(Z)-N-(1-(methylamino)-1-oxo-3-phenylbut-2-en-2-yl)benzamide (2b).** (Z)-2-phenyl-4-(1-



phenylethylidene)oxazol-5(4H)-one (**2a**, 0.1 g, 0.38 mmol) was dissolved in  $\text{CH}_2\text{Cl}_2$  (2 mL) and acetonitrile saturated with dry methylamine (0.15 mL) was added to it and the mixture was stirred for 15 min. A white precipitate was formed. The reaction mixture was concentrated in vacuo and washed with cold  $\text{CH}_2\text{Cl}_2$  ( $3 \times 3\text{ mL}$ ) and dried in vacuo to yield (Z)-N-(1-(methylamino)-1-oxo-3-phenylbut-2-en-2-yl)benzamide (**2b**, 0.098 g, 98%) as a

white powder that was used in the next step without further purification, m.p. 245 °C; UV (acetonitrile  $\lambda_{\text{max}}$  294 nm ( $\epsilon = 10300$ ); IR (ATR)  $\nu_{\text{max}}$  3278, 1638  $\text{cm}^{-1}$ ;  $^1\text{H}$  NMR (400 MHz,  $\text{DMSO-}d_6$ )  $\delta$  9.31 (s, 1H), 7.85 (quart,  $J = 4.76$  Hz, 1H), 7.65 (d,  $J = 7.7$  Hz, 2H), 7.45 (t,  $J = 8.05$  Hz, 1H), 7.36 (t,  $J = 7.6$  Hz, 2H), 7.25 (m, 4H), 7.19 (dd,  $J = 3.00$  Hz 1H), 2.65 (d,  $J = 4.6$  Hz, 3H), 2.24 (s, 3H);  $^{13}\text{C}$  NMR (125 MHz,  $\text{DMSO-}d_6$ )  $\delta$  167.05, 166.87, 142.09, 138.63, 134.77, 132.15, 128.92, 128.84, 128.50, 128.30, 128.13, 127.76, 26.76, 21.34; MS (ESI)  $m/z$  295; HRMS (ESI) calcd. for  $\text{C}_{18}\text{H}_{19}\text{N}_2\text{O}_2$   $m/z$  295.1441  $[\text{M}+\text{H}^+]$ , found  $m/z$  295.1447.

**(Z)-1-methyl-2-phenyl-4-(1-phenylethylidene)-1H-imidazol-5(4H)-one** (**2c**). (Z)-N-(1-



(methylamino)-1-oxo-3-phenylbut-2-en-2-yl)benzamide (**2b**, 0.1 g, 0.34 mmol)

was kept in furnace at 350 °C for 60 seconds to give an orange-yellow product which was purified by flash chromatography to yield the imidazolone as an orange-yellow oil (**2c**, 0.066 g, 70%) as a mixture of isomers.

Upon separation by chromatography a 7:1:: major:minor compounds were found which even on HPLC purification was not separated as there was facile isomerization to change one isomer into another. The compounds were tried to be crystallized but could not be done. The mixture of the compounds were tried to separate and identify by NMR signals, but nothing could be concluded based on NOE signals. Both the isomers showed correlation between the ortho proton of benzyl group and the allylic ethyl proton. The only differences found were a change in chemical shift and higher  $^{15}\text{N}$ - $^1\text{H}$  correlation for the major isomer.

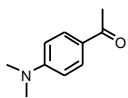
Major isomer: UV (acetonitrile)  $\lambda_{\text{max}}$  356 nm ( $\epsilon = 6600$ ); IR (ATR)  $\nu_{\text{max}}$  1640, 1626  $\text{cm}^{-1}$ ;  $^1\text{H}$  NMR (600 MHz,  $\text{CDCl}_3$ )  $\delta$  7.85 (m, 2H,  $-\text{CH}_{\text{ar}}$ ), 7.74 (m, 2H,  $-\text{CH}_{\text{ar}}$ ), 7.49 (m, 3H,  $-\text{CH}_{\text{ar}}$ ), 7.42 (m, 2H,  $-\text{CH}_{\text{ar}}$ ), 7.36 (m, 1H,  $-\text{CH}_{\text{ar}}$ ), 3.34 (s, 3H,  $-\text{NCH}_3$ ) 2.85 (s, 3H,  $-\text{CH}_3$ );  $^{13}\text{C}$  NMR (125 MHz,  $\text{CDCl}_3$ )  $\delta$  171.02, 158.94, 146.90, 140.02, 136.73, 131.04, 130.30, 129.73, 129.23, 128.92, 128.79, 128.65, 128.24, 128.05, 127.41, 127.05, 28.93, 18.50;  $^{15}\text{N}$  NMR (60.8 MHz,  $\text{CDCl}_3$ )  $\delta$



242, 199; MS (ESI)  $m/z$  277; HRMS (ESI) calcd. for  $C_{18}H_{17}N_2O$   $m/z$  277.1336  $[M+H^+]$ , found  $m/z$  277.1341.

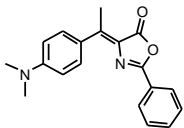
Minor isomer: UV (acetonitrile)  $\lambda_{max}$  359 nm ( $\epsilon$  =6650); IR (ATR)  $\nu_{max}$  1696, 1627  $cm^{-1}$ ;  $^1H$  NMR (600 MHz,  $CDCl_3$ )  $\delta$  7.78 (m, 2H,  $-CH_{ar}$ ), 7.54 (m, 3H,  $-CH_{ar}$ ), 7.49 (m, 2H,  $-CH_{ar}$ ), 7.42 (m, 3H,  $-CH_{ar}$ ), 3.21 (s, 3H,  $-NCH_3$ ), 2.62 (s, 3H,  $-CH_3$ );  $^{13}C$  NMR (125 MHz,  $CDCl_3$ )  $\delta$  168.10, 159.71, 149.53, 138.69, 137.39, 131.25, 131.11, 130.34, 129.76, 129.65, 129.29, 129.14, 128.99, 128.85, 128.70, 128.55, 128.43, 128.27, 128.13, 28.81, 22.78;  $^{15}N$  NMR (60.8 MHz,  $CDCl_3$ )  $\delta$  200; MS (ESI)  $m/z$  277; HRMS (ESI) calcd. for  $C_{18}H_{17}N_2O$   $m/z$  277.1336  $[M+H^+]$ , found  $m/z$  277.1341.

**1-(4-(dimethylamino)phenyl)ethanone (3)** was prepared following literature procedure.<sup>186</sup>



Briefly, 1-(4-aminophenyl)ethanone (0.1 g, 0.74 mmol) was taken in DMF (2 mL) and stirred for 10 min at room temperature. To the stirring solution was added  $K_2CO_3$  (0.205 g, 1.48 mmol) and MeI (0.138 mL, 2.2 mmol) and was further stirred for 48 hrs at 40 °C, quenched with cold water and extracted with ethyl acetate ( $3 \times 10$  mL). The organic layer was washed thoroughly with water ( $4 \times 10$  mL) concentrated under vacuo. The final product was purified by flash chromatography and recrystallized from DCM/PE to yield a white solid (0.078 g, 65%), m.p. 105 °C [lit. m.p. 105 °C].<sup>187</sup>

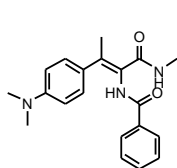
**(Z)-4-(1-(4-(dimethylamino)phenyl)ethylidene)-2-phenyloxazol-5(4H)-one (3a)**. THF (10 mL)



was chilled under  $N_2$  to  $-10$  °C. To it,  $TiCl_4$  (0.075 mL, 0.685 mmol) in  $CH_2Cl_2$  (0.2 mL) was added and stirred for 10 min. To the stirring solution, 1-(4-(dimethylamino)phenyl)ethanone (0.1 g, 0.61 mmol) was added and the mixture was stirred for five min, then 2-phenyloxazol-5(4H)-one (**II**, 0.196 g, 1.22 mmol) was added and stirred for a further 20 min. To the mixture, pyridine (0.15 mL) was added dropwise. The black mixture was stirred for a further 5 hours and was monitored by TLC until there were

no starting materials left. The reaction was then quenched with saturated ammonium chloride solution (3 mL) and extracted with ethyl acetate (3 × 10 mL). The organic layer was washed thoroughly with water (4 × 10 mL) and brine solution (2 × 10 mL) and concentrated under vacuo. The oxazolone was purified by flash chromatography and recrystallized from DCM/PE to yield a bright orange solid (0.075 g, 40%), m.p. 165 °C; UV (acetonitrile)  $\lambda_{\max}$  445 nm ( $\epsilon$  = 24500); IR (ATR)  $\nu_{\max}$  2918, 1735, 1627  $\text{cm}^{-1}$ ;  $^1\text{H}$  NMR (400 MHz,  $\text{CDCl}_3$ )  $\delta$  8.09 (m, 4H), 7.49 (m, 3H), 6.83 (m, 2H), 3.09 (s, 6H), 2.78 (s, 3H);  $^{13}\text{C}$  NMR (125 MHz,  $\text{CDCl}_3$ )  $\delta$  167.61, 160.04, 159.64, 158.71, 151.26, 149.31, 132.66, 132.16, 131.05, 128.85, 128.25, 127.73, 127.02, 126.50, 112.25, 111.94, 40.63, 17.45; MS (ESI)  $m/z$  307; HRMS (ESI) calcd. for  $\text{C}_{19}\text{H}_{19}\text{N}_2\text{O}_2$   $m/z$  307.1442  $[\text{M}+\text{H}^+]$ , found  $m/z$  307.1447.

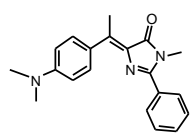
**(Z)-N-(3-(4-(dimethylamino)phenyl)-1-(methylamino)-1-oxobut-2-en-2-yl)benzamide(3b).** (Z)-



4-(1-(4-(dimethylamino)phenyl)ethylidene)-2-phenyloxazol-5(4H)-one (**3a**, 0.1 g, 0.33 mmol) was dissolved in  $\text{CH}_2\text{Cl}_2$  (2 mL) and acetonitrile saturated with dry methylamine (0.15 mL) was added to it and the mixture was stirred for 15

min. A white precipitate was formed. The reaction mixture was concentrated in vacuo and washed with cold  $\text{CH}_2\text{Cl}_2$  (3 × 3 mL) and dried in vacuo to give (Z)-N-(3-(4-(dimethylamino)phenyl)-1-(methylamino)-1-oxobut-2-en-2-yl)benzamide (**3b**, 0.11 g, 100%) as a white powder that was used in the next step without further purification, m.p. 137 °C; UV (acetonitrile)  $\lambda_{\max}$  314 nm ( $\epsilon$  = 12100); IR (ATR)  $\nu_{\max}$  3340, 3208, 1640  $\text{cm}^{-1}$ ;  $^1\text{H}$  NMR (400 MHz,  $\text{DMSO}-d_6$ )  $\delta$  9.26 (s, 1H), 7.74 (m, 3H), 7.47 (t,  $J$  = 7.5 Hz, 1H), 7.38 (t,  $J$  = 7.5 Hz, 2H), 7.13(d,  $J$  = 8.6 Hz, 2H), 6.59 (d,  $J$  = 8.9 Hz, 2H), 2.82 (s, 6H), 2.63 (d,  $J$  = 4.6 Hz, 3H), 2.18 (s, 1H);  $^{13}\text{C}$  NMR (125 MHz,  $\text{DMSO}-d_6$ )  $\delta$  167.58, 166.80, 150.45, 137.59, 134.81, 132.15, 129.36, 128.96, 128.58, 126.40, 112.41, 26.77, 21.08; MS (ESI)  $m/z$  338; HRMS (ESI) calcd. for  $\text{C}_{20}\text{H}_{24}\text{N}_3\text{O}_2$   $m/z$  338.1871  $[\text{M}+\text{H}^+]$ , found  $m/z$  338.1869.

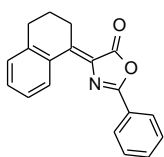
**(Z)-4-(1-(4-(dimethylamino)phenyl)ethylidene)-1-methyl-2-phenyl-1H-imidazol-5(4H)-one**



**(3c).** (Z)-N-(3-(4-(dimethylamino)phenyl)-1-(methylamino)-1-oxobut-2-en-2-yl)benzamide (**3b**, 0.1 g, 0.3 mmol) was kept in furnace at 350 °C for 60

seconds to give an orange-yellow product which was purified by flash chromatography to yield the imidazolone as a yellow solid (0.071 g, 65%), m.p. 178.5 °C; UV (acetonitrile)  $\lambda_{\text{max}}$  430 nm ( $\epsilon = 31400$ ); IR (ATR)  $\nu_{\text{max}}$  3314, 1679  $\text{cm}^{-1}$ ;  $^1\text{H}$  NMR (600 MHz,  $\text{CDCl}_3$ )  $\delta$  8.06 (m, 2H, - $\text{CH}_{\text{ar}}$ ), 7.77 (m, 2H, - $\text{CH}_{\text{ar}}$ ), 7.49 (m, 3H, - $\text{CH}_{\text{ar}}$ ), 6.73 (m, 2H, - $\text{CH}_{\text{ar}}$ ), 3.35 (s, 3H, - $\text{NCH}_3$ ), 3.03 (m, 6H, - $\text{N}(\text{CH}_3)_2$ ), 2.85 (s, 3H, - $\text{CH}_3$ );  $^{13}\text{C}$  NMR (150 MHz,  $\text{CDCl}_3$ )  $\delta$  171.08, 156.55, 151.31, 147.29, 134.36, 132.67, 130.59, 130.28, 128.74, 128.63, 127.10, 111.35, 40.25, 28.94, 17.52;  $^{15}\text{N}$  NMR (60.8 MHz,  $\text{CDCl}_3$ )  $\delta$  100, 200; MS (ESI)  $m/z$  320; HRMS (ESI) calcd. for  $\text{C}_{20}\text{H}_{22}\text{N}_3\text{O}$   $m/z$  320.1764  $[\text{M}+\text{H}^+]$ , found  $m/z$  320.1763.

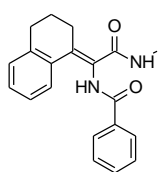
**(Z)-4-(3,4-dihydronaphthalen-1(2H)-ylidene)-2-phenyloxazol-5(4H)-one (4a).** THF (10 mL)



was chilled under  $\text{N}_2$  to -10°C. To it,  $\text{TiCl}_4$  (0.075 mL, 0.685 mmol) in  $\text{CH}_2\text{Cl}_2$  (0.2 mL) was added and stirred for 10 min. To the stirring solution, tetralone (0.0912 mL, 0.685 mmol) was added and the mixture was stirred for five min, then 2-phenyloxazol-5(4H)-one (**II**, 0.165 g, 1.03 mmol) was added and stirred for a further 20 min. To the mixture, pyridine (0.15 mL) was added dropwise. The black mixture was stirred for a further 5 hours and was monitored by TLC until there were no starting materials left. The reaction was then quenched with saturated ammonium chloride solution (3 mL) and extracted with ethyl acetate ( $3 \times 10$  mL). The organic layer was washed thoroughly with water ( $4 \times 10$  mL) and brine solution ( $2 \times 10$  mL) and concentrated under vacuo. The oxazolone was purified by flash chromatography and recrystallized from DCM/PE to yield a yellow solid (0.07 g, 35%),

m.p. 140 °C. [lit. m.p 140 °C]; UV (acetonitrile)  $\lambda_{\text{max}} = 365 \text{ nm}$  ( $\epsilon = 31000$ ); IR (ATR)  $\nu_{\text{max}}$  1789, 1756, 1636  $\text{cm}^{-1}$ ;  $^1\text{H}$  NMR (400 MHz,  $\text{CDCl}_3$ )  $\delta$  8.91 (m, 1H), 8.12 (m, 2H), 7.57 (m, 1H), 7.50 (m, 2H) 7.36 (m, 2H), 7.22 (m, 1H), 3.35 (t,  $J = 6.2 \text{ Hz}$ , 2H), 2.87 (t,  $J = 6.2 \text{ Hz}$ , 2H), 1.96 (quin,  $J = 6.2 \text{ Hz}$ , 2H);  $^{13}\text{C}$  NMR (125 MHz,  $\text{CDCl}_3$ )  $\delta$  167.11, 160.39, 148.86, 142.77, 133.17, 132.92, 132.70, 130.94, 128.97, 128.01, 126.29, 30.64, 28.27, 22.58; MS (ESI)  $m/z$  290; HRMS (ESI) calcd. for  $\text{C}_{19}\text{H}_{16}\text{NO}_2$   $m/z$  290.1184  $[\text{M}+\text{H}^+]$ , found  $m/z$  290.1181.

**(Z)-N-(1-(3,4-dihydronaphthalen-1(2H)-ylidene)-2-(methylamino)-2-oxoethyl)benzamide (4b).**



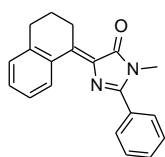
(Z)-4-(3,4-dihydronaphthalen-1(2H)-ylidene)-2-phenyloxazol-5(4H)-one (**4a**, 0.1

g, 0.35 mmol) was dissolved in  $\text{CH}_2\text{Cl}_2$  (2 mL) and acetonitrile saturated with dry

methylamine (0.15 mL) was added to it and the mixture was stirred for 15 min. A

white precipitate was formed. The reaction mixture was concentrated in vacuo and washed with cold  $\text{CH}_2\text{Cl}_2$  ( $3 \times 3 \text{ mL}$ ) and dried in vacuo to yield (Z)-N-(1-(3,4-dihydronaphthalen-1(2H)-ylidene)-2-(methylamino)-2-oxoethyl)benzamide (**4b**, 0.11 g, 100%) as a white powder that was used in the next step without further purification, m.p. 230 °C; UV (acetonitrile)  $\lambda_{\text{max}}$  300 nm ( $\epsilon = 50000$ ); IR (ATR)  $\nu_{\text{max}}$  3251, 1640  $\text{cm}^{-1}$ ;  $^1\text{H}$  NMR (400 MHz,  $\text{DMSO}-d_6$ )  $\delta$  9.71 (br, s, 1H), 7.91 (d,  $J = 4.21 \text{ Hz}$ , 1H), 7.85 (m, 2H), 7.52 (m, 1H), 7.43 (m, 3 H), 7.15 (m, 2H), 7.01 (m, 1 H), 2.74 (t,  $J = 6.6 \text{ Hz}$ , 2H), 2.66 (m, 5H), 1.79 (quin,  $J = 6.5 \text{ Hz}$ , 2H);  $^{13}\text{C}$  NMR (125 MHz,  $\text{DMSO}-d_6$ )  $\delta$  167.33, 166.65, 139.97, 135.67, 135.48, 132.28, 129.34, 129.04, 128.66, 128.45, 126.86, 125.94, 29.61, 28.71, 26.80, 25.15; MS (ESI)  $m/z$  321; HRMS (ESI) calcd. for  $\text{C}_{20}\text{H}_{21}\text{N}_2\text{O}_2$   $m/z$  321.1605  $[\text{M}+\text{H}^+]$ , found  $m/z$  321.1603.

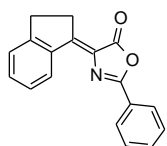
**(Z)-4-(3,4-dihydronaphthalen-1(2H)-ylidene)-1-methyl-2-phenyl-1H-imidazol-5(4H)-one (4c).**



(Z)-N-(1-(3,4-dihydronaphthalen-1(2H)-ylidene)-2-(methylamino)-2-oxoethyl)benzamide (**4b**, 0.1 g, 0.31 mmol) was kept in furnace at 350 °C for 60

seconds to give an orange-yellow product which was purified by flash chromatography to yield the imidazolone as a yellow solid (0.062 g, 65%), m.p. 133 °C; UV (acetonitrile)  $\lambda_{\text{max}}$  = 376 nm ( $\epsilon$  = 12000); IR (ATR)  $\nu_{\text{max}}$  1680  $\text{cm}^{-1}$ ;  $^1\text{H}$  NMR (600 MHz,  $\text{CDCl}_3$ )  $\delta$  8.93 (m, 1H,  $-\text{CH}_{\text{ar}}$ ), 7.82 (d,  $J$ =8.02 Hz, 2H,  $-\text{CH}_{\text{ar}}$ ), 7.51 (m, 3H,  $-\text{CH}_{\text{ar}}$ ), 7.29 (m, 2H,  $-\text{CH}_{\text{ar}}$ ), 7.17 (m, 1H,  $-\text{CH}_{\text{ar}}$ ), 3.44 (t,  $J$  = 6.46 Hz, 2H,  $-\text{CH}_2$ ), 3.36 (s, 3H,  $-\text{NCH}_3$ ), 2.84 (t,  $J$  = 6.25 Hz, 2 H,  $-\text{CH}_2$ ), 1.95 (quin,  $J$  = 6.35 Hz, 2 H,  $-\text{CH}_2$ );  $^{13}\text{C}$  NMR (150 MHz,  $\text{CDCl}_3$ )  $\delta$  171.14, 158.59, 146.31, 142.65, 134.78, 133.71, 133.66, 131.04, 130.06, 129.98, 128.87, 128.70, 128.66, 126.12, 30.69, 29.02, 28.13, 22.74;  $^{15}\text{N}$  NMR (60.8 MHz,  $\text{CDCl}_3$ )  $\delta$  200; MS (ESI)  $m/z$  303; HRMS (ESI) calcd. for  $\text{C}_{20}\text{H}_{19}\text{N}_2\text{O}$   $m/z$  303.1502  $[\text{M}+\text{H}^+]$ , found  $m/z$  303.1497.

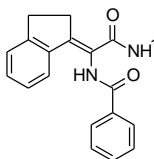
**(Z)-4-(2,3-dihydro-1H-inden-1-ylidene)-2-phenyloxazol-5(4H)-one (5a).** THF (10 mL) was



chilled under  $\text{N}_2$  to  $-10$  °C. To it,  $\text{TiCl}_4$  (0.083 mL, 0.76 mmol) in  $\text{CH}_2\text{Cl}_2$  (0.2 mL) was added and stirred for 10 min. To the stirring solution, indanone (0.1 g, 0.76 mmol) was added and the mixture was stirred for five min, then 2-phenyloxazol-5(4H)-one (**II**, 0.183 g, 1.14 mmol) was added and stirred for a further 20 min. To the mixture, pyridine (0.2 mL) was added dropwise. The black mixture was stirred for a further 5 hours and was monitored by TLC until there were no starting materials left. The reaction was then quenched with saturated ammonium chloride solution (3 mL) and extracted with ethyl acetate ( $3 \times 10$  mL). The organic layer was washed thoroughly with water ( $4 \times 10$  mL) and brine solution ( $2 \times 10$  mL) and concentrated under vacuo. The oxazolone was purified by flash chromatography and recrystallized from DCM/PE to yield a yellow solid (0.088 g, 42%), m.p. 155 °C; UV (acetonitrile)  $\lambda_{\text{max}}$  375 nm ( $\epsilon$  = 61000); IR (ATR)  $\nu_{\text{max}}$  1775, 1747  $\text{cm}^{-1}$ ;  $^1\text{H}$  NMR (400 MHz,  $\text{CDCl}_3$ )  $\delta$  8.76 (m, 1H), 8.17 (m, 2H), 7.53 (m, 3H), 7.40 (m, 3H), 3.37 (t,  $J$  = 5.6 Hz, 2H), 3.17 (t,  $J$  = 5.6 Hz, 2H);  $^{13}\text{C}$  NMR (125 MHz,  $\text{CDCl}_3$ )  $\delta$  167.10, 160.16, 155.45, 152.35, 139.26, 132.44, 132.12, 129.34, 128.91, 127.81, 127.50, 126.90, 126.41, 125.35, 30.87, 30.68;

MS (ESI)  $m/z$  276; HRMS (ESI) calcd. for  $C_{18}H_{14}NO_2$   $m/z$  276.1019  $[M+H]^+$ , found  $m/z$  276.1025.

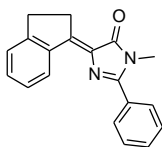
**(Z)-N-(1-(2,3-dihydro-1H-inden-1-ylidene)-2-(methylamino)-2-oxoethyl)benzamide (5b).** (Z)-



4-(2,3-dihydro-1H-inden-1-ylidene)-2-phenyloxazol-5(4H)-one (**5a**, 0.1 g, 0.36 mmol) was dissolved in  $CH_2Cl_2$  (2 mL) and acetonitrile saturated with dry methylamine (0.15 mL) was added to it and the mixture was stirred for 15 min.

A white precipitate was formed. The reaction mixture was concentrated in vacuo and washed with cold  $CH_2Cl_2$  ( $3 \times 3$  mL) and dried in vacuo to yield (Z)-N-(1-(2,3-dihydro-1H-inden-1-ylidene)-2-(methylamino)-2-oxoethyl)benzamide (**5b**, 0.11 g, 100%) as a white powder that was used in the next step without further purification, m.p. 248 °C; UV (acetonitrile)  $\lambda_{max}$  = 305 nm ( $\epsilon$  = 4200); IR (ATR)  $\nu_{max}$  3322, 3236, 1637  $cm^{-1}$ ;  $^1H$  NMR (400 MHz, DMSO- $d_6$ )  $\delta$  9.88 (br, s, 1H), 8.07 (d,  $J$  = 7.14 Hz, 2H), 7.79 (quart,  $J$  = 4.39 Hz 1H), 7.60 (m, 2H), 7.49-7.56 (m, 2H), 7.36 (d,  $J$  = 7.5 Hz, 1H), 7.25 (t,  $J$  = 7.5 Hz, 1H), 7.11 (t,  $J$  = 7.14 Hz, 1H), 3.18 (t,  $J$  = 6.77 Hz, 2H), 2.96 (t,  $J$  = 6.77 Hz, 2H), 2.66 (d,  $J$  = 4.8 Hz, 3H);  $^{13}C$  NMR (125 MHz, DMSO- $d_6$ )  $\delta$  167.12, 166.48, 149.53, 146.61, 140.08, 134.55, 132.48, 130.09, 129.22, 128.75, 127.26, 126.26, 126.15, 123.19, 32.15, 31.03, 26.90; MS (ESI)  $m/z$  307; HRMS (ESI) calcd. for  $C_{19}H_{19}N_2O_2$   $m/z$  307.1441  $[M+H]^+$ , found  $m/z$  307.1447.

**(Z)-4-(2,3-dihydro-1H-inden-1-ylidene)-1-methyl-2-phenyl-1H-imidazol-5(4H)-one (5c).** (Z)-

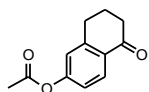


N-(1-(2,3-dihydro-1H-inden-1-ylidene)-2-(methylamino)-2-oxoethyl)benzamide (**5b**, 0.1 g, 0.33 mmol) was kept in furnace at 350 °C for 60 seconds to give an

orange-yellow product which was purified by flash chromatography to yield the imidazolone as a yellow solid (0.058 g, 62%), m.p. 128 °C; UV (acetonitrile)  $\lambda_{max}$  380 nm ( $\epsilon$  = 4600); IR (ATR)  $\nu_{max}$  1727, 1689  $cm^{-1}$ ;  $^1H$  NMR (600 MHz,  $CDCl_3$ )  $\delta$  8.83 (d,  $J$  = 7.69 Hz, 1H, -CH<sub>ar</sub>), 7.86 (m, 2H, -CH<sub>ar</sub>), 7.54 (m, 3H, -CH<sub>ar</sub>), 7.36 (m, 3H, -CH<sub>ar</sub>), 3.47 (t,  $J$  = 5.6 Hz, 2H, -CH<sub>2</sub>), 3.37 (s, 3H,

-NCH<sub>3</sub>), 3.20 (t,  $J$  = 5.6 Hz, 2H, -CH<sub>2</sub>); <sup>13</sup>C NMR (150 MHz, CDCl<sub>3</sub>)  $\delta$  170.80, 158.19, 152.75, 152.00, 140.03, 133.11, 131.33, 130.98, 130.11, 129.70, 128.90, 128.69, 127.34, 125.21, 31.04, 30.76, 28.96; <sup>15</sup>N NMR (60.8 MHz, CDCl<sub>3</sub>)  $\delta$  200; MS (ESI)  $m/z$  289; HRMS (ESI) calcd. for C<sub>19</sub>H<sub>17</sub>N<sub>2</sub>O  $m/z$  289.1333 [M+H<sup>+</sup>], found  $m/z$  289.1341.

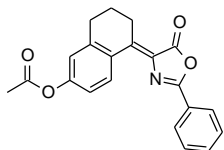
**5-oxo-5,6,7,8-tetrahydronaphthalen-2-yl acetate (6h).** 5-oxo-5,6,7,8-tetrahydronaphthalen-2-yl



acetate (**6h**, 0.5 g, 3.1 mmol) was added to acetic anhydride (5 mL) and 2 equivalent of sodium acetate (0.51 g, 6.2 mmol). The reaction mixture was

irradiated in a microwave reactor (SEM) for 3 min (300 W, 140 °C). The mixture was then poured in ice cold water and extracted with ethylacetate. The organic layer was washed thoroughly with water (4 × 25 mL) and concentrated in vacuo. Purification by flash chromatography gave the pure product (0.61 g, 97%), m.p. 62 °C [lit. m.p. 62.5 °C].<sup>188</sup>

**(Z)-5-(5-oxo-2-phenyloxazol-4(5H)-ylidene)-5,6,7,8-tetrahydronaphthalen-2-yl acetate (6a).**



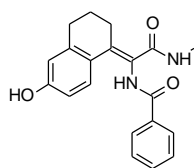
THF (10 mL) was chilled under N<sub>2</sub> to -10 °C. To it, TiCl<sub>4</sub> (0.052 mL, 0.49 mmol) in CH<sub>2</sub>Cl<sub>2</sub> (0.2 mL) was added and stirred for 10 min. To the stirring solution, 5-oxo-5,6,7,8-tetrahydronaphthalen-2-yl acetate (**6h**, 0.1 g, 0.49

mmol) was added and the mixture was stirred for five min, then 2-phenyloxazol-5(4H)-one (**II**, 0.12 g, 0.74 mmol) was added and stirred for a further 20 min. To the mixture, pyridine (0.2 mL) was added dropwise. The black mixture was stirred for a further 5 hours and was monitored by TLC until there were no starting materials left. The reaction was then quenched with saturated ammonium chloride solution (3 mL) and extracted with ethyl acetate (3 × 10 mL). The organic layer was washed thoroughly with water (4 × 10 mL) and brine solution (2 × 10 mL) and concentrated under vacuo. The oxazolone was purified by flash chromatography and recrystallized from methanol/water to yield a yellow-orange solid (0.068 g, 40%), m.p. 158 °C;

UV (acetonitrile)  $\lambda_{\text{max}}$  368 nm ( $\epsilon$  = 16000); IR (ATR)  $\nu_{\text{max}}$  1789, 1750, 1680 cm<sup>-1</sup>; <sup>1</sup>H NMR (400

MHz, CDCl<sub>3</sub>)  $\delta$  9.02 (d,  $J$  = 8.8 Hz, 1H), 8.11 (d,  $J$  = 7.14 Hz, 2H), 7.57 (t,  $J$  = 7.23 Hz, 3H), 7.50 (d,  $J$  = 7.14 Hz, 1H), 7.09 (dd,  $J$  = 8, 2.26 Hz, 1H), 6.98 (s, 1H), 3.34 (t,  $J$  = 6.50 Hz, 2 H), 2.87 (t,  $J$  = 6.22 Hz, 2 H), 2.33 (s, 3 H), 1.96 (quin,  $J$  = 6.36 Hz, 2 H); <sup>13</sup>C NMR (125 MHz, CDCl<sub>3</sub>)  $\delta$  169.28, 167.05, 160.46, 152.31, 147.63, 144.52, 134.82, 132.76, 130.63, 128.99, 128.01, 127.87, 126.14, 121.63, 119.63, 30.75, 28.05, 22.38, 21.37; MS (ESI)  $m/z$  348; HRMS (ESI) calcd. for C<sub>21</sub>H<sub>18</sub>NO<sub>4</sub>  $m/z$  348.1235 [M+H<sup>+</sup>], found  $m/z$  348.1236.

**(Z)-N-(1-(6-hydroxy-3,4-dihydronaphthalen-1(2H)-ylidene)-2-(methylamino)-2-**

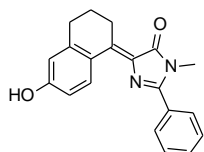


**oxoethyl)benzamide (6b).** (Z)-5-(5-oxo-2-phenyloxazol-4(5H)-ylidene)-5,6,7,8-

tetrahydronaphthalen-2-yl acetate (**6a**, 0.1 g, 0.29 mmol) was dissolved in CH<sub>2</sub>Cl<sub>2</sub> (2 mL) and acetonitrile saturated with dry methylamine (0.15 mL) was

added to it and the mixture was stirred for 15 min. A white precipitate was formed. The reaction mixture was concentrated in vacuo and washed with cold CH<sub>2</sub>Cl<sub>2</sub> (3 × 3 mL) and dried in vacuo to give (Z)-N-(1-(2,3-dihydro-1H-inden-1-ylidene)-2-(methylamino)-2-oxoethyl)benzamide (**6b**, 0.77 g, 80%) as a white powder that was used in the next step without further purification, m.p. 125 °C; UV (acetonitrile)  $\lambda_{\text{max}}$  303 nm ( $\epsilon$  = 15100); IR (ATR)  $\nu_{\text{max}}$  3364, 3273, 1644 cm<sup>-1</sup>; <sup>1</sup>H NMR (400 MHz, DMSO-*d*<sub>6</sub>)  $\delta$  9.61 (s, 1H), 7.85 (d,  $J$  = 7.5 Hz, 2H), 7.8 (quart,  $J$  = 4.57 Hz, 1H), 7.53 (t,  $J$  = 7.32 Hz, 1H), 7.45 (t,  $J$  = 7.4 Hz, 2H), 7.3 (d,  $J$  = 8.6 Hz, 1H), 6.54 (d,  $J$  = 2.2 Hz, 1H), 6.42 (dd,  $J$  = 8, 2.38 Hz, 1H), 2.58-2.72 (m, 7H), 1.75 (quin,  $J$  = 6.40 Hz, 2H); <sup>13</sup>C NMR (125 MHz, DMSO-*d*<sub>6</sub>)  $\delta$  167.64, 166.58, 157.94, 141.57, 135.83, 134.77, 132.20, 130.02, 129.03, 128.64, 126.24, 124.86, 115.43, 113.54, 29.97, 29.19, 26.80, 23.91; MS (ESI)  $m/z$  337; HRMS (ESI) calcd. for C<sub>20</sub>H<sub>21</sub>N<sub>2</sub>O<sub>3</sub>  $m/z$  337.1552 [M+H<sup>+</sup>], found  $m/z$  337.1552.

**(Z)-4-(6-hydroxy-3,4-dihydronaphthalen-1(2H)-ylidene)-1-methyl-2-phenyl-1H-imidazol-**

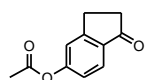


**5(4H)-one (6c).** (Z)-N-(1-(6-hydroxy-3,4-dihydronaphthalen-1(2H)-ylidene)-



2-(methylamino)-2-oxoethyl)benzamide (**6b**, 0.1 g, 0.30 mmol) was kept in furnace at 350 °C for 60 seconds to give an orange-yellow product which was purified by flash chromatography to yield the imidazolone as a yellow solid (0.057 g, 60%), m.p. 236 °C; UV (acetonitrile)  $\lambda_{\text{max}}$  389 nm ( $\epsilon = 250000$ ); IR (ATR)  $\nu_{\text{max}}$  3364, 3271, 1643  $\text{cm}^{-1}$ ;  $^1\text{H}$  NMR (600 MHz,  $\text{CDCl}_3$ )  $\delta$  8.91 (d,  $J = 8.75$  Hz, 1H,  $-\text{CH}_{\text{ar}}$ ), 7.79 (m, 2H,  $-\text{CH}_{\text{ar}}$ ), 7.53 (m, 3H,  $-\text{CH}_{\text{ar}}$ ), 6.73 (dd,  $J = 8.88, 2.77$  Hz, 1H,  $-\text{CH}_{\text{ar}}$ ), 6.59 (d,  $J = 2.81$  Hz, 1H,  $-\text{CH}_{\text{ar}}$ ), 3.42 (t,  $J = 6.44$  Hz, 2H,  $-\text{CH}_2$ ), 3.35 (s, 3H,  $-\text{NCH}_3$ ), 2.77 (t,  $J = 6.28$  Hz, 2H,  $-\text{CH}_2$ ), 1.91 (quin,  $J = 6.34$  Hz, 2H,  $-\text{CH}_2$ );  $^{13}\text{C}$  NMR (150 MHz,  $\text{CDCl}_3$ )  $\delta$  171.02, 157.64, 157.38, 146.59, 145.38, 136.07, 133.35, 130.90, 130.09, 128.98, 128.87, 128.68, 126.69, 115.02, 113.89, 30.97, 28.99, 28.30, 22.65;  $^{15}\text{N}$  NMR (60.8 MHz,  $\text{CDCl}_3$ )  $\delta$ ; MS (ESI)  $m/z$  319; HRMS (ESI) calcd. for  $\text{C}_{20}\text{H}_{19}\text{N}_2\text{O}_2$   $m/z$  319.1441  $[\text{M}+\text{H}^+]$ , found  $m/z$  319.1447.

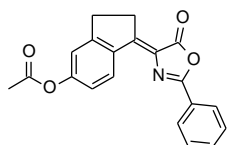
**1-oxo-2,3-dihydro-1H-inden-5-yl acetate (7).** 5-hydroxy-2,3-dihydro-1H-inden-1-one (**7h**, 0.5 g,



3.37 mmol) was added to acetic anhydride (5 mL) and 2 equivalent of sodium acetate (0.55 g, 7.74 mmol). The reaction mixture was irradiated in a microwave

reactor (SEM) for 3 min (300 W, 140 °C). The mixture was then poured in ice cold water and extracted with ethylacetate. The organic layer was washed thoroughly with water ( $4 \times 25$  mL) and concentrated in vacuo. Purification by flash chromatography gave the pure product (0.62 g, 97%), m.p. 93 °C [lit. m.p. 93-94 °C].<sup>189</sup>

**(Z)-1-(5-oxo-2-phenyloxazol-4(5H)-ylidene)-2,3-dihydro-1H-inden-5-yl acetate (7a).** THF (10

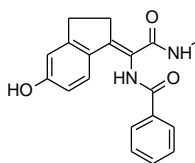


mL) was chilled under  $\text{N}_2$  to -10 °C. To it,  $\text{TiCl}_4$  (0.058 mL, 0.53 mmol) in  $\text{CH}_2\text{Cl}_2$  (0.2 mL) was added and stirred for 10 min. To the stirring solution, 1-oxo-2,3-dihydro-1H-inden-5-yl acetate (**7h**, 0.1 g, 0.53 mmol) was added

and the mixture was stirred for five min, then 2-phenyloxazol-5(4H)-one (**II**, 0.13 g, 0.85 mmol) was added and stirred for a further 20 min. To the mixture, pyridine (0.2 mL) was added

dropwise. The black mixture was stirred for a further 5 hours and was monitored by TLC until there were no starting materials left. The reaction was then quenched with saturated ammonium chloride solution (3 mL) and extracted with ethyl acetate (3 × 10 mL). The organic layer was washed thoroughly with water (4 × 10 mL) and brine solution (2 × 10 mL) and concentrated under vacuo. The oxazolone was purified by flash chromatography and recrystallized from methanol/water to yield a bright green-yellow solid (0.071 g, 40%), m.p. 198 °C; UV (acetonitrile)  $\lambda_{\text{max}}$  377 nm ( $\epsilon$  = 52500); IR (ATR)  $\nu_{\text{max}}$  1751, 1651  $\text{cm}^{-1}$ ;  $^1\text{H}$  NMR (400 MHz,  $\text{CDCl}_3$ )  $\delta$  8.79 (d,  $J$  = 8.6 Hz, 1H), 8.15 (m, 2H), 7.54 (m, 3H), 7.18 (m, 1H), 7.13 (dd,  $J$  = 8.51, 2.29 Hz, 1H), 3.44 (t,  $J$  = 5.85 Hz, 2 H), 3.22 (t,  $J$  = 5.85 Hz, 2H), 2.34 (s, 3H);  $^{13}\text{C}$  NMR (125 MHz,  $\text{CDCl}_3$ )  $\delta$  169.28, 167.15, 160.41, 154.10, 154.04, 153.81, 137.08, 132.58, 132.48, 130.45, 130.20, 128.99, 127.90, 127.74, 126.90, 126.40, 121.35, 121.02, 118.53, 31.05, 30.97, 21.36; MS (ESI)  $m/z$  334; HRMS (ESI) calcd. for  $\text{C}_{20}\text{H}_{16}\text{NO}_4$   $m/z$  334.1071  $[\text{M}+\text{H}^+]$ , found  $m/z$  334.1079.

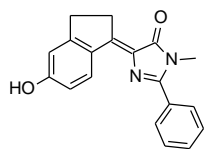
**(Z)-N-(1-(5-hydroxy-2,3-dihydro-1H-inden-1-ylidene)-2-(methylamino)-2-oxoethyl)benzamide**



**(7b).** (Z)-1-(5-oxo-2-phenyloxazol-4(5H)-ylidene)-2,3-dihydro-1H-inden-5-yl acetate (**7a**, 0.1 g, 0.3 mmol) was dissolved in  $\text{CH}_2\text{Cl}_2$  (2 mL) and acetonitrile saturated with dry methylamine (0.15 mL) was added to it and the mixture was stirred for 15 min. A white precipitate was formed. The reaction mixture was concentrated in vacuo and washed with cold  $\text{CH}_2\text{Cl}_2$  (3 × 3 mL) and dried in vacuo to yield (Z)-N-(1-(5-hydroxy-2,3-dihydro-1H-inden-1-ylidene)-2-(methylamino)-2-oxoethyl)benzamide (**7b**, 0.082 g, 85%) as a white powder that was used in the next step without further purification, m.p. 256 °C; UV (acetonitrile)  $\lambda_{\text{max}}$  306 nm ( $\epsilon$  = 18700); IR (ATR)  $\nu_{\text{max}}$  3251, 1652  $\text{cm}^{-1}$ ;  $^1\text{H}$  NMR (400 MHz,  $\text{DMSO}-d_6$ )  $\delta$  9.68 (s, 1H), 8.04 (d,  $J$  = 7.32 Hz, 2H), 7.58 (m, 2H), 7.50 (t,  $J$  = 7.2 Hz, 2H), 7.37

(d,  $J = 8.6$  Hz, 1H), 6.70 (s, 1H), 6.46 (dd,  $J = 8.0, 2.01$  Hz, 1H), 3.16 (t,  $J = 6.6$  Hz, 2H), 2.85 (t,  $J = 6.6$  Hz, 2H), 2.61 (d,  $J = 4.57$  Hz, 3H);  $^{13}\text{C}$  NMR (125 MHz, DMSO- $d_6$ )  $\delta$  167.38, 166.48, 159.76, 152.10, 147.06, 134.74, 132.337, 131.20, 129.18, 128.73, 127.50, 119.80, 115.07, 112.23, 32.48, 30.91, 26.91; MS (ESI)  $m/z$  323; HRMS (ESI) calcd. for  $\text{C}_{19}\text{H}_{19}\text{N}_2\text{O}_3$   $m/z$  323.1394  $[\text{M}+\text{H}^+]$ , found  $m/z$  323.1396.

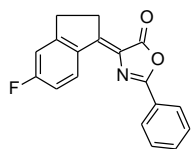
**(Z)-4-(5-hydroxy-2,3-dihydro-1H-inden-1-ylidene)-1-methyl-2-phenyl-1H-imidazol-5(4H)-one**



**(7c).** (Z)-N-(1-(5-hydroxy-2,3-dihydro-1H-inden-1-ylidene)-2-(methylamino)-2-oxoethyl)benzamide (**7b**, 0.1 g, 0.31 mmol) was kept in furnace at 350 °C

for 60 seconds to give an orange-yellow product which was purified by flash chromatography to yield the imidazolone (0.057 g, 60%), m.p. 247 °C; UV (acetonitrile)  $\lambda_{\text{max}}$  394 nm ( $\epsilon = 260000$ ); IR (ATR)  $\nu_{\text{max}}$  3384, 1675  $\text{cm}^{-1}$ ;  $^1\text{H}$  NMR (600 MHz,  $\text{CDCl}_3$ )  $\delta$  8.66 (d,  $J = 8.41$  Hz, 1H,  $-\text{CH}_{\text{ar}}$ ), 7.81 (m, 2H,  $-\text{CH}_{\text{ar}}$ ), 7.49 (m, 3H,  $-\text{CH}_{\text{ar}}$ ), 6.83 (m, 2H,  $-\text{CH}_{\text{ar}}$ ), 4.67 (b, s, 1H,  $-\text{OH}$ ), 3.42 (t,  $J = 5.54$  Hz, 2H,  $-\text{CH}_2$ ), 3.34 (s, 3H,  $-\text{NCH}_3$ ), 3.09 (t,  $J = 5.64$  Hz, 2H,  $-\text{CH}_2$ );  $^{13}\text{C}$  NMR (150 MHz,  $\text{CDCl}_3$ )  $\delta$  170.54, 161.14, 156.39, 155.19, 153.73, 131.84, 131.23, 130.65, 130.55, 130.34, 128.76, 128.52, 116.02, 111.58, 31.32, 30.86, 28.83;  $^{15}\text{N}$  NMR (60.8 MHz,  $\text{CDCl}_3$ )  $\delta$  200; MS (ESI)  $m/z$  305; HRMS calcd. for  $\text{C}_{19}\text{H}_{17}\text{N}_2\text{O}_2$   $m/z$  305.1287  $[\text{M}+\text{H}^+]$ , found  $m/z$  305.1290.

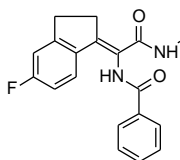
**(Z)-4-(5-fluoro-2,3-dihydro-1H-inden-1-ylidene)-2-phenyloxazol-5(4H)-one (8a).**



mL) was chilled under  $\text{N}_2$  to -10 °C. To it,  $\text{TiCl}_4$  (0.072 mL, 0.66 mmol) in  $\text{CH}_2\text{Cl}_2$  (0.2 mL) was added and stirred for 10 min. To the stirring solution, 5-fluoro-2,3-dihydro-1H-inden-1-one (**8**, 0.1 g, 0.66 mmol) was added and the mixture was stirred for five min, then 2-phenyloxazol-5(4H)-one (**II**, 0.16 g, 1.0 mmol) was added and stirred for a further 20 min. To the mixture, pyridine (0.2 mL) was added dropwise. The black mixture was stirred for a further 5 hours and was monitored by TLC until there were no starting materials left. The reaction was then quenched with saturated ammonium chloride

solution (3 mL) and extracted with ethyl acetate (3 × 10 mL). The organic layer was washed thoroughly with water (4 × 10 mL) and brine solution (2 × 10 mL) and concentrated under vacuo. The oxazolone was purified by flash chromatography and recrystallized from methanol/water to yield a yellow solid (0.071 g, 37%), m.p. 182 °C; UV (acetonitrile)  $\lambda_{\text{max}}$  = 374 nm ( $\epsilon$  = 2656); IR (ATR)  $\nu_{\text{max}}$  1767, 1657  $\text{cm}^{-1}$ ;  $^1\text{H}$  NMR (400 MHz,  $\text{CDCl}_3$ )  $\delta$  8.79 (dd,  $J$  = 8.0, 5.5 Hz, 1H), 8.15 (d,  $J$  = 7.14 Hz, 2H), 7.54 (m, 3 H), 7.1 (t,  $J$  = 8.4 Hz, 2H), 3.45 (t,  $J$  = 5.75 Hz, 2H), 3.22 (t,  $J$  = 5.48 Hz, 2H);  $^{13}\text{C}$  NMR (125 MHz,  $\text{CDCl}_3$ )  $\delta$  167.08, 166.78, 164.24, 160.34, 155.15, 155.06, 153.87, 135.62, 132.57, 131.30, 131.20, 128.98, 127.85, 126.36, 115.66, 115.43, 112.42, 112.20, 31.12, 31.00; MS (ESI)  $m/z$  294; HRMS (ESI) calcd. for  $\text{C}_{18}\text{H}_{13}\text{NOF}$   $m/z$  294.0929  $[\text{M}+\text{H}^+]$ , found  $m/z$  294.0930.

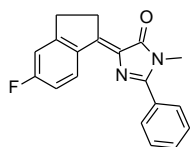
**(Z)-N-(1-(5-fluoro-2,3-dihydro-1H-inden-1-ylidene)-2-(methylamino)-2-oxoethyl)benzamide**



**(8b).** (Z)-4-(5-fluoro-2,3-dihydro-1H-inden-1-ylidene)-2-phenyloxazol-5(4H)-one (**8a**, 0.1 g, 0.34 mmol) was dissolved in  $\text{CH}_2\text{Cl}_2$  (2 mL) and acetonitrile saturated with dry methylamine (0.15 mL) was added to it and the mixture was stirred for 15 min. A white precipitate was formed. The reaction mixture was concentrated in vacuo and washed with cold  $\text{CH}_2\text{Cl}_2$  (3 × 3 mL) and dried in vacuo to give (Z)-N-(1-(5-fluoro-2,3-dihydro-1H-inden-1-ylidene)-2-(methylamino)-2-oxoethyl)benzamide (**8b**, 0.105 g, 95%) as a white powder that was used in the next step without further purification, m.p. 259 °C; UV (acetonitrile)  $\lambda_{\text{max}}$  303 nm ( $\epsilon$  = 31400); IR (ATR)  $\nu_{\text{max}}$  3318, 3224, 1637  $\text{cm}^{-1}$ ;  $^1\text{H}$  NMR (400 MHz,  $\text{DMSO}-d_6$ )  $\delta$  9.87 (br. s., 1H), 8.07 (d,  $J$  = 7.14 Hz, 2H), 7.80 (quart,  $J$  = 4.0 Hz, 1H), 7.56 (m, 4H), 7.20 (dd,  $J$  = 8.0, 2.01 Hz, 1H), 6.9 (dt,  $J$  = 8.0, 2.20 Hz, 1H), 3.22 (t,  $J$  = 6.86 Hz, 2H), 2.97 (t,  $J$  = 6.86 Hz, 2H), 2.66 (d,  $J$  = 6.86 Hz, 3H);  $^{13}\text{C}$  NMR (125 MHz,  $\text{DMSO}-d_6$ )  $\delta$  167.04, 166.49, 162.28, 152.55, 152.46, 144.45, 136.51, 134.47, 132.53, 129.23, 128.78, 127.89, 127.81, 122.83, 114.78, 114.56, 112.98, 112.77, 32.47, 31.04, 26.90; MS (ESI)  $m/z$  325; HRMS (ESI)

calcd. for  $C_{19}H_{18}N_2O_2F$   $m/z$  325.1352  $[M+H^+]$ , found  $m/z$  325.1352.

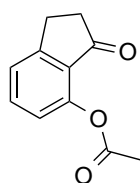
**(Z)-4-(5-fluoro-2,3-dihydro-1H-inden-1-ylidene)-1-methyl-2-phenyl-1H-imidazol-5(4H)-one**



(**8c**). (Z)-N-(1-(5-fluoro-2,3-dihydro-1H-inden-1-ylidene)-2-(methylamino)-2-oxoethyl)benzamide (**8b**, 0.1 g, 0.31 mmol) was kept in furnace at 350 °C for

60 seconds to give an yellow product which was purified by flash chromatography to yield the imidazolone (0.094 g, 57%), m.p. 154 °C; UV (acetonitrile)  $\lambda_{max}$  376 nm ( $\epsilon$  = 20816); IR (ATR)  $\nu_{max}$  3045, 2919, 1691  $cm^{-1}$ ;  $^1H$  NMR (600 MHz,  $CDCl_3$ )  $\delta$  8.82 (t,  $J$  = 4.8 Hz, 1H,  $-CH_{ar}$ ), 7.83 (d,  $J$  = 4.8 Hz, 2H,  $-CH_{ar}$ ), 7.56 (m, 3H,  $-CH_{ar}$ ), 7.05 (m, 2H,  $-CH_{ar}$ ), 3.49 (t,  $J$  = 5.93 Hz, 2H,  $-CH_2$ ), 3.37 (s, 3H,  $-NCH_3$ ), 3.20 (t,  $J$  = 5.93 Hz, 2H,  $-CH_2$ );  $^{13}C$  NMR (150 MHz,  $CDCl_3$ )  $\delta$  170.71, 165.89, 164.21, 158.30, 154.66, 154.60, 151.21, 136.28, 131.50, 131.44, 131.05, 130.02, 129.05, 128.94, 128.74, 128.67, 115.28, 115.13, 112.19, 112.15, 112.04, 112.00, 31.16, 31.12, 28.97;  $^{15}N$  NMR (60.8 MHz,  $CDCl_3$ )  $\delta$  200; MS (ESI)  $m/z$  307; HRMS (ESI) calcd. for  $C_{19}H_{16}N_2OF$   $m/z$  307.1247  $[M+H^+]$ , found  $m/z$  307.1247.

**3-oxo-2,3-dihydro-1H-inden-4-yl acetate (9).** 7-Hydroxy-2,3-dihydro-1H-inden-1-one (0.5 g,

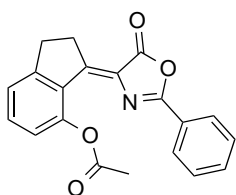


3.37 mmol) was added to acetic anhydride (5 mL) and 2 equivalent of sodium acetate (0.55 g, 7.74 mmol). The reaction mixture was irradiated in a microwave

reactor (SEM) for 3 min (300 W, 140 °C). The mixture was then poured in ice cold

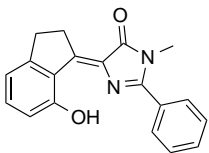
water and extracted with ethylacetate. The organic layer was washed thoroughly with water (4  $\times$  25 mL) and concentrated in vacuo. Purification by flash chromatography gave the pure acetoxyindanone (0.62 g, 97%), as white crystals. m.p. 76 °C [lit m.p. 75-77 °C].  $^{190}H$  NMR (400 MHz,  $CDCl_3$ )  $\delta$  7.58 (t,  $J$  = 7.80 Hz, 1H), 7.33 (d,  $J$  = 8.00 Hz, 1H), 6.97 (d,  $J$  = 7.70 Hz, 1H), 3.13 (t,  $J$  = 5.90 Hz, 2H), 2.66 (t,  $J$  = 5.90 Hz, 2H), 2.39 (s, 3H).

**(Z)-3-(5-oxo-2-phenyloxazol-4(5H)-ylidene)-2,3-dihydro-1H-inden-4-yl acetate (9a).** THF (10



mL) was chilled under N<sub>2</sub> to –10 °C. To it, TiCl<sub>4</sub> (0.058 mL, 0.53 mmol) in CH<sub>2</sub>Cl<sub>2</sub> (0.2 mL) was added and stirred for 10 min. To the stirring solution, 3-oxo-2,3-dihydro-1H-inden-4-yl acetate (*7-OAc indanone*; 0.1 g, 0.53 mmol) was added and the mixture was stirred for 5 min, then 2-phenyloxazol-5(4H)-one (*phenyl oxazolone*, 0.13 g, 0.85 mmol) was added and stirred for a further 20 min. To the mixture, pyridine (0.2 mL) was added dropwise. The black mixture was stirred for a further 5 hours and was monitored by TLC until the starting material had disappeared. The reaction was then quenched with saturated ammonium chloride solution (3 mL) and extracted with ethyl acetate (3 × 10 mL). The combined organic layer was washed thoroughly with water (4 × 10 mL) then brine solution (2 × 10 mL) and concentrated under vacuum. The oxazolone was purified by flash chromatography and recrystallized from methanol/water to yield a yellow solid (0.071 g, 40%), m.p. 192 °C; UV (acetonitrile)  $\lambda_{\text{max}}$  365 nm ( $\epsilon$  = 36800); IR (ATR)  $\nu_{\text{max}}$  1790, 1780, 1751, 1640 cm<sup>-1</sup>; <sup>1</sup>H NMR (400 MHz, CDCl<sub>3</sub>)  $\delta$  7.07 (m, 2H), 7.53 (m, 4H), 7.30 (d,  $J$  = 7.50 Hz, 1H), 7.06 (d,  $J$  = 7.87 Hz, 1H), 3.49 (t,  $J$  = 5.90 Hz, 2H), 3.18 (t,  $J$  = 5.90 Hz, 2H), 2.24 (s, 3H); <sup>13</sup>C NMR (125 MHz, CDCl<sub>3</sub>)  $\delta$  169.33, 166.99, 153.59, 153.47, 148.19, 133.46, 132.80, 131.56, 129.06, 128.07, 126.15, 123.06, 122.11, 32.68, 31.43, 22.12; MS (ESI)  $m/z$  334; HRMS (ESI) calcd. for C<sub>20</sub>H<sub>16</sub>NO<sub>4</sub>  $m/z$  334.1073 [M+H<sup>+</sup>], found  $m/z$  334.1079.

**(Z)-4-(7-hydroxy-2,3-dihydro-1H-inden-1-ylidene)-1-methyl-2-phenyl-1H-imidazol-5(4H)-one**



**(9c).** (Z)-3-(5-oxo-2-phenyloxazol-4(5H)-ylidene)-2,3-dihydro-1H-inden-4-yl acetate (*o-AcBPA*; 0.1 g, 0.30 mmol) was added to aqueous methylamine (40%; 0.1 mL) and potassium carbonate (0.04 g, 0.3 mmol) and the solution was refluxed under N<sub>2</sub> for three hours, cooled, extracted with ethyl acetate (2 × 10 mL), washed with water (3 × 50 mL) and concentrated *in vacuo*. The crude product was purified by flash

chromatography to provide the imidazolone **8c** (0.04 g, 45%) as a green-yellow solid, m.p. 192.5 °C; UV (acetonitrile)  $\lambda_{\text{max}}$  370 nm ( $\epsilon = 18600$ ), 410 nm ( $\epsilon = 21200$ ) nm; IR (ATR)  $\nu_{\text{max}}$  1686  $\text{cm}^{-1}$ ;  $^1\text{H}$  NMR (600 MHz,  $\text{CDCl}_3$ )  $\delta$  14.87 (s, 1H, -OH), 7.78 (d,  $J = 7.25$  Hz, 1H, -CH<sub>ar</sub>), 7.56 (m, 3H, -CH<sub>ar</sub>), 7.35 (t,  $J = 7.73$  Hz, 1H, -CH<sub>ar</sub>), 6.87 (d,  $J = 7.38$  Hz, 1H, -CH<sub>ar</sub>), 6.80 (d,  $J = 8.20$  Hz, 1H, -CH<sub>ar</sub>), 3.49 (t,  $J = 5.81$  Hz, 2H, -CH<sub>2</sub>), 3.45 (s, 3H, -NCH<sub>3</sub>), 3.18 (t,  $J = 7.73$  Hz, 2H, -CH<sub>2</sub>);  $^{13}\text{C}$  NMR (150 MHz,  $\text{CDCl}_3$ )  $\delta$  167.92, 157.45, 156.87, 154.26, 153.42, 135.53, 131.62, 129.27, 128.40, 128.31, 127.55, 125.57, 116.06, 115.76, 31.31, 30.89, 29.14; MS (ESI)  $m/z$  305; HRMS (ESI) calcd. for  $\text{C}_{19}\text{H}_{17}\text{N}_2\text{O}_2$   $m/z$  305.1295 [ $\text{M}+\text{H}^+$ ], found  $m/z$  305.1290.

## References

- (176) Adhikary, R.; Barnes, C. A.; Trampel, R. L.; Wallace, S. J.; Kee, T. W.; Petrich, J. W. *J. Phys. Chem. B* **2011**, *115*, 10707.
- (177) Eaton, D. F. *Pure Appl. Chem.* **1988**, *60*.
- (178) Stewart, W. W. *J. Am. Chem. Soc* **1981**, *103*, 7615.
- (179) Fischer, M.; Georges, J. *Chem. Phys. Lett.* **1996**, *260*, 115.
- (180) O'Connor, D. V.; Phillips, D. *Time Correlated Single Photon Counting, 3rd Edition*,; Academic Press, New York.
- (181) Burai, T. N.; Mukherjee, T. K.; Lahiri, P.; Panda, D.; Datta, A. *J. Chem. Phys.* **2009**, *131*, 034504.
- (182) Cook, A. H.; Harris, G.; Sir Heilbron, I. *J. Chem. Soc.* **1948**, 1060.
- (183) Conway, P. A.; Devine, K.; Paradisi, F. *Tetrahedron* **2009**, *65*, 2935.
- (184) Alías, M.; López, M. P.; Cativiela, C. *Tetrahedron* **2004**, *60*, 885.
- (185) Cativiela, C.; Diaz De Villegas, M. D.; Meléndez, E. *J. Heterocycl. Chem.* **1985**, *22*, 1655.

- (186) Herbivo, C.; Comel, A.; Kirsch, G.; Raposo, M. M. M. *Tetrahedron* **2009**, 65, 2079.
- (187) Bader, H.; Hansen, A. R.; McCarty, F. J. *J. Org. Chem.* **1966**, 31, 2319.
- (188) Knowles, A. M.; Lawson, A.; Boyd, G. V.; Newberry, R. A. *J. Chem. Soc. C: Organic* **1971**, 598.
- (189) Rioz-Martínez, A.; de Gonzalo, G.; Vicente, G. *Synthesis* **2010**, 1, 110.
- (190) Narine, A. A.; Wilson, P. D. *Can. J. Chem.* **2005**, 83, 413.





## Conclusions

In the first part of this thesis, we tried to rationalize the origin of the non-fluorescing nature of epicocconone, which is widely used as a fluorescent protein stain, and engineer its photophysics by virtue of synthetic modification. Photoisomerization has been found to be the origin of the ultrafast relaxation pathway of epicocconone, resulting in its feeble fluorescence. Four analogues were synthesized that helped understand the excited state process involved in epicocconone and its amine adduct. It has been found that photoisomerization did not alter the excited state dynamics of the epicocconone-amine adduct, indicating that the fluorescence originated from the heteronuclear ring system. It has also been found that the presence of the keto-enol moiety was necessary to have greater fluorescence in the amine adducts by the virtue of intermolecular H-bonding, while it affected only little in the excited state dynamics of the native compounds. Based on these observations and interpretations, two highly fluorescent analogues were synthesized that showed competence to be used as protein stains as well as dual stains.

In the second part, we synthesized several locked and unlocked GFP chromophore analogues to have a better understanding of the non-fluorescing behaviour of the isolated chromophore (*p*-HBDI). Despite locking the exocyclic single bond, the compounds were found to be non-fluorescent in solution, while strongly fluorescent in solid state. This substantiated the fact that isomerization of the exocyclic double bond to be the primary reason for the non-radiative channel. To restrict this rotation, the ortho-hydroxy analogue was synthesized with a phenyl substitution at the C(1) of the imidazolinone. Surprisingly, this compound exhibited an unprecedented dual fluorescence with a much lower quantum yield than that of the methylated analogue, reported earlier. This result showed the importance of the substituents at the imidazolinone and forms the basis of designing HBDI derivatives with very high quantum yield.



## Acknowledgment

I can still remember the beginning of the journey of my Ph.D. tenure. Almost half an era has passed; millions have breathed their last and a lot more were born. Technology, politics, religion and personal vendetta have triumphed over humanity with an inclining graph, but life continued. The day has eventually come. On the verge of submitting my thesis for *philosophiae doctor*, aka Ph.D., the highest one achievable in the realm of academics (D. Sc. or D. Litt. is not considered), I cannot help but question myself if I really deserve this. I often ask myself what exactly I have learnt academically and how much contribution I made to human civilization as well as to science in these years and yet I am unable to find definite answers. But, I certainly know that the past years have taught me to be patient, to endure and wait for the right moment. It helped me to have a ‘never say die attitude’ which made me stronger and stronger everyday as a human being. After all the ‘hard’ work and sometimes ‘hardly’ work, I have learnt to live my life to the fullest.

Acknowledging people is not an easy job for me as it literary means ‘acceptance of the truth or existence of something’ and I have encountered many persons who had a negative effect on me. I want to acknowledge their presence in my life by not mentioning them in this acknowledgment.

The foremost persons, whom I love the most, are my parents {my father; Mr. Amit Chatterjee (Baba), my mother; Mrs. Chitralkha Chatterjee (Ma)} and my younger brother (Tupai), who dreamt to see me graduating and never put any pressure upon me despite numerous hostile situations in their personal life. They are my best friends forever and the reason what I am today. Thanks to them as they only taught me to be a better person before becoming a good scientist. I hope I can keep their faith in the future too so that they can hold their head high. In this regard, I would also like to thank my cousin, Miss Pubali Basu for her love and support.

I thank Prof. Peter Karuso, my principal supervisor for his patience, meticulous correction of my thesis and helping me whenever required during the tenure of my candidature as a Ph.D. student along with my associate supervisor A/Prof. Fei Liu.

It is my privilege to thank Prof. Anindya Datta, my adjunct supervisor, for letting me work in his lab, helping me throughout the years and sharing his vast knowledge of the subject.

During my stay in Sydney, I came across many people with whom I made special bonding. I would especially want to thank Rajesh, Alpesh, Javed, Sowmya, Jashan, Gagan,

Karthik, Nima, Carlo, An, Kaushikda, Sonali Boudi and Sristi for their presence, constant love and support during my stay. A very, very special thanks to Wendy, Michael, Ketan, Kavita, Girish and Andre to bother me in the lab and to Ron who was always there with me.

Tupurdi, Rakeshda and Shnaajh must be mentioned with whom I had wonderful times in Melbourne and who, by their cordial love never made me feel out of my country.

Amongst my friends in Mumbai, Late Atanu Mitra (Atanuda) and Punamdi would come first, followed by Tarakda, Siva, Nancy, Anasuya, Snigdha, Sucheta, Krishna, Vijaykant, Avinash, Sohikul(Sr.), Sohikul (Jr.), Vaishalidi, Ramya, Ravi and Rugmini madam in the list of thanksgiving. A special thanks to the Bengali group; Manasda, Uddipta, Antara, Sohom, Aniket, Ushak, Gouri, Nilapratim, Sukanta and Anweshan, who consistently made my stay in IIT Bombay funny, enjoyable and cheerful and pampered me with loads of delicious cuisines.

I would like to express my gratitude to Mr. Sujoy Chakraborty and Dr. Vivek Chatterjee for their constant support, love and help for the last eleven years.

I thank CBMS Department, Macquarie University and Department of Chemistry, IIT Bombay for providing me the opportunity to be a part of these departments with state of the art research facilities and also to Australian Research Council for my funding.

Last but not the least, I must mention about Poulomi, my wife, who was always beside me even during the most pathetic times and pacified me to forget everything and start a new chapter.